STRUCTURE PROPERTY CORRELATION OF FRICTION STIR WELDED Al-Ce-Si-Mg ALUMINIUM ALLOY AND OPTIMIZATION OF PROCESS PARAMETERS USING SOFT COMPUTING TECHNIQUES

Thesis

Submitted in partial fulfillment of the requirements for the degree of

DOCTOR OF PHILOSOPHY

by

AUSTINE DINESH D'SOUZA

DEPARTMENT OF MECHANICAL ENGINEERING

NATIONAL INSTITUTE OF TECHNOLOGY KARNATAKA

SURATHKAL, MANGALORE-575 025

October 2021

STRUCTURE PROPERTY CORRELATION OF FRICTION STIR WELDED Al-Ce-Si-Mg ALUMINIUM ALLOY AND OPTIMIZATION OF PROCESS PARAMETERS USING SOFT COMPUTING TECHNIQUES

Thesis

Submitted in partial fulfillment of the requirements for the degree of

DOCTOR OF PHILOSOPHY

by

AUSTINE DINESH D'SOUZA

(Registration No: ME16P01)

Under the Guidance of

Dr. Shrikantha S. Rao
Professor
and

Dr. Mervin A. Herbert
Associate Professor

DEPARTMENT OF MECHANICAL ENGINEERING

NATIONAL INSTITUTE OF TECHNOLOGY KARNATAKA
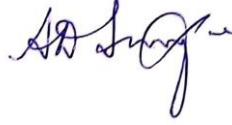
SURATHKAL, MANGALORE-575 025

October 2021

DECLARATION

by the Ph.D. Research Scholar

I hereby declare that the Research Thesis entitled "**Structure property correlation of friction stir welded Al-Ce-Si-Mg aluminium alloy and optimization of process parameters using soft computing techniques**", which is being submitted to the **National Institute of Technology Karnataka, Surathkal** in partial fulfillment of the requirements for the award of the Degree of Doctor of Philosophy in Mechanical Engineering, is a *bonafide report of the research work carried out by me*. The material contained in this thesis has not been submitted to any other University or Institution for the award of any degree.

Name of the Research Scholar   : **AUSTINE DINESH D'SOUZA**

Register No.   : **165087 - ME16P01**

Signature of Research Scholar   :

Department of Mechanical Engineering
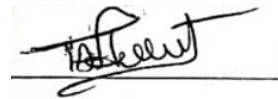
Place: NITK -Surathkal

Date: 18/10/2021

CERTIFICATE

This is to certify that the Research Thesis entitled "**Structure property correlation of friction stir welded Al-Ce-Si-Mg aluminium alloy and optimization of process parameters using soft computing techniques**", submitted by **Mr. Austine Dinesh D'Souza** (**Register Number: 165087 - ME16P01**) as the record of the research work carried out by him, is accepted as the *Research Thesis* submission in partial fulfillment of the requirements for the award of degree of Doctor of Philosophy.

Dr. Shrikantha S. Rao
Research Guide
Date: 18/10/2021

Dr. Mervin A Herbert
Research Co-Guide
Date: 18/10/2021

Dr. S. M. Kulkarni
Chairman-DRPC
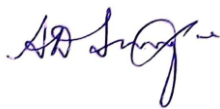Date: 18/10/2021

Acknowledgements

Austine Dinesh D'Souza

Abstract

The demand for Aluminium alloys for uses as structural material is growing day by day, due to their distinct benefit of high strength to weight ratio. However, these alloys show a great challenge during welding by conventional methods due to the physical properties being dissimilar to steel and other materials and the property of improved hardness. Solid state welding method offers an alternative to conventional welding methods and leads to the improved joint efficiency due to microstructural alteration. Researchers around the world are carrying out wide-ranging experiments on one such process known as Friction Stir welding or FSW to join the materials effectively in solid state.

In the present research study, the evolution of microstructure at the weld zone during friction stir welding of Al-Ce-Si-Mg aluminium alloy (Al-10Mg-8Ce-3.5Si and Al-5Mg-8Ce-3.5Si), as well as the effect of Friction Stir Welding (FSW) on joint strength was carried out. The microstructural study of the FSW joint has been carried out using Scanning electron microscopy as per ASTM E112-12(2012). An EDAX analysis as per ASTM F1375-92(2012) and an Optical emission spectrometry as per ASTM E1251-11 have been carried out to ascertain the chemical composition. An x-ray diffraction has been carried out as per ASTM F2024 - 10(2016) to ascertain the phases present in the alloy. The tensile testing has been done as per ASTM E8-04 and Vickers hardness test as per ASTM E92–17.

It is very difficult to identify the process variables to obtain the desired joint strength by conducting numerous individual experiments. Therefore, to analyse the welding process variables, the orthogonal array technique (OA) type Taguchi design of experiment helps in arriving at the best possible solution. Design of Experiments were adopted to find out the influence of various input process parameters on mechanical properties such as ultimate tensile strength (UTS), hardness and grain size of the joint and to predict the UTS of the joint.

The Taguchi experiments showed that the tool pin shape, speed of tool rotation and speed of welding have a bearing on the quality of the FSW joints in

aluminium alloys. It was observed that the grain size at Nugget Zone (NZ) is dependent on the speed of tool rotation, speed of welding, tool pin shape and composition of the aluminium alloy. The grain size at the bottom of the NZ was found to be decreasing as compared to the top of the NZ. It was observed that highest hardness was found at NZ. Minimum hardness was obtained at HAZ and all the tensile specimens fractured at HAZ. Optimal joint strength was obtained for a speed of tool rotation of 1000 rpm, speed of welding of 20 mm/min, tool of triangular pin shape and 10% (wt%) of Mg (Al-10Mg-8Ce-3.5Si) aluminium alloy. The Taguchi orthogonal array-based design has shown that the Tool pin shape has greater significance in increasing the joint strength, followed by speed of welding, Material composition and speed of tool rotation. A speed of tool rotation 1000rpm, speed of welding 20 mm/min, Triangular Profile Tool (TPP) tool and Al-10Mg-8Ce-3.5Si aluminium alloy were obtained as the optimum variables of the process. The percentage contribution of each of the input process variables on optimum output quality characteristics was also found out and found to be lying well within the confidence interval of 95% suggested by the Taguchi design.

Further work is carried out to predict the model for aluminium alloy joints fabricated using friction stir welding using Artificial neural network (ANN) technique. The Multilayer perceptron neural network (MLP) with error back propagation learning algorithm is selected as it can predict the ultimate tensile strength, percentage of elongation and hardness of the joint for given rotation speed welding speed, tool pin profile and composition of the material. The validation of the predicted model is performed by conducting validation experiments. The prediction is done by the model, and later it is analysed to assist the suitability of the ANN prediction model.

The present work has shown that the prediction results with ANN are more superior to those predicted using statistical methods like Taguchi Techniques.

Contents

List of Figures

and welding speed of 10 mm/min, (b) Speed of tool rotation of l000 RPM and welding speed of 15 mm/min, (c) Speed of tool rotation of l000 RPM and welding speed of 20 mm/min, (d) Higher magnification image showing the dimples, pullout, decohesion and cracked AlSiMg particles.

List of Tables

Nomenclature

Adj MS	Adjusted mean squares
R-Sq(adj)	Adjusted R square value
Adj SS	Adjusted sum of squares
AS	Advancing Side
AA	Aluminium alloys
Al_2O_3	Aluminium Oxide
ASTM	American Society for Testing and Materials
AI	Artificial Intelligence
ANN	Artificial Neural Network
Trainbfg	BFGS quasi-Newton backpropagation
BM	Base Material
BP	Back Propagation
CPP	Circular Profile Pin
DF	Degrees of freedom
DSCP	Direct current straight polarity
DCRP	Direct Current Reverse Polarity
EDM	Electrical Discharge Machine
El %	Elongation Percentage

EDX	Energy Dispersive X-Ray Analysis
FFNN	Feed forward neural network
FEM	Finite Element Analysis
F	Fischer ratio
FSW	Friction Stir Welding
GA	Genetic Algorithm
GD	Gradient descent
Traingda	Gradient descent with adaptive learning rate backpropagation
Traingdx	Gradient descent with momentum and adaptive learning rate backpropagation
HAZ	Heat Affected Zone
n	Input numbers to hidden neurons
IMF	Intrinsic Mode Functions
LBW	Laser beam welding
LR	Learning rate
η	Learning rate variable
Trainlm	Levenberg-Marquardt backpropagation
LM	Levenberg-Marquardt
LMGD	Levenberg-Marquardt Gradient Decent
Xmax	Maximum value in the data range
MSE	Mean squared error

MIG	Metal Inert Gas
Xmin	Minimum value in the data range
MLP	Multilayer perceptron
α	Momentum term or the momentum factor
NN	Neural Network
xn	Normalised value of input data
NZ	Nugget Zone
OA	Orthogonal Array
m	Output numbers to hidden neurons
% El	Percentage Elongation
X	Predicted data
t-1	Previous training step
P	Probability that 95% confidence level exceeds
RNN	Recurrent neural network
RE	Relative Error
Trainrp	Resilient backpropagation
RS	Retreating Side
RSM	Response Surface Methodology
Trainscg	Scaled conjugate gradient backpropagation
SEM	Scanning Electron Microscope

Seq MS	Sequential mean of squares
D/d	Shoulder diameter to pin diameter
ML	Sliding Torque
SPP	Square Profile Pin
MT	Sticking Torque
SZ	Stir Zone
TMAZ	Thermo-Mechanically Affected Zone
TPP	Triangular Profile Pin
TIG	Tungsten Inert Gas
UTS	Ultimate Tensile Strength
VHN	Vickers Hardness Number
XRD	X-Ray Diffraction
YS	Yield strength

CHAPTER 1

INTRODUCTION

1.1   GENERAL BACKGROUND OF THE RESEARCH WORK

In the current period of reliance on diminishing fossil fuel energy sources, a great thrust has been laid on improving the fuel efficiency of the thermal engines used in different applications like automobiles, aircrafts, marine and other equipment. To enhance the efficiency of the engines, it is essential to decrease the mass of the engine as well as improved performance features even at higher temperatures. Also, an effort has been made to operate these engines using a common fuel, requiring the material of the engine to withstand high temperatures. Also, the aircraft manufacturers look for light weight, durable and thermally stable materials for engine design. Taking this into consideration, a lot of research work has been pointed at creating special alloys which will give the desired outcomes. One such material which can cater to these requirements and which is of recent origin is aluminium cerium silicon magnesium (Al-Ce-Si-Mg) alloy (Sims et al. 2016). This alloy has been found to be able to retain its properties even at raised temperatures. This alloy is durable, light in weight, can be easily casted and the alloying element cerium is copiously available and is marginally low in cost in comparison to other alloying elements. This is found to be suitable for general engine cylinder heads and aircraft engine cylinder heads with very long and thin fins.

Most of the alloys with exceptionally good properties are not easy to cast. But the Al-Ce-Si-Mg alloy has casting properties equivalent to the 3000 series aluminium-silicon alloys. One of the alloying elements used in Al-Ce-Si-Mg alloy is called Cerium, which is a rare earth element which is available easily. The addition of alloying element cerium forms an intermetallic which is stable up to 1093ºC, which makes the alloy stable even at high operating temperatures. In addition to the enhanced mechanical properties at elevated temperatures, the aluminium-cerium alloy has low density compared to pure aluminium. The density of the standard pure aluminium is 2.68 g/c.c.,

whereas that of Al-Ce-Si-Mg alloy is 2.49 g/c.c., which is significant particularly for aircraft engines (Sims et al. 2016). The magnesium addition to the aluminium alloy enhances the alloy strength through solid solution strengthening and increases their strain hardening capacity. These alloys are the highest strength non-heat-treatable aluminium alloys and are, therefore, used extensively for structural applications. Some common applications for these alloys are truck and train bodies, buildings, armored vehicles, ship and boat building, chemical tankers, pressure vessels and cryogenic tanks. The addition of magnesium and silicon to aluminium produces the compound magnesium-silicide (Mg_2Si). The formation of this compound provides heat-treatability. They are extensively used in making of extruded shapes. Some of the common applications for the these alloys are handrails, drive shafts, automotive frame sections, bicycle frames, tubular lawn furniture, scaffolding, stiffeners and braces used on trucks, boats and many other structural fabrications. (Kori et al. 1999; Miller et al. 2000).

The usage of this new Al-Ce-Si-Mg alloy in engines has necessitated requirement of having a method for joining these alloys. One such method which meets these requirements is the method of Friction stir welding or FSW which could be effectively used for joining these aluminium alloys (Jannet et al. 2014).

The suitability of joining this newly developed high-performance alloy i.e., Al-Ce-Si-Mg alloy using FSW has been considered as the subject of this research study. The research work is mainly focussed on studying the micro-structure and mechanical properties of the Al-Ce-Si-Mg alloy weld connection made using friction stir welding, while varying the parameters (or variables) used in the process.

1.2 BACKGROUND OF FSW TECHNIQUE

Friction stir welding or FSW in short, is a recently established metal joining technique and has been in use for welding purposes since 1991. Since in FSW, the melting does not happen and joining occurs below the melting temperature of the material, a high-quality weld is produced. This feature marginally mitigates the bad effects of high heat input, such as distortion, and removes the defects of solidification. FSW also is

extremely efficient, since it does not generate any fumes, and does not use any filler material, to make this method environmental friendly (Defalco 2009).

FSW was devised by The Welding Institute (TWI) during December 1991 (Liu et al. 2014; Ma et al. 2018; Verma and Misra 2015). Since its inception, the method has garnered an unprecedented world-wide interest, and these days FSW is used in research and production in many industrial sectors such as, automotive, shipbuilding, railways, aerospace, coolers, heat exchangers, electronic housings, and nuclear waste containers etc.

FSW has been proved itself to be an popular method for joining aluminium, copper, brass, and other low-melting-temperature materials (Defalco 2009; Kumar, HM Anil et al. 2014). The recent phase in FSW research has been targeted at expanding the usefulness of this technique in high-temperature-melting materials, for example nickel-based alloys and carbon and stainless steels, by designing tools that are able to withstand elevated pressures and temperatures required for joining these materials successfully.

The FSW procedure can be treated as a solid-phase key-hole welding method, because to accommodate the tool pin, a hole is created. The rotating pin is then moved along the weld line during the welding sequence (Kallee and Nicholas 2000; Thomas and Nicholas 1997). In FSW, a cylindrical, shouldered tool with a contoured pin is made to rotate and slowly plunged into the weld connection between two pieces of sheet or plate material that are to be joined together (Mendez and Eagar 2001). The parts need to be clamped firmly onto a backing plate in a fashion that prevents the abutting weld connection faces from being forced apart or moved out of position in any other direction. The frictional heat is produced between the wear-resistant welding tool and the workpiece material. This heat makes the workpieces to soften without reaching the melting point and permits the tool to navigate along the weld line. The ensuing plasticized material is channeled from the leading side of the tool to the trailing side of the tool pin and is forged together by the close contact of the tool shoulder and the pin profile. This creates a solid-phase bond between the two pieces (Gori and Uniyal 2015; Meilinger and Torok 2013).

A superior quality weld is produced by FSW method due to its inherent advantages over the conventional arc and other welding procedures. In FSW, the complete melting of the base material does not happen due to partial plasticizing of the base material and joining taking place well below the melting temperature. This feature also gives it the distinct edge over conventional welding processes, due to its low heat addition characteristics, thus mitigating solidification related complications. FSW method does not use any flux and hence does not release any hazardous gases, which makes it extremely healthy to use and environmental friendly method (Malik et al. 2014). Even though earlier, the FSW was used for materials having low temperature of melting, such as copper, aluminium and brass etc., later, its use was extended to materials having high temperature of melting like, steel, nickel and titanium alloys due to the developments in special tool materials with enhanced hardness and other properties (Threadgilll et al. 2009; Wan and Huang 2018).

The method originally was limited to low-melting-temperature materials because initial tool materials could not hold up to the stress of "stirring" higher-temperature materials such as steels and other high-strength materials. This problem was solved recently with the introduction of new tool material technologies such as polycrystalline cubic boron nitride (PCBN), tungsten rhenium, and ceramics. The use of a liquid-cooled tool holder and telemetry system has further refined the method and capability (Defalco 2009). Tool materials utilized in FSW of high- temperature-melting materials must have high "hot" hardness for abrasion resistance, in addition to chemical stability and good toughness at elevated temperatures. Material developments in different tool materials are progressing quickly with each material contributing specific benefit for each of the applications (Chiteka 2013; Kumar et al. 2014; Rai et al. 2011)

The quality characteristics of the output weld such as material flow pattern, micro-structure changes like grain size modification and mechanical properties like hardness, tensile stress etc. are influenced by various input process parameters (or process variables) (Balasubramanian 2008; D'Souza et al. 2019a; Dwivedi 2014; Guo et al. 2014; Karthikeyan and Senthil Kumar 2011; Prabhu et al. 2016). The important input process parameters are tool geometry (tool pin contour, tool pin dimension, tool collar dimension, tool collar thrust face contour), welding parameters (speed of tool rotation,

4

direction of tool rotation, tool feed along the line of weld, tool inclination angle, tool forces) and weld connection design (edge butt joint, T-butt joint, square butt joint, simple lap joint, multiple lap joint, T-lap joint, and fillet joint) etc. (Ghazanfar et al. 2013; Thangaiah et al. 2018). The study of influence of input process parameters like speed of tool rotation, tool feed in the direction of weld and tool pin contour have become important topics of interest to the researchers in the area of FSW and are broadly covered in this research paper (Banik et al. 2019; D'Souza et al. 2019; Suresha et al. 2011). These parameters have a considerable bearing on the quality of the weld connection produced. The research is mainly aimed at finding the effect of these input process parameters on output weld quality characteristic (response); the ultimate tensile stress (UTS) of the FSW weld connection produced with plates of Al-Ce-Si-Mg aluminium alloy material.

The weld connection strength of the material in FSW method are governed by welding parameters. Therefore, it is highly recommended for utilizing some sort of technique to optimize the process parameters. An engineering approach is used to resolve such problems to build a mathematical model. Several research have used mathematical models to analyze, predict and optimize the process parameters of FSW of aluminium alloy. But these approaches lead to single objective prediction are optimization technique, which once again creates a new model in order to optimize another output variable. In order to predict several output parameters based on input parameters, for highly complex and non-linear systems, the artificial intelligent technique (AI) is preferred. AI technique assists industries for multi objective predication and optimization.

1.3 BACKGROUND OF TAGUCHI DESIGN OF EXPERIMENTS TYPE MATHEMATICAL MODEL OPTIMIZATION TECHNIQUE

To evaluate the influence of input process parameters on weld output quality, researchers have followed conventional testing methods like changing the parameters

one by one and maintaining other parameters steady. This type of experimental method is very laborious and needs more resources. And to overcome these limitations, the statistical tools like Design of Experiments (DOE) by Taguchi approach (method) were used (Jayaraman et al. 2009a; Lakshminarayanan and Balasubramanian 2008; Palani et al. 2015). With the statistical methods, by conducting a relatively a smaller number of experiments than the conventional methods, the significant factors that affect the quality of the weld could be obtained. In the Taguchi design even though the interaction effects of these input process parameters could be studied, these have not been considered in this analysis to save the cost and time. Additional experiments may be required to be conducted if the combined effects of these interactions need to be studied (Abbas and Abdulkadhum 2019; Ghetiya et al. 2016; Kumar et al. 2015a; Mishra and Jain 2019).

Taguchi technique could effectively be used for solving the problems related to the optimization of process parameters for any FSW work. This method helps in improving the performance of the method or system with a considerable saving in time and cost, which eventually leads to improved design and better product (Kumar et al. 2018; Montgomery 2017). Taguchi method, or alternatively called the Robust Design Method, significantly enhances engineering output (Besterfield et al. 2011; Dehnad 1990). Robust Design method helps ensure quality of the product, by carefully considering the noise factors (include environmental variations during the product's handling, manufacturing deviations, and component wear and tear) and the cost of breakdown.

For solving numerous complicated problems in manufacturing companies, the Taguchi method or robust design of products and processes, which takes into consideration the combined effect of the experimental design theory and quality loss function concept, has been made use of. In addition, this technique also decides the most significant parameters for the optimum result (Lakshminarayanan and Balasubramanian 2008). The optimum process parameters obtained from the Taguchi method are not sensitive to the changes in the environmental and other noise factors. The number of experiments goes up with the increase in the number of process parameters. With the aim of reducing this complexity, the Taguchi method makes use of a special orthogonal array design to

analyze the full method variable domain only with a small number of experiments (Jayaraman et al. 2009a). Taguchi technique classifies three classes of quality characteristics in the analysis of Signal/Noise ratio, i.e. the lower-the-better, the larger-the-better and the nominal the-better. The S/N ratio for each of method variable is calculated using S/N ratio analysis. Irrespective of the class of the quality characteristics, a larger S/N ratio matches to the better-quality characteristics. Therefore, the optimal level of method variable is the level of maximum S/N ratio. Moreover, a statistical analysis of variance (ANOVA) can be carried out to find out which method variable is statistically important for each of the quality characteristics (Elangovan et al. 2009; Elatharasan and Kumar 2013).

1.4 BACKGROUND OF ARTIFICIAL NEURAL NETWORK TYPE ARTIFICIAL INTELLIGENCE OPTIMIZATION TECHNIQUE

The term Artificial Intelligence (AI) or Artificial Intelligent technique was coined by John McCarthy, in the year of 1956. Artificial neural network (ANN) is a subcategory of AI system. Artificial Neural Network (ANN) plays a dynamic application in the field of biology, electronics, computer science. mathematics and engineering (Okuyucu et al. 2007). It is considered as the computing system, wherein, it mimics the working of human brain. The ANN procedure learns and recognizes the relationship between the input and output patterns by training the network. The development of such a model and using such a model is quite simple. but more effective as compared to other techniques. It comprises of number of interconnected neurons, wherein it saves the information in the memory based on the given set of input and output patterns. The memory gets updated, in case if there is any new information addressed to the same location, but without losing the old information (Ghetiya and Patel 2014; Zurada 1992).

Multilayer perceptron neural network (MLP) is one of the most common neural network architectures used for function approximation, classification, and prediction problems. The MLP consists of an input, hidden and output layers, each consisting of several neurons. Each neuron processes the input and its output is transmitted to the

7

neurons in the subsequent layer (Vaira and Padmanaban 2018). The architecture of MLP is a multilayered feed forward neural network, where the information flow is unidirectional. Each neuron in the network includes a non-linearity at the output. A commonly used form of non-linearity is the sigmoidal non-linearity. MLP is trained by using one of the supervised learning algorithms of which the best known is back propagation algorithm. There are two passes: a forward pass and a backward pass through the different layers of the network. An input pattern is submitted and propagated through the network layer by layer in the forward pass, and a set of outputs are produced as the actual response of the network. The synaptic weights are all fixed during the forward pass, and in the backward pass, depending upon the error between the actual output and the target output, all the synaptic weights are adjusted. Until all the input patterns from the training set are learnt with an acceptable overall error, this method is continued. The trained network itself operates in a feed forward manner, during the testing phase. (Vaira and Padmanaban 2018; Yousif et al. 2008).

1.5   SUMMARY OF THE PROPOSED RESEARCH WORK

The present research work is aimed at investigating the suitability of a metal joining method of Friction stir welding or FSW on a newly developed material, i.e., Aluminium Cerium Magnesium Silicon (Al-Ce-Si-Mg) alloy plates. The research is also aimed at ascertaining the superiority of the weld connection characteristics such as micro-structure, grain size, hardness, tensile stress etc., produced by FSW with that produced using conventional welding processes such as arc welding. It is also intended to conduct the research experiments with a varying the input parameters of the process. To obtain the desired weld connection strength, since it is very difficult to identify the process parameters by conducting numerous individual experiments, the orthogonal array technique (OA) type Taguchi design of experiment was made use of, in arriving at the best possible combination of input process parameters.

8

Further work is carried out to predict the model for aluminium alloy joints fabricated using friction stir welding. The Multilayer perceptron neural network (MLP) with error back propagation learning algorithm is selected as it can predict the ultimate tensile strength, percentage of elongation and hardness of the weld connection for given tool rotation speed, welding speed, profile of pin of tool and composition of the material. The validation of the predicted model is performed by conducting validation experiments. The prediction is done by the model, and later it is analyzed to assess the suitability of the ANN prediction model

1.6   THESIS ORGANIZATION

In this research study, a methodical investigation is conducted to explain the performance of Al-10Mg-8Ce-3.5Si and Al-5Mg-8Ce-3.5Si Aluminium alloys joined by FSW process. The influences of process parameters involved in the welding of aluminium alloys have been explored. Also, a exhaustive design of experiments analysis is carried out with the help of orthogonal array (OA) type Taguchi technique and later a prediction model was proposed by Taguchi as well as Multilayer Perceptron type ANN technique. The research was carried out in various stages and these have been summarized into six chapters. The details of the summary of research work has been explained as follows.

Chapter 1 explains the historical background of the proposed research work along with the problems encountered during research work and the impetus to take up the present research work. An outline of the planned research work with specific objectives is also detailed in this chapter.

Chapter 2 includes a step by step detailed and critical review of the literature in the area of FSW of aluminium alloys. The influence of conventional welding method on strength of the aluminium alloys is highlighted. Brief explanation of FSW method and material flow are discussed here. The metallurgical and mechanical characterization of FSW material is briefly explained. The effect of process parameters on the weld connection quality is discussed in this chapter. A mathematical model is created for

analysis and optimization and prediction of material is enumerated. Various types of defects occurring during the FSW method are explained in this chapter.

Chapter 3 covers the exhaustive description of the investigational and measurement procedures, used to get the results for tests like tensile test, hardness measurement, grain size etc., of Al-10Mg-8Ce-3.5Si and Al-5Mg-8Ce-3.5Si Aluminium alloys which are joined by FSW method. The detailed step by step method involved in the stir casting of aluminium alloys, welding of these aluminium alloys to get a good quality weld, preparation of specimen for different experiments, mechanical testing for measurement of hardness and tensile test are also discussed here.

Chapter 4 deals with the analysis of the weld connection quality of the friction stir welded aluminium alloys, analysis of process parameters of FSW welded aluminium alloys using Taguchi technique and prediction of weld connection strength and hardness of aluminium alloys using Taguchi and ANN techniques. A detailed analysis of metallurgical and mechanical properties of the aluminium alloys has been discussed here. In FSW, an attempt has been made to explore the working range, in order to obtain the defect free weld connection by varying the speed of tool rotation, welding speed and tool pin contour. The detailed nature of defects and cause of the defects have been discussed in this chapter. Further analysis is carried out on those specimens which were free from defects and their metallurgical and mechanical characterizations are discussed. Taguchi design of experiments was carried out to analyze the influence of process parameters on weld output quality. Further, the optimization and prediction of weld connection strength is carried out to find out the fitness of the model. A prediction and multi-objective optimization were carried out using Artificial Neural Network technique.

Chapter 5 covers the overall conclusion drawn from the present research work and scope for further   research work in this field of study is elaborated.

CHAPTER 2

LITERATURE REVIEW

INTRODUCTION

The demand for Aluminium alloys is rising rapidly for use as structural material, owing to their advantageous characteristic of high strength to weight ratio (Dursun and Soutis 2014; Miller et al. 2000; Starke and Staley 2010). However, these alloys pose a great challenge during welding by conventional methods due to the physical properties being dissimilar to steel and other materials and the property of improved hardness (Balasubramanian et al. 2009; Kumagai 2003; Yamamoto et al. 1992). Solid state welding method offers an alternative to conventional welding methods and also leads to the improved weld connection efficiency due to microstructural alteration. Researchers around the world are carrying out wide-ranging experiments on one such method known as Friction stir welding or FSW to join the materials effectively in the solid state (Mishra and Ma 2005; Thomas and Dolby 2002).

The significance of the current work on FSW of Al-10Mg-8Ce-3.5Si aluminium alloy has been highlighted in the chapter 1. The present chapter focuses on work which has been carried out by different researchers in the field of synthesis of aluminium alloy, FSW of alloys, FSW of aluminium alloys and application of Taguchi Design of Experiments type of soft computing techniques for optimization of parameters of FSW process. A systematic, exhaustive, and critical literature survey is carried out and presented in the present chapter. The survey carried out provides information and direction for methodical approach of the experimental work and analysis of the present work. The survey is classified into the following comprehensive divisions:

- Aluminium alloy synthesis
- Aluminium alloy welding

- FSW Concept

- Selection of material

- Flow pattern of material during welding

- Micro-structure evolution at the weld region

- Study of mechanical properties of the weld connection

- Influence of process parameters on weld quality

- Analysis, Prediction, and optimization of weld properties

- Defects in FSW weld connection

- Applications of FSW

2.1 ALUMINIUM ALLOY SYNTHESIS

Aluminium and aluminium alloys possess many exceptional qualities that lead to wide range of uses, together with enhanced oxidation and corrosion resistance, superior thermal and electrical conductivities, high reflectivity, low density, reasonably high ductility and high strength, and relatively cheaper in price (ASM International 1993a; Davis 2001).

Aluminium with a density of 2.7 g/cm^3 (0.1 lb/in^3) is a relatively lightweight material available in abundance (Barnhisel and Bertsch 1982; Davis 2001). Pure aluminium and its alloys possess the face-centered cubic (FCC) structure, which is stable up to its melting point at 657 °C (1215 °F). Because the FCC structure comprises multiple slip planes, this crystalline structure significantly helps in contributing to the superior formability to the aluminium alloys.

Aluminium alloys show a decent blend of ductility and strength. Aluminium alloys are the easiest to form and machine among all metals. The precipitation-hardening alloys can be formed in a comparatively soft state and then heat treated to much higher strength levels after completing these forming operations. Moreover, aluminium and its alloys are non-toxic and when compared to any of the structural materials, they are one among the easiest to recycle (McLean 1965).

Aluminium is the most abundant metal in the Earth's crust, but it was not until the 1800s that elemental aluminium was successfully extracted. Even the first processes

developed were inefficient and extremely expensive. The scenario altered during 1886 to 1888 with the nearly simultaneous development of the Hall-Héroult method for electrolytic reduction and the Bayer method for cheap production of alumina (Al_2O_3) from bauxite ore (Grjotheim et al. 1977; Hind et al. 1999; Jarrett 1987; Øye and Huglen 1990; Whittington 1996).

2.1.1 Types of Aluminium Alloys

Aluminium alloys are generally classified into three distinct groups: wrought non-heat-treatable alloys, wrought heat-treatable alloys, and casting alloys (Enright 1987; Heinz et al. 2000; Miller et al. 2000; Rambabu et al. 2017). This is depicted in Figure 2.1 and Figure 2.2

2.1.1.1 Wrought non-heat-treatable alloys

For strengthening of wrought non-heat-treatable alloys the method of precipitation-hardening cannot be used and primarily the cold working method is adopted for hardening (Sanders et al. 1989; Vasudevan and Doherty 1989). The wrought non-heat-treatable alloys mainly comprise the commercially available pure aluminium alloy series (1*xxx*), the aluminium-manganese series (3*xxx*), the aluminium-silicon series (4*xxx*), and the aluminium-magnesium series (5*xxx*). While some of the 4*xxx* series alloys can be hardened by heat treatment, other aluminium alloys can be hardened only by cold working method.

2.1.1.2 Wrought heat-treatable alloys

Wrought heat-treatable alloys can be precipitation-hardened to develop reasonably high strength values (Robinson et al. 2014; Russo et al. 1970). These alloys include the 2*xxx* series (Al-Cu and Al-Cu-Mg), the 6*xxx* series (Al-Mg-Si), the 7*xxx* series (Al-Zn-Mg and Al-Zn-Mg-Cu), and the aluminium-lithium alloys of the 8*xxx* alloy series. The 2*xxx* and 7*xxx* alloys, which develop the highest levels of strength, are the main alloys utilized in construction of metallic aircraft structures.

2.1.1.3 Casting alloys

Casting alloys consist of both heat-treatable and non-heat-treatable alloys. The most important series consist of the 2*xx.x* series (Al-Cu), the 3*xx.x* series (Al-Si + Cu or Mg), the 4*xx.x* series (Al-Si), the 5*xx.x* series (Al-Mg), the 7*xx.x* series (Al-Zn), and the 8*xx.x* series (Al-Sn). The 2*xx.x*, 3*xx.x*, 7*xx.x*, and 8*xx.x* alloys can be strengthened by precipitation-hardening, but the properties obtained are not as good as those obtained for the wrought heat-treatable alloys (Enright 1987; Vasudevan and Doherty 1989).
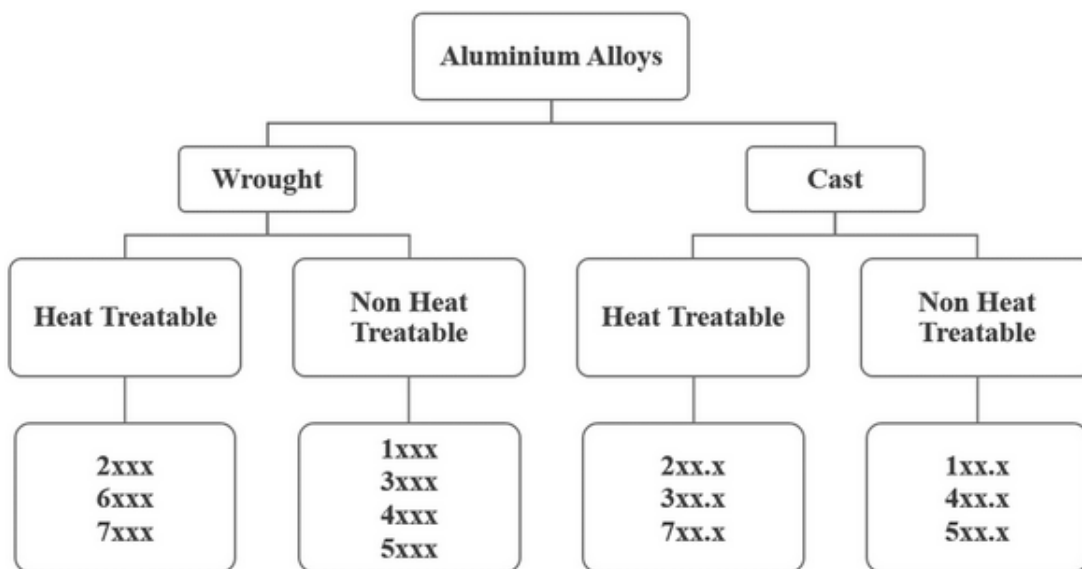
Figure 2.1 Classification of aluminium alloy (Courtesy: Davis J.R. 2001)
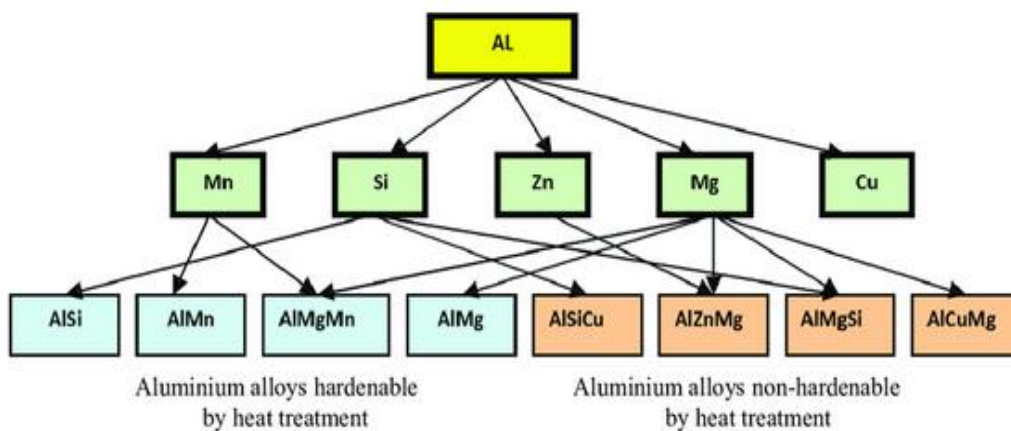
Figure 2.2 Aluminium alloy ingredients and combinations (Courtesy: Davis J.R. 2001)

2.1.2 Melting and Fabrication of Aluminium Alloys

2.1.2.1 Fabrication of Aluminium alloys (General)

An aluminium alloy is a composition consisting mainly of aluminium to which other elements have been added. The alloy is made by mixing the elements when aluminium is in molten state (liquid), which cools to form a homogeneous solid solution. The other elements may make up as much as 15 percent of the alloy by mass (ASM International 1993b; Davis 2001)

2.1.2.2 Fabrication of Cerium based Aluminium alloys

Al-Ce alloys were cast in binary composition of 6 - 16 wt. % Ce. The pure aluminium bars were liquefied and kept at approximately 785º C. Also, the ternary and quaternary alloys with small percentages of Si and Mg were prepared. Cerium was added last in the case of the binary and ternary alloys, and molten alloy was allowed to reach the above temperature. The quaternary alloy was transferred from the remaining heel of the alloy beneath. While adding cerium, an extremely quick exothermic reaction was concluded with the molten mass temperature increasing almost 25º C in a duration of 5 minutes. The temperature rise was attributed to the strong associative interaction among the Al and Ce atoms ensuing in a high enthalpy of mixing that is traditionally accompanied with the development of intermetallic compounds during the process of solidification (Sims et al. 2016). The casting was transferred into polymer coated sand molds at 785º C. From the already formed ternary alloy, the quaternary alloy was prepared.

Mg is commonly used as a strengthening additive in aluminium alloys (Davis 2001; Kaufman and Rooy 2014). Hence, it is chosen as a ternary additive to the Al-Ce system. The ease of casting was not reduced on addition of a small weight % of Mg. Mg will not influence the thermodynamics or phase composition of the Al-Ce binary system significantly, instead, it reinforces the matrix phase by creating intermetallic Al-Mg precipitates and metastable groups. Intermetallic precipitates are helpful for increasing

the strength of the ductile aluminium matrix without influencing the already present $Al_{11}Ce_3$.

Silicon has two outcomes if added to traditional aluminium alloys: Silicon helps the alloy to enhance the ease of casting, and silicon, when combined with Mg, usually precipitates a Mg_2Si strengthening phase (Chakrabarti and Laughlin 2004) . Silicon significantly hinders the castability of the Al-Ce-X system. However, in the case of Al-Ce-X alloys, high silicon percentage reduces the castability in comparison with the standard silicon aluminium outcomes.

The binary Al-Ce shows excellent castability. This excellent castability is attributed to a combination of improved fluidity of the melt and the near isothermal solidification of the Al-Ce alloy. The fluidity of the melt is predominantly depends on the enthalpy of formation (Flemings et al. 1961). Development of the Al-Ce intermetallic phases is strongly exothermic. The exothermic reaction noticed after the addition of Ce to the melt could then be attributed to the surge in fluidity of the melt and, thus, to enhanced castability.

Post casting process, the test rods were subjected to heat-treatment to assess the efficacy of heat-treatment on mechanical properties. The schedule used for heat treatment was a standard T6 schedule. Test rods were heated to 537º C and kept at that temperature for 8 hours. After the completion of this solutionising step, the test rods were quenched in water and aged artificially for 3 hours at 155º C. The quaternary alloy Al-Ce-Si-Mg has a much more standard response to a T6 heat-treatment when compared to the binary or ternary alloy. They have improved tensile and yield strengths, but inferior ductility than the binary or ternary alloys. The transition of phase that happens while heat-treating seems to be the cause for the improvement in mechanical properties.

For high-temperature applications, Al-Ce alloys have the best replacement possibilities for heavier steel and cast-irons. Al-Ce alloys could be casted over a wide range of cerium percentages, which are compatible with the modern casting practices, and hence require little or no change in the existing foundry infrastructure. Mechanical properties such as tensile strength as high as 252 N/mm^2 and yield strength as 128 N/mm^2. High-

temperature mechanical properties combined with the good thermodynamic properties and physical stability post heat-treatment recommend that Al-Ce-X alloys hold tremendous potential for high-temperature applications. Variation in composition is possible within the Al-Ce-X alloy family; both the Si and Mg have the possibility to be alloyed with Al-Ce to produce an easily modifiable microstructure and mechanical properties. The impairment of silicon on castability is negative, but it is hypothesized that by reducing the silicon percentage, a good castability can be provided, while keeping the room temperature strength of the Al-Ce-Si-Mg alloy same (Sims et al. 2016).

2.1.3 Heat treatment

Aluminium alloys are normally annealed to make them soft to enhance their ductility, and the heat-treatable aluminium alloys are precipitation-hardened to strengthen them (Field and Moran 1985).

Annealing is a method to increase ductility, while reducing the strength and hardness. Annealing could be used for both the heat-treatable and non-heat-treatable grades of cast and wrought aluminium alloys (Campbell 2006). The annealing operations are carried out during complex cold forming processes to permit further forming without the risk of sheet cracking. The most formable, most ductile, and softest condition for aluminium alloys is formed by complete annealing to the 'O' condition (soft annealed condition). When cold-worked aluminium alloys are heated to an adequately high temperature for a reasonably extended time. Annealing will happen in three stages: recovery, recrystallization, and grain development (Jazaeri and Humphreys 2004; Miodownik 2002). The internal stresses produced because of cold working are reduced during recovery, with considerable strength loss and a recovery of ductility to some extent. During the process of recrystallization, new unstrained nuclei generate and develop until they collide with each other to generate a new recrystallized crystallite element structure. Heating for prolonged duration and at elevated temperatures will typically result in grain development, which is generally not desirable (Campbell 2006).

In an alloy, to take a substantial amount of an alloying element into solid solution, it is heated to an elevated temperature, in precipitation-hardening (ASM International

1993b; Campbell 2006). It is then quickly cooled (quenched) to room temperature, trapping the alloying elements in solution. On heating the alloy to an intermediate temperature again, the base metal discards the alloying element in the form of a very fine precipitate, which is only a few angstroms in diameter (1 Å = 10^{-9} m). The fine precipitate produces matrix strains in the lattice that behave as hurdles to the movement of dislocations and offer opposition to slip, and thereby improving the strength and hardness. Precipitation hardening comprises of the following three steps:

- Solution heat treating
- Fast quenching to low temperature
- Ageing

During the process of solution heat treating, the alloy is raised to such a high temperature that the added heat is sufficient to place the soluble alloying elements in solution. After holding for long enough time at the solution treating temperature for diffusion of the solute atoms into the solvent matrix to happen, the alloy is quenched at a low temperature (e.g., room temperature) to retain the alloying elements trapped in solution. The alloying elements which are trapped in solution form a uniform distribution of very fine particles by precipitation during aging. At room temperature, after a few days, some aluminium alloys will harden (The method is termed as natural aging), while some other alloys are hardened by artificial means, by heating to an intermediate temperature (artificial aging). The condition of the alloy is designated as the T4, if it is aged at room temperature (solution heat treated and naturally aged), and its condition is designated as T6, if it is aged by heating to an intermediate temperature again (solution heat treated and artificially aged). The cold working heat treating, will improve the properties of certain alloys and this condition of the alloy is termed as the T3 condition (solution heat treated, cold worked, and then naturally aged), as T8 condition (solution heat treated, cold worked, and then artificially aged), and as T9 condition (solution heat treated, artificially aged, and then cold worked). In T7 condition (solution heat treated and over aged) the alloy is deliberately aged beyond its highest strength by aging at an elevated temperature, and this condition is utilized with

some high-strength alloys for improvement of fracture toughness and its resistance to corrosion (Hirsch 2014; Rometsch et al. 2014).

2.2   WELDING OF ALUMINIUM ALLOYS

The most widely used joining methods for aluminium alloys are Tungsten Inert Gas (TIG), Metal Inert Gas (MIG), Variable Polarity Plasma Arc (VPPA) and Electron Beam (EB) welding and friction stir welding (FSW) (Hirsch 2014; Malarvizhi and Balasubramanian 2011; Mathers 2002; Mishra and Ma 2005; Wan and Huang 2018; Woodward et al. 2000) These processes allow us to obtain optimum mechanical properties with minimum distortion due to the high heat intensities provided by these sources. However, the high conductivity, high reflectivity, high reactivity, and high coefficient of thermal expansion make welding of aluminium alloys difficult. The high heat input associated with high thermal conductivity and high coefficient of expansion could lead to severe distortion of parts during welding. Careful control of welding parameters is a must to get a sound weld in aluminium alloys.

Many techniques have been proposed to join aluminium alloys (Çam and Mistikoglu 2014). Figure 2.3 represents the classification of welding method used to join the aluminium alloys. In solid state welding process, the joining temperature is less than the melting temperature of the base material. Thus defects related to solidification are completely eliminated (Olabode et al. 2013).

The successful application of FSW in joining of aluminium alloy as compared to other welding techniques, made the researchers to think about use of FSW method for joining aluminium alloys. Since few years, the method of friction stir welding (FSW) has emerged as a preferred solid state welding method to join aluminium alloys (Balasubramanian et al. 2009; R. Nandan et al. 2008). Recently, friction stir processing (FSP) was developed for micro-structural modification of metallic materials (Ma 2008; Mehdi and Mishra 2016; Zhang et al. 2012). In the present review article, the contemporary state of development and understanding of the FSW and FSP are addressed. Specific stress has been laid on mechanisms responsible for the creation of welds and development of micro-structural refinement, and influences of FSW/FSP

parameters on final resulting microstructure and mechanical properties (Balasubramanian and Lakshminarayanan 2008; Mishra and Mahoney 2007).
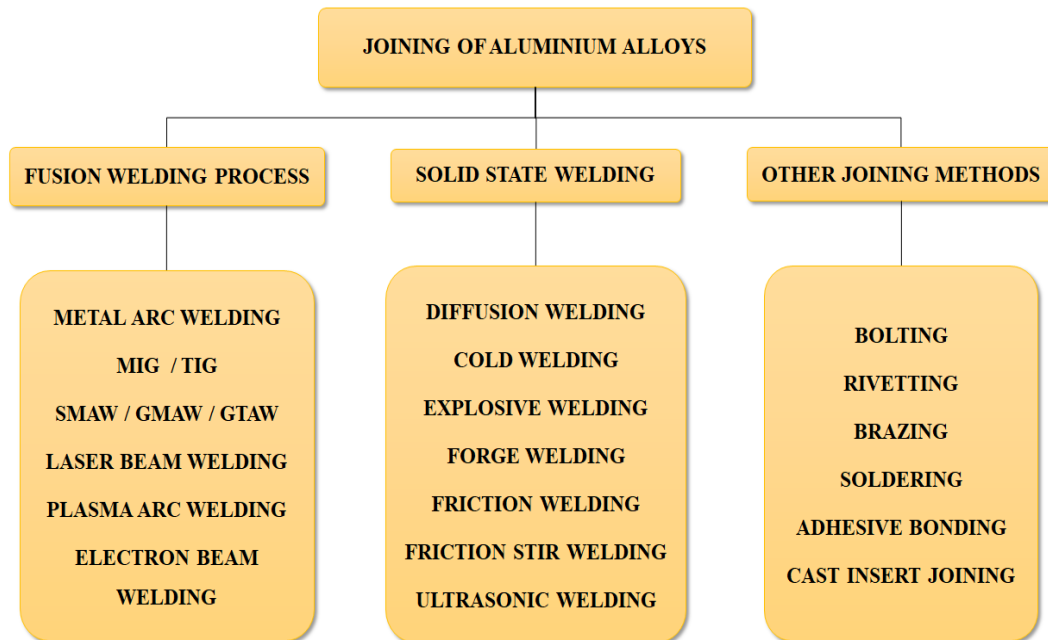
Figure 2.3 Classification of welding processes of aluminium alloys

Yamamoto et al. (1992) in his research publication discusses about the possibility of welding of aluminium alloys by MIG welding technique. In the beginning, aluminium due to the difficulty of non-availability of a suitable welding method, was used in limited fields. The developments of new welding processes such as tungsten inert gas (TIG) and metal inert gas (MIG) widened the scope of welding of some of aluminium alloys (Barnes and Pashby 2000; Mathers 2002). The main limitation of these techniques is the formation of porosities and hot cracking, due to both the ingress of the oxygen and the effect of excessive strain at the welding joint, which resulted from the melting and solidification sequences (Barnes and Pashby 2000; Ilyushenko and Nesterenkov 2006; Mathers 2002; Mukhopadhyay et al. 2006; Roberge 1999; Thomas et al. 2001; Threadgilll et al. 2009).

The micro-structure of the weldment is modified compared to parent alloy. That also leads to changes in the mechanical properties. Welding method needs to be controlled

to get optimum properties (Wang et al. 2006). Wrought aluminium alloys such as AA1xxx, AA3xxx, AA5xxx, AA6xxx and AA7xxx copper free alloys, are joined easily by fusion welding process. AA5xxx alloys offer superior welding properties than rest of the alloys. AA2xxx and high strength AA7xxx alloys are difficult to join with fusion welding process (Roberge 1999). An arc welding process called Tungsten inert gas (TIG) is used for welding of aluminium and its alloys. In TIG welding method a non-consumable tungsten rod is utilized as a welding electrode. To prevent alloy oxidation if any, an inert gas like argon is supplied around the electrode to act as a shielding gas. A fast arc welding method known as Metal inert gas (MIG) that uses a continuously fed wire of metal as an electrode and filler metal. An inert gas, like argon or helium is supplied into the welding pool to prevent oxidation of the workpieces which are being welded. MIG process is utilized for welding of bodies of cars, storage tanks and big structures (Barnes and Pashby 2000; Polmear 2005; Wagner et al. 2015). Resistance welding is made by heating the surfaces to be joined by flow of an electric current coupled with an application of pressure. The produced heat melts the mating surfaces and subsequently accomplishes the joining of the parts. Resistance welding finds applications in the aerospace industry. Another method of welding called Laser beam welding is carried out by a beam laser focused at the joint of the workpieces being welded. A molten metal pool which is in dynamic equilibrium with the metal vapor is produced. The commonly used lasers for welding are CO_2 and neodymium yttrium-aluminium garnet (Nd-YAG). Compared to other arc welding processes, the Laser welding method is characterized by reduced thermal distortion, higher process speed and better weld joint characteristics. In addition to these advantages, the laser welding possesses many disadvantages, like inadequate penetration depth, hot cracking, process risks and huge cost. The depth of penetration depends on the supplied power and it varies from 2 to 6 mm. The maximum depth of penetration obtained with CO_2 lasers is 6 mm. Laser welding finds its applications in automotive industry. A method of welding called Electron Beam Welding (EBW) is carried out with the production of a beam of high energy density electrons inside a vacuum chamber. The cost of this process is comparatively high, and it is best suited for welding of close square weld joint in a single pass for thin parts, like foils (Ilyushenko and Nesterenkov 2006; Mathers 2002; Wagner et al. 2015). A process called Fine plasma arc welding is

adopted with a high voltage current is subjected to an ionized gas. Plasma arc welding is comparatively of higher cost and finds its applications in welding method called spot welding. The problems combined with the laser welding are also associated with plasma welding. The weld connection integrity is comparatively higher (Barnes and Pashby 2000). The method of solid-state welding is probably the oldest technique of welding for joining variety of workpieces, for example using a hammer to join two workpieces. This procedure is carried out for wide array of temperatures and pressures (Younes 2010). Solid-state welding is best suited for welding of the aluminium alloys such as AA2xxx and AA7xxx, which are impossible to weld using the method of fusion welding (Polmear 2005; Younes 2010).

Malarvizhi et al. (2011), for welding aluminium alloy AA2219, with square butt joints and with no addition of any filler material, employed friction stir welding (FSW), electron beam welding (EBW), and gas tungsten arc welding (GTAW) processes. For the welded joints, the tensile properties in the transverse directions were assessed. It was seen that the FSW joints with post-weld aging showed improved fatigue properties in comparison to GTAW and EBW joints. This is mostly due to the development of dynamically recrystallized, very fine grains and even dispersal of fine precipitates in the weld zone.

Squillace et al. (2004) conducted experiments on AA2024-T3 aluminium alloy butt joints to compare tungsten inert gas (TIG) method and friction stir welding (FSW). They showed that, in TIG joints, there is drop in mechanical properties, primarily due to the material experiencing high temperatures. In the case of a FSW joint, due to lesser temperatures incurred and extreme plastic deformations induced by the tool movement, a small decline in mechanical properties is observed in the nugget region, and thermo-mechanically affected zone (TMAZ), whereas, in the heat affected zone (HAZ), because of lower temperature of melting, a slight enhancement of above properties is observed. In nugget region, however, a slight regaining in hardness, with respect to the TMAZ region, is recorded, because of the recrystallisation of very fine structure of grains.

Maggiolino and Schmid (2008) conducted a comparative study among the corrosion resistance of AA6082-T6 and AA6060-T5 weld joint surfaces produced using metal

inert gas (MIG) and friction stir welding (FSW) techniques. The morphological analysis of the surface was used to find the corrosion resistance of the joint surfaces. From the results it was clear that the weld joint surfaces obtained using FSW had greater corrosion resistance than that obtained using MIG welding technique.

The effect of welding processes (FSW and TIG) on the fatigue properties of 5052 aluminium-welded joints was reported by Wang et al. (2008). The results show that the fatigue properties of FSW welded joints are better than those of TIG welded joints.

The comparative studies held by Muñoz et al. (2008) of microstructure and mechanical characteristics of solid-state welds (FSW) and fusion welds (TIG) on heat-treatable aluminium alloy Al–4.5Mg–0.26Sc indicated that the effect of TIG welding process is comparatively more than the FSW process on hardening of the precipitates. These outcomes result in a considerable reduction in mechanical properties of TIG weld joints and a post-weld heat treatment helps in partial recovery of these properties.

Zhao et al. (2010) carried out a comparison study on the influences of TIG welding and FSW processes on metallurgical and mechanical properties of joints of Al–Mg–Sc alloy plates. The studies showed that the mechanical properties of FSW connection are much better than those of TIG welded joint. Moreover, tensile stress and yield stress of FSW weld connection are 19% and 31% higher than those of TIG joint, respectively. Due to the low welding temperature during FSW method and the excellent thermal stability of Al_3 (Sc, Zr) particles, the cold working micro-structures can be well preserved.

He et al. (2011) conducted a study on comparisons of the metallurgical and mechanical properties of Al-Mg-Mn-Sc-Zr alloy weld joints produced by TIG and FSW welding processes. The strength of FSW and TIG welded joints decreased as compared to the base metal but strength of FSW welded joints higher than the TIG welded joints. The loss of substructure strengthening and a very little loss of precipitation strengthening of Al_3(Sc, Zr) cause the decreased strength of FSW welded joint. But for the TIG welded joint, the disappearance of both the strain hardening and most precipitation strengthening effect of Al_3(Sc, Zr) particles contributed to its softening. At the same time, the grains in weld nugget zone of FSW welded joints were finer than those in the molten region of TIG welded joints.

23

The experiments carried out by Anjaneya and Prasanna (2013), on AA6061 joints welded by MIG and FSW showed that FSW produced 10-100 times smaller grains in the micro-structure than the MIG welding. MIG welding produced the less tensile stress than FSW. The amount of heat input affected the weld material hardness and the width of hardness was determined by shoulder diameter and heat input. The FSW reduced production cost, pre operations and increased the weld quality.

The evaluation studies done by Jannet et al. (2014) explained the mechanical properties of welded joints of 6061-T6 and 5083-O aluminium alloy obtained using friction stir welding (FSW) and conventional fusion welding. Better tensile stress was obtained with FSW welded joints. The width of the Heat affected zone of FSW was narrower than Fusion welded joints.

A research study on comparison of Direct current straight polarity (DCSP) TIG welding and friction stir welding (FSW) of aluminium alloy AA2219 by Sasidharan et al. (2017) revealed that the Ultimate Tensile stress (UTS) of DCSP TIG welded weld connection and the UTS for FSW weld connection were at 58.5% and 65.4% respectively, compared to the parent metal. Percentage elongation for FSW weld connection has also been found to be more than that of parent metal. From the micro-structure study, it is seen that FSW joints are having fewer micro porosities compared to DCSP TIG welded joints.

The tests performed by Kumar et al. (2014) for TIG, MIG and FSW welding of aluminium alloy AA6061 revealed that the heat input in case of FSW is less than that of TIG and MIG welding processes. FSW weld connection efficiency was 19.4% higher as compared to TIG welded joints and 35.5% higher as compared to MIG welded joints.

2.2.1 Prospective issues in joining of Aluminium alloys

Aluminium alloys are prepared by mixing of aluminium with various alloying elements and melting them together to get the required alloy. Aluminium and its alloys are used in fabrications because of their low weight, good corrosion resistance and weldability. Although, normally most of the aluminium alloys have low strength, some of the alloys with more complex alloying compositions can have superior mechanical properties

equivalent to those of steels. The various types of aluminium alloys can be used for fabricating various components without impairing corrosion and mechanical properties of the material or introducing imperfections into the weld. A number of issues are faced by the user while joining and fabrication of aluminium alloys (Çam and İpekoğlu 2017; Mathers 2002). The defects commonly occurring during welding of aluminium alloys by FSW are shown in Figure 2.4 (Podržaj et al. 2015; Qian et al. 2013).
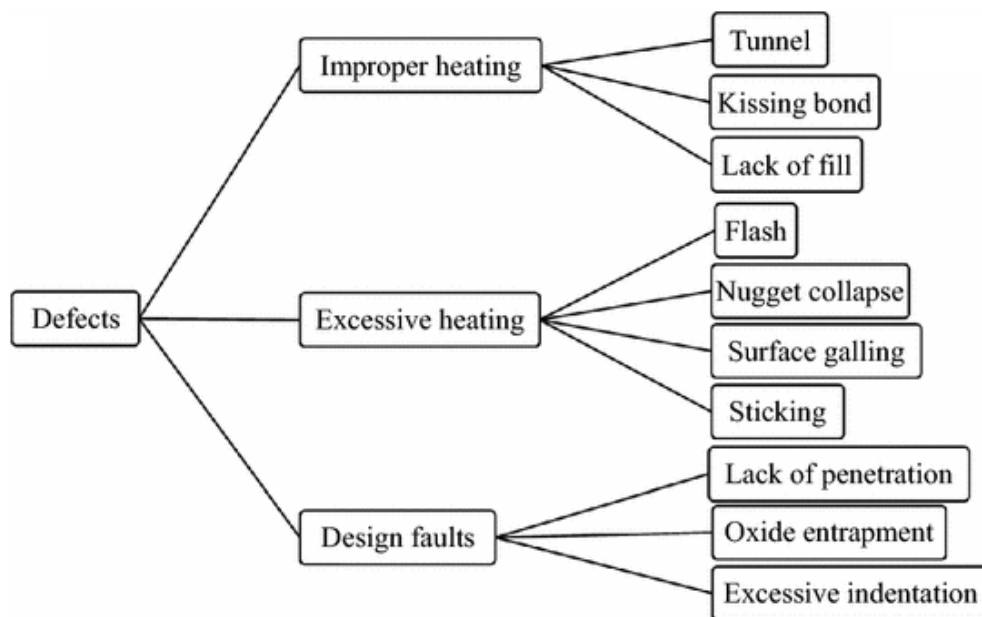
Figure 2.4 Defects in friction stir welded aluminium alloy joints (Courtesy: Podržaj et al. 2015)

2.2.1.1 Gas porosity

Gas Porosity in aluminium weld joints can be of two types.

a) Hydrogen induced porosity and

b) Inter-dendritic shrinkage porosity and both are caused by entirely different factors.

Former one is caused by the presence of hydrogen in the weld owing to unfavorable welding conditions such as improper cleaning, moisture in electrode, shielding gases and oxide layer, presence of hydrocarbons in the form of oil, paint, grease etc. The presence of hydrogen porosity in the weld metal mainly occurs due to high difference in solubility of hydrogen in liquid and solid state of aluminium alloy. During

solidification of the weld metal, the excess hydrogen is rejected at the advancing solid-liquid interface in the weld which in turn leads to the development of hydrogen induced porosity especially under high solidification rate conditions as high cooling rate experienced by the weld pool increases tendency of entrapment of hydrogen (ASM International 1993a; Cramer and Covino 2003). Excessive hydrogen porosity can severely reduce strength, ductility and fatigue resistance of aluminium welds due to two reasons a) reduction in effective load resisting cross-sectional area of the weld joints and b) loss of metallic continuity owing to the presence of gas pockets which in turn increases the stress concentration at the weld pores. It also reduces the life of aluminium welds. Therefore, to control hydrogen induced porosity in aluminium, the following approaches can be used (Çam and Ventzke 2000; Canaby et al. 1991; Rongshi et al. 2007).

    i.   Proper cleaning of surfaces, baking of the electrodes to drive off moisture and

    ii.   Removing the impurities from weld surface

    iii.   Addition of Freon to the shielding gas,

    iv.   Churning the weld pool during weld solidification using suitable electro-magnetic fields. Inter-dendritic porosity in weld mainly occurs due to poor fluidity of molten weld metal and rapid solidification. Preheating of plates and increasing heat input (using high current and low welding speed) help in reducing the inter-dendritic porosity.

2.2.1.2   Inclusion

In general, presence of any foreign constituent (one which is not desired) in the weld can be considered as inclusion and these may be in the form of gases, thin films and solid particles. High affinity of aluminium with atmospheric gases increases the tendency of formation of oxides and nitrides (Taylor 1996) (having density similar to that of aluminium) especially when;

    i.   Protection of weld pool is not enough,

    ii.   Proper cleaning of filler and base metal has not been done,

iii. Shielding gases are not pure enough and therefore making oxygen and hydrogen available to molten weld pool during welding,

iv. Gases are present in dissolved state in aluminium itself and tungsten inclusion while using GTA welding.

Mostly, inclusion of oxides and nitrides of aluminium are found in weld joints in case of un-favourable welding conditions. Presence of these inclusions disrupts the metallic continuity in the weld. Therefore, these inclusions provide site for stress concentration and become a source of weakness leading to the deterioration in mechanical and corrosion performance of the weld joints (Broek 1973; Jaradeh and Carlberg 2007; Sabatino et al. 2005). Ductility, notch toughness and fatigue resistance of the weld joints are very adversely affected by the presence of the inclusion. To reduce the formation of inclusion in weld it is important to give proper attention to.

i. Avoid sources of atmospheric gases,

ii. Developing proper welding procedure specification (selection of proper electrode, welding parameters, shielding gases and manipulation of during welding), and

iii. Manipulation of GTAW torch properly so as to avoid the formation of tungsten inclusion.

2.2.1.3   Oxide inclusions and oxide filming

A clean, smooth and protected surface is important in pre-weld aluminium structures to ensure good aluminium weldments except in high energy density welding processes like hybrid laser beam welding (LBW) (using pulsed metal inert gas (MIG)) (Mathers 2002). Oxide formation in aluminium occurs due to the strong chemical affinity of aluminium for oxygen on exposure to air. The aluminium oxide thickness increases as a result of thermal treatment, moist storage conditions and electrochemical treatment (anodizing) (Campbell 2006; Cotell et al. 1994; Sulka and Stepniowski 2009; Zaraska et al. 2010). Aluminium alloys melt at about 660°C. Therefore, the layer must be removed by pickling or dry machining just before weld.

2.2.1.4   Solidification (hot) cracking or hot tearing

In aluminium alloys cracking of weld is another major reason of concern due to its comparatively higher thermal expansion, huge variation in volume on solidification, and wide range of temperature of solidification. The weld crack sensitivity of heat-treatable aluminium alloys is mainly a reason for concern, because of additions of higher amounts of alloying elements in these alloys (Taylor 1996). The weldability of aluminium alloys could be defined as the resistance it offers to cracking of weld due to the catastrophic effect of these cracks in the weld on properties of the weld joint. In aluminium alloys, the weld cracking could be divided into two main categories depending on the crack position and, mechanism responsible for cracking, that is, solidification cracking and liquation cracking (Çam and İpekoğlu 2017).

The solidification type of cracking occurs inside the fusion region and usually appears at the midpoint of the weld or at the termination craters while the liquation cracking occurs next to the fusion region and may or may not be visible easily. Hot tearing, or solidification cracking is noticed during solidification shrinkage occurring due to high levels of thermal stress, when the weld pool undergoes different stages of solidification (Coniglio et al. 2008; Warrington and Mccartney 1989). The hot tearing sensitivity of any given aluminium alloy is influenced by a combination of metallurgical, thermal, and mechanical, factors (ASM International 1993a). The type of restraint of welded assemblies plays an important part in crack sensitivity by accumulating the stress on the solidifying weld. Hot tearing arises inside the weld fusion region and is influenced by the parameters of welding process and composition of weld metal. High heat input causes such as slow speeds of welding, and high weld currents and are assumed to be contributing to solidification cracking of the weld. Moreover, it may also happen in low-heat input welding procedures, such as laser beam welding provided the heat input is satisfactorily high. Similarly, concave fillet weld bead profile results higher solidification cracking tendency than those of convex weld bead profile. In the same lines, other related materials characteristics of base metal such as increase in thickness of plate, high thermal expansion of coefficient and wider solidification temperature in general increase the residual stresses and so also the solidification cracking tendency. Apart from the residual tensile stresses, strength and ductility of weld metal in terminal

28

stage of solidification also predominantly determine the solidification cracking tendency (Kah et al. 2015; Sheikhi et al. 2009; Xiao and Zhang 2014).

2.2.1.5 Liquation cracking

In the liquation type of cracking, an important element of the HAZ for precipitation hardenable alloys is the thin boundary layer adjacent to the fusion region that is referred to as the partially melted region. This region forms when eutectic phases or constituents that have low melting points (melting points below the melting point of the bulk material) liquate, or melt, at grain boundaries during welding. It occurs in precipitation harden able alloys because of the relatively large amount of alloying additions available to form eutectic phases. During welding, these phases liquate and if sufficient stress is present, may be accompanied by tears. Under extreme conditions, continuous cracks may form along the fusion region interface. As expected, higher heat input widens the partially melted region and makes it more prone to cracking (Çam and Mistikoglu 2014). composition of the filler alloy is highly important in deciding whether the cracks form in this liquated region or not (Gittos and Scott 1981). Filler alloys that have low solidification temperatures provide less susceptibility to liquation cracks, since the solidification shrinkage strains occur at lower temperatures (Katoh and Kerr 1987).

2.2.1.6 Reduced strength in the weld and HAZ

HAZ is formed next to the fusion region which results in degradation of properties of the base metal in joining, especially during fusion welding. The degradation in properties is caused by modifications in microstructure, associated with high temperatures felt in this region. In the case of heat-treatable aluminium alloys, the HAZ is characterized by dissolution and growth of precipitates. In 2xxx series of aluminium alloys, the dissolution takes place in the HAZ region, whereas for 6xxx series alloys the primary modification is the growth of precipitates (Enjo and Kuroda 1982). This problem is more noticeable, that is, the degree of coarsening of precipitates is higher and width of the HAZ region created is bigger, if the input heat provided in the welding process is larger, for example as in the case of arc welding. Even though the type of these HAZs vary, they are all thermally dependent and diffusion controlled (Kou 1987).

29

Measuring the hardness across the HAZ region is one of the methods to estimate the width and range of the HAZ. The welding method and process parameters which determine the degree of base metal degradation for the metallurgical changes of the HAZ of alloys of aluminium are dependent thermally. Preheating and High input of heat intensifies both the width and extent of the HAZ. This is particularly valid for the precipitation harden-able aluminium alloys.

2.2.1.7   Lack of fusion

Shielding gas protects the molten weld pool from the atmosphere, which is important because aluminium has a tendency to react with atmospheric air to form oxide and nitrides (Mathers 2002). The shielding gases commonly used in welding aluminium and its alloys are inert gases such as argon and helium. Argon is used as a shielding gas for manual and automatic welding. Argon is cheaper than helium, and the use of argon produces a more stable arc and smoother welds. However, argon gives lower heat input and lower attainable welding speed, and therefore there is the possibility of a lack of fusion and porosity in thick sections. In addition, use of argon can result in a black sooty deposit on weld surfaces, although this can be wire brushed away. It has been observed that with helium shielding gas, the arc voltage is increased by 20%, resulting in a higher, hotter arc, deeper penetration, and wider weld beads. This implies that the criticality of arc positioning (aids avoidance of missed edge and insufficient penetration defects) is lower with helium. There is a reduction in the level of porosity and lack of fusion when helium shielding gas is used because the weld pool is hotter and there is slower cooling, which allows hydrogen to diffuse from the weld pool.

2.2.1.8   Reduced corrosion resistance

Aluminium alloys are corrosion resistant in atmosphere, but often have poor corrosion resistance when submerged in aqueous environments. Aluminium corrosion resistance is also often only high in a restricted range of pH value. Aluminium corrosion rates are very low when the chemical stream pH value is between approximately 4 and 7, but the corrosion rates are very high when the pH value is either below 4 or above 7 (Tait 2005). The corrosion behavior of aluminium and its alloys is intimately connected with the behavior of the surface oxide film, which effectively passivates the aluminium

surface under a variety of environmental conditions in the pH value range of 4–9. Any corrosion of aluminium in this pH value range may be of the pitting type, the most commonly encountered form of aluminium corrosion is when the of halide ions presence is observed, especially that of chloride ions (Li et al. 2009).

2.2.1.9 Reduced electrical resistance

Conductivity in metal is a measure of a material's ability to transmit heat, or electricity (or sound). The reciprocal of conductivity is resistance, or the ability to reduce the flow of those. Pure metals will tend to provide the best conductivity. In most metals, the existence of impurities restricts the flow of electrons. Compared to pure metals, then, elements which are added as alloying agents could be considered "impurities". So, alloys tend to offer less electrical conductivity than pure metal. If different properties provided by alloying are required (for additional hardness or strength, for example) it is important to choose the alloy additions that do not significantly affect conductivity if that is also important (Olsen n.d.)

2.3 CONCEPT OF FSW

FSW, for joining of aluminium alloys, is comparatively a new concept (Gibson et al. 2014; R. Nandan et al. 2008; Ulysse 2002). After solidification the metallurgical and mechanical properties of the weld region are altered. Also, the growing demand for light weight material ushered in the search for alternative way of joining aluminium alloys. Finally in the year 1991, "The Welding Institute", Cambridge (Lauro et al. 2011), developed a concept to join aluminium through solid state, named as friction stir welding (FSW). The concept is similar to milling method but instead of material being removed, the material is being joined. The method can be carried out on commercial FSW machine. A typical FSW machine is shown in Figure 2.5. This welding method is recognized to be energy efficient, environment friendly and versatile (Mishra and Ma 2005).

In conventional fusion welding techniques, the weld connection is formed by melting the base material with or without the addition of filler material. Whereas FSW requires a stable frictional heat generating element, constant movement of the workpiece, and

31

homogeneous deformation to consolidate the material (E. Taban 2013; Malarvizhi and Balasubramanian 2011).

Figure 2.5 FSW machine (Courtesy: ETA Technology Pvt. Ltd. India)

Figure **2.6** schematically illustrates the FSW process. A non-consumable tool consisting of shoulder and pin and made of harder material is used. The rotating tool is plunged into the butting surfaces until the shoulder makes contact with the workpiece surface and moves along the weld connection line, As the welding tool is plunged into the butt joint, the pin will help to produce frictional heat followed by plastic deformation of the metal, and the shoulder will help to produce heat as well as compaction of the material below it. The weld connection is formed due to the frictional heat as primary heat source and deformation heat under the influence of applied normal force as secondary heat source (Buffa et al. 2006; Doude et al. 2015).

The three primary functions of the tool are: 1) Produce sufficient heat in the workpiece by friction between the rotating tool (pin and shoulder) and the butted workpiece. 2) Impart proper movement of the plasticized material to form the joint. 3) Provide reservoir of hot metal beneath the tool shoulder. The localized heat produced by friction softens the material around the pin and combines with the tool rotation and translation,

which leads to the movement of the plasticized material from the leading side to the trailing side of the pin. Thus, softer plasticized material will fill the gap as the tool moves in forward direction. The tool shoulder will restrict the escaping of soft plasticized material flow up to a level equivalent to the shoulder position, i.e. approximately to the top surface of the workpiece. As a result, the thrust force is exerted by the revolving tool against the workpiece along the butt line, thereby compacting the softened deformed material underneath the tool shoulder. Due to this, solid-state weld connection is produced without melting.

The advancing side (AS) refers to the side where tool rotation velocity vectors and direction of welding tool movement are in same direction. In the case of Retreating side (RS), the tool rotation velocity vector, and direction of welding tool movement are in opposite direction. The process parameters are tool geometry, axial force, speed of tool rotation, traverse speed and tool tilt angle. The angle between the tool axis and normal to the surface of the workpiece is called tool tilt angle (Rodrigues et al. 2009; Seighalani et al. 2010; Su et al. 2003)
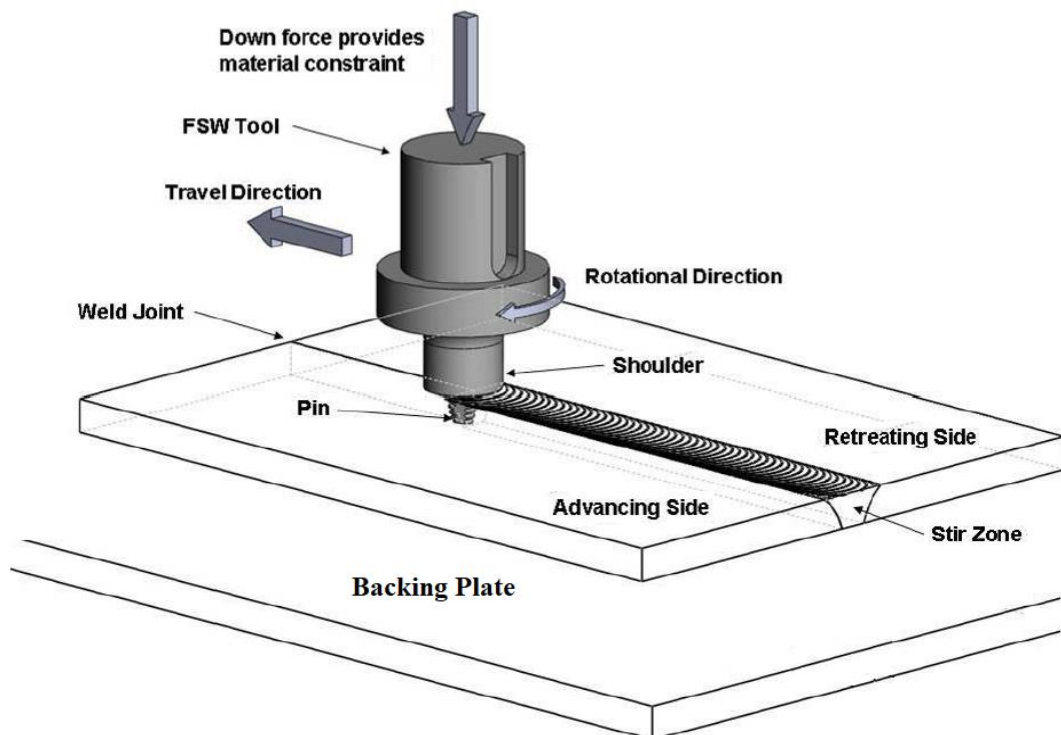
Figure 2.6 FSW terminology (Courtesy: Thompson and Thomas 2011)

The schematic diagram showed in Figure 2.7 (a to f) depicts the step by step procedure followed in FSW process. The initial stage is plunging of the tool as shown in Figure 2.7 (a). During this stage, the rotating tool at constant speed approaches the workpiece. The plunging depth depends on thickness of the workpiece and thrust force. Figure 2.7 (b) indicates the dwell time after the plunging operation, where velocity vector in each axis is zero. The next stage is welding, where the rotating tool is moved along the direction of the weld and other two axis velocity vectors remain zero as shown in the Figure 2.7 (c). Material flow is mainly dependent on two effects. First, is the extrusion method where the plasticized material is propelled by combined effect of axial force and movement of the tool pin. Second is the driving force, which is produced due to the rotation of the pin (Elangovan et al. 2008; Elangovan and Balasubramanian 2008; Shettigar and Manjaiah 2017). The details of material flow are being discussed in succeeding sections. Figure 2.7 (d) indicates the second dwell period after the rotating tool reached the final stage. The velocity vector in each axis is zero. The final stage of the welding method is shown in the Figure 2.7 (e) where the tool is retracted from the weld region. During this stage, the z-axis velocity vector is constant and the other two axis velocity vectors remain zero.
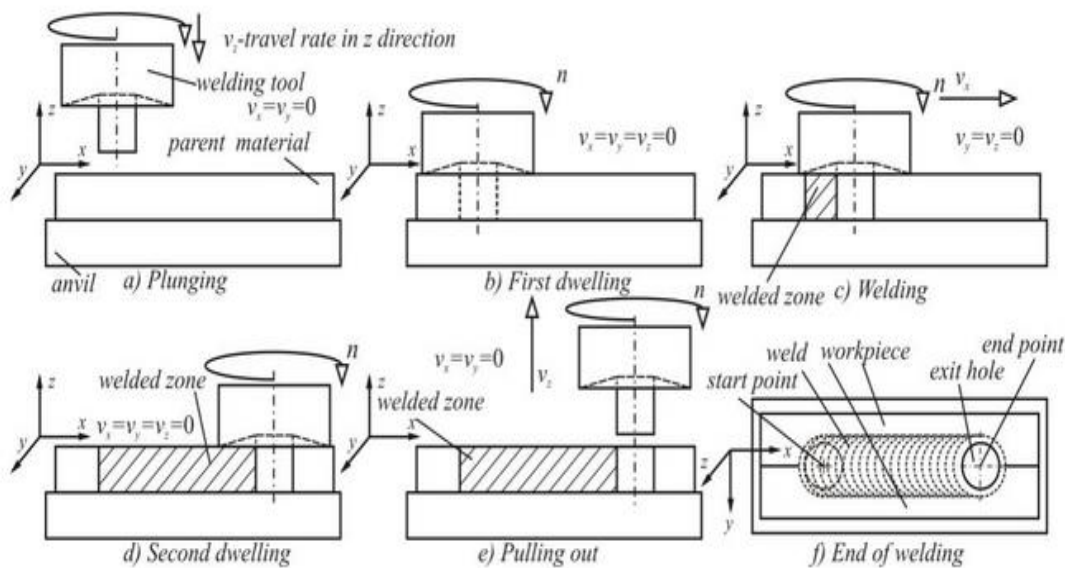
Figure 2.7 Stages in FSW method (Courtesy: Mijajlović and Milčić (2012)

2.4   MATERIAL SELECTION

In the present era of dependency on depleting fossil fuel energy sources, a great importance has been given to increase the fuel efficiency of the thermal engines used in diverse applications. To boost the efficiency of the engine, it is necessary to reduce the weight of the engine and have better performance characteristics even at elevated temperatures. Keeping this in mind, a lot of research has been aimed at producing special alloys which give desired results. One such material which can meet these requirements and which is of recent origin is aluminium cerium magnesium alloy (Sims et al. 2016). This alloy has been found to be able to retain its properties even at high temperatures. This alloy is durable, lightweight, easy to cast and the alloying element cerium is abundantly available and is relatively cheaper compared to other alloying elements.

A new alloy has been developed recently called Aluminium-Cerium Alloy which can withstand high temperatures and is placed as high temperature grade aluminium alloy. This is found to be suitable for general engine cylinder heads and aircraft engine cylinder heads with very long and thin fins as shown in Figure 2.8 (Sims et al. 2016) . Most of the alloys with exceptionally good properties are not easy to cast. But the aluminium-cerium alloy has casting properties equivalent to the 3000 series aluminium-silicon alloys. The alloying element used in aluminium-cerium is called Cerium, which is a rare earth element which is available easily. The addition of alloying element cerium forms an intermetallic which is stable up to $1093^{o}C$, which makes the alloy stable even at high operating temperatures like 300° C. In addition to the enhanced mechanical properties at elevated temperatures, the aluminium-cerium alloy has low density compared to pure aluminium. The density of the standard pure aluminium is 2.68 g/c.c., whereas Al-Ce-Si-Mg alloy is 2.49 g/c.c. Hence in a typical 20-pound automatic engine cylinder head there is a total aluminium mass reduction of 1.4 pounds, which is significant particularly for aircraft engines.
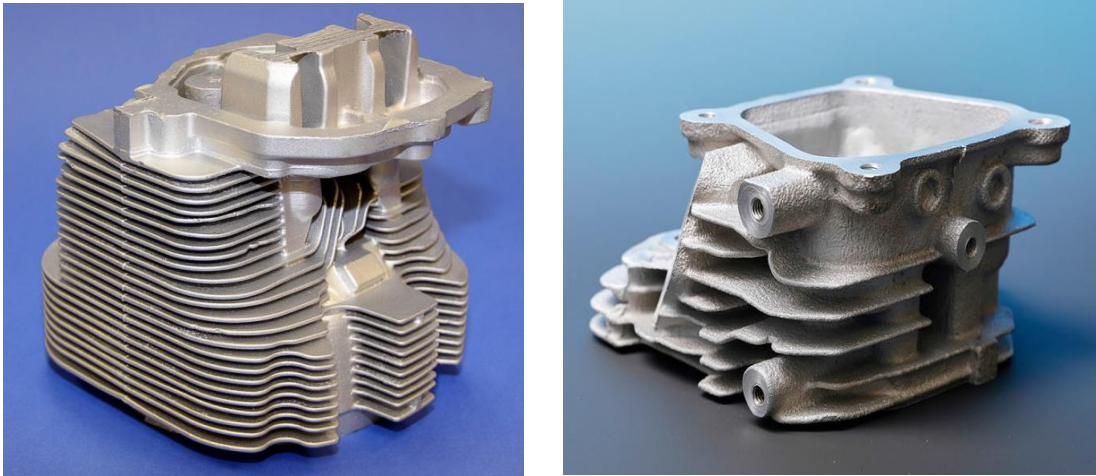
Figure 2.8 Engine blocks made using Al-Ce-Si-Mg alloy. (Courtesy: Sims et al. 2016).

Use of this new aluminium cerium magnesium alloy in engines has created a requirement for the method of joining these alloys. One such method is Friction stir welding or FSW which could be effectively used for joining aluminium alloys (Fukuda 2000; Jannet et al. 2014; Mehdi and Mishra 2016). This newly developed high-performance alloy i.e., Aluminium-Cerium-Silicon-Magnesium (Al-Ce-Si-Mg) alloy has been intended to be used for the Friction stir welding. The research work is aimed at studying the micro-structure of (Al-Ce-Si-Mg) alloy weld connection made using FSW with varying the different parameters used in the process.

A range of Al-Mg-Ce-Si alloys were available with varying percentages of each of the alloying elements with a wide range of properties. Since the alloys Al-10Mg-8Ce-3.5Si and Al-5Mg-8Ce-3.5Si had similar composition and percentage of only one the alloying elements varying, which made a better choice for comparison of properties of friction stir welded joints. In addition to that, both these alloys had excellent properties like, high temperature withstanding capacity, easy weldability, enhanced strength, lightweight, easily available, economical, and other properties. Based on these reasons the above alloys were chosen for these experiments.

2.5   MATERIAL FLOW PATTERN

Many mechanisms have been proposed to describe the material flow during FSW. It involves complex material movement and plastic deformation (Kumar and Kailas 2008; Leitão et al. 2012; da Silva et al. 2011). Material flow pattern is predominantly dependent on the welding parameters, tool geometry, and type of weld connection design. As soon as the rotating tool plunges into the base material, a cavity is formed in the base material. The shape of the cavity is dependent on the pin profile. There is a plasticized material formed around the pin and beneath the shoulder. This plasticized material is enclosed by the surrounding cooler base material and backing plate at the bottom. This arrangement along with tool rotational direction and tool movement decide the material flow path. During the tool movement the soft metal from the leading side is progressively plasticized and then moves to the trailing side through the retreating side b) two different modes: namely shoulder and pin driven flows.

Soft plasticized material flows through retreating side and the soft plasticized material gets deposited behind the tool forming the weld connection (Colegrove and Shercliff 2005; Colligan 1999; Fonda et al. 2004). Figure 2.9 represents the material flow pattern. Colligan (1999) made an effort to explain the material flow pattern in AA6061 and AA7075. Small steel balls known as tracer were embedded in to the previously made grooves which are parallel to the welding direction at different distances. Radiographic examination of the welded components revealed different material flow at different parts of the material. The thread profile in the pin helps in forcing the stirred material in downward direction. Remaining material in the weld region is extruded around retreating side of the pin and got deposited. Xu et al. 2001 stated that the flow pattern is not symmetric on advancing side and retreating side. The plasticized material flow, at the top surface, up to one third thickness of the weld region is governed by the tool shoulder rather than the thread of the pin (Guerra et al. 2003; Seidel and Reynolds 2001) Near the top surface of the weld, a considerable quantity of plasticized material moves from retreating side to the advancing side due to the shape of the tool. Hence, movement of the material causes vertical mixing in the weld and complex circulation of the material along the longitudinal axis of the weld.
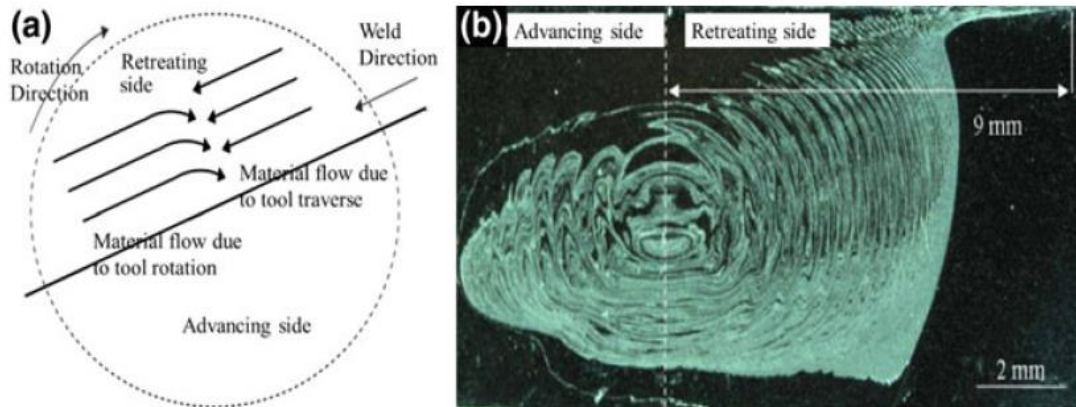
Figure 2.9 Schematic of metal flow pattern (Courtesy: Hamilton et al. 2008) (a) Top of the Nugget zone (b) Cross section of nugget region

2.5.1   Mechanism of Friction Stir Weld Formation

In the case of shoulder driven FSW, the material flows from the retreating side and gets deposited on advancing side of the base material with forging action induced by the tool. Whereas, in the case of pin drive, material flows layer by layer around the pin, due to the extrusion phenomenon and the layers continuously get stacked in the weld line. The shearing action of the tool shoulder and extrusion of the soft plasticized material around the pin cause layer by layer material transfer (Sinha et al. 2008). Once this pin driven material interacts with the shoulder driven material on the retreating side, the plasticized material gets transferred from the retreating side to the advancing side. There will not be any change in the structure details of layers in the pin driven material. Further increase of shoulder interaction results in merging of pin driven and shoulder driven material. The weld connection will be formed if the method develops sufficient temperature and hydrostatic pressure to transfer the shoulder driven and pin driven material to fill the weld cavity (Kumar and Kailas 2008). The material flow in the FSW method is summarized schematically in Figure 2.10.
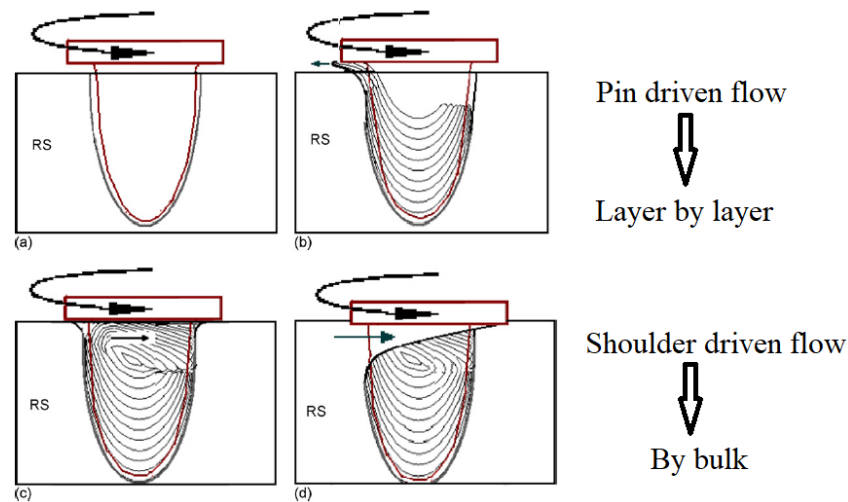
Figure 2.10 Material flow at different shoulder interaction in the transverse section of the weld (Y–Z plane) (a) Creation of weld cavity during plunging, (b) Cross-section of the layers in the pin-driven flow, (c) Merging of pin- and shoulder-driven material flow region and (d) Drawing of base material into weld nugget. (Courtesy: Kumar and Kailas 2008)

2.5.2   Role of FSW Tool in Material Flow

As reported by Hamilton et al. (2008) and Rajiv S. Mishra (2007), resemblance was found between the resultant micro-structure of hot worked aluminium extrusion and forging, with that of the features obtained through friction stir welding. Figure 2.11 (a-b) show the different mechanical processing zones formed during friction stir welding. Hence, modelling of FSW method can be treated as metal working which includes conventional metal working zones of preheat, initial deformation, extrusion, forging, and cool down (Kumar and Kailas 2008). Preheating region is ahead of the pin. The rise in the temperature at preheating region is due to frictional heat developed by rotating tool and deformation heat. The heat rate expansion of preheat region is dependent on the thermal properties of the workpiece material and rate at which welding method is carried out. Initial plastic region is formed as the tool moves in the forward direction (Gratecap et al. 2012). As a result, material is heated above the critical temperature and the amount of stress exceeds the critical flow stress of the material, resulting in material flow. The plasticized material in this region is forced to move upward in the shoulder region and downward in the extrusion region (Guerra et al.

2003). From the investigation done on the Friction stir welds of very thin plates of the AA6016-T4 aluminium alloy by Rodrigues et al. (2009), it was concluded that the differences in tool geometry and welding parameters induced significant changes in the material flow path during welding as well as in the micro-structure in the weld nugget.
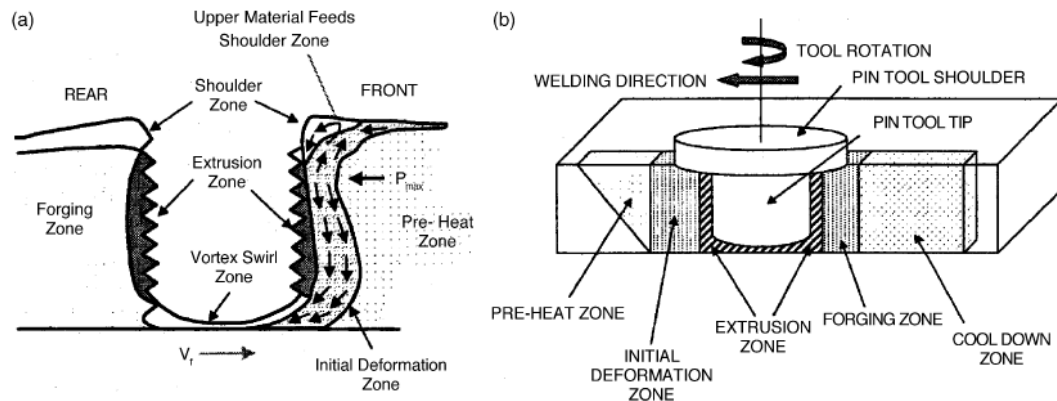
Figure 2.11 (a) Metal flow patterns and (b) Metallurgical processing zones developed during FSW (Courtesy: Mishra and Ma 2005)

Vertex swirl region is formed beneath the pin tip due to rotation of the pin. A small amount of material experiences the vertex flow pattern in this region (Mehta et al. 2013; Ouyang et al. 2006; Shettigar and Manjaiah 2017a). A finite amount of material moves around the pin from the leading side to the trailing side of the pin known as extrusion zone. The magnitude of temperature and stress is not enough to allow the material flow in this region and critical isotherm defines the width of the extrusion zone. Next to the extrusion region is the forging region where plasticized material is forced into cavity formed by forward movement of the tool under hydrostatic pressure condition. The shoulder of the tool assists in moving the material in cavity and also provides downward forging force. The softer material at shoulder region is forcefully dragged from the retreating side to the advancing side. At the final stage, the material gets cooled under natural or forced cooling condition post heat zone. The plasticized material at weld region experiences three types of flows (Guo et al. 2014; Hamilton et al. 2008a; da Silva et al. 2011). Initially, near the tool, a slug of softened material is rotated around the tool pin under the influence of the rotating tool and also results in friction between the workpiece and the tool. Secondly, during tool rotation, the threaded portion of the pin

moves the softened plasticized material in the close proximity of the pin in the downward direction, which in turn, results in driving an equal amount of plasticized material which is farther away from the pin, in the upward direction. Finally, there is a relative motion between the tool and the workpiece. The combined effect of this material flow results in formation of the joint. The rate at which the heat is transferred into the tool along with the parameters of welding and properties of material affects the width of the recirculating plasticized material flow region (Chen et al. 2013; Hamilton et al. 2008a; Su et al. 2015).

Zhang et al. (2007) and Liu et al. (2018) reported that, the material flow at advancing side and retreating side are different. Figure 2.12 and Figure 2.13 show the material flow during FSW. The simulation of the material flow was carried out by them using finite element analysis. They reported that the softer material on the advancing side organizes itself into a fluidized bed near the pin and starts moving around it. At any circumstances, the material in the retreating side does not enter the rotational zone. However, on the advancing side, the material rotating around the pin, accumulates itself in the wake behind the pin after several rotations. The study also revealed the speed of tool rotation has small effect on the material behavior on both the sides (Bisadi et al. 2013; Jamshidi Aval et al. 2011; da Silva et al. 2011).
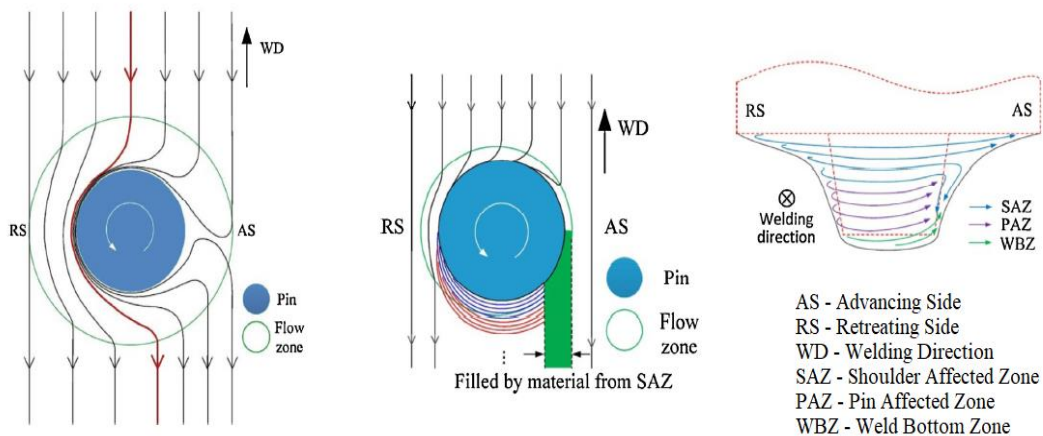
Figure 2.12 Material flow patterns around the FSW tool (Courtesy: Liu et al. 2018) (a) Two-dimensional material flow in SAZ (b) Two-dimensional material flow in PAZ (c) Three-dimensional material flow around the pin

41
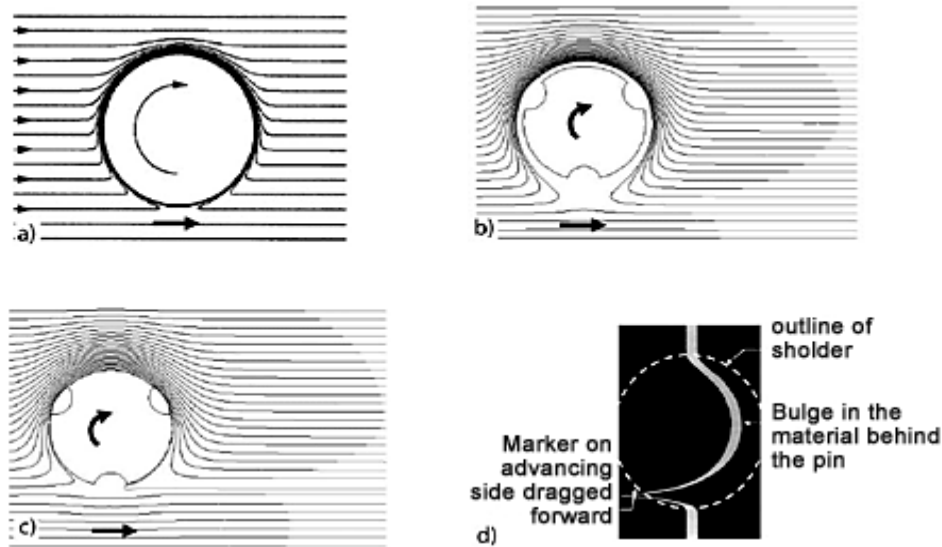
Figure 2.13 Material flow pattern around the FSW tool pin (Courtesy: Threadgill et al. 2009) (a) Typical path of flow of material around the pin rotating in clockwise direction in FSW (Courtesy: Seidel and Reynolds 2003)   (b, c) Influence of interfacial boundary conditions (**b** stick; **c** slip) on flow predicted with profiled tool (Courtesy: Colegrove and Shercliff 2004) d) Flow induced by pin (Courtesy: Reynolds 2008)

Figure 2.14 shows the material flow pattern in a pin. The profile of the pin helps in ensuring that the material, deformed plastically is completely distributed around the pin, and also from the top portion of the weld to the bottom portion of the weld and vice versa (Chen et al. 2018; Chowdhury et al. 2010; Su et al. 2015; Zhao et al. 2006). Fernandez et al. (2010), have reported that the threaded profile pin produces 25% reduction in mean particle size compared to thread less pin which produces 7% reduction in mean particle size. The thread pitch also plays an important role in joining. If the pitch is in the range of 1.4 and 2.0 mm, then it will act like a drill rather than a stirrer. This effect results in the workpiece material curl outward in the form of chips. Similar mechanical and metallurgical properties were exhibited when thread profile pin pitch used was 0.85 and 1.1 mm. (Boz and Kurt 2004; Elangovan et al. 2008; Moosabeiki et al. 2012) have reported that the thread pin helps in plastic flow and moves the material downward direction, when the thread direction is opposite to the spindle rotation direction.
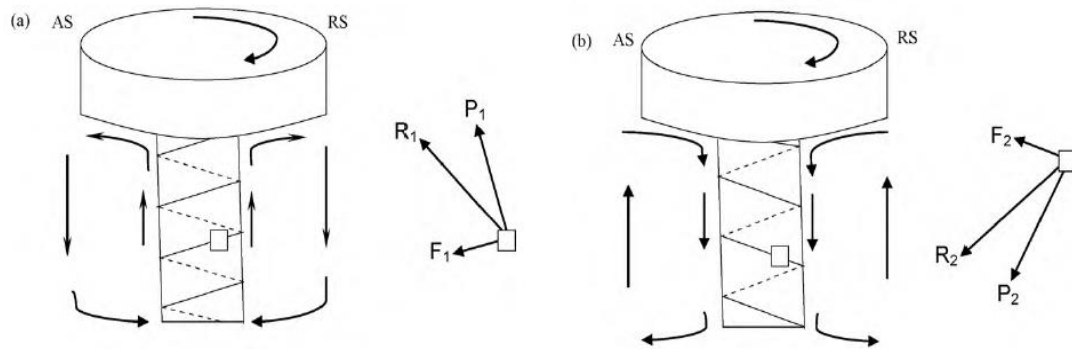
Figure 2.14 Helical material flow in threaded pin (Courtesy: Chowdhury et al. 2010) (a) Right-hand thread (RHT) and (b) Left-hand thread (LHT) pin tools in the clockwise rotation.

Doude et al. (2014); Hoyos et al. (2016); Reynolds (2008) have reported that the plastically deformed material flow in FSW method at weld region can be studied by marker tracer technique. The lead and titanium wire were used as a marker material and were placed on the advancing side at a distance of 1.3 mm below the top surface of the material. On the advancing side of the tool, periodically distributed trace patterns which comprised of arc shaped segments have been observed.

Pin breaking technique was reported by Chen and Cui (2009) to study the material flow in threaded profile pin. It is reported that, for each revolution of the tool, the sheared layer completely gets separated from the pin. As the tool advances, a cavity is formed behind the tool on advancing side and retreating side. This cavity is filled by the flow of separated layer forced by the shear region material and thus forms a nugget.

2.6   EVOLUTION OF MICRO-STRUCTURE AT WELD ZONE

Significant attention has been paid to the study of microstructural evolution of the friction stir welded aluminium alloys. Aluminium alloys demonstrate variety of crystallographic textures, grain size and grain morphologies that depend on the material composition and heat treatment The first attempt at classifying micro-structures was made by Barcellona et al. 2006; Shercliff et al. 2005; Threadgill et al. 2009. Figure 2.15 shows different zones of micro-structure developed at weld region after welding. The system divides the weld region into distinct regions as follows.

A. Unaffected Base Material (BM).

B. Heat Affected Zone (HAZ).

C. Thermo-Mechanically Affected Zone (TMAZ).

D. Nugget Zone or Stir Zone (NZ or SZ).
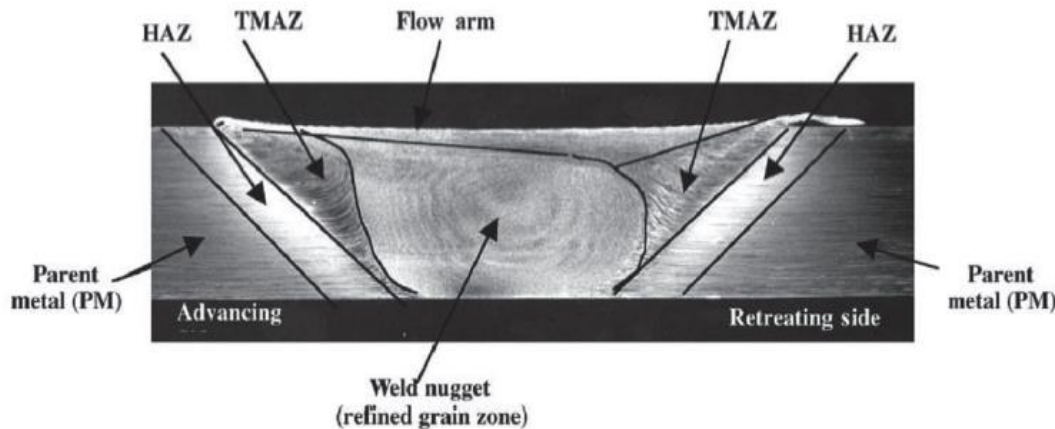
Figure 2.15 Different zones of micro-structure at weld region (Courtesy: Mishra and Ma 2005)

2.6.1   Unaffected Base Material

This material lies far away from the weld premise that has not been deformed and it may have experienced a thermal cycle of negligible magnitude during the welding. This thermal cycle does not affect the micro-structure or mechanical properties of the weld material.

2.6.2   Heat Affected Zone

In this zone, there will not be any plastic deformation. But, thermal energy of the FSW method is experienced by this region and facilitates reforming of the grain at HAZ. Therefore, grains in this region are slightly larger as compared to the base material. In precipitation strengthening alloys, thermal energy causes over ageing of precipitates which results in deterioration of mechanical properties (Jata 2000; Soundararajan et al. 2005; Zhang and Zhang 2008). The heat input to the workpiece at HAZ is a function of the welding parameters. So far, the researchers have highlighted that welding parameters considerably depend on the nature and purpose of the process. Therefore there is considerable variation in the width and property of the HAZ (Kwon et al. 2009; Mishra and Ma 2005).

Figure 2.16 (a-e) shows the typical micro-structure images of the TMAZ, the HAZ, BM and the NZ, investigated by Zhang et al. (2018), on friction stir welded material. On the advancing side elongated and extremely extruded grains have been observed in the TMAZ (Figure 2.16 (a)). But on the retreating side, an unclear interface between TMAZ and NZ has been observed (Figure 2.16 (b)). However, the HAZ (Figure 2.16 (c)) exhibits a grain structure which is similar to the BM (Figure 2.16 (d)), since HAZ is not subjected to any thermal cycle and not undergoing any plastic deformation.

2.6.3   Thermo Mechanically Affected Zone

TMAZ is a region which is characterized by the plastic deformation of the grains (Hu et al. 2012a; Ouyang and Kovacevic 2002). It is a region which is in close proximity to the nugget zone and thus it is exposed to higher temperature. The cause of the plastic deformation in TMAZ is due to the shearing of the grains induced by traverse of the tool and tool rotation. The plastic deformation in the TMAZ varies with its proximity to the nugget zone as well as to its depth in the weld.
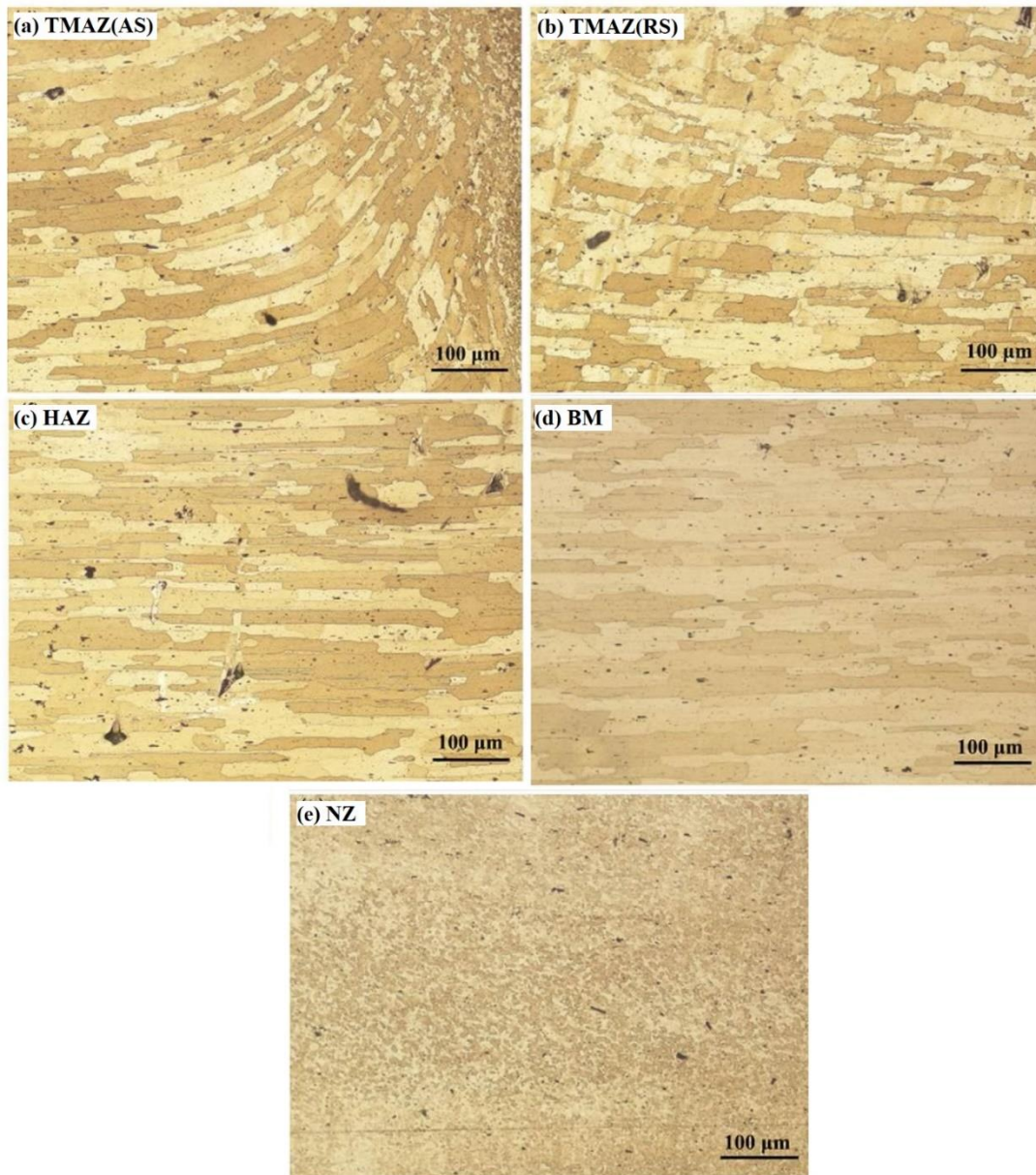
Figure 2.16 Typical micro-structure images of the TMAZ, HAZ and BM of FSW welded AA2195-T8 (a) TMAZ on the AS (b) TMAZ on the R.S. (c) HAZ (d) BM and (e) NZ. (Courtesy: Zhang et al. 2018)

The higher degree of deformation in the grains is identified towards the tool shoulder and nearer to the weld. The deformation of the grains is found to decrease as the distance of the grains from centre line of weld increases (Kwon et al. 2009; Mishra and Ma 2005). It is hard to recognize the boundary between the TMAZ and HAZ. However to define the outer boundary of the TMAZ, a method has been developed based on the angular distortion (Altenkirch et al. 2008a; Cavaliere et

al. 2006; Woo et al. 2006). Since, the TMAZ experiences significantly higher temperature, the strengthening precipitates in the vicinity of the nugget zone get dissolved and the strengthening precipitates in areas near to HAZ coarsen, leading to significant deterioration of strength. The exact boundary between the coarsened particles and dissolved particles is highly dependent on welding parameters. Thus the final distribution of the precipitates is a function of the time-temperature history of the region (Mehdi and Mishra 2016; Woo et al. 2006). TMAZ is a transition zone, between the parent metal and nugget zone created by the FSW) The grains appear to be elongated in the direction around the nugget zone (Balasubramanian et al. 2009; Jata 2000). This transition region between the parent metal and nugget zone on the advancing side is sharp, while on the retreating side appears to be relatively spread over (Krasnowski et al. 2015; Wan et al. 2014).

2.6.4   Nugget Zone

A Nugget Zone is characterized by fully re-crystalized area, sometimes called as Stir Zone (Ma 2008; Mehdi and Mishra 2016; Rhodes et al. 1997; Sato and Kokawa 2003; Su et al. 2003). It also is the region previously occupied by the tool pin. The variation in the size of the nugget zone depends on welding process parameters, built temperature, tool geometry and thermal conductivity of the material. Mishra and Ma (2005) reported that the nugget shape can be sub categorized by basin shape and elliptical shape. Sato et al. (1999) reported that the basin a shaped nugget is formed in FSW of AA6063-T5 plate. The wider nugget shape is formed on upper surface due to extremely higher heat generated at tool shoulder and material interface. Meanwhile Rhodes et al. (1997) and Su et al. (2003) have reported on the elliptical nugget shape formed in AA7075-T6 plates. Ma (2008) has investigated the shape of nugget at different process parameters. It is concluded that, lower speed of tool rotation produces basin-shape tool pin and higher speed of tool rotation produces elliptical shape. (Chen et al. 2018) distinguished the flow pattern of material, near the top, bottom, and middle regions of the weld, which result in a weld nugget of inverse trapezoidal shape. The generalized butt weld connection profile and other weld connection profiles with typical nuggets are depicted in Figure 2.17 (a) and (b), respectively (Khaled 2005).
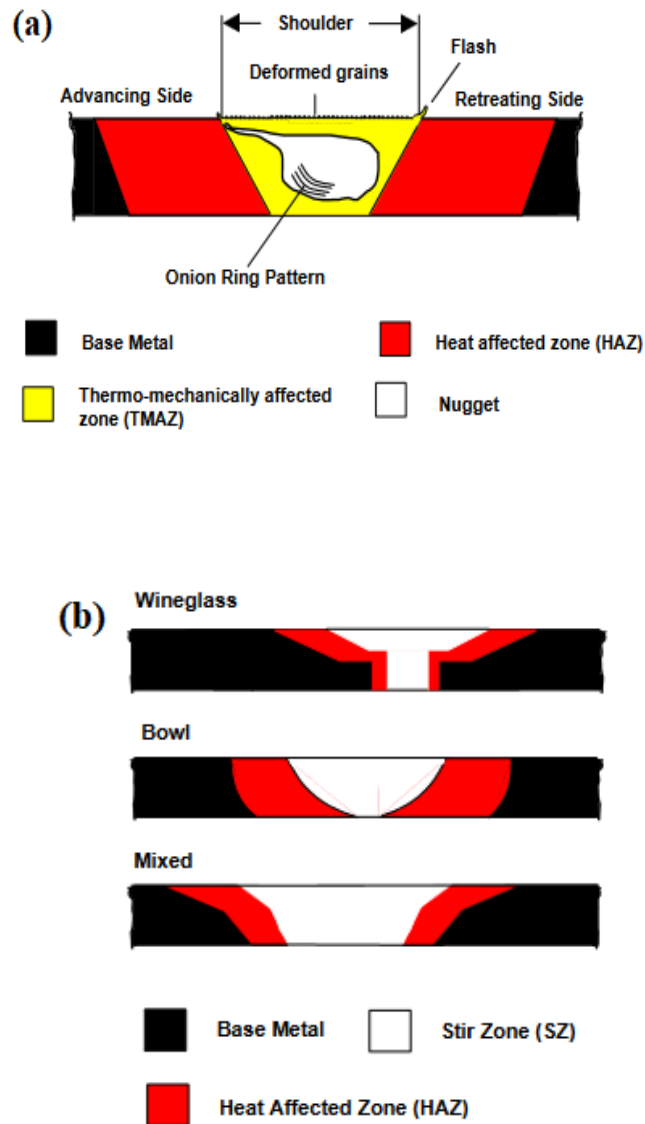
Figure 2.17 (a) Generalized butt weld connection profile   (b) Other types of FSW weld connection profiles (Courtesy: Khaled 2005)

2.6.5   Effect of Pin Diameter on Nugget Size

Seidel and Reynolds (2001) revealed the relationship between the nugget size and pin size. Figure 2.18 illustrates the effect of pin diameter on nugget size. It is described that the size oldie nugget is slightly larger than the diameter of the pin, except at the bottom of the weld where the pin is tapered to a hemispherical termination. Further, it was observed that the nugget zone leads

to a round shape with a maximum diameter at the middle of the weld due to increase in the pin diameter.
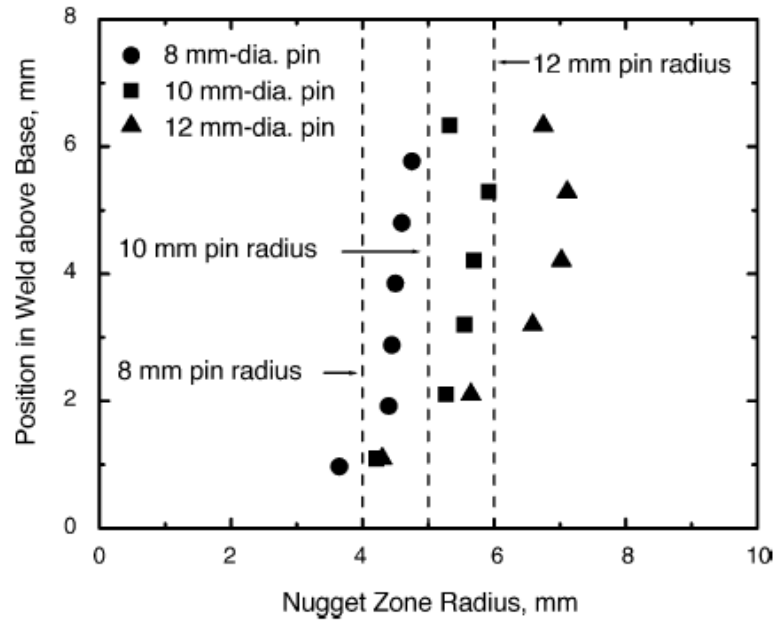
Figure 2.18 Effect of pin diameter on nugget size in an FSW of Al 2195-T8 (Courtesy: Mishra and Ma 2005; Reynolds 2000)

2.6.6 Significance of Grain size in FSW

As per strengthening principle, restricting, or hindering dislocation motion renders a material harder and stronger. As FSW method is associated with plastic deformation, slip or dislocation motion takes place. The grain boundary acts as an obstacle to the dislocation motion for two reasons as follows:

- The dislocation of the grains of different orientation is due to the increase in the mis-orientation of the crystallography.
- The disorder in the grain boundary resulted to the incoherence of slip planes of grains.

The fine-grained material is stronger and harder compared to the coarse grain. According to the Hall-Petch equation, the yield stress varies with respect to the grain size (Sato et al. 2003).

$$\sigma_Y = \sigma_\circ + \frac{k_Y}{\sqrt{d}}$$

49

Where "d" is the average grain diameter, "σ_o" is the friction stress representing the overall resistance of the crystal lattice to dislocation movement and "k_y" is a constant called locking variable representing the relative hardening contribution of grain boundaries as obstacles to slip across the grain boundaries (Ilkhichi et al. 2015; Rajakumar et al. 2010b).

Figure 2.19 shows the influence of grain size on the yield stress of the Friction stir welded joints made with different welding parameters (Afrin et al. 2008; Rajakumar and Balasubramanian 2012). It illustrates that the yield stress depends on the grain size. As the grain size decreases, the yield stress increases. Grain size can be synchronized by the plastic deformation and the rate of the solidification from liquid phase followed by a suitable heat treatment.
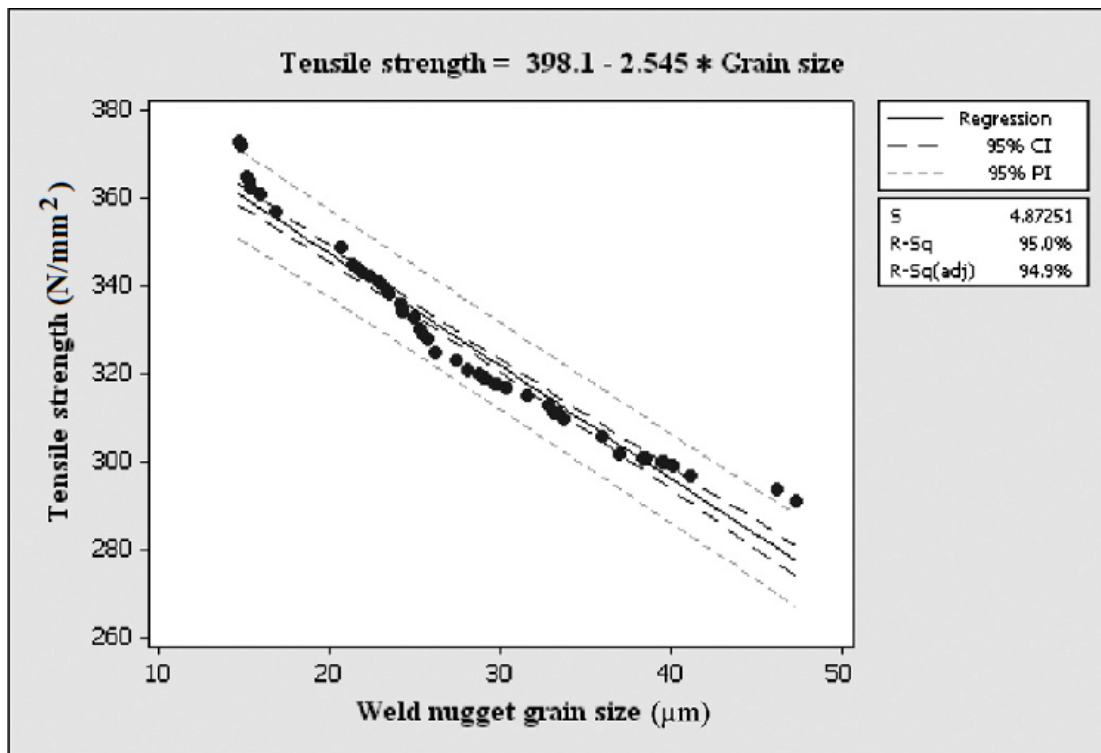
Figure 2.19 Influence of Grain size on the yield stress for AA7075-T6 (Courtesy: Rajakumar and Balasubramanian 2012)

Figure 2.20 shows the grain size distribution in various locations of nugget zone of weld joint prepared by friction stir welding AA7050. The grain size tends to increase at the top of the nugget zone and in turn decreases as one moves towards the bottom of the nugget zone. Su et al. (2003)

revealed that the grain size varies from the retreating side to advancing side in a 6.35 mm thick plate. The average grain size ranges from 5.3 microns at the top to 3.2 microns at the bottom. Similarly, the grain size varies from 5.1 microns on the advancing side to 3.5 microns on the retreating side. The variation in the grain size is due to the variation of temperature and heat dissipation in the nugget zone (Hassan et al. 2003a; Yan et al. 2005). Because the bottom of workpiece is in contact with the backing plate which acts as a heat sink, the peak temperature is lower, and the thermal cycle is shorter compared to the nugget top. The combination of lower temperature and shorter heat flow path at the nugget bottom effectively retards the grain growth and results in bigger recrystallized grains. It is evident that with the increase in plate thickness, the temperature difference between bottom and top of the weld nugget increases, resulting in increased difference in grain size (Liu et al. 2015; Xu et al. 2013).
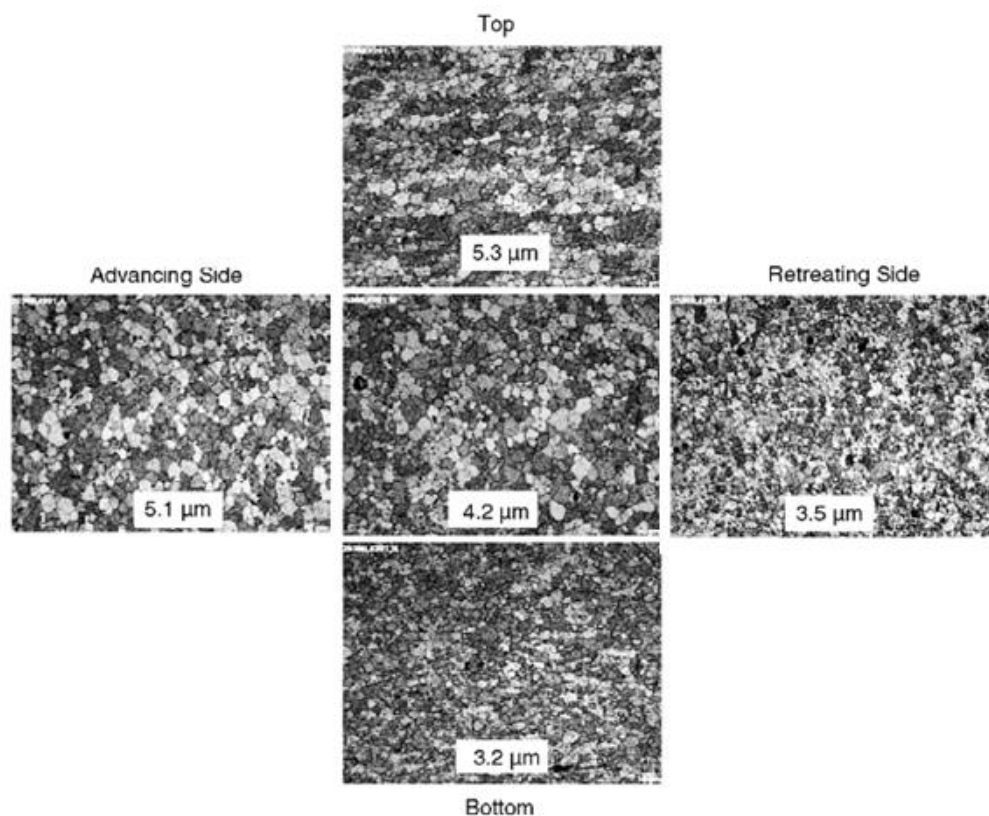
Figure 2.20 Typical Grain size distribution in various locations of A17050 weld nugget (Courtesy: Mishra and Ma 2005)

2.7 EFFECT OF PROCESS PARAMETERS ON QUALITY OF WELD

The weldability of the aluminium alloy welded by FSW is dependent on the process parameters, material, and tool geometry. The process parameters are speed of tool rotation, welding speed and thrust force.

2.7.1 FSW tools

FSW tool is an essential component to achieve success in the welding process. A non-consumable rotating tool usually comprises of a round shoulder and a pin of different shapes. The primary purpose of the tool is to provide heat to the workpiece by friction and deformation and moves the soft plasticized material around it to form the joint. Due to severe stresses and high temperature developed at the pin during welding, it is considered as a weakest component (Debroy et al. 2012; Elangovan and Balasubramanian 2008a; Rai et al. 2011). Improper selection of tool material and shapes lead to tool wear, which impacts not only the tool life but also the weld characteristics (Chen et al. 2018; Rai et al. 2011; Tao et al. 2017; Zeng et al. 2019).

(Debroy et al. 2012) have studied the durability of the tool for FSW of aluminium alloys. The durability of the tool is dependent on the type of tool and workpiece, method variable, weld connection thickness and shape of the tool. (Chen et al. 2018; Mehta et al. 2015) have performed the joining of dissimilar metal, which consisted soft metal aluminium on one side and hard metal AISI 1080 steel on the other side. It showed lot of porosities at weld region and breakage of tool. Intermetallic compounds were also observed at the nugget zone due to worn out tool. The mechanical properties of AA6061 using threaded tool was studied by (Zeng et al. 2019). The effect of the tool wear on the mechanical properties of the welded aluminium alloys was quite evident from the tensile test of the welded components. Therefore, it is essential to elucidate on the features of tool material and as well as tool shapes.

2.7.1.1 Tool Materials

Advances in tool materials have allowed the method to be used for increasingly demanding applications; however, the degradation of FSW tools in the form of wear

(Gibson et al. 2014), has remained an issue, highlighted by (Wang et al. 2014), who reported that tool wear in FSW leads to a decrease in the stirring action and a lack of the vertical movement of the weld material through the plate thickness.

Several publications have been found on the selection of tool material. Before selecting the tool material it is important that, tool should be as simple a shape as to manufacture, to reduce cost of production and generate sufficient stirring effect (Kumar et al. 2016b; Padmanaban and Balasubramanian 2009; Seighalani et al. 2010). Initially the FSW was developed to join the soft metal like aluminium alloys, which are easily stirred with tool steel (Chen et al. 2018; Rai et al. 2011; Rajakumar et al. 2011; Rodrigues et al. 2009; Threadgilll et al. 2009). Steel materials are easily available, and it can be machined to desired shape and size at low cost, and material characteristics can be established. But in the case of welding of aluminium alloys, the presence of hard particles stimulates more tool wear Zeng et al. (2006) have made an attempt to study the tool wear in FSW of AA6061-alloy plates. The study revealed that, as the speed of tool rotation increases the tool wear also increases.

From the work carried out so far on selection of the tool material and self-optimized tool wear, it appears that there is definitely an improvement in tool as it wears and stirring effect are concerned. (Fujii et al. 2006) have conducted study on the welding of 7020-T6 aluminium alloys using collared tool with pin made of steel material and with three different types of pin shapes. The simplest shape (column without threads), the ordinary shape (column with threads) and the triangular prism shape pins were used to weld the aluminium alloys. For 6061-T6 alloy whose deformation resistance is relatively low, the tool shape does not significantly affect the micro-structures and mechanical properties with steel as the tool material. Ikuta et al. (2012) have studied the tool wear of threaded screw tool made of steel for friction stir spot lap welding of Al 5754/Al 6111 and friction stir butt joints Al 5052/Al 6061 aluminium alloys using threaded and half thread tools. It could be seen from the experiments that, the thread on the rotating pin has limited influence on the mechanical properties of the friction stir spot lap joints. Self-optimized tool shape had been obtained after some experiment with the FSW tool without threads. Such optimized shape produces good quality of weld without any tool wear. In most of the cases, the tool wear occurs due to improper selection of process parameters. High speed of tool rotation and low welding speed leads to tool wear rapidly. Rai et al. (2011), have reported the process parameters for self-optimized tool shape. The study suggested that when speed of tool

rotation decreases and welding speed increases, the tool wear initially goes down due to filling of work material in the threads. After some distance is travelled by the tool (>3m), there will not be any wear due to self-optimized shape. Table 2.1 represents list of literature review of type of tool material and workpiece material of FSW of aluminium alloys.

2.7.1.2 Tool Geometry

Tool geometry plays a vital role in the FSW process, to move the material and, also to direct the traverse rate. An FSW tool comprises of shoulder and pin with different profiles. The heat is generated due to the friction between the workpiece and the pin during plunging stage (Aval 2015a; Ilangovan et al. 2015b). Some heat is also generated due to the deformation of the material. As soon as the tool shoulder comes in contact with the work material, the area of contact between the shoulder and the workpiece increases. Hence, frictional contact between workpiece and shoulder increases, which leads to generate larger amount of heat. Majority of the heat generated in thin sheet is produced by the shoulder (Casalino et al. 2014). However, in thick sheets the pin produces majority of the heat. From heating point of view, the relative ratio of shoulder to pin diameter is important. In the study carried out by Padmanaban and Balasubramanian (2009), it is revealed that the shoulder also confines the plasticized softer material. During welding process, the plasticized soft material is extruded from advancing side to the retreating side of the tool. This material is trapped by the shoulder and deposited along the weld connection to produce smooth surface finish. The second purpose of the tool is to stir and move the material. (Mishra and Ma 2005) has reported that the homogeneity of micro-structure and mechanical properties are governed by the tool design and as well as welding speed and speed of tool rotation of the tool. Carlone and Palazzo (2013); Lorrain et al. (2010); Yang et al. (2012) reported that the most dominant factors arc pin to shoulder diameter ratio, shoulder surface angle, pin shape and pin size. The various tool geometry parameters which affect the weld quality are discussed below.

Table 2.1 Type of base material, tool material and tool shape utilized in FSW of alloys of aluminium

Sl. No.	Base Material	Tool Material	Tool Shape	Reference
1.	1100 AA to 6061AA	Carbon Steel	Round	Murr et al. (1998)
2.	6061-T6AA to 7075-T6AA	Steel	Round Threaded	Colligan (1999)
3.	6061AA to 2024AA	Tool Steel	Round Threaded	Ouyang and Kovacevic (2002)
4.	6061AA	D2 tool steel heat-treated to HRc = 62	Round	Guerra et al. (2003)
5.	7075-T7351AA	1. MP159, 2. Dievar tool steel, 3. MP159 pin, H13 shoulder	Threaded	Colegrove and Shercliff (2003)
6.	5083AA	Tool Steel	Round	Hirata et al. (2007)
7.	6082-T6AA	Steel	Round	Scialpi et al. (2007)
8.	6061-T6AA	H13 steel	Round	Sorensen and Stahl (2007)
9.	7020-T6AA	Steel	Frustrum & Round	Kumar et al. (2008)
10.	2017AA to 6013AA	Tool Steel	Round	Mroczka et al. (2008)
11.	2024-T3AA to 7075-T6AA	Tool Steel	Round	Khodir and Shibayanagi (2008)
12.	RDE-40AA	High-Carbon Steel	Round Threaded	Balasubramanian and Lakshminarayanan (2008)
13.	6061-T6AA	H13 steel	Round Threaded	Atharifar et al. (2009)
14.	6111-T4AA	H13 steel	Square	Bakavos and Prangnell (2009)
15.	5754AA	H13 steel	Round	Badarinarayan et al. (2009)
16.	5052AA	H.S.S.	Round	Kumbhar et al. (2011)
17.	6061AA to 5086 AA	H.S.S.	Round Taper	Ilangovan et al. (2015)
18.	7075-T7351AA	H13 steel	Triflute, Trivex	Colegrove and Shercliff (2017)
19.	5059AA	H.S.S.	Taper Threaded	Babu et al. (2017)
20.	6063AA	H.S.S.	Round	Sashank et al. (2018)

2.7.1.3 Tool Shoulder Diameter

Significant attention has been devoted to study the effect of tool shoulder diameter of the FSW tool (Elangovan and Balasubramanian 2008a; Mehta et al. 2011). The tool shoulder generates most of the heat and its control on the plasticized material largely establishes the material flow field. Kumar and Kailas (2008) and Mehta et al. (2011) studied the influence of tool shoulder diameter on thermal cycle, power requirements, peak temperature, and torque during FSW of AA7074-T6. Figure 2.21 shows the variation of peak temperature with shoulder diameter. The study revealed that the temperature increases with increasing diameter of the shoulder. For defect free weld, the tool shoulder must prevent the escape of the plasticized material, and the total torque, even the traverse force should not be extreme. Elangovan and Balasubramanian (2008); Kumar and Kailas (2008) and Mehta et al. (2011), have revealed that amount of heat generated increases with the increase in tool shoulder diameter due to larger contact area, thus resulting in a wider TMAZ and HAZ regions. Therefore, it has been perceived that as the diameter decreases the amount of frictional heat generated reduces. The weld quality deteriorates due to lesser friction leading to lack of weld merging. Therefore, only a tool with an optimal shoulder diameter results in the highest strength. Arora et al. (2012) have suggested a method, by taking into account the sticking torque (MT) and sliding torque (ML) torque components, to regulate the optimal shoulder diameter. Figure 2.22 illustrates the variation of sliding torque, sticking torque and total torque with shoulder diameter. The torques intended are selected based on stress flow inside the workpiece, tool geometry and the axial pressure. They reported that the optimal diameter of the tool shoulder can be found by analyzing the variation of sticking torque with diameter of the shoulder.

2.7.1.4 Tool Shoulder Surface

Literature survey reveals that, the tool shoulder surface is also an essential aspect of the tool design. Several features were adopted in the surface to increase material deformation, to ensure proper mixing of material, to obtain smoother surface finish and to act as reservoir for the forging action (Mishra and Ma 2005; Rai et al. 2011; Venkateswarlu et al. 2013; Vilaça and Thomas 2011). Commonly used features are shown in

56
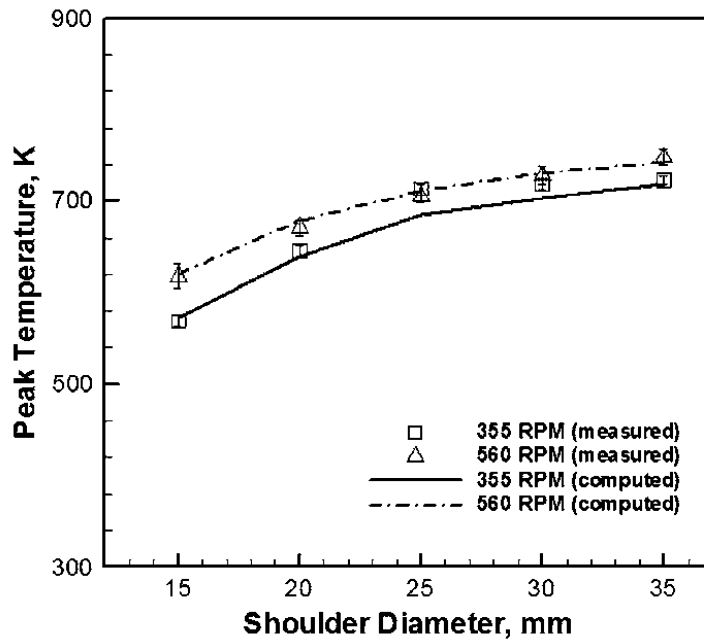
Figure 2.21 Graph of shoulder diameter versus temperature during FSW of AA7075-T6. (Courtesy: Mehta et al. 2011)
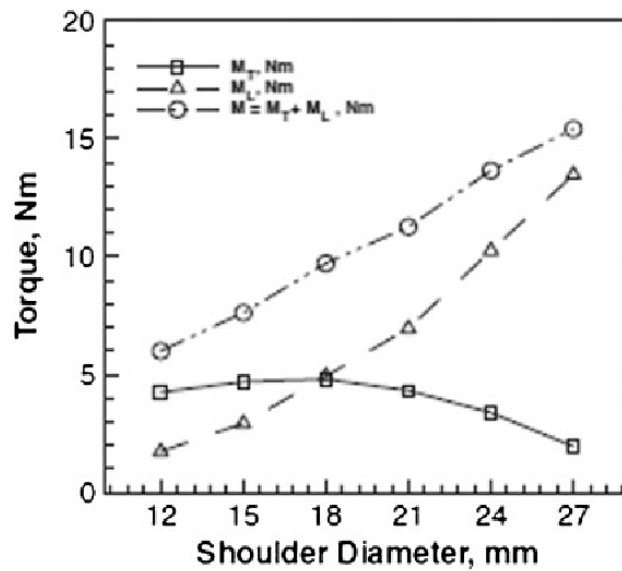
Figure 2.22 Graph of Variation of sliding torque, sticking torque and total torque with shoulder diameter of AA 6061 FSW joints. (Courtesy: Rai et al. 2011)
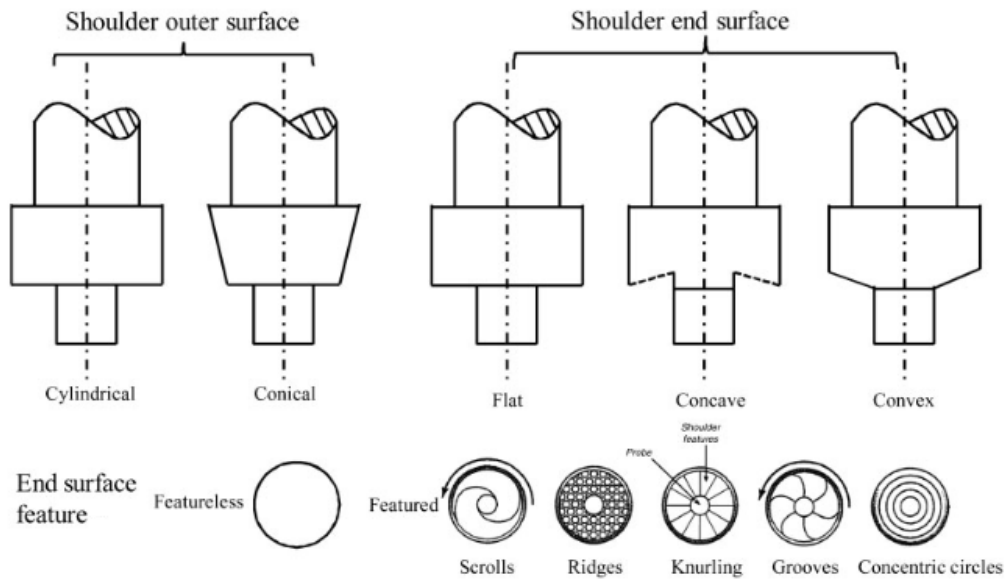
Figure 2.23 Tool shoulder geometries (Courtesy: Zhang et al. 2012)

Figure 2.23. Zhang et al. (2012) have explained that concave shaped tool produces good quality weld. It is simple in design and easy to manufacture. A small angle (6 to 10º) is made in the tool from the edge of the shoulder to the pin base. A small quantity of material is forced into this cavity during final stage of plunging of the tool and the material thus stored acts as a reservoir for the forging action of the tool shoulder. During forward traverse movement of the tool, new soft material is forced into this cavity and displaces the stored material into the flow of pin. Murthy et al. (2018), have investigated FSW of AA6082 aluminium alloy using concave shaped shoulder. The concave shape of shoulder produced smooth surface finish. Rai et al. (2011) and Venkateswarlu et al. (2013), have further studied the surface concavity effect on mechanical properties. The study involved, varying the surface concavity by addition of flat surface at the shoulder periphery. The result showed higher tensile stress obtained for 2 mm flat shoulder surface followed by concavity of 7º, which was perceived to be more appropriate for achieving adequate tensile strength. Trueba et al. (2015) by way of their FSW investigations on aluminium alloy 6061-T6, have shown that a FSW tool having a raised spiral design shoulder, produces a weld with a best combination of surface quality and mechanical properties.

2.7.1.5 Tool Pin Geometry

There have been many tool pin geometries reported in the literature to obtain improved mechanical properties (Boz and Kurt 2004; Colegrove and Shercliff 2017; Elangovan and Balasubramanian 2008a; Sued et al. 2014). The profile of the pin designed must be in such a way that it retains the maximum plasticized material in weld cavity (Kumar et al. 2008). The most commonly designed and used pin profiles are cylindrical or tapered with or without threads. Complex pin profiles such as square profile, triangular profile, Flared-Triflute, Skew-stir are also have been used (Thomas et al. 2003). In threaded profile, the pin produces higher heat and vertical flow of the material in the direction of thread (Sued et al. 2014). Generally clockwise rotation is used for left hand threaded tool and anticlockwise rotation of the tool is used for right hand tool (Mishra and Ma 2005). The study by Boz and Kurt (2004), has revealed that, the threaded profile pin with high pitch acts like a drill rather than stirrer, which spill the material in the form of chips Fernandez et al. (2010) and Seidel and Reynolds (2001), reported that the improved mechanical property has been obtained for a threaded profile pin with 0.8 and 1.1 pitches. (Elangovan and Balasubramanian 2008a), used different tool geometries for processing of AA2219. The shape used for the study and its dynamic orbit is shown in the Figure 2.24. The square and triangle shaped tool pin are associated with eccentricity which allow the incompressible material movement around the pin profile (Ouyang et al. 2002; Thomas and Nicholas 1997). Because of the eccentricity of the pin, the dynamic orbit is related to the eccentricity of the rotating plasticized material (Shettigar and Manjaiah 2017a; Thomas and Nicholas 1997). The path for the flow of plasticized material is identified by the ratio of static volume and dynamic volume. It in turn leads to the pulsating stirring action in the plasticized flowing material due to flat surface.

2.7.1.6 FSW Tool Pin Diameter

Rajakumar et al. (2011) have highlighted on the importance of tool pin diameter on producing good quality of weld in FSW. The pin diameter is responsible for deciding the volume of material being stirred. Suppose the tool diameter is smaller, then the volume of material stirred also is less

and vice-versa. The combined effect of smaller pin diameter, lower welding speed and higher speed of tool rotation causes higher heat input to a smaller volume of material which results in turbulent material flow and coarse grain structure. On the other hand, large pin diameter with lower welding and speed of tool rotation causes lower heat input to maximum volume of material. This effect will lead to inadequate material flow and insufficient plasticization (Khan et al. 2015b). Larger pin diameter with respect to shoulder diameter resulted in insufficient heat generation due to wider contact area and produced defects in advancing side of TMAZ region (Rajakumar et al. 2011). The shape of the tool pin influences the flow of plasticized material and affects weld properties Choi et al. (2011). Figure 2.25 shows the shapes of some of the commonly used tool pins. A triangular or 'trifluted' tool pin increases the material flow as compared to a cylindrical pin (Hirasawa et al. 2010).

Figure 2.24 Effect of pin profile on dynamic orbit and pulsating action (Courtesy: Shettigar and Manjaiah 2017)

The effects of shape of tool pin on micro-structure and tensile stress of dissimilar friction stir welded AA5083-H111 and AA6351-T6 aluminium alloys were studied by (Kumar et al. 2008; Palanivel et al. 2012; Schneider et al. 1991), using three various speeds of tool rotation of 600 RPM, 950 RPM and 1300 RPM and five different shapes of tool pin of straight square (SS), straight hexagon (SH), straight octagon (SO), tapered square (TS), and tapered octagon (TO). The macrostructure of all the fifteen joints

obtained with combinations of speed of tool rotation and shapes of tool pin, revealed that the joints fabricated using shapes of tool pin SS, SH and SO are defect free. A tunnel at the bottom of the weld connection is always present when tapered shapes of tool pin are used at all speeds of tool rotation (Chen et al. 2019; Schneider et al. 1991; Su et al. 2015). A sound weld connection forms when proper combinations of those factors are met with. The macrostructures suggest that sufficient frictional heat is formed to plasticize both the aluminium alloys at all speeds of tool rotation using straight pin profiles which yielded defect free welds (Mohanty et al. 2013; Seighalani et al. 2010). A straight pin profile tool has more contact area compared to tapered tool. The transportation of plasticized material from advancing side to retreating side is uniform from top to bottom of the weld connection when straight pin profile tool is employed (Chiteka 2013; Guo et al. 2014). The interaction between tool and plasticized material is less in tapered pin profile tool owing to lesser contact area. Inadequate sweeping of plasticized material and reduction in frictional heat leave a tunnel at the bottom of the joint (Mohanty et al. 2013; Seighalani et al. 2010; Venkateswarlu et al. 2013). Figure 2.26 images of various shapes of tool pin used for study.
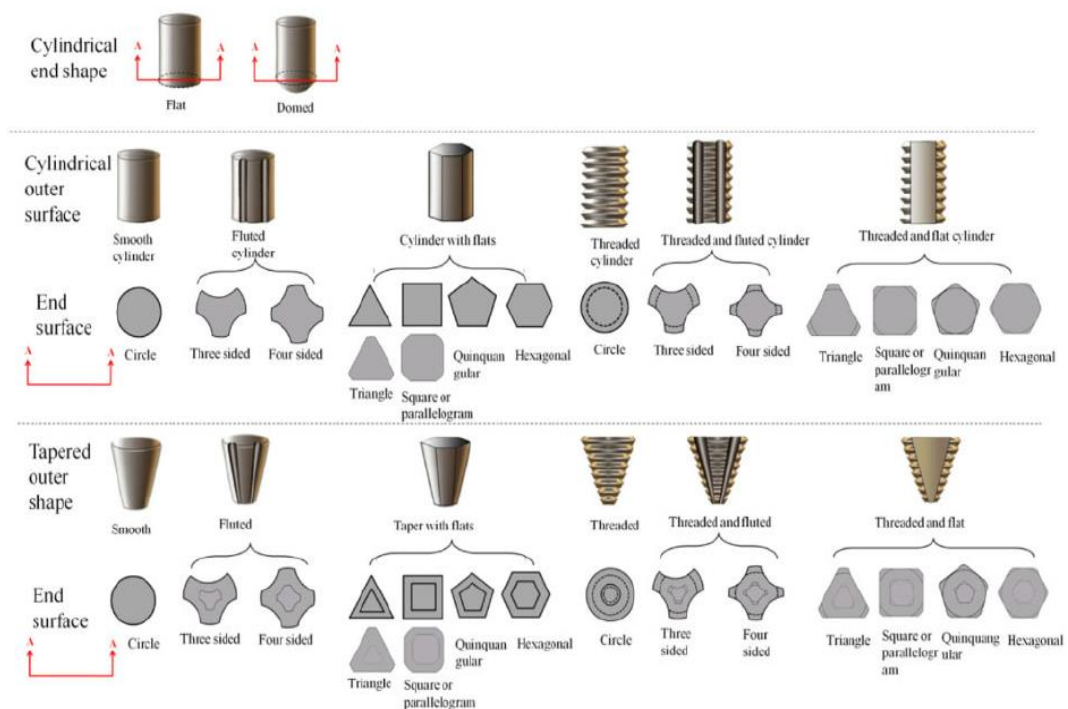
Figure 2.25 Shapes of some of the commonly used tool pins (Courtesy: Zhang et al. 2012)

61

Figure 2.26 FSW Tools manufactured for welding (Courtesy: Mazak Megastir Inc., U.S.A.)

The enhancement of the tensile properties in the joints produced by square pin tool is due to the difference in dynamic orbit created by the eccentricity of the rotating tool of the FSW method (Guo et al. 2014; Palanivel et al. 2012; Senthil et al. 2020). The relationship between the static volume and dynamic volume decides the path for the flow of plasticized material from the leading edge to the trailing edge of the rotating tool properties (Mosleh et al. 2016; Trimble et al. 2015b; Zhang et al. 2012). Figure 2.27 shows the effect of shapes of tool pin on the ultimate tensile stress (UTS) of the friction stir butt welded aluminium alloy plate joints.
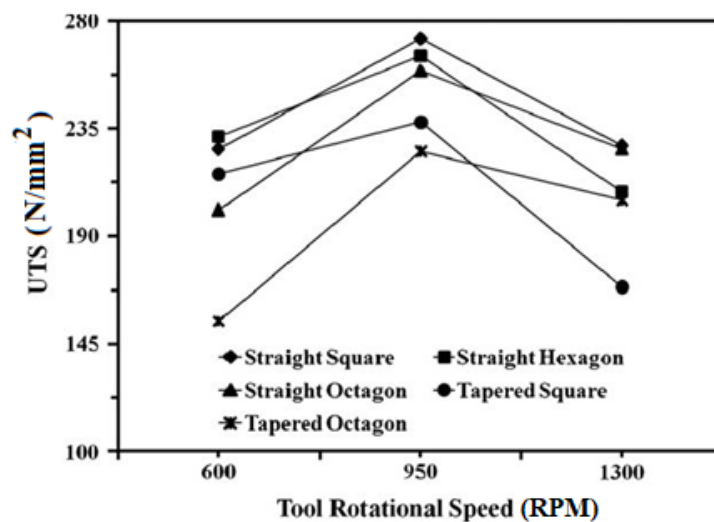
Figure 2.27 Effect of shapes of pin of tool on the ultimate tensile stress (UTS) (Courtesy: Palanivel et al. 2012)

It is evident from the table that the effect of shape of tool pin on the UTS is lowest for the tapered octagon pin tool. The reason is that the joints fabricated using straight tool profiles had no defects while tapered tool profiles caused a tunnel defect at the bottom of the joints under the experimental conditions considered (Rai et al. 2011; Shettigar and Manjaiah 2017a) Three different regions namely unmixed region, mechanically mixed region and mixed flow region were observed in the weld zone. The speed of tool rotation and pin profile influenced the formation of mixed flow region (Hao et al. 2013a; Kumar et al. 2013; Peel et al. 2003). The joints fabricated using tapered tool profiles and slow speeds of tool rotation showed absence of mixed flow region. The weld connection fabricated using medium speeds of tool rotation and straight square pin profile yielded highest strength. The variation in tensile stress of the dissimilar joints was attributed to material flow behavior (Rao et al. 2013; Sato et al. 2005; Yu et al. 2018), loss of cold work in the HAZ of the joint, dissolution and over aging of precipitates of alloy and formation of macroscopic defects in the weld region (Gungor et al. 2014).

The effect of tool profile on the weld connection efficiency is also similar to that of tensile stress (Elangovan et al. 2008a; Khodir and Shibayanagi 2008; Shen et al. 2013). The weld connection efficiency is high when the alloy is welded using square pin tool and low when it is welded with straight cylindrical pin tool. Table 2.2 shows the influence of shapes of tool pin on mechanical properties of the friction stir welded AA6061 aluminium alloy nugget zone material produced at 1200 RPM.

Features such as threads and flutes on the pin are believed to increase heat generation rate due to larger interfacial area, improve material flow and affect the axial and transverse forces (Elangovan et al. 2008b; Hattingh et al. 2008; Nandan et al. 2008; Tang et al. 2015) have studied the friction stir processing of AA6061 alloy of aluminium using five different shapes of tool pins (plain cylindrical, threaded cylindrical, tapered cylindrical, square, and triangular). It is found that the square shape of tool pin produces mechanically sound and metallurgically defect free welds compared to other shapes of tool pin and straight cylindrical tool experienced much less wear than the flat faced tools (Elangovan and Balasubramanian 2008b; Thube 2014).

Table 2.2 Effect of shapes of tool pin on mechanical properties of the weld joint made by friction stir welding of AA6061 alloy of aluminium at 1200 RPM (Courtesy: Elangovan et al. 2008)

Sl. No.	Shape of tool pin	Hardness (VHN)	Yield Stress (N/mm^2)	UTS (N/mm^2)	Percentage Elongation (%)	Joint Efficiency (%)
1.	Square	87	145	183	15.5	64
2.	Triangular	75	145	178	13.8	62
3.	Straight Cylindrical	60	127	160	13.2	54
4.	Taper Cylindrical	70	132	165	14.2	57
5.	Threaded Cylindrical	72	132	166	15.0	57

Babu et al. (2009), conducted research of FSW on AA2219 aluminium alloy plates by making use of tools with pin profiles triangular, square, straight cylindrical, tapered cylindrical and threaded cylindrical. Of the five pin profiles tested, the joints fabricated using the square pin profiled tool exhibit the highest tensile strength. The triangular pin profiled tool showed tensile properties almost matching those of the square pin, followed in order of descending performance by the threaded, taper and straight cylindrical pins. The reason for superior properties resulting from the use of a tool pin with flat faces, like square and triangular pins, is because tools with non-circular profiles will allow plasticized material to pass around the probe. Pin profiles with flat faces are associated with eccentricity. This eccentricity of the rotating object is related to dynamic orbit. This eccentricity must, to a greater or lesser extent be part of the FSW method characteristics. The relationship between the static volume and swept volume decides the path for the flow of plasticized material from the leading edge to the trailing edge of the rotating tool. In addition, the triangular and square pin profiles produce a pulsating stirring action in the material flow (Babu et al. 2018; Elangovan et al. 2008a; Nadikudi et al. 2015; Yuqing et al. 2017). Colegrove et al. (2006), studied four shapes of tool pin, namely, trivex, triflute, triflat, and cylindrical for welding of aluminium alloy AA7449 and from the pressure analysis studies they exhibited that the greatest difference in pressure could be attained with the tool of triflat shape followed by the

tools of triflute and trivex shapes. Also, the successful production of weld had the similar ranking.

2.7.2 Effect of Speed of tool rotation

The study of effect of speed of tool rotation on weld quality showed that proper mixing and adequate heat generation is dependent on the speed of tool rotation (Bisadi et al. 2013; Kumar and Thansekhar 2014; Rajakumar et al. 2011). At lower speed of tool rotation, heat generated is less and also mixing of material is not proper, irrespective of the welding speed. Elangovan et al. (2008) and Vidakis et al. (2016), have studied the effect of speed of tool rotation on ultimate tensile stress (UTS). The result revealed that, heat liberated due to friction is predominantly dependent on speed of tool rotation. If heat generated is less then heat supplied to the base material is also less, and it affects the softening of the material and consequently the material flow. As a result, lower value of UTS is found in FSW of aluminium alloys. At high speed of tool rotation, heat generated is more. Therefore, heat supplied also is more. Hence, softer plasticized material is available at NZ which results in turbulence in material flow and coarse grains formed at NZ. Ashok Kumar and Thansekhar (2014), have studied the effect of speed of tool rotation on UTS. The study exhibited that as the speed of tool rotation increases, the UTS also increases up to a certain value and further increase in speed of tool rotation decreases the UTS (Dinaharan et al. 2012; Palanivel et al. 2012; Rajakumar et al. 2011). Kwon et al. (2009) showed that in the friction stir welded 5052 aluminium alloy plates, the grain size in the friction-stir-welded region (SZ) is smaller than that in the base metal and is decreased with a decrease of the speed of tool rotation. In all speeds of tool rotation, the SZ exhibits higher average hardness than the base metal.

2.7.3 Effect of Welding speed

The welding speed only decides the quantity of heat supplied to the base material to be joined (Rajakumar et al. 2011)(Kumar and Thansekhar 2014). If the heat generation is less, then heat supplied will be relatively less and vice versa. Characteristics of friction stir welded joints are influenced by material flow and temperature distribution across

the weld which are dictated by pin/shoulder geometry and welding parameters. Peel et al. (2003); R. Nandan et al. (2008) and Rajakumar and Balasubramanian (2012), have reported that the Ultimate Tensile stress (UTS), percentage elongation (EL) and weld connection efficiency decrease with increase in welding speed. Further, the minimum hardness region shifts from Heat affected zone to weld nugget zone on increasing the welding speed and decreasing the tool speed of tool rotation. Stirring becomes insufficient at higher speeds of welding. The material then does not travel enough to the Retreating Side (RS) from the Advancing Side (AS) of the tool. The increase in the welding speed leads to lower heat generation with faster cooling of the plasticized material thereby reducing the softened area. Khodir and Shibayanagi (2008) have proven that grain size decreases with increasing welding speed during FSW of dissimilar AA2024 and AA7075 aluminium alloys. This could be attributed to the lower temperature caused by the lower heat input associated with faster welding speed, where the grain size decreases with decreasing heat input. Rahmi and Abbasi (2017) have studied the ratio of rotational/ welding speed (ω/v) in friction stir welding. By increasing (ω/v), a slight decrease in the effective tensile properties is observed. This was due to increased heat input and softening of the material in these regions. Furthermore, increasing (ω/v) ratio results in the formation of a larger weld nugget because of an increase in heat input and an easier material flow. Therefore, the probability of formation of ''incomplete root penetration'' defect is reduced when (ω/v) ratio increases. Miroslav Mijajlović and Dragan Milčić (2012); Dong et al. (2013); Tiwari and Shukla (2013) and Selamat et al. (2016), have reported that, as welding speed increases the tensile properties also increase. This is due to lower heat input at higher welding speed which weakens the growth and transformation of 'θ' precipitates. This leads to narrowed softened region as well as shifting of the weakest location to TMAZ just adjacent to NZ with reduced strength loss during tensile testing (Aydin et al. 2012; Liu et al. 2017; Rajamanickam et al. 2009).

2.7.4   Effect of Axial Force

Another variable which has to be considered during FSW is axial force. Only limited data is available to understand the effect of axial force on tensile stress Banik et al.

(2019); Elangovan et al. (2008); Hattingh et al. (2008); Jayaraman et al. (2009) and Kumar and Kailas (2008), have reported that, the material flow pattern mainly depends on the axial force. Inadequate plasticized material was obtained at top surface of the weld due to lower axial force. Kumar and Kailas (2008), have reported that bonding occurs when a pair of surfaces is brought in the vicinity of inter atomic forces. Axial force propels the plasticized material in the weld region to complete the extrusion process. Axial force is also responsible for the plunge depth of the pin. When the axial force is relatively low, there is a tunnel defect found at the bottom of the weld zone. If axial force is excessive, the material flow in the form of flash, on either side of the weld region, that is, on both AS and RS. This leads to thinning of the weld connection thereby reducing the strength of the weld (Elangovan et al. 2008). Elangovan et al. (2008) have expressed their thought on the effect of axial force increasing the tensile stress of AA6061 alloy weld connection fabricated by FSW. Coarse grains with clustered strengthening precipitates were obtained at axial force of 6 kN. When axial force is 8 kN, coarse grain with fine and uniformly distributed strengthening precipitates were obtained. Jayaraman et al. (2009) have reported that the tensile stress increases with increasing axial force up to a certain limit and then it decreases. At lower axial force, improper material flow forms defect in the weld zone. Hence, UTS was low. At higher axial force, the non-uniform distribution of Si particles and thinning effect led to a decrease in the UTS.

2.8   MECHANICAL PROPERTIES

2.8.1   Hardness

The available data found from the literature about mechanical properties of friction stir welded aluminium alloys is discussed here. Hassan et al. (2003) based on their study on the hardness of the friction stir welded high strength AA7010 alloy of aluminium, have reported that at low heat inputs, which is due to slow spindle speeds at a given welding speed, there will be a significant variation in grain dimension and hardness from the bottom to top of the weld, such that the biggest grain size and maximum

67

hardness is obtained at the top of the nugget (Habibnia et al. 2012; Ilkhichi et al. 2015; Kamp et al. 2009). As the spindle speed is raised with respect to the speed of tool traverse, the heat input increases, the micro-structure tends to become more homogeneous, and the hardness and grain size goes up. The increased input of heat intensifies the nugget solute concentration, which results in improvement of the tensile properties and hardness of the nugget zone (Topic et al. 2009; Xie et al. 2008). This is due to a decrease in density of coarse second phase particles and a better response to post weld natural aging. Kumar et al. (2015) have reported that in comparison to the parent material, there is reduction in hardness in the weld nugget area (NZ) and improvement in hardness in the TMAZ for high strength AA7075 aluminium alloy. Rao et al. (2015) also reported similar observations during welding of AA7075-T651 aluminium alloy. The over aging and dissolving of the metastable precipitates lead to the decrease in the hardness in NZ. But the presence of the fine equiaxed grains and the resolution of the dissolved precipitates partially remedy the loss of hardness. The improved hardness in NZ is attributed to the recovery of the dissolved precipitates and the fine equiaxed grains in NZ. FSW generates a region of relatively low hardness value around weld centre. This region extends up to the transition region of TMAZ and HAZ. The HAZ region showed a decrease in hardness arising from the coarsening of the precipitates in this region. The dissolution of strengthening precipitates ($MgZn_2$) in HAZ may be attributed to the reduction in hardness (Kumar et al. 2015). Sato et al. (2002) have conducted hardness tests on T4 and T5 heat treated 6063 aluminium alloys. They concluded that in the as-welded condition, 6063-T5 aluminium alloy was softened around the weld centre, whereas 6063-T4 aluminium alloy showed homogeneous hardness profiles. Various speeds of tool rotation values did not result in significant differences in the hardness profile in these welds, except for the width of the softened region in the weld of 6063-T5 aluminium alloy. Post weld aging raised the hardness in most parts of the welds, but the increase in hardness was small in the stir zone produced at the lower speeds of tool rotation. This is due to a similar distribution of the strengthening precipitates in the grain interiors and the presence of a precipitation-free region (PFZ) adjacent to the grain boundaries in all the welds. Microstructural analyzes suggested that the small increase in hardness in the stir zone produced at the lower speeds of tool rotation was caused by an increase in the volume fraction of PFZs. The

influence of FSW on evolution of micro-structure and mechanical properties of 5052 aluminium alloy plates have been studied by Kwon et al. (2009). They proved that, at all speeds of tool rotation, the friction-stir-welded region exhibits higher average hardness than the base metal. (Lakshminarayanan et al. 2009) have conducted comparative studies on AA6061 aluminium alloy plates which were welded using three different welding methods, Namely, gas tungsten arc welding (GTAW) and gas metal arc welding (GMAW) and friction stir welding (FSW). From this investigation, it is found that FSW joints of AA6061 aluminium alloy showed superior weld region mechanical properties like tensile stress and hardness, compared with GTAW and GMAW joints, and this is mainly due to the formation of very fine, equiaxed micro-structure in the weld zone. Dong et al. (2013) have carried out detailed research on FSW joints of 6005A-T6 aluminium alloy plates and the effect of welding speed on micro-structure and hardness of the FSW weld connection material. They reported that the hardness of nugget zone (NZ) depended on the level of natural aging of NZ at various speeds of welding. The thermo-mechanically affected zone (TMAZ) is characterized by elongated grains with a high density of dislocations. The welding speed had not a significant effect on hardness in this zone. The heat affected zone (HAZ) contains the transformation of precipitates and coarsening of precipitates. The HAZ close to the weld connection centre line exhibited the minimum hardness due to the coarsening of precipitates while the HAZ far from it having a high hardness level was mainly related to coherent precipitates. The HAZ hardness and weld connection strength has an increased tendency with increase in the welding speed. It is due to the increase the density of precipitates. Rahimzadeh Ilkhichi et al. (2015) conducted extensive experimental and mathematical studies on determination of grain Size and hardness of the friction stir-welded AA7020 aluminium alloy plate joints. They predicated from the studies that with an increase the heat input, the hardness of the joints decreased, whereas the grain size increased continuously. In addition, the optimized condition for achieving the lowest grain size and highest hardness of the joints was derived from the analysis. Ilangovan et al. (2015) investigated the Effect of shape of tool pin on hardness of friction stir welded dissimilar AA6061–AA5086 aluminium alloy joints. They found that the usage of tool with threaded profile of pin contributes to improved flow of materials among two alloys and the creation of a stir zone free of defects. This also

results in increased hardness readings within the stir zone and increased tensile strength capacity in comparison to tools with unthreaded profile of pin. The hardness rise is ascribed to the development of grains of fine size and intermetallics inside the stir zone, and, the decreased size of weaker zones, like HAZ and TMAZ, resulted in improved tensile properties. From the investigation done on the Friction stir welds of very thin plates of the AA6016-T4 aluminium alloy by Rodrigues et al. (2009), it was concluded that The welds produced with the conical shoulder (HW) displayed a larger nugget grain size with few coarsened precipitates as opposed to the welds done with the scrolled shoulder (CW), which showed a smaller grain size containing many coarsened precipitates. These differences in micro-structure conducted to a reduction in hardness around 15% in the CW welds contrary to the HW welds. Svensson et al. (2000) had based their FSW investigative studies on aluminium alloys AA5083 and AA6082 have published that, the hardness was same throughout the welded region within AA5083, whereas a minimum in hardness was noticed within the AA6082 welds. The position of the fracture clearly matched the region of lowest hardness. The weld thermal cycle significantly affected very fine scale precipitation in AA6082. The hardening precipitate had transformed into the non-hardening precipitate in the region of minimum hardness. This is perhaps is the important cause for the minimum hardness. Results were similar for similar experiments on aluminium alloy AA7075.

2.8.2 Tensile Properties

Publications related to the evolution of tensile properties of friction stir welded alloys of aluminium are plenty. Aydin et al. (2009) have investigated the tensile properties of friction stir welded joints of 2024 aluminium alloys in different heat-treated-states. They concluded that the tensile properties of the joints increase with precipitation-hardening of the base material and the tensile properties of the joints were all lower than those of the base materials or were equivalent to those of the base material, but lower elongation than that of the base material. From their experiments it is also implied that the tensile properties of these joints were not the same on the two sides of the weld centre, but the tensile properties on the advancing side (AS) were weaker than those on the retreating side (RS). Elangovan et al. (2008) worked on experiments for indicating

the effect of shape of tool pin and speed of tool rotation upon mechanical properties like tensile stress of friction stir welded AA6061 alloy of aluminium. The authors also showed that the joints prepared utilizing tool with square profiled pin, at a speed of tool rotation of 1200RPM produced better tensile properties when compared with tools with other types of tool pin shapes. The research studies done by Liu et al. (2017) on friction-stir-welded joints of 2017-T351 aluminium alloy for tensile properties and fracture locations showed that, the tensile properties and fracture locations of the joints are significantly affected by the welding process parameters. A maximum ultimate stress of the joints obtained was equivalent to 82% of that of the base material. It was also seen that, even though the voids-free joints fractured near or at the interface between the weld nugget and the thermo-mechanically affected zone (TMAZ) on the advancing side, the fracture occurs at the weld centre when the void defects exist in the joints. Sivaraj et al. (2014) in their research work discussed the influence of post weld heat treatment upon tensile properties of a joint of armor grade aluminium alloy AA7075-T651 made using friction stir welding. In their studies it was proved that the solution treatment followed by ageing heat treatment cycle was found to be slightly advantageous in improving the tensile properties of the joints of aluminium alloy AA7075-T651 plates prepared using friction stir welding. Sharma et al. (2012) did investigative studies on the effect of welding parameters on micro-structure and mechanical properties of friction stir welded joints of AA7039 aluminium alloy and proposed that, the tensile stress and other mechanical properties increase with decreasing welding speed / increasing rotary speed i.e. with increasing heat input per unit length of welded joint. It was also seen that, the high heat input joints fractured from Heat affected zone (HAZ) adjacent to thermo-mechanically affected zone (TMAZ) on advancing side, while low heat input joints fractured from weld nugget along zigzag line on advancing side. Jamshidi Aval (2015) during the due course of their research studies on influence of pin profile on the mechanical and microstructural behaviors on friction stir welded AA6082-AA7075 plate butt Joint, concluded that, the longitudinal samples show lower yield and tensile strengths than the base material itself. Also, a comparison of the micro-hardness profiles and longitudinal tensile strengths indicated that there is a correlation between the tensile stress of longitudinal specimens and the micro-hardness in different regions in the weld, since the stir zone shows less

71

hardness and strength than the base material. The longitudinal tensile specimens show greater strength than the transverse tensile specimens. Also, it was evident that, the strength of all samples continuously increased as the natural aging time increased. In each series of welds made using different tools, a decrease in weld pitch resulted in decreased strength of the welds and coarser grain sizes in the weld nugget. It was clear that the greater strength of samples welded using tool with increased weld pitch is related to adequate working of the plasticized metal in the stir zone of these samples in response to the pulsation effect of the pin profile. (Ahmed et al. 2017) conducted and presented the findings of their research on FSW of similar and dissimilar AA7075 and AA5083 aluminium alloys. They have published in their research journal that, the weld connection strength of the FSW welded weld connection of dissimilar aluminium alloy AA7075/AA5083 was observed to range as follows. The dissimilar joints exhibited ultimate tensile stress ranged between 245 and 267 N/mm^2 with weld connection efficiency ranged between 77 and 87% relative to the strength of AA5083BM and fracture strain ranged between 3 and 5.6%., under various welding conditions. As per the research findings of Silva et al. (2015), the FSW weld connection strength of AA6082-T6 alloy plates ranged between 45 and 76% of the AA6082 base material (BM) strength. The dissimilar FSW welded joints of AA6061/AA5086, as reported by Ilangovan et al. (2015), revealed up to 65% of the strength of the AA5086 base alloy. The weld connection strength of FSW welded AA2024 ranged between 76.7% and 94.6% of the AA2024 base alloy strength as reported by Aydin et al. (2009). The weld connection strength of FSW joined dissimilar AA6061-T6/AA7075-T6 alloys revealed 70% of the strength of the AA6061-T6 base alloy (Cole et al. 2014).

A research by Vidakis et al. (2016) on FSW of 2mm thick AA1050 alloy sheets revealed that welded joints had decreased tensile properties (ultimate strength, Young's modulus and strain) as compared to the parent material. The calculated ultimate stress values ranged from 57 to 91% of the base metal and the calculated strain values ranged from 25 to 43% of the base metal. The Young's modulus decreased as well. However, weld connection efficiencies ranged from 80 to 100% of the base metal. Liu et al. (2006) in his research work on 2219-T6 aluminium alloy discusses about the result of post weld heat treatment (PWHT) and infers that, the PWHT significantly influences the tensile

properties of the FSW joints. After the heat treatment, the tensile stress of the joints increases and the elongation at the fracture of the joints decreases. The maximum tensile stress of the joints is equivalent to 89% of that of the base material. The fracture location characteristics of the heat-treated joints are similar to those of the as welded joints. The defect free joints fracture in the HAZ on the retreating side (RS) and the joints with a void defect, fracture within the weld zone (WZ) on the advancing side (AS). From the research studies conducted by Takhakh and Abdullah (2012), on FSW of Al3003H14 aluminium alloy, the following conclusions could be arrived at. The mechanical properties of Friction stir welded aluminium alloy are influenced by process parameters. Hardness drop was observed in the weld region. The softening was mostly evident in the nugget zone because that Al3003H14 is a strain hardened tempered non-heat-treatable alloy. The optimum efficiency for joints was 89% of the ultimate tensile stress of the base metal. Dong et al. (2013) by way of their FSW experiments on 6005A-T6 aluminium alloy showed that, the tensile properties of FSW joints have an increased tendency with increasing the welding speed. The weld connection efficiency ranges between 71% and 80%. The results FSW experiments conducted by Liu et al. (2003) on aluminium alloy 1050-H24 showed that, the degree of softening and tensile properties of the joints are significantly affected by the welding process parameters, such as welding speed and speed of tool rotation. The maximum tensile stress of the joints obtained is equivalent to 80% of that of the base material. Trueba et al. (2015) by way of their FSW investigations on aluminium alloy 6061-T6, have shown that a FSW tool having a raised spiral design shoulder, produces a weld with a best combination of surface quality and mechanical properties like tensile stress etc. Svensson et al. (2000) based on their investigative studies on FSW of aluminium alloys AA5083 and AA6082 and have demonstrated that, in alloy AA5083 fracture usually happened near the centre of the weld, whereas AA6082 usually fractured in the heat affected zone. The tensile strength of joints made using FSW in aluminium alloy AA6082 was less than the strength of the parent material and the position of the fracture always coincided with the region of minimum hardness. The weld thermal cycle significantly influenced the very fine scale precipitation in AA6082 aluminium alloy. The hardening precipitates had transformed to the non-hardening precipitates in the region of least hardness. This is perhaps the main cause for the reduced tensile strength. Results were comparable for

a similar study on AA7075 alloy of aluminium. Table 2.3 presents the mechanical properties of friction stir welded aluminium alloys.

Table 2.3 Mechanical properties of friction stir welded aluminium alloys.

Sl. No.	Base Material	Base Material UTS (N/mm^2)	Joint Yield Strength (N/mm^2)	Joint UTS (N/mm^2)	Percentage Elongation (%)	Joint Efficiency (%)	Reference
1.	2014-T651	483	330	445	10	92.2	Dawes et al. 2000; Dracup and Arbegast (1999); Kadaganchi et al. (2015)
2.	2024-T3	478	290	425	14	90.0	Kubit et al. (2018); Magnusson et al. (2000); Sutton et al. (2002)
3.	2024-T351	493	348.9	434	17.5	90.0	Dracup and Arbegast (1999); Strombeck et al. (2000)
4.	2024Al /7075Al	475/ 595	277.2	405.1	5.6	81.9	Cederqvist and Reynolds (2001); Jung et al. (2009)
5.	2195-T8	593.0	355	406.8	8.4	69.0	Dracup and Arbegast (1999); Zhang et al. (2018)
6.	2219-T87	475.8	310.3	334	6.4	65.0	Dracup and Arbegast (1999); Zhao et al. (2017)
7.	2519-T87	480	278	379	10.5	79.0	Liang et al. (2012); Sabari et al. (2016)
8.	5005-H14	185	93	118	11	75.0	Khaled (2005); Strombeck et al. (1999)
9.	5083-O	298	140	344	10	119	Dawes et al. (1996, 2000); Dracup and Arbegast (1999); Han et al. (2009);Svensson et al. (2000)
10.	6013-T4	320	247	300	8.7	94.0	Heinz and Skrotzki (2002); Guoliang et al. (2010)

11.	6013-T6	375	207	322	81	64.0	Derry and Robson (2008); Heinz and Skrotzki (2002)
12.	6056-T78	332	158	247	5.9	74.0	Denquin et al. (2002); Lafly et al. (2006)
13.	6061-T6	324	162	252	7.2	79.0	Dracup and Arbegast (1999); Strombeck et al. (2000)
14.	6061-T6 to 5083-O	280	184	200	8.7	71.4	Jannet et al. (2014); Kim et al. (2008)
15.	6061 to 7050	310/524	137	193	8.2	62.3	Rodriguez et al. (2015)
16.	6063-T5	216	122	162	9.5	72.0	Sato et al. (2001); Tra et al. (2012)
17.	6351-T6 to 5083-H111	310/308	204	273	14	88.0	Palanivel et al. (2012, 2014)
18.	7020-T6	385	240	352	12.2	84.0	Golezani et al. (2015); Strombeck et al. (1999)
19.	7050Al	515	270.3	394.4	5.0	73.9	Kamp et al. (2009)
20.	7050-T7451	558	304	429	6.0	81.0	Dracup and Arbegast (1999); Hirsch and Lücke (1988)
21.	7075-T7351	472.3	422.0	455.1	10.8	96.0	Colegrove and Shercliff (2003); Dracup and Arbegast (1999)
22.	7075Al-T7451	524	470.2	533.7	13.5	98.1	Paglia et al. (2007); Zhou et al. (2016)
23.	7075-T651	622	365	468	15	75.0	Ouyang and Kovacevic (2002); Shah and Badheka (2016)
24.	7475-T76	490	407	465	92	94.9	Donne et al. (2000); Sutton et al. (2002)

2.9   PREDICTION, OPTIMIZATION AND ANALYSIS TECHNIIQUE

The most critical point in solving engineering problems is modelling and analysis of the correlation between input and output parameters. In general, there are two crucial modelling techniques used. They are known as analytical and empirical models.

Empirical models are further bifurcated into statistical model and neural network models.

2.9.1 Tensile Properties

Statistical model uses determined form (polynomial form) and parameterization (fixed in parametric form). In this process, the goal is to obtain measure of both complicity and particular fact in a data set. Several techniques have been proposed by the researchers to improve the weld connection efficiency of the friction welded materials to meet the required weld connection strength. In the case of FSW of aluminium alloys, the weld connection strength depends on the process parameters like; tool material, tool geometry, tool pin shape, tool tilt angle, tool axial thrust, tool rotatory speed, welding speed etc. (D'Souza et al. 2019; Krasnowski et al. 2015; Krishna Pal Singh Chauhan 2017; Meshram S. 2018; Murthy et al. 2018; Nik et al. 2017; Prabhu et al. 2016; Sharma et al. 2012; Shashi Kumar et al. 2016; Yang et al. 2012). Nowadays, focus is concentrated on how to increase the weld connection efficiency by adapting the prediction and optimization techniques (Jayaraman et al. 2009a; Pang et al. 2014; Rambabu et al. 2015). (Jayaraman et al. 2009a) have developed second order polynomial equation to predict and analyze the effect of method variable on UTS of the cast aluminium alloy A319, joined using FSW process. They have reported that the speed of tool rotation is the most predominant factor in prediction model followed by welding speed, while the axial force is the least significant factor to predict the UTS. (Lakshminarayanan and Balasubramanian 2008) have reported that optimization of process parameters of friction stir welded RDE-40 aluminium alloy can be achieved using Taguchi technique. The selected process parameters were speed of tool rotation, welding speed and axial force. Report reveals that, optimization method has been successfully implemented to automate the FSW process. The tensile stress was at maximum when speed of tool rotation, welding speed and axial force at level 2 of the method with 3 levels. The percentage contribution of the parameters was as follows, with speed of tool rotation at the top, the welding speed being the second and axial force being the last. (Palanivel et al. 2011) have also investigated effect of process parameters, on UTS of friction stir welded AA6351 aluminium alloy, using

mathematical model. Input process parameters considered are speed of tool rotation, welding speed and axial force. The increase in the speed of tool rotation, welding speed and axial force leads to the increase in the ultimate tensile strength; and it reaches a maximum value and then decreases. This trend is common for yield stress and percentage of elongation. Similar outcome is also justified by Heidarzadeh et al. (2012) for joints prepared by friction stir welding of AA6061-T4 aluminium alloy, Shanmuga Sundaram and Murugan (2010) for joints prepared by friction stir welding of AA2024-T6 and AA5083-H321 aluminium alloys, (Babu et al. 2009) for joints prepared by friction stir welding of AA2219 alloy of aluminium and Palani et al. (2015) for joints prepared by friction stir welding of AA8011 alloy of aluminium. Multi objective optimization of FSW parameters, for joining of dissimilar AA5083/AA6063 aluminium alloys using hybrid approach was reported by Gupta et al. (2018). A multi objective optimization of parameters of FSW process called grey relational analysis has been used to optimize the weld parameters in FSW of AA8011 for multi performance characteristics namely tensile strength, micro-hardness and power consumption by Ghetiya et al. (2016). Senthil et al. (2020) carried out multi objective optimization of the FSW method using Response Surface Methodology (RSM) based desirability function approach for joining aluminium alloy AA6063-T6 pipes. Kasman and Yenier (2014)have reported that full quadratic multiple regression equation could be used to analyze the relation between input parameters and output parameters of FSW of AA5754/AA7075 aluminium alloys. It has showed linear and square relationship between response control factor and response parameters. Kasman and Yenier (2014) have used central composite design matrix to predict and optimize the process parameters during friction welding of dissimilar FSW of AA5754/AA7075 aluminium alloys. Similar studies were held by Babajanzade Roshan et al. (2013) on FSW method of AA7075 aluminium alloy.

2.9.2   Neural network model

Artificial Neural Network (ANN) was developed by Minsky at MIT. It has been extensively used as prevailing technique by researchers in various institutions, trades, and government organization to deciphering several problems like method control and

automation, signal/image processing, prediction of breakdown/malfunctioning of the system and production method optimization (Lim and Gweon 1999; Mohanty et al. 2013; Yousif et al. 2008; Zurada 1992). The motivation behind the recognition and implementation of ANN is due to its success in solving the nonlinear problems which have no relationship between input and output parameters (Tansel et al. 2010).

ANN is a data processing network, identifying the unknown dependency relationship between the input and output parameters. The ANN network is expressed by a number of interconnected information processing units. It is more suitable for predicting the behavior of huge complex and nonlinear systems with large number of input and output parameters. The prediction system is purely based on mapping capacity obtained through the architecture of the network and learning system adopted to train the network with experimental input and output data. The network acquires the knowledge by investigating the patterns during training of the network (input and their corresponding output data), and then the network is able to use this knowledge to predict the behavior of unknown input parameters. Based on the architecture, ANN`s are classified as single layer feed-forward network, Multilayer feed-forward neural network and Recurrent neural network (Das et al. 2015, 2019).

Manufacturing method is complex in nature and highly nonlinear. It consists of large number of input data and there is lack of relation between input and output using mathematical model to describe the behavior of the process. Only a few studies have been reported in the literature in the field of prediction of mechanical properties of Friction stir welded aluminium alloys using ANN. Dewan et al. (2016); Gupta et al. (2018); Muthu Krishnan et al. (2018); Shanavas and Dhas (2018); Shehabeldeen et al. (2019) attempted to predict the mechanical properties of friction stir welded aluminium alloys, using ANN model. Single layer feed-forward neural network with back propagation learning algorithm was used to train, test and predict the mechanical properties. The input parameters taken into consideration were speed of tool rotation and welding speed, and output parameters were yield strength, tensile strength, elongation, hardness at HAZ and hardness of the weld metals. A good correlation had been observed between the measured values and predicted values. (De Filippis et al. 2016; Shanavas and Dhas 2018; Yousif et al. 2008) have investigated the performance

of neural network using Gradient Decent (GD) and Levenberg-Marquardt (LM) learning method. LM learning algorithm uses 2nd order Taylor series performance index, and the GD learning algorithm uses 1st order approximation. Hence, LM learning showed better performance than the GD. Jayaraman et al. (2009); Khourshid et al. (2015); Lakshminarayanan and Balasubramanian (2009), have compared Response Surface Method (RSM) with ANN model for predicting the tensile stress of Friction stir welded aluminium alloy AA7039. Buffa et al. (2009); Fratini et al. (2009), investigated the prediction of average grain size during FSW method using ANN and FEM. The output values of the FEM model were fed into the ANN model to predict the output. Input parameters of the network are strain rate, plastic strain, temperature, and Zener Hollowman parameters. Feed forward with back propagation model was made use of to predict the grain size accurately. Further, the same model was used to check the predictability for lap weld connection and T joints, and found good predictability. Chiteka (2014); Weglowski (2013), reported that multilayer perception model had accurately predicted tensile stress using speed of tool rotation, welding speed and tool profile as input parameters.

2.10 DEFECTS IN FSW

Defects in any form adversely affect the functionality of a component. FSW is a solid-state welding process. Therefore, defects related to melting and solidification, like porosity, crack, deleterious phase, intermetallic phases etc. were completely eliminated. However, defects like pin hole, tunnel defect, worm holes, piping defects, less penetration depth, kissing bond were found in the weld region due to improper selection of process parameters (Balasubramanian 2008; Dickerson and Przydatek 2003; Kah et al. 2015; Khan et al. 2015; Lombard et al. 2008; Movahedi et al. 2012; Rui M. Leal 2004). Under optimum method condition, both material flow and energy balance were obtained. In hot working process, sufficient heat is generated to reduce the resistance of the material to deform. Meantime, heat will also influence the changes in the micro-structure like grain growth, recrystallization, grain reorientation and dissolution of strengthening precipitate. Chemical composition of the material plays a vital role in material resistance to deform and changes its micro-structure. Some

materials undergo changes in metallurgical characteristic at very low temperature, and some material does not undergo any changes until higher temperatures were attained. Too cold processing condition refers to nonbonding and void formation. Hot processing condition refers to excessive material flow and it leads to material expulsion like flash and unwanted degradation of mechanical properties (Casalino et al. 2014; Hovanski et al. 2015; Kumar et al. 2015c; Lakshminarayanan et al. 2009; Padmanaban and Balasubramanian 2009; Zhang et al. 2006).

Hot processing conditions are achieved in two ways. 1) The temperature generated is higher than the solidus temperature of the material. 2) Temperature generated approaches the solidus but the heat loss from the direct deformation region is sufficiently slowed down so as to result in unwanted thermal softening of the work material. This results in degradation of the mechanical properties of the welded materials (Lohwasser and Chen 2010). Due to excessive heat generated by the FSW process, the surface contains blisters or surface galling (Arbegast 2008; Leal et al. 2008). Further increase in the heat causes thermal softening of the material beyond the boundary of tool shoulder. Subsequently the tool shoulder, instead of confining the material, starts ejecting the material in the form of surface flash (Arbegast 2008; Kumar and Kailas 2008; Leitão et al. 2012; Mohamed M. Ghanem 2018; Palanivel et al. 2014). Hence, insufficient material available at the weld region leads to formation of defects near the surface region of the weldment. In some cases, due to excessive thermal softening during FSW which is carried out under thrust force instead of tool position control system, the material directly under the shoulder will no longer be able to withstand the axial thrust force acting on it. This leads to thinning of the material whereby material thickness reduces. Due to fixed length of the pin and thinning effect of the material, the pin may rub against the backing plate, which ruptures the material at the root of the weld and excessive material will spill out from the weld region in the form of flash (Chauhan et al. 2018; Kumari et al. 2015; Singh et al. 2011a). This is shown in the Figure 2.28 as "Excessive Flash". Excessive flow of soft material from shoulder driven region to pin driven region leads to formation of nugget collapse Adamowski et al. (2007) and Arbegast (2008), have reported that tunnel or worm defects occur due to insufficient or extremely high speed of tool rotation accompanied

with too low a thrust force which leads to inappropriate mixing of material. Chionopoulos et al. (2008) have reported that, the defects also occur due to improper design of the tool. Screw type of tool is able to join only few components as compared to conical type tool. Chen et al. (2019); Muthukrishnan and Marimuthu (2010); Shettigar and Manjaiah (2017) and Takhakh and Abdullah (2012) have reported that high speed of tool rotation and welding speed led to the formation of tunnel defect at the intersection of NZ and TMAZ. Elangovan et al. (2009); Jayaraman and Balasubramanian (2013) and Zhang et al. (2007), notified the development of tunnel defect in weld region and revealed that the tunnel defect is formed at higher as well as lower welding speed with higher speed of tool rotation.

Khan et al. (2015) and Oosterkamp et al. (2004) have notified the formation of kissing bond in FSW. The study revealed that development of the kissing-bond was due to the oxide layer break up. The breakup of oxide layer was due to inadequate stretch of the contact surfaces around the welding pin. Kadlec et al. (2015); Sato et al. (2005) and Zhou et al. (2006) observed the micro-structure around zigzag line in an FS-welded Al alloy using TEM. During the method of FSW, the oxide layer on the butt surface is fragmented into particles and the particles are distributed along the cross section of zigzag line. Chen et al. (2006) and Kumar et al. (2016), have investigated on the defects found in the FSW. The study revealed that the kissing bond was formed due to insufficient frictional force and heat generation. It is very difficult to find out kissing bond using non-destructive process. Sato et al. (2005) and Taheri et al. (2019), reported that the presence of kissing bond promotes cracks. Lack of penetration of the tool pin is observed due to insufficient plunging of the tool due having shorter tool length. Shorter tool length may be due to wearing out of the tool. The wormhole initiation near the bottom of the weld is due to increase in the welding speed with speed of tool rotation being held constant. At low processing temperatures, tools made of brittle materials will lead to the formation of warm holes. The size of the wormhole increases with the welding speed because of inadequate material flow towards the bottom of the weld. There are indications that the welding speed to speed of tool rotation ratio is an important factor in the formation of the wormhole defect Adamowski et al. 2007; Daniela Lohwasser and Zhan Chen 2010; Dinaharan et al. 2012; Rajakumar et al. 2011;

Sharma et al. 2012b; Shettigar and Manjaiah 2017, have identified various defects which are presented in Figure 2.28. They concluded that the square shape of tool pin has higher eccentricity and produced least defect content in the weld. The eccentricity is described as the ratio of the dynamic volume swept by the tool to the static volume of the tool. The flat faces led to a pulsating action which in turn led to more effective stirring.
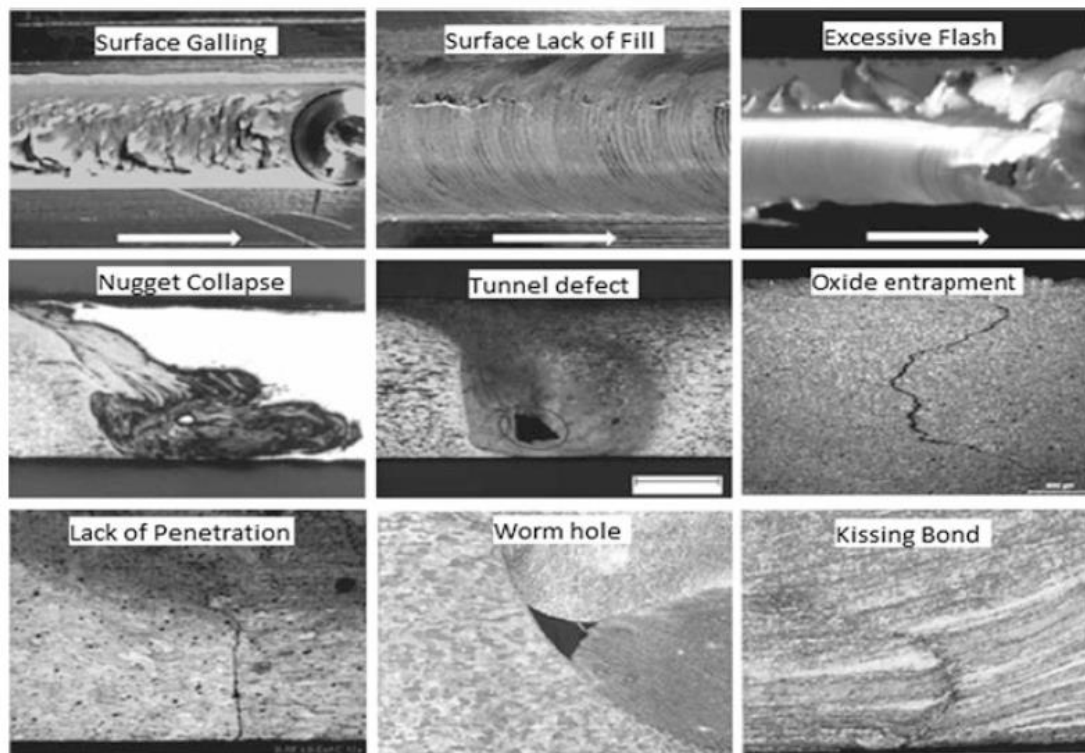
Figure 2.28 Types of defects in friction stir welded joints (Courtesy: Daniela Lohwasser and Zhan Chen 2010; Shettigar and Manjaiah 2017)

2.11 APPLICATIONS OF FSW (Courtesy : (Mishra and Ma 2005)(Threadgilll et al. 2009)(Dursun and Soutis 2014)

2.11.1 Shipbuilding and marine industry

The shipbuilding and marine industries were the first industry sectors which have opted and adopted the method for commercial applications (Midling and Oosterkamp 2009; Midling et al. 1999). The method is suitable for the following applications:

- Offshore accommodation
- Marine and transport structures
- Panels for decks, sides, bulkheads, and floors
- Aluminium extrusions
- Helicopter landing platforms
- Refrigeration plant
- Masts and booms, e.g. for sailing boats.

2.11.2 Aerospace industry

Now, aerospace industry is fabricating prototype and production parts by FSW (Heinz et al. 2000; Starke and Staleyt 1996; Wanhill 2013). Opportunities exist to weld skins to spars, ribs, and stringers for use in military and civilian aircraft. The Eclipse 500 aircraft, in which ~60% of the rivets are replaced by friction stir welding. This offers significant advantages such as reduced manufacturing costs and weight savings compared to fabrication and machining from solid. Longitudinal butt welds in Al alloy fuel tanks for space vehicles have been friction stir welded and successfully used. The method could also be used to increase the size of commercially available sheets by welding them before forming. The FSW method can therefore be considered for:

- Wings, fuselages, empennages
- Cryogenic fuel tanks for space vehicles
- Aviation fuel tanks
- External throw away tanks for military aircraft
- Military and scientific rockets

- Repair of faulty MIG welds
- Various primary and secondary structural components

2.11.3   Railway industry

The bullet trains are made up of aluminium extrusions which can be welded by FSW such as goods wagons, rolling stock of railways, railway tankers, underground carriages, trolley cars (Kawasaki et al. 2000; Otsuka and On 2008).

2.11.4   Land Transportation industry

The FSW method is being opted by automotive companies for their commercial applications (Bassett and Birley 2000; Campbell and Stotler 1999; Thomas and Nicholas 1997). The applications are as follows:
- Chassis cradles
- Wheel rims
- Space frames
- Truck bodies
- Tail lifts for truck
- Mobile cranes
- Armor plate vehicles

2.11.5   Other industries

FSW can also be considered for:
- Electric motor housings (in production)
- Refrigeration panels
- Cooking equipment and kitchens
- Gas tanks and gas cylinders etc.

2.12   SUMMARY AND GAP IN KNOWLEDGE

This review of literature inferred that the aluminium alloys play a vital role in the applications requiring high strength and higher stiffness by weight compared to traditional structural metals and their alloys. The increase in the strength to weight ratio by addition of alloying elements to aluminium, improves the strength and is very useful in aerospace and automobile industries. Fusion welding of these alloys poses lot of difficulties due to formation of harmful intermetallic phases and segregation of precipitate particles. Research revealed that a square profile pin and threaded profile pin tool are the most promising tools for FSW of aluminium alloys. It is observed that very little research work has been carried out in the field of aluminium alloys and not much has been discussed about FSW of aluminium-cerium-silicon-magnesium (Al-Ce-Si-Mg) alloy of aluminium, which comes under the category of quaternary alloy. Hence, this alloy is taken up for investigation to study the effectiveness of FSW in joining them and to correlate the structure property relationships. Tool geometry plays a vital role in producing sound welds. Apart from the limited availability of information in open literature due to the proprietary nature of tool designs, it is known that a concave shoulder and cylindrical threaded pin are widely used for welding tool features. Although, there is some literature available on optimization of process parameters and prediction of output quality characteristics of friction stir welded joints of different aluminium alloys using design of experiments (DOE) techniques, there is little information available about the similar studies on Al-Ce-Si-Mg aluminium alloy. Hence the DOE technique has been selected for optimization of input process parameters and prediction of output quality characteristics of the FSW welded joint. Also, the FSW method being dynamic in nature, the Multilayer perceptron model will be ideal as a prediction tool. Not much has been done in applying MLP type ANN technique or any of its variants in analysis of FSW process.

The present work elucidates on the study of the influences of the welding and the process parameters on the microstructural changes and mechanical properties of joints prepared using friction stir welding Al-Ce-Si-Mg alloy of aluminium.

The present work elucidates on the study of influences of the welding and the process parameters on the microstructural changes and mechanical properties of friction stir welded Al-10Mg-8Ce-3.5Si and Al-5Mg-8Ce-3.5Si aluminium alloys.

2.13   STATEMENT OF PROBLEM

A design engineer involved in the construction of aerospace, automotive vehicles, and other structures, will be interested in the materials and processes with superior properties. New developments in the materials utilized in the aerospace and automotive industries have significantly improved the scope and opportunities within these areas. However, these developments also necessitate the use of complex methods like suitable joining technique. Joining is frequently essential in important structural parts that are exposed to both static and dynamic loads of high magnitude, needing maximum strength and durability.

The FSW method is essentially a solid-state technique for joining, possessing many benefits over traditional welding procedures. The decrease in weight and increase in strength are important factors in the automotive and aerospace industries. To utilize FSW in joining of important parts, it is necessary a have thorough understanding of the characteristics of friction stir welds exposed to loads of static and dynamic nature. A standard aluminium alloy that could be benefited from the application of friction stir welding / processing would be A356 (As-cast AlSiMg Alloy), which is used in the high-strength components in the aerospace and automobile industries because they offer a combination of high strength with good casting characteristics (Din and Campbell 1996; Ma et al. 2006; Zhang and Zheng 1996). However, some mechanical properties of cast alloys, in particular, ductility, toughness, and fatigue resistance, are limited by three microstructural features: porosity, coarse acicular Si particles, and coarse primary aluminium dendrites(Atxaga et al. 2001; Seniw et al. 2000). Because of these drawbacks, a new AlSiMg alloy has been developed with an addition of element Cerium. Al-Ce based alloys are highly castable across a broad range of compositions. Nano scale intermetallics dominate the micro-structure and are the theorized source of the high ductility. In addition, room temperature physical properties appear to be competitive with existing aluminium alloys with extended high temperature stability of

the nanostructured intermetallic (Sims et al. 2016). Hence, recently the usage of AlSiMg alloy with Cerium added has increased. In industrial scenario, these cerium-based alloys are normally riveted, laser welded, or MIG welded. But these procedures may add weight, may degenerate macroscopic properties, or may be expensive and unreliable, and deteriorate the strength. If sufficient research on FSW joints of aluminium alloy Al-Ce-Si-Mg is carried out, it could offer a cost-effective alternative to the above joining techniques.

In applications such as industries, the joints are exposed to complex forces and moments and a wide variety of environmental conditions. Besides complex loading situations, the friction stir welded joints produce extremely variable micro-structures with residual stresses that influence the material performance. Eventually, the combination of the static and dynamic loading and inherent material properties can cause failure of the weld connection more quickly than is anticipated. If all the environmental conditions and loads were considered together in a single test, segregation of factors that govern failure would be tough. Tests with both static and dynamic loadings were made use of to approximate the behavior of friction stir welds in practical applications. In this way, data pertaining to the performance of the weld connection was obtained for the two primary loading types. This information allows better understanding the behavior of friction stir welded parts.

The present report outlines the common production welding processes, identifies the problems associated with them, discusses the friction stir welding (FSW) method in detail and outlines its development. Al-Ce-Si-Mg aluminium alloy, which is difficult to weld by conventional welding processes was chosen for FSW study.

2.14   OBJECTIVES OF THE PRESENT RESEARCH WORK

The aim of this research study is to quantify the inter-relation between speed of tool rotation, welding speed, shape of tool pin and percentage of cerium in the alloy, and to correlate the evolution of micro-structure with mechanical properties using Taguchi technique. Using single approach method, the evolution of micro-structure at weld region of Al-Ce-Si-Mg aluminium alloy for different combinations of speed of tool

rotation, welding speed and shape of tool pin are analyzed. Looking at the on-going developments in FSW, the following objectives have been derived:

1. To elucidate the role of process parameters like speed of tool rotation, welding speed, shape of tool pin and work material composition for obtaining defect free welds in FSW of the following Al-Ce-Si-Mg aluminium alloys, namely, non-heat-treated Al-10Mg-8Ce-3.5Si and Al-5Mg-8Ce-3.5Si.

2. Microstructural analysis of alloys joined through FSW technique, to study the grain distribution and micro-structure at the welded zone and to assess the mechanical properties of the welded alloys.

3. To analyze and investigate the effect of process parameters on FSW of alloy through statistical methods, develop a suitable nonlinear regression model relating the effects of input process parameters on the output quality characteristics like ultimate tensile stress (UTS) of the weld joint and predict the UTS of the joint by statistical approach.

4. Formulation of a suitable Artificial Neural Network based model to simulate the relationship of FSW process parameters and their influence on hardness and weld joint strength of the aluminium alloys.

2.15 SCOPE

Based on the proposed objective, the scope for the research work in FSW of aluminium alloys includes:

1. Experimentally investigating the impact of process parameters like shape of tool pin, speed of tool rotation, welding speed on the tensile strength, hardness and weld joint efficiency of the friction stir welded aluminium alloys.

2. Exploring the possibility of microstructural studies to ascertain the type of micro-structure, grain size and grain distribution of the friction stir welded Ai-Ce-Si-Mg aluminium alloys and to device methods to study the mechanical properties such as hardness and ultimate tensile stress of friction stir welded aluminium alloy joints.

3. Analyzing and investigating the effect of process parameters on FSW of alloy through statistical techniques like Design of Experiments and developing suitable nonlinear regression equation to relate the effect of input process parameters on the output quality characteristics, namely UTS of the weld joint and predicting the UTS of the joint.

4. Developing of ANN with Multilayer Perceptron model to correlate the FSW parameters with hardness, ultimate tensile strength, and percent elongation of the aluminium alloys.

2.16   DIRECTIONS FOR FUTURE RESEARCH

The aim of present study is to form a knowledge base for the future research pertaining to static and dynamic performances of weld joints of aluminium alloy Al-Ce-Si-Mg, made using friction stir welding process. Developments in this field would pave way for the feasibility of using the friction stir welding method for the above aluminium alloy in the aircraft and automotive industries, leading to substantial reduction in cost of production and advances in component strength, over conventional welding techniques used with Al-Ce-Si-Mg aluminium alloys. This research work also has a secondary objective of deciding inter-relationships among the static and dynamic performances of butt-welded connections of the Al-Ce-Si-Mg aluminium alloy plates and the micro-structural features ensuing from diverse sets of parameters of the friction stir welding process.

CHAPTER 3

RESEARCH METHODOLOGY

INTRODUCTION

Literature survey presented in Chapter 2 reveals enormous amount of research work going on in the field of welding of aluminium and its alloys. As seen in the literature review a fair amount of work is going on in the field of joining of aluminium alloys using solid state technique. The present study focuses on the evolution of micro-structure at weld region during FSW of Al-Ce-Si-Mg aluminium alloy (Al-10Mg-8Ce-3.5Si and Al-5Mg-8Ce-3.5Si), as well as the effect FSW on weld connection strength. The investigation of mechanical properties of FSW joints obtained with various combinations of input (speed of tool rotation, welding speed and tool profile) is carried out at specific points of experimentation only, giving a glimpse of the potential of FSW of the said aluminium alloy. The user industry however needs more data, so that the method can be optimized based on either the control of the input parameters or the output parameters. The commercial acceptance of the technological breakthrough is Therefore, the problem at hand. The data, however, if expanded to include more combinations of the input parameters providing the corresponding mechanical properties as outputs, will become more useful to the ultimate user, that is, the industries. The optimization technique proposed, as discussed in Chapter 1 will provide the solution for improving the database for correlation of welding parameters with micro-structure and the resultant mechanical properties. An overview of the investigations carried out is categorized as follows:

- ❖ Arrangement and preparation of sample plates of Al-Ce-Si-Mg aluminium alloys, namely Al-10Mg-8Ce-3.5Si & Al-5Mg-8Ce-3.5Si and characterization of these alloy plates using Scanning Electron Microscope (SEM) and X-Ray Diffraction (XRD).

- ❖ Performing friction stir welding on aluminium alloy plates of Al-Ce-Si-Mg and then identifying the common range of defect free welds for different tool pin shapes, speeds of tool rotation and speeds of welding.
- ❖ Determining the consequent changes in microstructural and mechanical properties at the joint of the friction stir welded alloy plates, through Scanning Microscopy, hardness test and tensile test.

- ❖ Analysis of the effect of process parameters on mechanical properties by Taguchi type Design of Experiments technique.
- ❖ Prediction of mechanical properties of the aluminium alloy joints by using soft computing techniques.

Initially, arrangement of materials and design of tool are carried out, followed by planning of experiments for different stages mentioned above. A schematic representation of the overall methodology is as shown in Figure 3.1 and can be represented as graphical abstract in Figure 3.2. The details of the experiments to be carried out are presented in the subsequent sections.

3.1 MATERIAL PREPARATION

Recent survey shows that several methods have been employed for manufacturing of aluminium alloy. In the present research work, Aluminium-Cerium-Silicon-Magnesium alloy (Al-Ce-Si-Mg) is used as the experimental material for the research work of friction stir welding. These alloys were prepared by casting (Jayaraman and Balasubramanian 2013; Liu et al. 2004). The chemical compositions of the aluminium alloys Al-10Mg-8Ce-3.5Si & Al-5Mg-8Ce-3.5Si are listed in Table 3.1. The mechanical properties of the aluminium alloys Al-10Mg-8Ce-3.5Si & Al-5Mg-8Ce-3.5Si are listed in Table 3.2.

Al-Ce alloys were cast in binary composition of 6–16 wt.% Ce (Sims et al. 2016). Commercially pure aluminium ingots were melted and held at approximately 785°C.

Ternary and quaternary alloys with small Si and Mg additions were also prepared similarly. In the case of the binary and ternary alloy, cerium was added last, and melt could return to above temperature. The quaternary alloy was poured from the remaining heel of the alloy below. During cerium addition, a highly exothermic reaction was observed with the melt temperature rising almost 25°C in 5 min. This temperature increase is correlated with strong associative interactions between the Al and Ce atoms resulting in a high enthalpy of mixing that is typically associated with the formation of intermetallic compounds during solidification. The total mass of each melt was approximately 25 kg, and castings were poured into polymer bound sand molds at 785°C.
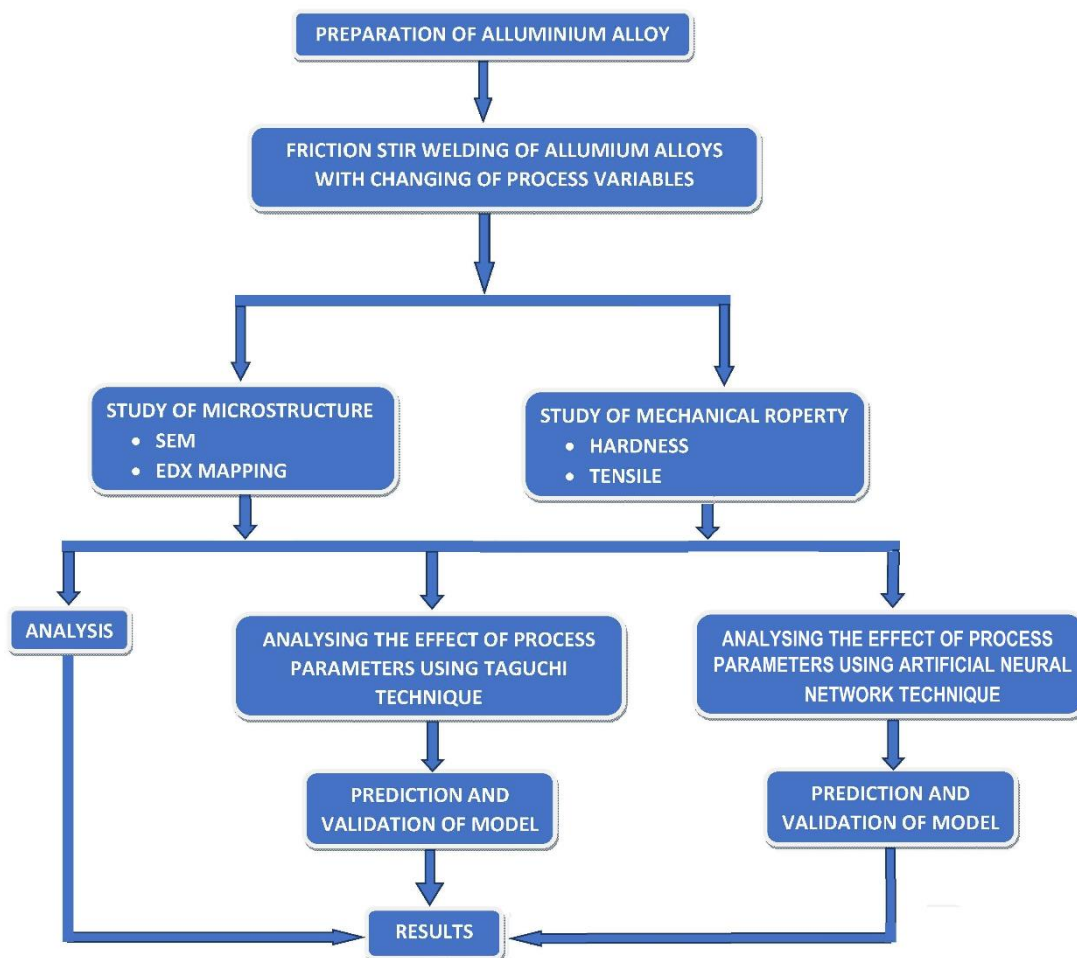
Figure 3.1 Schematic representation of the experimental methodology
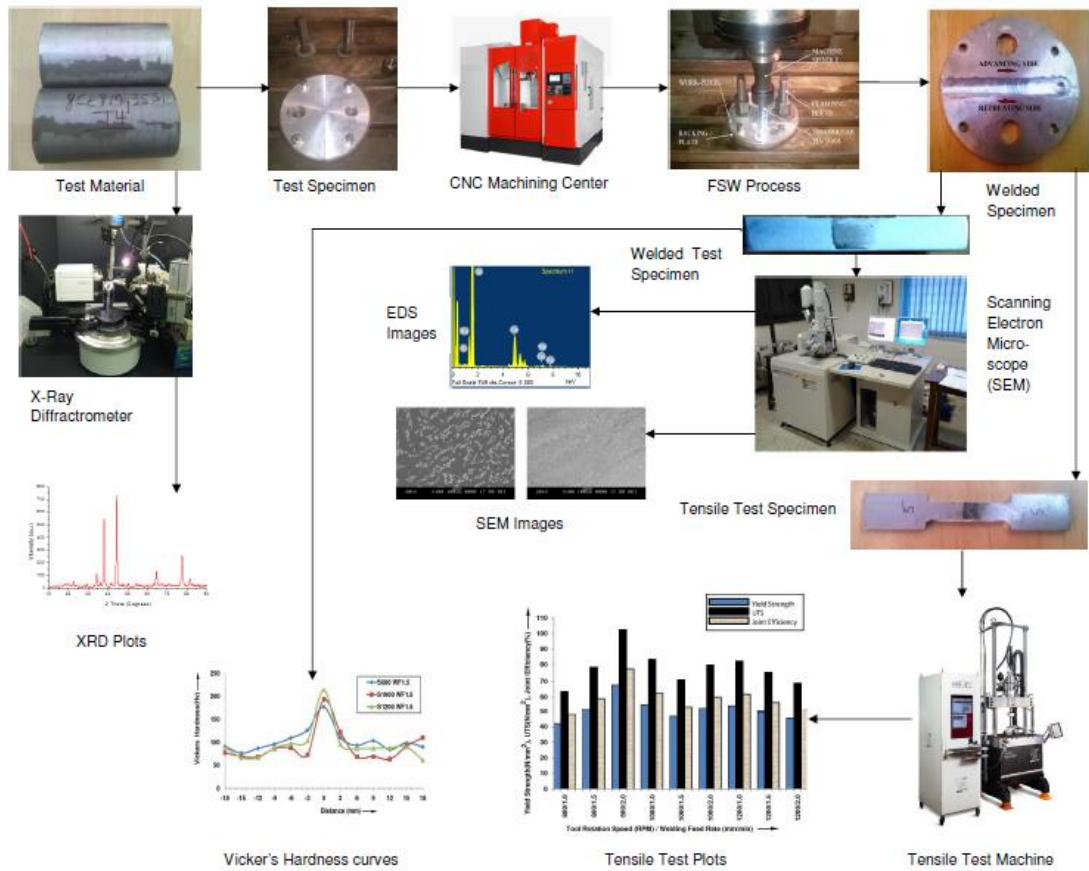
Figure 3.2 Graphical abstract of the experimental methodology

The quaternary alloy was made from the already formed ternary alloy. The alloy most compatible with existing casting practices is Al-12Ce, where the number preceding the alloying element is its concentration in weight percent (Sims et al. 2016). The two alloys used for research experiments are Al-10Mg-8Ce-3.5Si and Al-5Mg-8Ce-3.5Si which fall in the Al-Ce-Si-Mg group of alloys.

The cast aluminium alloy rods were machined to get the test plates of required shape and size with the help of a CNC machining Center.

Table 3.1 Chemical composition of aluminium alloy Al-10Mg-8Ce-3.5Si and Al-5Mg-8Ce-3.5Si

Alloy / Elements	Element percentages in alloy							
	Al	Ce	Si	Mg	Zn	Ti	Fe	Mn
Al-10Mg-8Ce-3.5Si	79.28	7.109	3.239	9.942	0.85	0.042	0.188	0.122
Al-5Mg-8Ce-3.5Si	82.48	8.003	3.821	5.016	0.142	0.39	0.309	0.191

Table 3.2 Mechanical properties of aluminium alloy Al-10Mg-8Ce-3.5Si and Al-5Mg-8Ce-3.5Si used for FSW

Alloy	Mechanical properties		
	Yield stress (N/mm^2)	Ultimate Tensile stress (N/mm^2)	Percentage Elongation (%)
Al-10Mg-8Ce-3.5Si	81.7	154.1	4.66
Al-5Mg-8Ce-3.5Si	78.4	146.7	6.34

3.2 FSW MACHINE

Based on the previous researches, it is inferred that the basic requirement of the FSW machine is similar to the milling machine (Klobčar et al. 2013; Manisegaran et al. 2018; Siddiqui et al. 2014). The welding tool must be mounted on spindle with variety of speed. The power required to drive the spindle must be minimum 5.5KW / 7.5HP. The spindle must be in vertical direction. The bed of the machine must be rigid and sturdy. The X-axis table movement must be automatic with variety of welding feed rates. Based on above parameters, vertical machining center with 5.5 KW power, maximum spindle speed of 8000 RPM range and infinitely variable feed rate of 0 to 600 mm/min has been selected. Figure 3.3 shows a vertical machining center machine used for friction stir welding.

Figure 3.3 Vertical Machining Center

3.3   EXPERIMENTATION

The material used in this study was Al-10Mg-8Ce-3.5Si & Al-5Mg-8Ce-3.5Si aluminium alloys. The abutting weld connection faces were secured by placing the plates on the steel backing plate (130 mm in diameter, and 10 mm in thickness) and clamping it firmly in order to prevent the plates from moving apart. The backing plate is required to resist the normal forces associated with friction stir welding. The friction stir method was carried out using a BFW CNC vertical machining center (Spindle power of 5.5KW). The FSW was carried out at different combinations of speeds of tool rotation and speeds of welding, using three different types of FSW tools.

The alloy Al-Ce-Si-Mg was produced by preparing a melt of pure aluminium, cerium, silicon magnesium and other elements as indicated in Table 3.1, under a controlled melting method in a crucible furnace and pouring it into metal molds to form the alloy in the shape of circular rods of diameter 130mm (Sims et al. 2016). The circular plates of thickness 6 mm were cut out of these circular rods and split equally along a centre

line into two equal semicircular plates. Suitable holes were drilled in these plates for clamping them onto the machine table along with the backing plate as shown in Figure 3.4.

MACHINE TABLE

PLATES TO BE JOINED

HOLES FOR CLAMPING TO M/C TABLE

JOINING LINE

BOLTS FOR FIXING TO BACKING PLATES
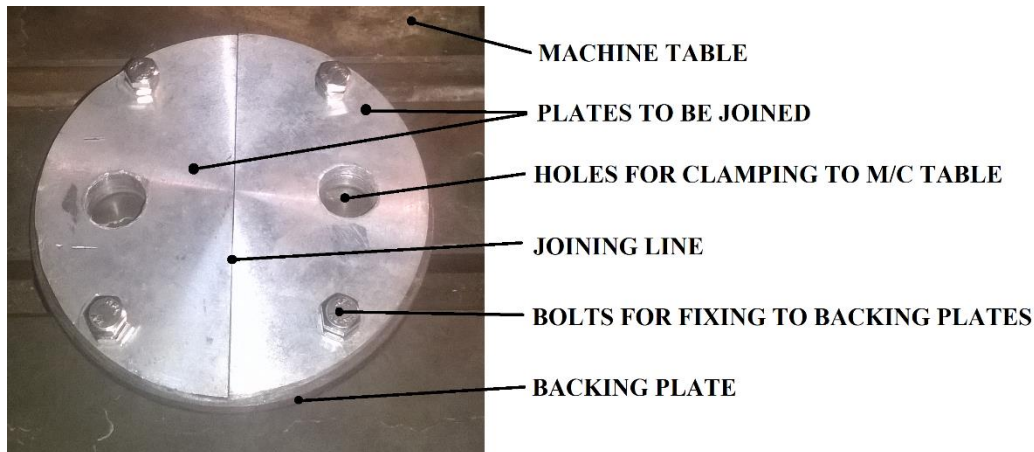
BACKING PLATE

Figure 3.4 Experimental material plates for FSW

The abutting weld connection faces were secured by placing the plates on the steel backing plate and fixing with screws, in order to prevent the plates from moving apart. The backing plate is required to resist the normal forces associated with friction stir welding. The friction stir method was carried out using a BFW milling machine (5.5KW). The FSW process was conducted at different combinations of speed of tool rotation, welding speed, and using three different types of FSW tools.

To carry out the FSW operation on the plates clamped on to the machine table, the rotating tool is plunged into the abutting edges of the plate till the tool shoulder touches the surface of the workpiece with sufficient axial force. To attain the required frictional heating, the tool was held at the initial plunge position, with shoulder touching the surface of the work, for a dwell period of 15 seconds. Then, the machine table was made to move at a pre-determined welding speed. The method resembles the end milling operation with the rotating tool travelling along the weld connection line with circular ripples over the work surface. The tool is retracted as soon as the plunged tool

96

reaches the extreme end of the weld connection (Kumar and Kailas 2008; Perovic et al. 2012; Sidhu and Chatha 2012; Thomas and Nicholas 1997).

The weld so formed would will be hot, necessitating a cooling period of 20 minutes at the clamped condition (Altenkirch et al. 2008b; R. Nandan et al. 2008). Then the welded workpiece was removed, and a new set of workpieces is clamped for subsequent welding. The combination of speed of tool rotation and welding speed adopted to carry out FSW operations are listed in Table 3.3.

Table 3.3 FSW Experimental schedule

		Speed of tool rotation (RPM)					
		600	800	1000	1200	1400	1600
Speed of welding (mm/min)	5	✓	✓	✓	✓	✓	✓
	8	✓	✓	✓	✓	✓	✓
	10	✓	✓	✓	✓	✓	✓
	15	✓	✓	✓	✓	✓	✓
	20	✓	✓	✓	✓	✓	✓
	25	✓	✓	✓	✓	✓	✓
	30	✓	✓	✓	✓	✓	✓

3.4 TOOL DESIGN

Three types of tool geometries were selected for experimentation based on the literature survey and a new type of tools were designed to study the effect of different pin profiles. The plasticized material flow path is enhanced by adding features to the pin (Hasan et al. 2018; Marzbanrad et al. 2014; Zettler et al. 2005). They have reported that, enhancement in mixing capacity of a given geometry is achieved due to the changes in the swept volume to static volume ratio. Swept volume refers to the volume being swept by the pin while rotation and static volume corresponds to the actual volume of the pin. The ratio of the swept to static volume of square pin profile is 1.57 (Ilangovan et al. 2015b; Shettigar and Manjaiah 2017a). Similarly, for a straight thread pin profile, it is 1.09 (Gharaibeh et al. 2016; Herbert et al. 2016; Jain et al. 2015; Thube 2014). Left

hand threaded pin profile when rotated in clockwise direction, results in the material being drawn in the downward direction by the threads along the pin surface. This phenomenon leads to improved mixing action (Elangovan and Balasubramanian 2008a; Zhang et al. 2012). Aluminium alloy welded with square and triangular pin tool profiles have shown good quality of weld with higher ultimate tensile stress and lower yield stress at low welding speed. These pins because of their straight plane surfaces, produce pulsating effect, which led to the reduction in grain size (Elangovan et al. 2008b). The round tool pin shape also shows moderately good results. Based on these outcomes, the triangle, square and round pin profiles have been chosen to get good quality of weld with improved ultimate and yield strengths. The height of the pin should be a little less than the weld depth or depth of workpiece. The depth of the workpiece is 6 mm. Hence, height of the pin is taken as 5.7 mm (Threadgilll et al. 2009; Verma and Misra 2015; Zhao et al. 2006). The most commonly used shoulder diameter range varies from 2.5 to 3 times the thickness of the plate for aluminium alloys (Arora et al. 2012; Mehta et al. 2011). In most of the cases, diameter to pin ratio was used in the analysis of FSW joint. Hence shoulder to pin diameter ratio is kept at 2.5 and shoulder diameter to thickness of the plate is maintained at 2.66. Since CNC vertical machining center is used to perform welding operation, the shoulder is designed to be of concave shape, with an inclination of 7° to the perpendicular to the axis of rotation of the tool (Casalino et al. 2014; Hasan et al. 2013; Leal et al. 2008; Murthy et al. 2018; Scialpi et al. 2007). It serves as an accumulator and generates sufficient heat during welding. In-order to avoid the overheating and under heating, the shoulder and pin diameter ratio has to be maintained which will be less than 4 and more than 2 (Ahmed et al. 2017; Babu et al. 2017; Khan et al. 2015a; Ugender et al. 2014). The height of the shoulder should be more than the diameter of the shoulder, which helps to remove heat at a faster rate during and after the welding (Liu et al. 2005). The other end of the tool must contain proper holding facility. The tool material must comprise properties like withstanding impact load during plunging, high temperature resistance, compressive load and wear resistance (Amini et al. 2014; Debroy et al. 2012; Kumar et al. 2016b). Hence High carbon high chromium steel (HCHCr) type tool steel material (M2 tool steel) with 60±2 HRc case hardened, has been selected since it possesses most of the above referred properties. The coefficient of the friction 'μ' is mainly reliant on the

hardness of the FSW tool. The coefficient of the friction 'μ' and the friction occurred between the tool and base material is directly proportional to each other. Therefore, it can be interpreted that the tool hardness will decide the heat generated in the FSW method (Rajakumar et al. 2011). The strength of the weld connection is entirely dependent on the heat generated at the weld zone. If heat generated at weld region is inadequate, then it leads to the deterioration of the strength of the joints. The increase in the heat produced at weld region will lead to the formation of defects on the retreating side of thermo mechanically affected region (TMAZ), in turn instigating the grain growth and thus causing in severe clustering of the precipitates at NZ. This results in generating lower hardness at NZ. Rajakumar et al. (2011) reported that the superior strength was attained when the joints were fabricated using tool hardness ranging from 45 HRc to 55 HRc. The details of various heat treatment processes adopted in practice are discussed below (ASM-Volume 4A, 2013).

3.4.1 Heat treatment of tool

With proper selection of heat treatment, HCHCr (High Carbon High Chromium) type M2 tool steel material can be used as FSW tool material for joining of the aluminium alloys using FSW process. Steel in annealed condition mainly consists of ferrite and alloy of carbides. These structures can be transformed into martensitic structure to provide necessary tool properties, by adopting appropriate heat treatment or hardening process. Based on the heat treatment process, it can be divided into following areas (ASM-Volume 4A, 2013).

3.4.1.1 Preheating

Preheating method does not involve any hardening reaction from metallurgical point of view. But however, it serves three main purposes which are discussed below (ASTM-Volume 16).

(1) Reduction of thermal shock: When cold tool is placed inside the warm or hot furnace, thermal shocks are produced. By reducing the thermal shock, the hazards and

undesirable distortion or cracking are minimized. It also releases some of the stresses developed during machining and/or forming process.

(2) It also helps in increasing the productivity of the equipment by reducing the amount of time of exposure in the ease of high-heat furnace.

(3) In case high-heat furnace is not neutral to the surface of tool, preheating of tool in high-heat furnace will result in reducing the amount of carburization and decarburization.

In case of commercial salt bath hardening process, preheating of the high-speed tool is conducted in two stages. Initial stage of preheating is carried out for temperature range between 650ºC and 760ºC. At final stage, preheating temperature range is maintained between 815ºC and 900ºC. In vacuum heat treatment process, the furnace is heated slowly from 790ºC to 845ºC in single stage.

In this study, the fabricated tools were preheated in resistance type electric furnace under two-step preheat method. In the first step, the fabricated tools were heated to a temperature of 650ºC for a soak time of 10 minutes and in the next step, the preheat was carried out at 900ºC and soaked at that temperature for 15 minutes.

3.4.1.2   Austenitizing (Hardening)

Austenitizing is a second stage heating method and, it is time / temperature dependent reaction. Austenite begins to form at about 760°C, and preheating to a temperature slightly above this, will minimize the stresses that might be cropping up because of the transformation. The properties of high-speed tool steels are influenced by dissolving of various complex alloy carbides during Austenitizing. These alloy carbides do not dissolve to any appreciable extent unless the steel is heated to a temperature within 28°C to 56°C of their melting point. This temperature is dependent upon the particular high-speed tool steel being treated and is in the range of 1150°C to 1290°C. Approximately 2 to 6 min of holding time is generally recommended for high-speed tool steel, depending upon the type of high-speed tool steel, tool configuration,

and cross-sectional size. Lowering of the hardening temperature (under hardening) usually improves the impact toughness while lowering the hot hardness. As the hardening temperature is raised, both the heat-treated room-temperature hardness and hot hardness increase.

In this study, the pre-heated HCHCr M2 tool steel FSW tools were heated to an austenitizing temperature of 1220°C with a soak time of 5 minutes.

3.4.1.3   Quenching

The quenching or cooling of the workpiece from the austenitizing temperature is designed with the objective of transforming the austenite formed at high temperature to a hard-martensitic structure. The rate of cooling, which must be controlled, is dictated by the analysis of the particular steel. Sometimes, high-speed steels are quenched in two steps, initially in a molten salt bath maintained at approximately 540°C to 595°C or an oil quench, followed by air cooling to near ambient temperature. The simplest of quenching is cooling in air, where again only tool steels with smaller and / or thinner cross sections would air quench rapidly.

In this study, the hardened tools were allowed to cool using compressed air. Figure 3.5 shows time versus temperature plot showing sequences required to properly heat treat high-speed tool steels (ASM_Handbook_Vol-16, 1995, Page 120)

3.4.1.4   Tempering

Tempering serves to relieve the stress and transform retained austenite of the quenching step to fresh martensite. Secondary hardness is enhanced further owing to the occurrence of some precipitation of complex carbide. It is this method of transforming retained austenite and tempering of newly formed martensite that dictates a multiple tempering procedure. High-speed tool steels require tempering of 2 to 4 times for a soak time of 2 to 4 hours each. As with austenitizing temperatures and quenching rates, the number of tempers is decided by the specific grade.
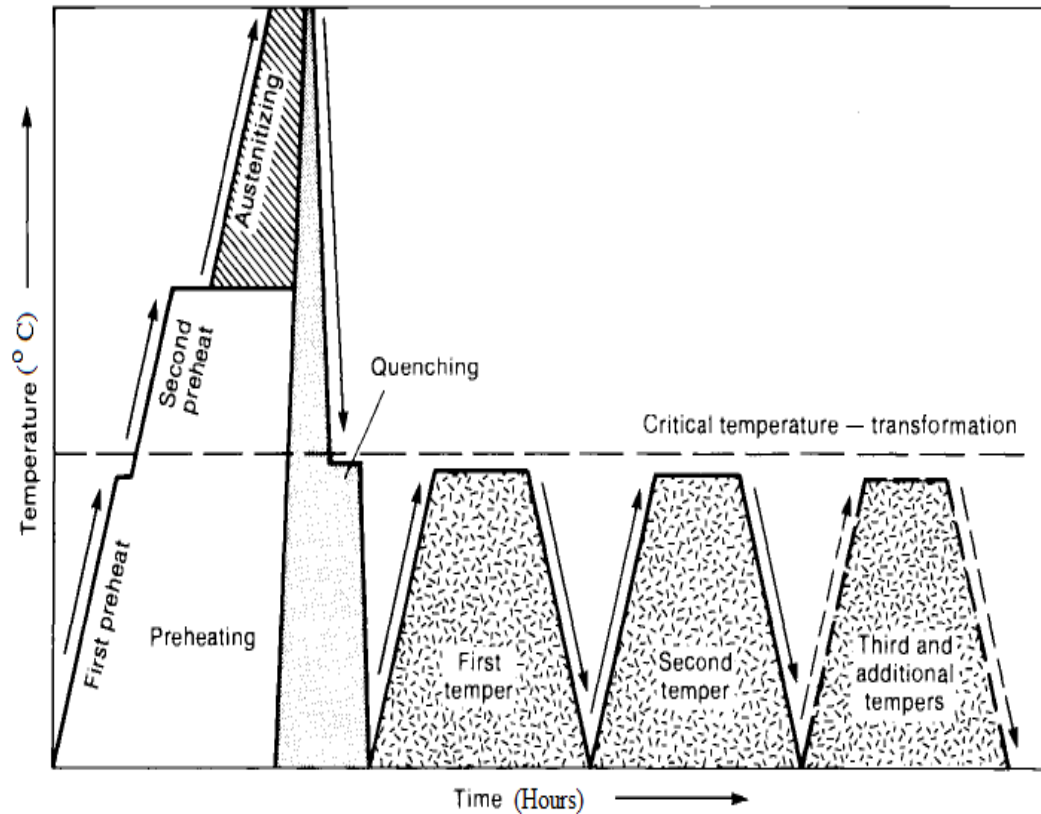
Figure 3.5 Time versus temperature plot illustrating sequences required to properly heat treat high-speed tool steels (Courtesy: ASM_Handbook_Vol-16, 1995, Page 120)

Figure 3.6 shows the tempering curve for HCHCr M2 tool steel. Hardening optimizes the transformation of retained austenite to fresh martensite during the tempering sequence. The right (higher) side of the secondary hardness peak curve, shown in Figure 3.6 should be preferred, and the left (lower) side is avoided. In this study, the used FSW tools were triple tempered at 650°C at a soak time of 2 hours followed by oil bath quenching. Hardness achieved was 60±2 HRc.

In this study, 3 types of tool are fabricated, and heat treated to attain a tool hardness of 60±2 HRc. Figure 3.7 is a schematic representation of FSW tools. (Triangle, square and round pin profile tool). Henceforth, Triangular Profile Pin tool is represented by TPP, Square Profile Pin tool represented by SPP and Circular / Round Profile Pin tool represented by CPP. Figure 3.8 shows the FSW tool after heat treatment and tempering.
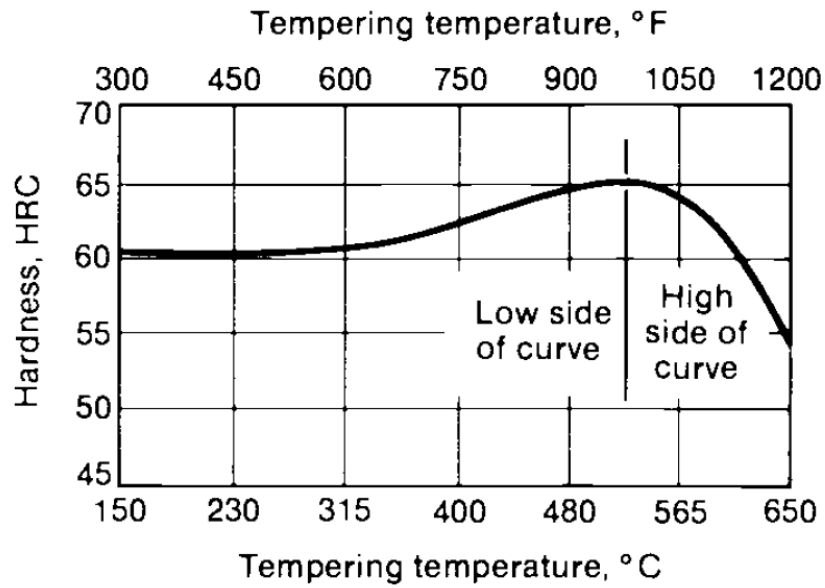
Figure 3.6 Tempering curve for HCHCr M2 tool steel (Courtesy: ASM_Handbook_Vol-16, 1995, Page 122)
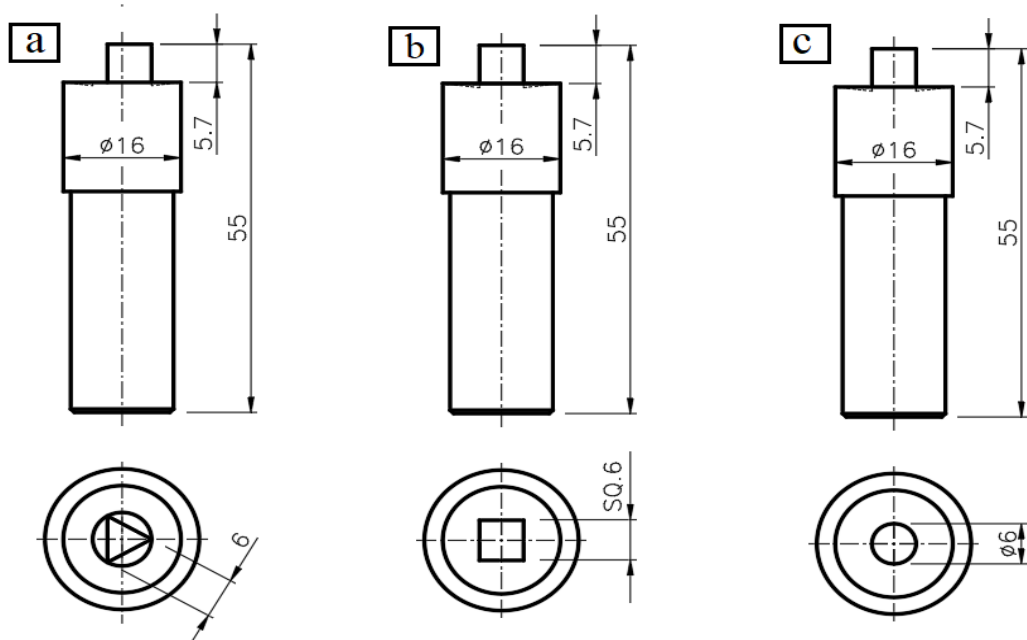
Figure 3.7 Schematic drawings of FSW tools (a) Triangular profile pin (TPP), (b) Square profile pin (SPP) and (c) Circular / Round Profile Pin tool (CPP)

103
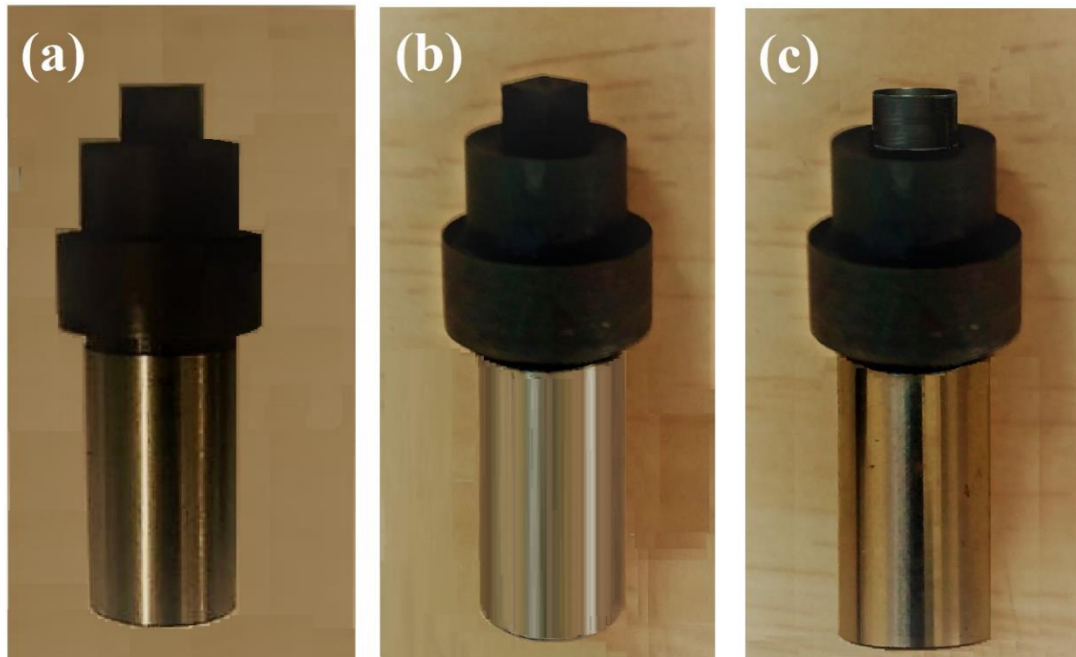
Figure 3.8 Photographs of fabricated and heat treated FSW tools with (a) Triangular profile pin (TPP), (b) Square profile pin (SPP) and (c) Circular / Round Profile Pin tool (CPP)

3.5   FIXTURE DESIGN

The primary purpose of a fixture is to reduce the setting time of the specimen during operation. The fixture was designed in such a way that it has to hold the specimen rigidly and should facilitate quick changing of the part. The type of the weld connection is butt joint. There is no constraint on the length or diameter of the specimen. Because the aluminium alloy is supplied in 130 mm diameter rods, the weld specimens were made as circular plates of diameter 130 mm. There was no separate fixture made for this purpose. Instead, a circular backup plate of diameter equal to the specimen was provided as support to the abutting semicircular plates to be friction stir welded. These test plates were clamped to the backup plate using four bolts as shown in Figure 3.9. The aluminium alloy plates which are to be welded along with the backup plates are rigidly clamped to the machine table using T-bolts using two numbers of holes provided in the weld and backup plate assembly. The purpose of backing plate is to support the workpiece during welding. The backing plate is made of mild steel. The upward lifting

and lateral movement of the plates during welding is arrested by the T-bolts provided for clamping the plate assembly to the machine table. The entire welding setup has been illustrated in the Figure 3.4.
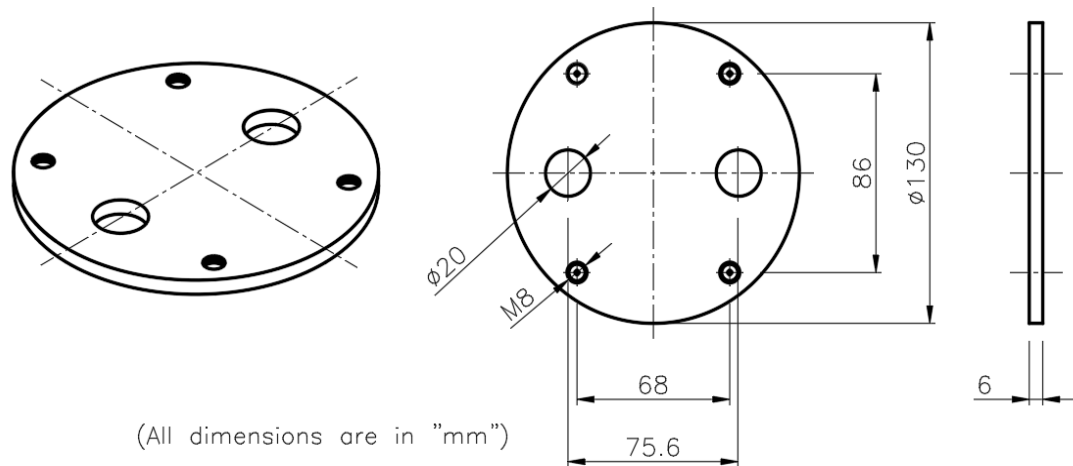
Figure 3.9 Schematic sketch of the backup plate used to support FSW plates

3.6   SECTIONING OF TEST SPECIMENS OF Al-Ce-Si-Mg ALUMINIUM ALLOY WELD CONNECTION FABRICATED THROUGH FRICTION STIR WELDING

Figure 3.10 illustrates the way in which the Al-Ce-Si-Mg aluminium alloy plate joined through FSW method, is sectioned and shaped to obtain the specimens for microstructural characterization, tensile testing, and hardness studies. The surfaces selected for the microstructural study and hardness measurements were selected across the weld connection and perpendicular to the direction of welding. The samples were cut using wire EDM (Electrical Discharge Machine) of Suzhou Baoma Make, Servo Control High Quality Wire Cut EDM machine Model-BM400C-CT as depicted in Figure 3.11.
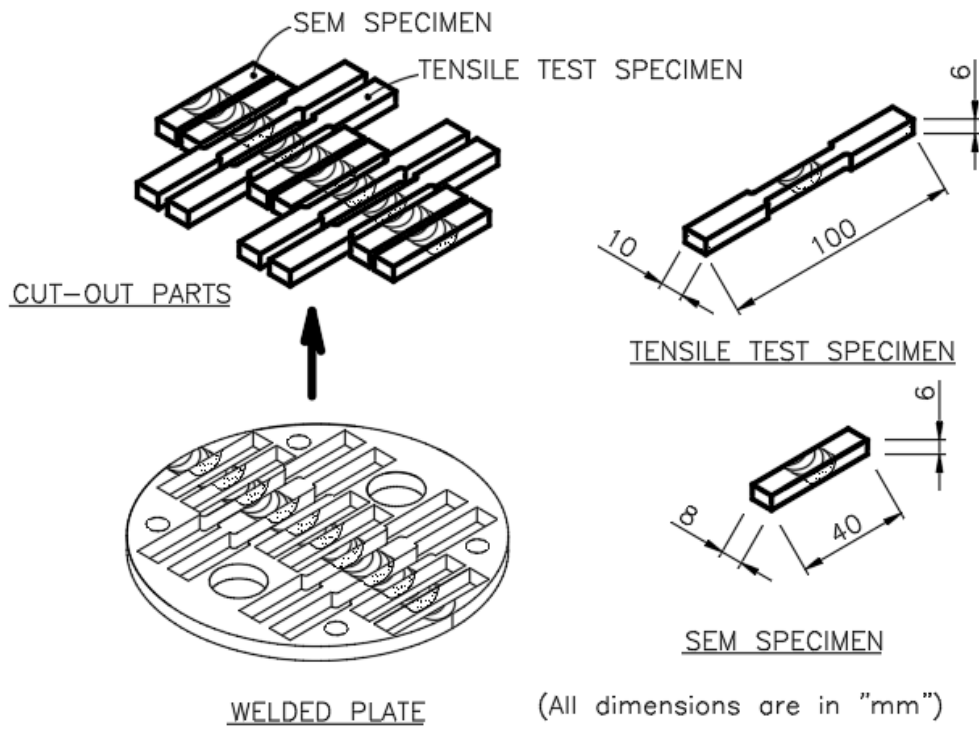
Figure 3.10 Cut-out Scheme of sections selected for characterization

Figure 3.11 Servo Control High Quality Wire Cut EDM machine (Model: BM400C-CT, Make: Suzhou Baoma)

3.7 CHARACTERIZATION OF Al-Ce-Si-Mg ALUMINIUM ALLOY WELD CONNECTION FABRICATED THROUGH FRICTION STIR WELDING

3.7.1 X-Ray Diffraction Analysis

X-Ray diffraction was carried out on Al-10Mg-8Ce-3.5Si and Al-5Mg-8Ce-3.5Si aluminium alloy samples using an X-ray diffractometer model DX-GE-2P, JEOL as shown in Figure 3.12. It operates with Cu-Ka, at 40KV and 20 mA, to identify the phases present in the as-cast and friction stir welded specimens. The 2θ range is $20°$ to $80°$ selected for all the aluminium alloy specimens in such way that it will cover all the major intense peaks of the phases. Since the maximum temperature developed during FSW is at NZ, the nugget zone samples were selected for the analysis. The size selected for this purpose is 7mm $\times$ 6 mm $\times$ 3mm. The diffracted data were analyzed using the JCPDF data files to recognize the peaks linked to various constituent phases.
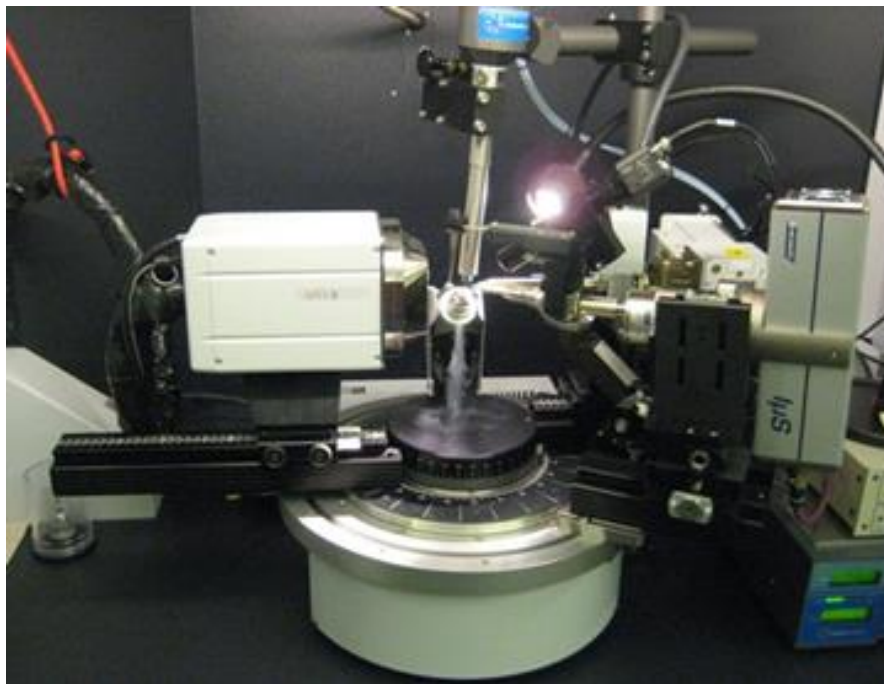
Figure 3.12 Photograph of X-Ray Diffraction machine (Model: DX-GE-2P, Make: JEOL)

3.7.2 Microstructural Analysis

Scanning Electron Microscope (SEM) is an extremely useful investigative tool for presenting surface features of the specimen. Figure 3.13 shows the photograph of SEM machine model JSM-6380LA, JEOL. Observations have been made using secondary electron imaging modes, accompanied by use of Energy Dispersive X-Ray Analysis (EDX) on the welded aluminium alloy, to reveal the micro-structure at different regions. The operating voltage is 20kV. Figure 3.14 represents the regions where micro structural images have been captured for joints which were fabricated using TPP and SPP tool. Images have been captured at top region of the nugget, (labeled as 'a' in Figure 3.14), middle region of the nugget, (labeled as 'b' in Figure 3.14), bottom region of nugget, (labeled as 'c' in Figure 3.14). Advancing the TMAZ (labeled as 'd' in Figure 3.14), and retreating side region (labeled as 'e' in Figure 3.14). The mean size of the grain was measured using line intercept method as per American Society for Testing and Materials standard ASTM_E112-12 (2012).

Figure 3.13 Photograph of SEM machine (Model: JSM-6380LA, Make: JEOL)
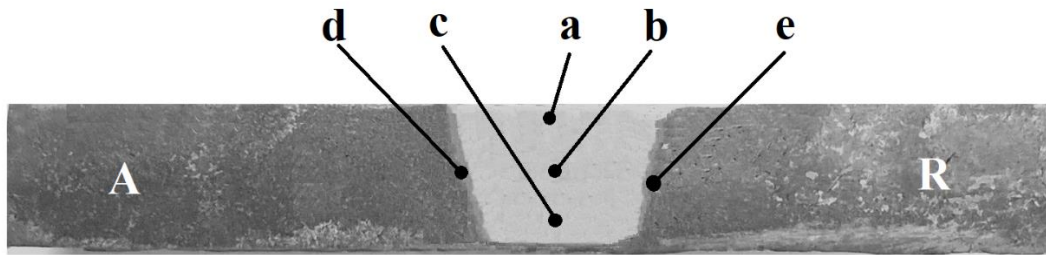
Figure 3.14 Macrostructure image of FSW specimen, showing (a) Nugget top region, (b) Nugget middle region, (c) Nugget bottom region (d) Retreating side TMAZ, and (e) Advancing side TMAZ respectively (A) Advancing side (R) Retreating side.

Figure 3.15 shows the locations of SEM images of weld region of aluminium alloy, friction stir welded using TPP tool. The marks 'a' to 'g ' in the figure represent the regions where micro structural images have been captured and markings (i) to (ii) represent the shoulder driven, triangular profile pin driven regions.
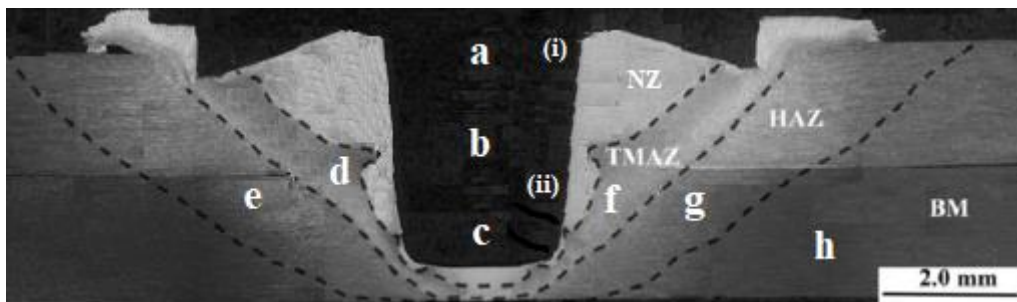
Figure 3.15 Micro-structure images of aluminium alloy weld connection friction stir welded using TPP tool, showing (a) Base Material Zone, (b) the NZ near the top of TPP, (c) TMAZ at advancing side, (d) TMAZ at retreating side, (e) HAZ at advancing side, and (f) HAZ at retreating side. (Courtesy: Shen et al. 2013)

3.7.3 Mechanical Testing

3.7.3.1   Hardness test

The welded alloy weld region samples have been tested for hardness, yield strength, ultimate tensile stress, and elongation percentage. Vickers hardness tester is used to

measure the hardness of the material. The measurement of hardness of the weld zone was made on the same plane on which microstructural studies were conducted. Vickers Hardness Tester (VM- 120) was used to make Vickers Hardness measurements using an indentation load of 5 kg for 15 sec. The hardness measurements were made at locations starting from mid-point of the weld nugget zone, and then across the weld, at every 3 mm intervals on both sides of the center line of the weld nugget zone. The size of the specimen and measured distances used for the hardness test are as shown in the Figure 3.16. At the end of hardness test on each sample, the diagonal length of indentation was carefully measured. The Vickers Hardness Number is calculated using equation 3.1

$$H_v = \frac{1.854\,P}{d^2} \tag{3.1}$$

Where "P" represents the load in terms of "kg" applied during indentation and "d" presents the mean diagonal length (mm) of the indentation mark on the test specimen. While taking hardness readings on a specimen, care is taken to see to it that the indentation marks are separated by at least a distance of three times the diagonal length. This is done to ensure that the accuracy of the hardness readings is not affected due to elastic deformations and to minimize the errors in measurement of diagonal length.

(All dimensions are in "mm")
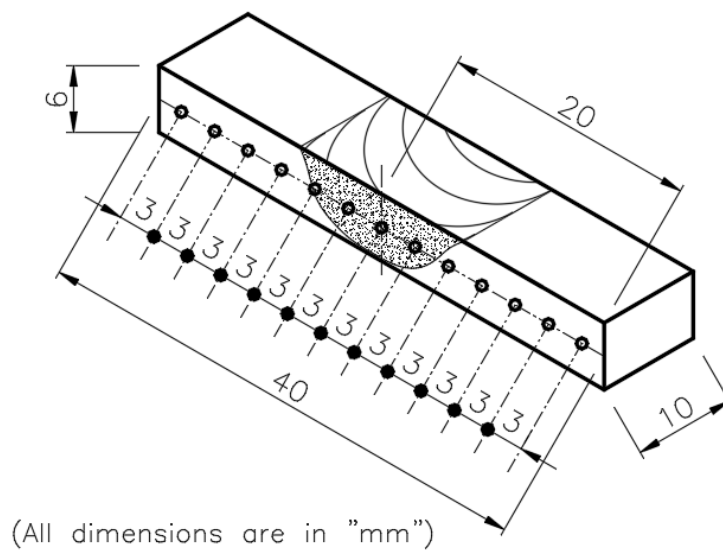
Figure 3.16 Hardness test specimen showing hardness measurement locations

3.7.3.2   Tensile test

The machining of the tensile test specimens was done as per ASTM E8-04 (2013) standard. The fractured surfaces of the tensile tested specimens were studied for microstructural analysis using SEM. The tensile tests were carried out for as-cast Al-Ce-Si-Mg aluminium alloy and welded specimens at various speeds of tool rotation, speeds of welding, and tool pin shapes. The tensile test schedule is shown in Table 3.4. The tensile tests were conducted using a computerized, servo hydraulic driven, fatigue testing machine of 50kN capacity (Make: BISS-ITW, India, Model: Median). The computerized fatigue testing machine has servo hydraulic drive with a maximum loading capacity of 50kN. The minimum load sensing capacity is 20N (2kg). The cross-slide speed selected to perform the tensile test is 0.5 mm / min. For each case, 3 samples were considered for the tensile test. The average value of the tensile stress of these samples was used in further analysis. The schematic diagram of the tensile test specimen is shown in Figure 3.17, which were prepared as per the standard (ASTM E8-04 2013). The machined tensile test specimens have been shown in Figure 3.18. Figure 3.19 and Figure 3.20 show the tensile test machine and its gripper arrangement used for clamping the test specimen during the tensile test.

The weld connection efficiency (%) (Weld connection strength) of the each friction stir welded weld connection is calculated by using the equation 3.2 (Kumar and Murugan 2014);

$$\text{Weld connection efficiency (\%)} = \frac{\text{Average strength of the weld connection}}{\text{Base material strength}} \times 100 \qquad (3.2)$$

The error in prediction of each process parameters are called as relative error (RE) and represented in terms of percentage. The equation is as shown in equation 3.3 (Ghetiya and Patel 2014);

$$\text{Relative error (\%)} = \frac{(\text{Experimental UTS} - \text{Predicted UTS})}{\text{Base material strength}} \times 100 \qquad (3.3)$$
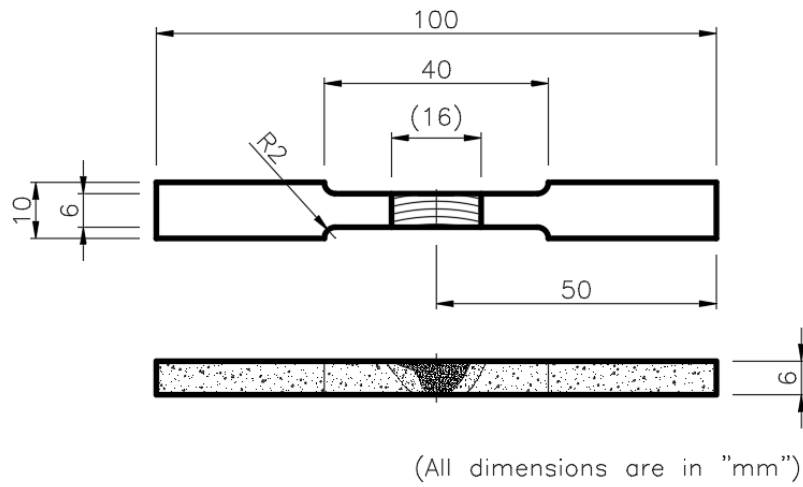
Figure 3.17 Schematic diagram of tensile test specimen
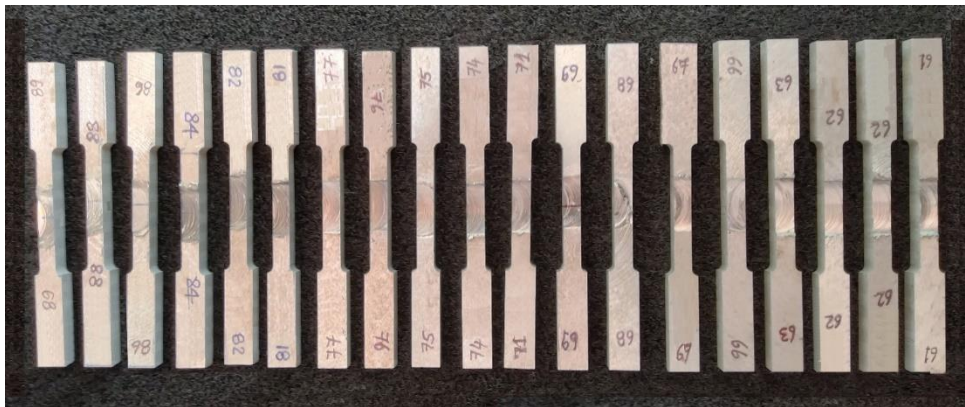
Figure 3.18 Machined tensile test specimens

Table 3.4 Tensile testing schedule of FSW of aluminium alloy

Sl. No.	Material	FSW process parameters		
		Speed of Rotation (RPM)	Welding speed (mm/min)	Tool pin shape
1.	Aluminium alloy Al-10Mg-8Ce-3.5Si	800, 1000, 1200	10, 15, 20	TPP, SPP, CPP
2.	Aluminium alloy Al-5Mg-8Ce-3.5Si	800, 1000, 1200	10, 15, 20	TPP, SPP, CPP

Figure 3.19 Fatigue testing machine of 50kN capacity, make: BISS India

Figure 3.20 Mechanical wedge grippers for clamping tensile test specimen

3.8   DESIGN OF EXPERIMENT AND ANALYSIS

The primary objective of design of experiment and analysis is to provide a brief explanation about how effectively one can reduce and control the method variation, by projecting which parameters affect the performance of the process. Variation in the outcome can be reduced by suitably varying the method variable values.   In this research work, Orthogonal Array (OA) is used to conduct the experiments. OA is one method, most flexible in accommodating a variety of situations. Design of experiment consists of two or more parameters, with different sets of levels. Each level is varied in statistical manner. The outcome of the test combinations observed, and the complete set of results is analyzed to determine the influencing factors. The experiments were conducted to analyze the performance of the process. Design of experiments is used to cut the cost and time of experiments general model of method has been shown in Figure 3.21. In any process, there are some parameters which can be controlled (X) and some parameters which cannot be controlled (Y). The objectives of the experiments are:

1. Identifying the variable which is more significant on the outcome of Y.
2. Defining and setting of Y in such way that it is always nearer to the desired nominal value.
3. Y is dependent on X. The change in X will lead to vary Y, thus the variability occurred in Y should be of a smaller value.
4. Determining and setting the influential X in such way that the effects of Z parameters should be reduced.
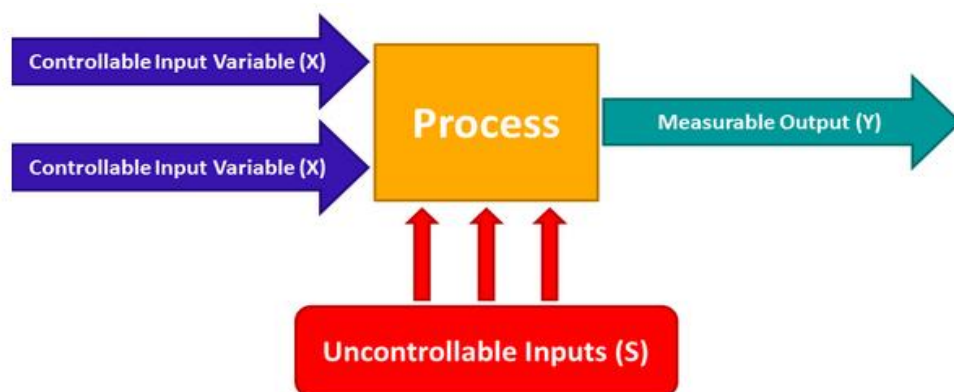
Figure 3.21 Basic model of D.O.E. Method (Courtesy: www.quality-one.com)

The Design of Experiment (DOE) involves three stages, namely, 1) Planning stage, 2) Processing stage and 3) Analyzing stage. OA is a best suitable technique for design of Experiments that operate consistently on a varying range of conditions. The key objective is to identify factor setting, which is nothing but the welding parameters that diminishes the output variation by regulating the method towards the target. A method designed with this goal will produce more consistent output. An experiment designed with this objective will enhance the performance of system.

3.8.1 Phases of Taguchi experiment

The executions of an OA experiment have distinct steps as mentioned below.

1. Definition of the problem - Thoroughly recognize and understand the nature of the problem.
2. Define the objective of the experiments
3. Identify the quality characteristics which are most relevant to the problem.
4. Select the influencing factors which affect the quality characteristics.
5. Identify the control and noise factors
6. Selection of factor levels
7. Selection of suitable OA.
8. Select possible interactions which influence on the quality characteristics
9. Conducting experiments with appropriate data collection.
10. Analysis and interpretation of experimental results.
11. Conduct confirmatory run of the experiment.

The control factors for welding of aluminium alloys are tabulated in the Table 3.5. The welding method consists of three control factors, namely, speed of tool rotation, welding speed and tool profile. Three levels per factors were selected based on the initial stage of experiment. The selected level is in such a way that it must be free from defects such as pin hole, worm hole and tunnel defect. The experiments were conducted for alloys Al-10Mg-8Ce-3.5Si and Al-5Mg-8Ce-3.5Si. Therefore, composition level is also selected as one of the input parameters. Since it has 2 levels, mixed level OA is selected for the analysis. According to Taguchi design of experiments method, the

available designs for analysis are L18, L36 and L54. The number of degrees of freedom in less than the 18. Therefore, L18 is used for the analysis. The implication of OA design will reduce the experiments from 54 to 18 experiments. L54 design is called as mixed full level experiment. Here all the experimental data are considered for the experiments.

Table 3.5 Control factors at different levels of the experiment

Control Factor	Level-1 (Low)	Level-2 (Medium)	Level-3 (High)
Alloy Composition	5	10	-
Speed of Tool Rotation (RPM)	800	1000	1200
Speed of Welding (mm/min)	10	15	20
Tool Pin Geometry	Triangular	Square	Cylindrical

3.8.2 Signal-to- noise ratio

Based on the output behavior, a suitable control factor can be selected in order to keep the variation to optimum level. The variation occurred at the output can be measured by transformation of the repetition data to another value by using Taguchi technique. The transformation is indicated by signal-to-noise ratio (S/N). Based on the type of features there are three S/N ratios available. In that, larger is the better equation used to analyze the UTS (Chien et al. 2011; Lakshminarayanan and Balasubramanian 2008). The S/N ratio for larger the better criterion is given by.

$$\frac{S}{N}\textbf{ratio } = -\textbf{10} \times \textbf{log}_{10}\left\{\frac{\left[\Sigma\left(\frac{1}{Y^2}\right)\right]}{n}\right\} \qquad (3.4) \ \ (\text{Besterfield et al. 2011})$$

Where 'n' is the number of experiments and 'Y' is the experimental value of the required quality characteristics.

3.8.3 Analysis of Variances

Analysis of variance (ANOVA) is a statistical technique is made use of to predict the process parameters and their interactions significantly affect the quality characteristics (Liao et al. 2004). ANOVA uses tests based on variance ratios to determine whether significant differences exist among the means of several groups of observations, where each group follows a normal distribution. The percentage contribution can be used to determine the significant variable which affects the performance characteristics. Also, F-test is named after Fisher (1925), can be used to identify the variable which has a substantial consequence on the quality characteristics based on 95% confidence level. Usually, if the value of "F" is higher than the variable, it has a greater influence on the performance. ANOVA is performed using Minitab 18.1® (2017), to determine the design parameters and their interaction, which significantly affect the performance characteristics.

3.9 NEURAL NETWORK MODEL

The aim of this study is to assist in building a model using neural network for the purpose of predicting the weld connection strength and hardness of aluminium alloy joined through FSW. The following model was developed for prediction of mechanical properties of FSW joint. Namely, Multilayer Perceptron (MLP) type ANN model was used. The learning algorithm used in this study was BFGS quasi-Newton back propagation method. The following sections cover information on training methods and architecture used in the current research study.

3.9.1 Architecture of Multi-Layer Perceptron model

The Multilayer perceptron (MLP) type of ANN technique has been used to resolve successfully the divisive and complex engineering problems. These problems were successively solved by training them with an effective error back propagation algorithm (Haykin 2007; Sumathi and Paneerselvam 2010). The various algorithms those could be used for training are Traingda (Gradient descent with adaptive learning rate

backpropagation), Traingdx (Gradient descent with momentum and adaptive learning rate backpropagation), Trainrp (Resilient backpropagation), Trainscg (Scaled conjugate gradient backpropagation), Trainbfg (BFGS quasi-Newton backpropagation), Trainlm (Levenberg-Marquardt backpropagation) etc. The errors occurred during learning method were resolved by using learning rule such as Adaptive Filtering, Gradient Decent or Least Mean Square algorithm. The architecture comprises of three kinds of layers namely input layer. hidden layer, and output layer. The direction of signal flow is from input layer to output layer in a forward direction. Hence it is termed as Feed Forward Neural Network. The processed data in the network will pass through numerous layers without any presence of feedback connections. Figure 3.22 depicts a schematic presentation of Multi-Layer Perceptron feed forward neural network with input and output parameters. The configured neural network must work in such a way that the anticipated results are obtained from a set of inputs provided. The weights are basically set in two different manners. One method is to set the weights based on the previous knowledge. The other way is by providing the data as a train to learn the pattern of output by means of learning rules. The back-propagation algorithm executes in two different ways for a given epoch of training data and these ways are known as the sequential mode or batch mode. In sequential mode the neuron weights fully depend on the pattern basis. Whereas in the case of batch mode, the adjustment of all synaptic weights and biases are completely based on epoch basis. In the back-propagation learning, the sequential mode is the most regularly used mode. Networks must be trained in such a way that the errors between the desired and targets are minimal. There are two types of error specification, one is by the number of epochs specification and the other is by the error value specification. In specification by the number of epochs, the training data will run up to the specified epoch number and as soon as it reaches stated value, the testing of the data is completed. In the case of error criterion, the training data will run up to the reach specified value of error. In the current research work, MLP architecture is made use of for training and predicting the mechanical properties of the weld joints fabricated with the help of FSW process. The input parameters are speed of tool rotation, welding speed, tool pin contour and aluminium alloy material composition. The predicted output parameters are ultimate tensile strength (UTS), elongation percentage, and hardness at the weld zone of the joint.
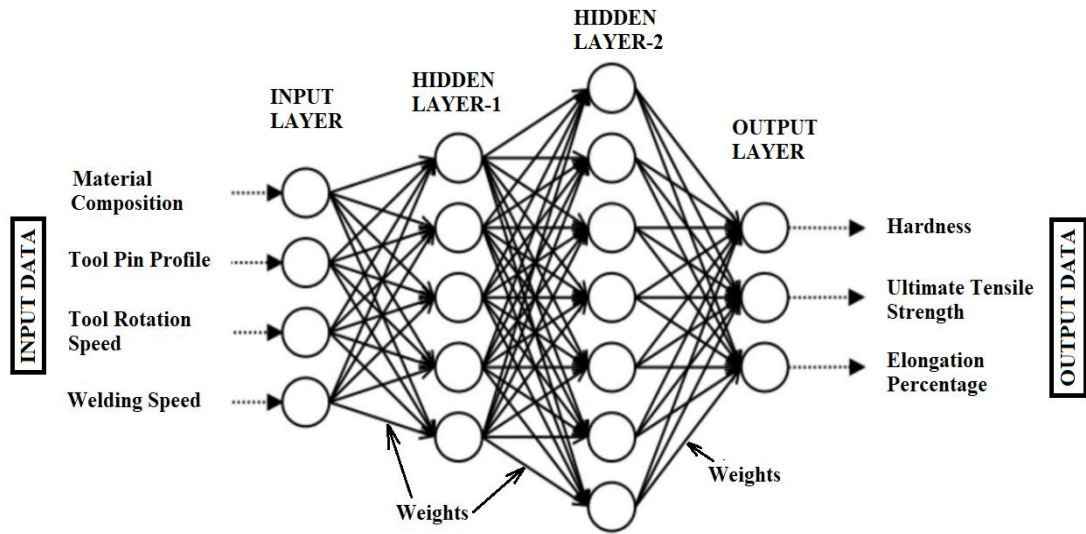
Figure 3.22 Multilayer Perceptron feed forward neural network Architecture (Buffa et al. 2009)

3.9.2 Steps in developing a neural network

3.9.2.1 Identification of input variable

For modelling output variable(s) under study, the input parameters are very important and suitable variable selection procedures are used for selection of right input parameters for the process. From the literature review, it was found that, weld connection strength of aluminium alloy joints prepared through FSW is mainly dependent on the speed at which spindle operates, welding speed at which the table moves along respective axes (X, Y), type of tool pin contour, thrust force, rigidity of the machine as well as the type of material, and so on. The most important parameters are speed of tool rotation, welding speed, type of tool pin contour and type of material selected for predicting the weld connection strength, percentage elongation and hardness at the centre of the joint.

3.9.2.2 Formation of training and validation sets

The data set is categorized in to three discrete sets which are termed as training set, testing set, validation set. The neural network uses the training set in order to learn the patterns and the training set is considered as the prime set. The testing set is used to

appraise the generalization ability of a trained network. The validation dataset is applied to the trained network in order to verify the performance of the established network. In total, 54 sets of experiments were conducted. Out of these 54 sets, 46 data sets were used for the training the networks, 8 sets of data were used for testing validation of the network. Additional data sets were also tried out for validation. If the data being collected to develop the model lies in the range [x_{min}, x_{max}], then the validation and the test data also need to be generated in the range [x_{min}, x_{max}]. The training data can also be generated in the same range. In the region near the extremes i.e. at the boundaries, it is advisable that training data may be sampled slightly beyond the bounded values of data. The reason is to enhance the performance of the model.

3.9.2.3   Pre-processing and Post-processing of Data

In most of the cases, the input space contains more than one variable. For the data collected, each of the input may have a range different from others. Similarly, the quantity of outputs may be more than one and each may have a range different from others. Hence each of the inputs and the outputs need to be normalized by its own normalizing factors. Therefore, it is necessary to preprocess the raw input and output data or otherwise there will be impediment to the satisfactory performance of the network. In the complete model design and development, this phase is very critical.

There are two methods of data pre-processing. These are transformation method and the normalization method. In the transformation method, the raw input data is manipulated to create a single input to a network, while normalization transforms a single input data to be distributed evenly and scales it into a workable range for the network (Ghetiya and Patel 2014; Gupta et al. 2018b; Nigalye 2013; Okuyucu et al. 2007). As stated earlier, it is desirable that the knowledge of the processes and systems for which the model is developed be known, as it will help to understand the underlying features of the process. All this will help the network to be trained in a better fashion resulting in better performance of the network. Normalization of data is the last step in data pre-processing. The goal is to distribute the data in such a way that it is spread uniformly across the data range. This applies to both the input as well as the output data. The values should be scaled in such a way that the range of the input and output

data matches with the range of the summing and squashing device, the neuron. Thus, it imperative that in other type of transformation also, normalization as a final pre-processing step is indispensable. It is possible to scale the raw input data within any range. However, for our work the data is scaled between '0' and '1' using the following normalizing function.

$$x_n = \left[\frac{(x - x_{min}) \times 0.8}{(x_{max} - x_{min})}\right] + 0.1 \qquad (3.5)$$

In the above equation 'x_n' denotes the normalized value, 'x_{min}' is the minimum and 'x_{max}' is the maximum value in the range (Guangzong et al. 2010; Nigalye 2013; Smith et al. 1997). Upon training the network to a required degree of performance, it is expected that the network will provide the output values that are well understood by the end user. In order to achieve this, the post- processing of the data becomes necessary. In this step, the outputs of the network in the normalized form are de-normalized using the following equation (Smith et al. 1997).

$$x = \left\{\frac{[(x_{max} - x_{min}) \times (x_n - 0.1)]}{0.8}\right\} + x_{min} \qquad (3.6)$$

3.9.2.4 Hidden layers concept

The hidden layer provides the network with its ability to generalize. In theory the approximation of the continuous function is attained by the presence of single hidden layer with adequate hidden neurons. In practice, the neural network with one hidden layer is widely used and rarely the two hidden layers are used.

3.9.2.5 Hidden nodes concept

In order to select the ideal number of hidden neurons there were no proper guidelines mentioned. The hidden neurons are calculated based on the thumb rules. The approximation of the required number of hidden neurons was obtained by using a geometric pyramid rule which was anticipated by Timothy Masters (1993). For a three-layer neural network, the number of hidden neurons with 'n' inputs and 'm' output

neurons is found by minimum square root of 'n x m' neurons. Hence, by considering minimum hidden layer at the first hidden layer and starting from 4 neurons, the best results were attained at 7 neurons. Likewise, considering minimum hidden layer at the second hidden layer, the best results attained at 4 neurons. Figure 3.23 represents the number of neurons in the hidden layer verses mean square error (MSE) during the training the network. It can be seen from the graph that as the number of neurons increases the mean square error increases. This is due to increase in the complicity of the equation. Hence, it consumes more time to understand the relationship among the input and output.
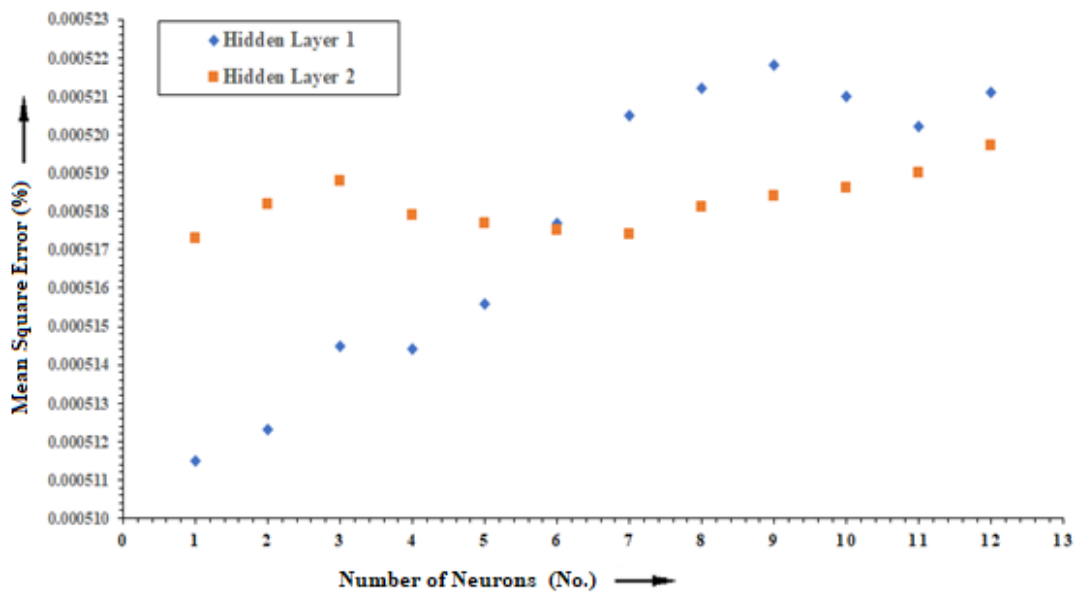
Figure 3.23 Number of hidden layers 1 and 2 versus mean square error (Shettigar et al. 2016)

3.9.2.6   Output nodes concept

If the outputs are broadly spaced in the network with multiple outputs, then it leads to inferior results as compared to a network with single output. The output parameters are weld connection strength, percentage elongation and hardness at the middle of the joint.

3.9.2.7 Concept of Activation function

Activation functions are mathematical formulae that determine the output of a processing node. The unit takes its net input and an activation function is applied over it. Nonlinear functions such as tanh, log, sigmoid are used as activation functions. The network can sometimes get paralyzed and even it may indicate the inhibit training due to the larger values produced. So, transfer functions are used to avoid such situations. In the case of network learning generally the sigmoidal transfer function is used because as it is nonlinear and continuously differentiable. The most prevalent function used is the sigmoid function, which is unipolar continuous. The sigmoid function is denoted as follows (Guangzong et al. 2010; Nigalye 2013; Smith et al. 1997).

$$f(x) = \frac{1}{1+e^x} \qquad (3.7)$$

For the outputs, one may select an activation function to suit the distribution of target values. For binary (0/1), the logistic function is ideally suited (Jordan 1995). Thus, the logistic function (sigmoid function) has been used as the activation function.

3.9.2.8 Initial Weights

The weights of the network are usually initialized at small random values. The weight initialization has a profound influence on the way the network learns. If one starts out with equal weights and the network solution requires that the weights be unequal, then learning will not proceed in proper direction. The network may fail to learn from the training data due to either the error stabilizing or due to increase in error as training continues. If one continues training the network even when the region of low plateau has reached, it may result in drifting of weight, which is not desirable. The error then increases, and the network mapping quality suffers. To counter this, it is desirable to start with a fresh random weight set.

3.9.2.9 Learning Rate

Learning rate variable determines the quantum of adjustment of weight done at each stage and is responsible for the rate at which the convergence of the network happens. A wrong selection of this variable can end in difficulties of convergence. The effectiveness of the use of back propagation algorithm depends on choice of an appropriate value for learning rate coefficient. There is no information available on selection of learning rate variable and it depends upon the type of relationship that exists in the data set (Reddy et al. 2005). So, the learning rate coefficient is unique for each problem being modelled and must be arrived at by trial and error method. Use of too low a learning rate variable (η) will lead to very slow convergence. A too high value of 'η' causes the network to oscillate or diverge thereby leading to non-convergence. Under this situation no learning will take place. Rumelhart et al. (1986) reported that for most cases of computations, a value of $\eta = 0.25$ and $\alpha = 0.9$ gives best results. Usually 'η' is the quantum of weight adjustment for each iteration. Its value varies from 0.1 and 0.9. During training process, the learning rate is varied between 0.1 and 0.9, and it is noticed that the learning rate of 0.3 yields better results.

3.9.2.10   Momentum Factor

The crux of back propagation algorithm is the evaluation of how much each weight contributes to the error output. This is a credit assignment problem. A continuously differentiable function of the weights should be the objective function in Neural Network (NN) training. Therefore, evaluation of the credit assignment is easily possible. Therefore, it may appear that the use of Back Propagation (BP) training scheme is a guarantee for network convergence. But this is not the case though. This is because the error surface on the error v/s weight plane may have several local minimums, besides possessing a global minimum. There is quite a likelihood that the training may get stuck in the local minimum and may not move on this plane. Secondly, there may be some stationary points on the error profile. The stationary points also inhibit the learning method in the BP algorithm. The purpose of introducing the

momentum term in the training scheme of a Feed Forward Neural Network (FFNN) is to accelerate the convergence of the network by overcoming these issues. The method involves supplementing the current adjustments in weight with a fraction of the adjustment in weight in the preceding time step. The current weight adjustment then takes the form shown below (Guangzong et al. 2010; Nigalye 2013; Smith et al. 1997).

$$\Delta w(t) = -\mu \, \Delta E(t) + \alpha \, \Delta w(t - 1) \qquad (3.8)$$

The arguments 't' and (t-1) in the above equation indicate the current and previous training steps. The term 'α' is called as the momentum term or the momentum factor. The advantage of using the momentum term is that it gives a supplementary momentum to the downward descending movement. This method can help the network to climb out of the local minima and move further down the slope of error profile. The larger the momentum term, as can be seen from above equation, the larger will be its impact on convergence. Typically, 'α' is chosen between 0.1 and 0.9. During training process, momentum factor is varied from 0.1 to 0.9, and it is found here that momentum factor of 0.5 yields very good results.

CHAPTER 4

RESULTS AND DISCUSSION

INTRODUCTION

Present chapter elucidates on the characterization of the as-cast Al-Ce-Si-Mg aluminium alloys Al-10Mg-8Ce-3.5Si and Al-5Mg-8Ce-3.5Si. To study the effectiveness of Ce in these alloys, a systematic characterization of these alloys has been carried out using XRD, SEM/EDX microanalysis. In addition, mechanical properties like tensile properties and hardness are evaluated. An orthogonal array type Design of Experiments (DOE) techniques have been used to study the correlation between input and output parameters of FSW process. Taguchi and ANOVA analyses have been carried out to predict the mechanical properties like ultimate tensile strength, hardness, and elongation percentage etc., based on input process parameters.

The results of the studies are presented and discussed in-depth in this chapter through the following sections.

4.1 MICROSTRUCTURAL AND MECHANICAL CHARACTERIZATION OF AS-CAST Al-Ce-Si-Mg ALUMINIUM ALLOYS

4.1.1 Microstructural and Mechanical Characterization of As-cast Al-10Mg-8Ce-3.5Si aluminium alloy

The microstructural study of the as-cast aluminium alloy has been carried out to identify the phases and examine the grain structure and are explained in the following sections.

4.1.1.1 X-ray Diffraction Analysis

The quaternary Al-10Mg-8Ce-3.5Si aluminium alloy stands out from the binary and ternary alloys in micro-structure morphology, phase constitution, and heat treatment results. The alloy exists in the as-cast state as three phases. The smallest is AlSiMg accounting for less than 2 wt%. The main three phases present are the Al (FCC) phase, the intermetallic $Al_{11}Ce_3$ and AlSiMg. $Al_{11}Ce_3$ shows both primary and eutectic solidification in the as-cast state. The silicon not accounted for in AlSiMg is dissolved in the aluminium matrix (Sims et al. 2016; Zhang et al. 2004).

Figure 4.1 shows the XRD patterns of the as-cast Al-10Mg-8Ce-3.5Si aluminium alloy. The phases present in the as-cast Al-10Mg-8Ce-3.5Si aluminium alloy were determined to be α-Al, α-$Al_{11}Ce_3$ and AlSiMg, obtained for alloys solidified under conventional conditions. Some of the reflections in the XRD pattern could not be identified in the XRD plot shown. Furthermore, the broad hump, typical characteristic of amorphous phases, appears in the XRD pattern of the as-cast alloy (Zhang et al. 2004). The XRD pattern comprises of two sets of Bragg reflections: the intense reflections from the α-Al (332) region axis and the weak ones from the α-$Al_{11}Ce_3$ (311) region axis. There exist the following orientation relationships; α-Al (332) to α-$Al_{11}Ce_3$ (311) and α-Al (220) to α-$Al_{11}Ce_3$ (130). Also, the following orientation relationships have been determined; α-Al (001) to α-$Al_{11}Ce_3$ (010) and α-Al (020) to α-$Al_{11}Ce_3$ (002). The peaks in the XRD plots of as-cast Al–8Ce alloy composed of α-Al cells with intercellular α-$Al_{11}Ce_3$, that indicates amorphous phase which gives the alloy required castability and ductility to make it an ideal material for welding (Zhang et al. 2004). In the XRD pattern for Al-Ce-Si-Mg materials, in addition to sharper peaks there are also broad diffraction ranges which correspond to the presence of amorphous composition along with the crystalline particles. A distribution of small percentage of amorphous material in the matrix does not impede ductility. Amorphous materials also exhibit ductile behaviour under elevated temperature. Ductile behaviour of amorphous metals, their ability to sustain localized flow at high nominal stresses, is attributed to a mechanism which alleviates the severe stress conditions prevailing near potential cleavage flaws. The improvement in ductility is accompanied by the property of enhancement of castability of the alloy material (Lagos and Das 2016).

4.1.1.2 Scanning Electron Microscope (SEM) Analysis

Figure 4.2 (a) presents the SEM image of the as-cast Al-Ce-Si-Mg aluminium alloy Al-10Mg-8Ce-3.5Si, exhibiting typical primary α-Al dendrites with inter-dendritic α-Al/α-$Al_{11}Ce_3$ eutectic (Hawksworth et al. 1999; Zhang et al. 2004). The average size of the grains of as-cast Al-10Mg-8Ce-3.5Si aluminium alloy was measured to be 100.0±0.25 μm. Figure 4.2 (b) represents the Optical microscope images of Al-10Mg-8Ce-3.5Si. The micro-structure of the as-cast Al-10Mg-8Ce-3.5Si aluminium is hypoeutectic and composed of primary α-Al dendrites (α-phase) with inter-dendritic lamellar flake α-Al / α-$Al_{11}Ce_3$ eutectic. Figure 4.2 (c) EDX spectrum showing peaks of Al, Mg, Ce & Si in the dendritic structure and intermetallic base of as-cast Al-10Mg-8Ce-3.5Si aluminium alloy.
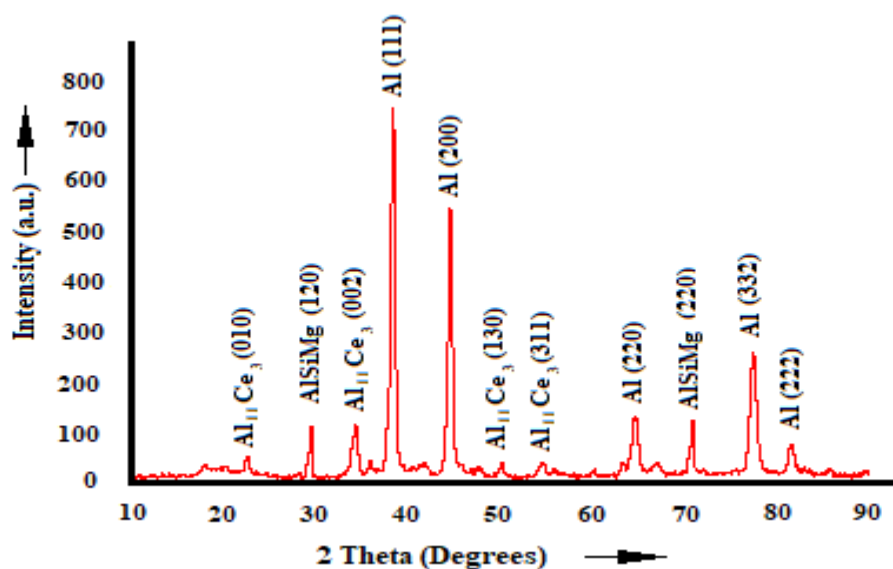
Figure 4.1 XRD pattern displaying the peaks of α-Al, $Al_{11}Ce_3$, AlSiMg in as-cast Al-10Mg-8Ce-3.5Si aluminium alloy

Figure 4.3 (a to h) represent the SEM/EDX area mapping of the base Al-10Mg-8Ce-3.5Si aluminium alloy showing the elements A1, Ce, Si, Mg, Zn, Ti, Fe and Mn respectively. The EDX map of the Al-10Mg-8Ce-3.5Si aluminium alloy in Figure 4.2 (c) shows peaks which belong to these elements near the grain boundaries in the as-cast state.

The micro-structural evolution of Al-10Mg-8Ce-3.5Si aluminium alloy could be explained as shown in Figure 4.2. Solidification has no effect on the phase constitution but has a marked effect on the micro-structure. The equilibrium α-Al and α-Al$_{11}$Ce$_3$ phases are identified in the as-cast Al-Ce-Si-Mg alloy of aluminium Al-10Mg-8Ce-3.5Si. The micro-structure of the as-cast alloy comprises of α-Al cells with intercellular α-Al$_{11}$Ce$_3$ (Zhang et al. 2004). Both primary α-Al dendrites and primary Al$_{11}$Ce$_3$ undergo significant morphological changes as the boundaries of the coupled region are approached. It also exhibits the asymmetrical region of coupled eutectic growth by the corresponding AlSi systems. This behavior of the Al/eutectic boundary of the coupled region stems from a relatively steep rate of decrease of the eutectic growth temperature compared with that for the α-Al dendrites. (Hawksworth et al. 1999; Waterloo and Jones 1996). The Al-10Mg-8Ce-3.5Si aluminium alloy exists in the as-cast state as three phases. The smallest is AlSiMg accounting for less than 2 wt%. The main two phases present are the aluminium (FCC) phase and the intermetallic Al$_{11}$Ce$_3$, both reflected in Figure 4.2. Al$_{11}$Ce$_3$ shows both primary and eutectic solidification in the as-cast state. The silicon not accounted for in AlSiMg is dissolved in the aluminium matrix (Sims et al. 2016). The analysis of SEM images of as-cast Al-10Mg-8Ce-3.5Si alloy was composed of α-Al cells with intercellular α-Al$_{11}$Ce$_3$, which indicates amorphous phase which gives the alloy the required castability and ductility to make it ideal material for welding (Hawksworth et al. 1999; Zhang et al. 2004).

The conclusions drawn from the SEM/EDX studies could be confirmed by chemical analysis tests as shown in Appendix V. The chemical composition obtained for Al-10Mg-8Ce-3.5Si aluminium alloy by SEM/EDX/Chemical analysis have been summarized in Table 3.1.

4.1.1.3 Mechanical properties of Al-10Mg-8Ce-3.5Si aluminium alloy

Hardness is the measure of resistance of the material to plastic deformation by indentation. The Vickers hardness value of Al-10Mg-8Ce-3.5Si aluminium alloy was found to be 98±1 VHN. In the alloy, the ductility remains high despite the large intermetallic phase fraction present in the alloy. This phenomenon could prove useful

129

in applications requiring alloys to be optimized for resistance to creep failure (Collins 1993). Tensile and yield strengths are improved over commercial pure aluminium (CPA). Cerium does not appear to provide dispersion strengthening in the as-cast state. The lower tensile and yield strengths are accompanied by an increase in ductility. Although the coarsening is minimal because there is no diffusion into the aluminium, the bulk mechanical properties of the alloy become more like those of pure aluminium, with lower tensile stress and high ductility. The ternary Al-Ce-Si-Mg system shows a marked increase in tensile strength, which is likely due to $Al_{11}Ce_3$ and AlSiMg particles dispersed throughout the aluminium matrix causing localized dislocations (Sims et al. 2016). Usually, the harder the material, the higher is its tensile strength, and the lower is its ductility.
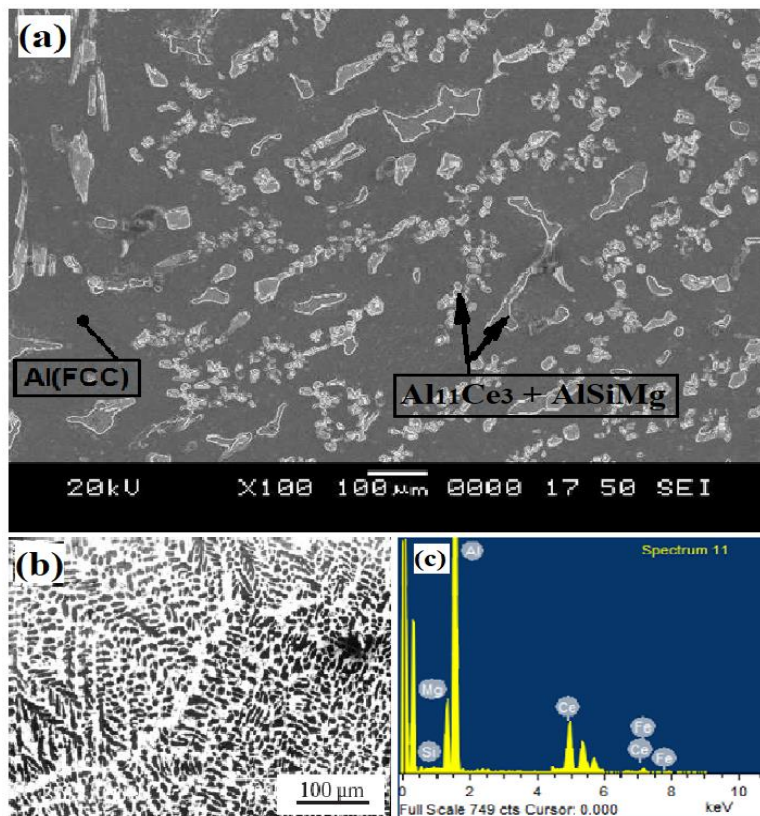
Figure 4.2 (a) SEM image of the as-cast Al-Ce-Si-Mg aluminium alloy Al-10Mg-8Ce-3.5Si, exhibiting typical primary α-Al dendrites with inter-dendritic α-Al / α-$Al_{11}Ce_3$ eutectic (b) Optical microscope images of Al-10Mg-8Ce-3.5Si (c) EDX spectrum showing peaks of Al, Mg, Ce & Si.

130
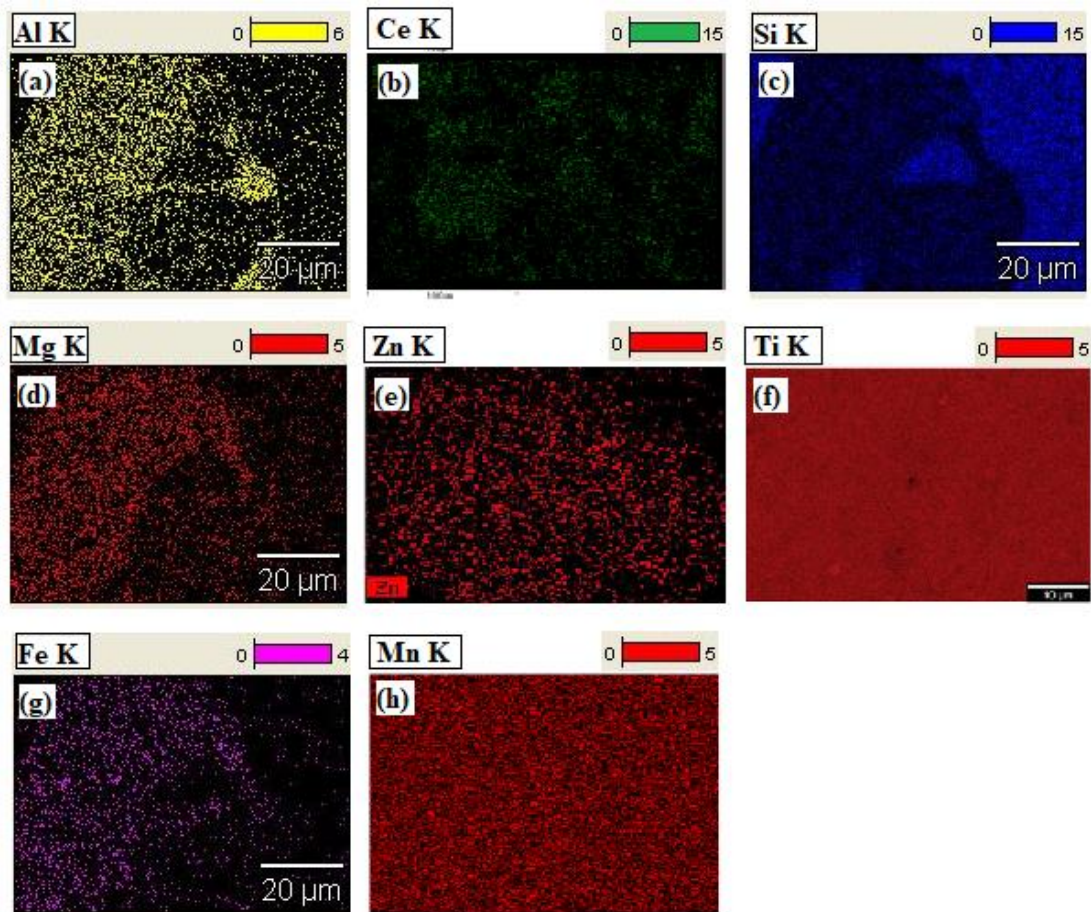
Figure 4.3 SEM images of base material EDX maps of Al-10Mg-8Ce-3.5Si aluminium alloy (a) Aluminium, (b) Cerium, (c) Silicon, (d.) Magnesium, (e) Zinc, (f) Titanium, (g) Iron and (h) Manganese

Tensile properties are generally a function of micro-structure, distribution of phases present like the aluminium (FCC) phase and the intermetallic $Al_{11}Ce_3$. The load displacement plots obtained from the tensile test are analyzed to estimate the yield stress (YS), ultimate tensile stress (UTS) and percentage elongation (El%). The fracture surface obtained from tensile test is examined to study the mechanism of failure. The YS, UTS and El% of Al-10Mg-8Ce-3.5Si aluminium alloy are 101.7 ± 4 N/mm^2, 154 ± 4.5 N/mm^2 and $4.66\% \pm 0.3$ respectively.

Figure 4.1 shows the SEM micrograph of the fracture surface of Al-10Mg-8Ce-3.5Si aluminium alloy. The fracture surface exhibits dimples and tear ridges confirming to a mixture of the ductile-brittle fracture. At the bottom of the tear ridges, the α-Al and

131

intermetallic $Al_{11}Ce_3$ & AlSiMg particles are observed. The voids originate at the matrix-particle interface due to the presence of particles inside the dimples. Furthermore, fracture surface dendritic nodules indicate that the fracture propagates through inter-dendritic separation.
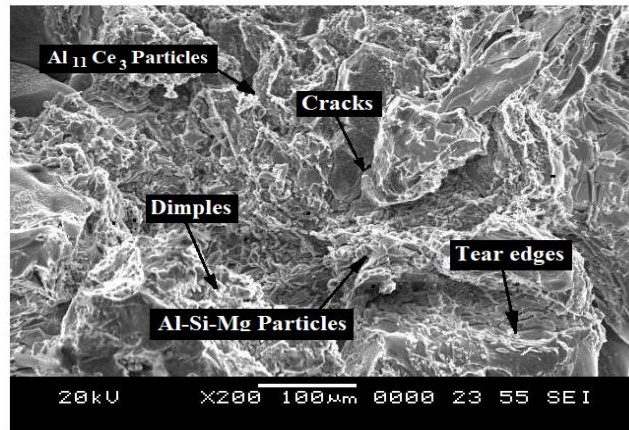
Figure 4.4 SEM micrograph showing the typical fracture surface of Al-10Mg-8Ce-3.5Si aluminium alloy.

4.1.2 Microstructural and Mechanical Characterization of As-cast Al-5Mg-8Ce-3.5Si aluminium alloy

The microstructural study of the as-cast aluminium alloy has been carried out to identify the phases and examine the grain structure and are explained in the following sections.

4.1.2.1 X-ray diffraction analysis

The quaternary Al-5Mg-8Ce-3.5Si aluminium alloy is similar to quaternary Al-10Mg-8Ce-3.5Si aluminium alloy in micro-structure morphology, phase constitution, and heat treatment results but with reduction in strength caused by decreased solid solution strengthening and reduced strain hardening ability, due to the lower percentage of magnesium (Mg) in the alloy mix (Singh et al. 2011b; Somasekharan and Murr 2004). The alloy exists in the as-cast state as three phases as explained in section 4.1.1.1 (Sims et al. 2016; Zhang et al. 2004).

Figure 4.5 shows the XRD patterns of the as-cast Al-5Mg-8Ce-3.5Si aluminium alloy showing peaks of α-Al, α-$Al_{11}Ce_3$ and AlSiMg as in the case of Al-10Mg-8Ce-3.5Si

aluminium alloy, explained in section 4.1.1.1. The peaks in the XRD plots of as-cast Al-5Mg-8Ce-3.5Si aluminium alloy were composed of α-Al cells with intercellular α-$Al_{11}Ce_3$, which indicates amorphous phase which gives the alloy required castability and ductility to make it ideal material for welding (Zhang et al. 2004).

4.1.2.2   Scanning Electron Microscope (SEM) Analysis

Figure 4.6 (a) presents the SEM image of the as-cast Al-Ce-Si-Mg aluminium alloy Al-5Mg-8Ce-3.5Si, exhibiting typical primary α-Al dendrites with inter-dendritic α-Al/α-$Al_{11}Ce_3$ eutectic (Hawksworth et al. 1999; Zhang et al. 2004). The average grain size of the as-cast Al-5Mg-8Ce-3.5Si aluminium alloy was measured to be 117.6±2.3 µm. Figure 4.2 (b) represents the Optical microscope images of Al-5Mg-8Ce-3.5Si. The micro-structure of the as-cast Al-5Mg-8Ce-3.5Si aluminium alloy is hypoeutectic and composed of primary α-Al dendrites (α-phase) with inter-dendritic lamellar flake α-Al / α-Al11Ce3 eutectic. Figure 4.2 (c) EDX spectrum shows peaks of Al, Mg, Ce & Si in the dendritic structure and intermetallic base of as-cast Al-5Mg-8Ce-3.5Si aluminium alloy.
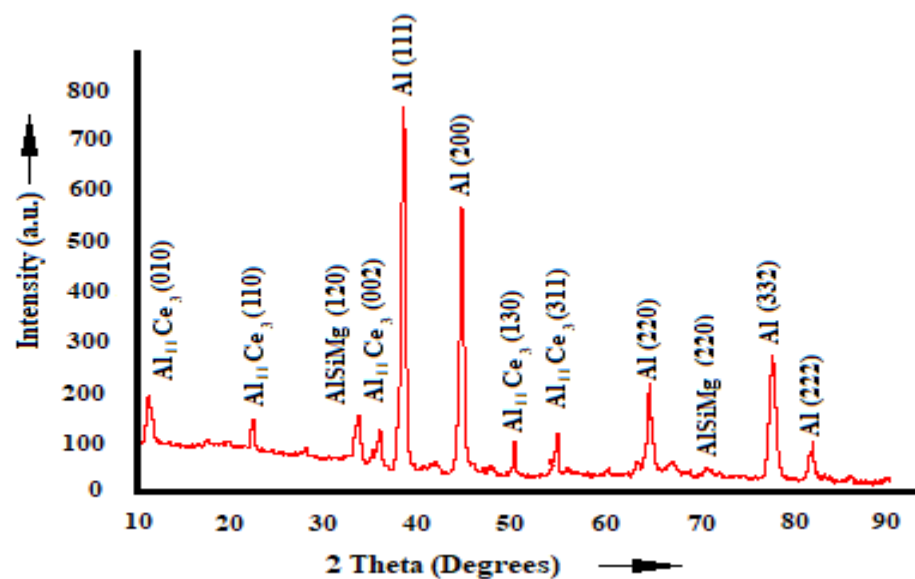
Figure 4.5 XRD pattern showing the peaks of α-Al, $Al_{11}Ce_3$, AlSiMg in as-cast Al-5Mg-8Ce-3.5Si aluminium alloy

The micro-structure evolution of the Al-5Mg-8Ce-3.5Si aluminium alloy is similar to the Al-10Mg-8Ce-3.5Si aluminium alloy in micro-structure morphological changes, phase constitution, heat treatment results and crystal growth as explained in the section 4.1.1.2. But the solidification method has shown no effect on the phase constitution but has shown a marked effect on the micro-structure. Figure 4.7 (a to h) represents the SEM/EDX area mapping of the base aluminium alloy Al-5Mg-8Ce-3.5Si showing the elements A1, Ce, Si, Mg, Zn, Ti, Fe and Mn respectively. The EDX map of the Al-5Mg-8Ce-3.5Si aluminium alloy in Figure 4.6 (c) shows peaks which belong to these elements near the grain boundaries in the as-cast state.

The conclusions drawn from the SEM/EDX studies could be confirmed by chemical analysis tests as shown in Appendix V. The chemical composition obtained for Al-5Mg-8Ce-3.5Si aluminium alloy by SEM/EDX/Chemical analysis have been summarized in Table 3.1.

4.1.2.3   Mechanical properties of Al-5Mg-8Ce-3.5Si aluminium alloy

Hardness is the measure of resistance of the material to plastic deformation by indentation. The Vickers hardness value of Al-5Mg-8Ce-3.5Si aluminium alloy was found to be 81.6±1.8 VHN. The hardness value of the Al-5Mg-8Ce-3.5Si aluminium alloy is decreased by 16.7 %, as compared to the Al-10Mg-8Ce-3.5Si aluminium alloy. The decrease of hardness value is because of the existence of less quantity of hard particles which act as obstacles to the motion of dislocation and also due to increase in the grain size (Collins 1993).

Despite the huge intermetallic phase fraction existing in the alloy, the ductility remains high even in the aluminium alloy Al-5Mg-8Ce-3.5Si. Yield and tensile strengths are also improved over commercial pure aluminium (CPA).

From the load displacement plots obtained from the tensile test it is found that the values of yield stress (YS), ultimate tensile stress (UTS) and percentage elongation (E1%) of Al-5Mg-8Ce-3.5Si aluminium alloy are 88.0±3 N/mm^2, 135.8 ±2 N/mm^2 and 5.5 ± 0.4 % respectively.

The fracture surface obtained from tensile test is examined to study the mechanism of failure. Figure 4.8 illustrates the SEM micrograph of the fracture surface of Al-5Mg-8Ce-3.5Si aluminium alloy. The fracture surface exhibits dimples and tear ridges confirming to a mixture of the ductile-brittle fracture. At the bottom of the tear ridges, the α-Al and intermetallic $Al_{11}Ce_3$ particles are observed. The voids are initiated at matrix particle interface due to the presence of particles inside the dimples. Moreover, dendritic nodules of the fracture surface indicate that fracture propagates through inter-dendritic separation.
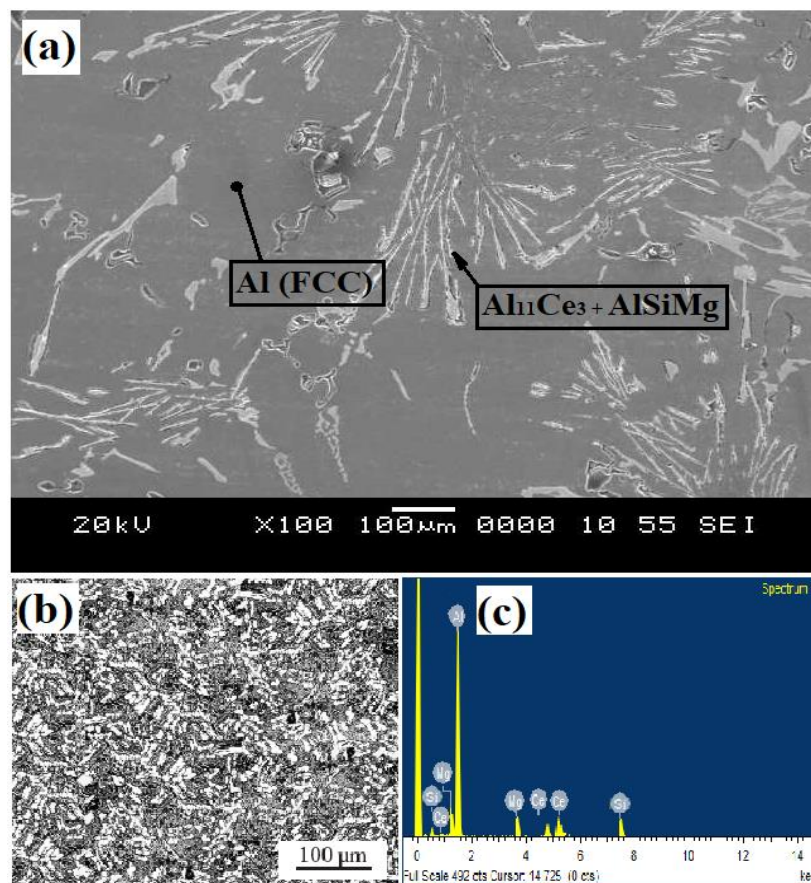
Figure 4.6 (a) SEM image of the as-cast Al-Ce-Si-Mg aluminium alloy Al-5Mg-8Ce-3.5Si, exhibiting typical primary α-Al dendrites with inter-dendritic α-Al/α-Al11Ce3 eutectic (b) Optical microscope images of Al-5Mg-8Ce-3.5Si (c) EDX spectrum showing peaks of Al, Mg, Ce & Si.
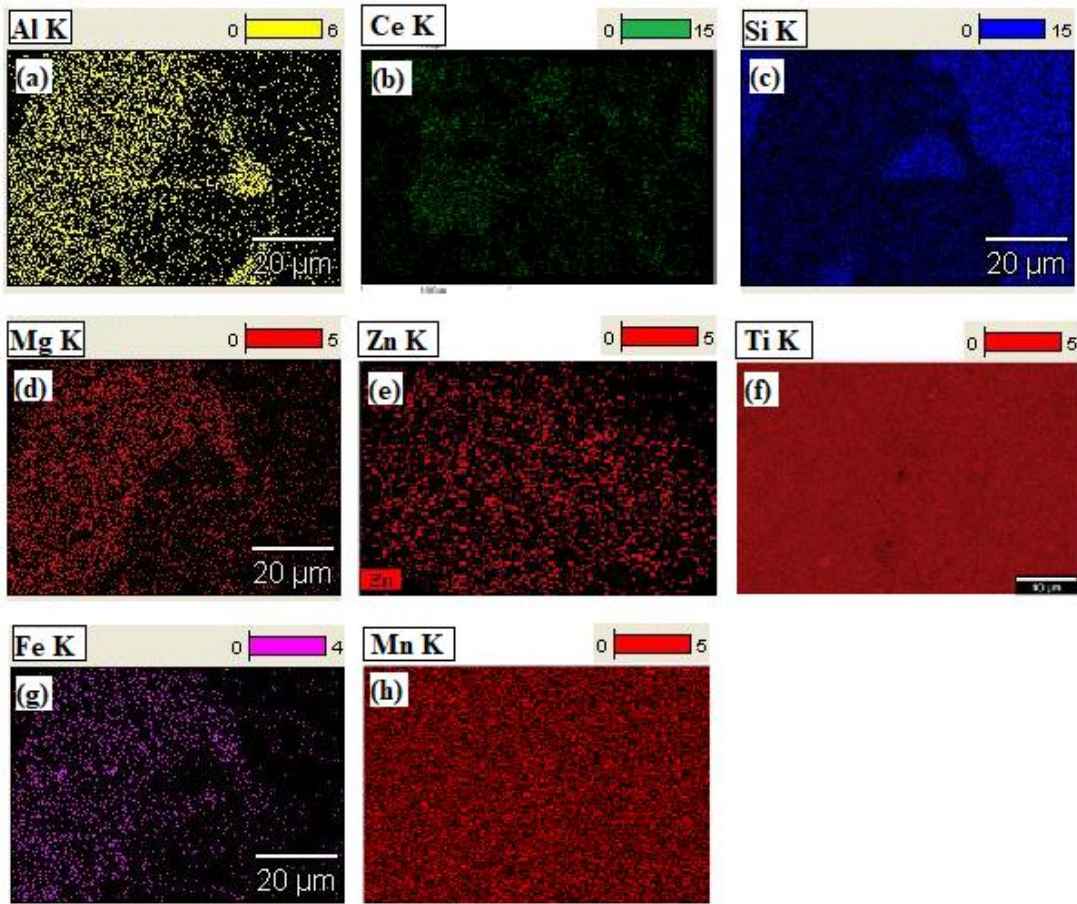
Figure 4.7 SEM images of base material EDX maps of Al-5Mg-8Ce-3.5Si aluminium alloy (a) Aluminium, (b) Cerium, (c) Silicon, (d.) Magnesium, (e) Zinc, (f) Titanium, (g) Iron and (h) Manganese
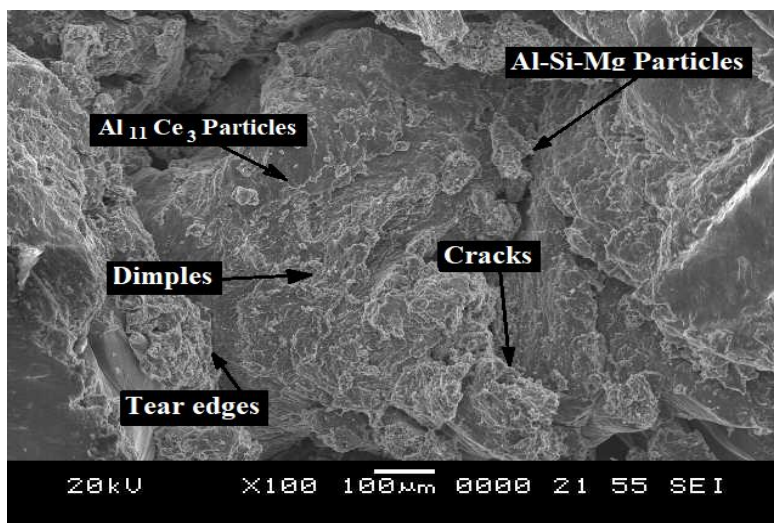
Figure 4.8 SEM micrograph showing the fracture surface of Al-5Mg-8Ce-3.5Si aluminium alloy.

4.2 FSW OF Al-10Mg-8Ce-3.5Si AND Al-5Mg-8Ce-3.5Si ALUMINIUM ALLOY

The welded specimen has been shown in Figure 4.9. The change in the structural feature and hardness at the weld region with respect to process parameters of friction stir welded Al-10Mg-8Ce-3.5Si and Al-5Mg-8Ce-3.5Si aluminium alloy material have been investigated and correlated.

Semicircular geometry has been obtained on the surface of the weld (Figure 4.9), which is identical to that produced during milling process. This is due to the rubbing action of tool shoulder on the workpiece surface (Hou et al. 2014; Kwon et al. 2009; Mahmoud et al. 2008). Smooth semicircular geometry is obtained for all types of joints. Excessive flashes and voids were not observed on the surface of the weld. At the end of the weld, a key hole is made by the pin, which is the result of tool retraction from the weld (Huang et al. 2011; Zhang et al. 2014; Zhou et al. 2012).
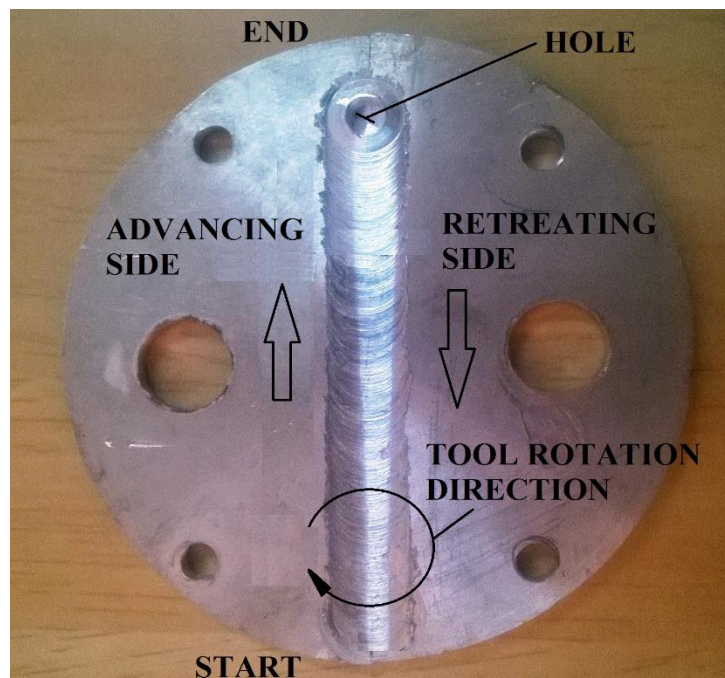
Figure 4.9 Friction stir welded Al-10Mg-8Ce-3.5Si or Al-5Mg-8Ce-3.5Si aluminium alloy specimen

4.2.1 Working range identification for different pin profile tools
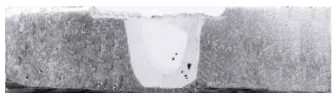
The first stage of the experimental study consisted of identifying the range of process parameters to get the defect free weld joints with the usage of tools with different pin shapes. When a perfect combination of process parameters is selected, a good weld connection could be attained. In this study, the speed of tool rotation, welding speed and tool pin shapes are the parameters considered. In the Table 4.1 a list of nature of defects occurring during the welding of the aluminium alloy is tabulated for different combinations of process parameters. At a speed of tool rotation of 800 RPM and a welding speed of 8 mm/min of the TPP tool, small amount of heat is produced. Whereas increased amount of heat production is noted for combination of input process parameters like, speed of tool rotation of 1200 RPM and welding speed of 23 mm/min. In the remaining cases (Table 3.5 shows experimental details), either tunnel hole, worm hole or pin hole defects have been detected. In the case of CPP tool, the lower heat input condition was observed at a speed of tool rotation of 800 RPM and a welding speed of 10 mm/min. On the other side, higher heat input condition has been observed at a speed of tool rotation of 1200 RPM and a welding speed of 23 mm/min. The SPP tool exhibited defect free working range similar to that of TPP tool conditions. The heat induced at the time of welding is largely depends on the speed of tool rotation irrespective of the welding speed. Only, the welding speed determines the amount of heat input provided to the base material (Kah et al. 2015; Rajakumar et al. 2010a; Sharma et al. 2012a). Therefore, heat induced at the time of welding is directly proportional to the heat supplied to the weld zone. Hence, at a slower speed of tool rotation, a smaller amount heat is induced, and the heat supplied to the weld zone is also small. Enough heat is not absorbed by the deformed material and the resistance to material flow goes up (Liu et al. 2018a; Zhu et al. 2016). As a consequence, the hot forging effect induced by the tool is not experienced by the material and it leads to the development of worm holes and pin holes in the stir zone. When the speed of tool rotation is high, due to increased frictional heat, the heat induced in the nugget zone is also high. This leads to more rigorous mixing and stirring of materials, due to which a turbulence in the flow of material ensues (Guerdoux and Fourment 2009; Rajakumar et al. 2010a). The heightened turbulence in the flow of material leads to the development
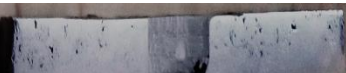
of a defect known as tunnel defect (Elangovan and Balasubramanian 2008b; Jayaraman et al. 2009a; Lakshminarayanan et al. 2011). It is detected that as the welding speed increases, the tunnel hole size also increases (Khan et al. 2015b; Leal et al. 2004). Higher welding speed results in less heat input to the weld zone, leading to lack of bonding and defects formation (Liu et al. 2012; Nakata et al. 2000; Zhang et al. 2015).

4.2.2 Identification of process parameters

Upon conducting several trial experiments, the feasible working ranges were identified for speed of tool rotation, welding speed, tool pin shape and weight percentage, by analyzing the weld region for macro and micro level defects such as tunnel defect, wormhole, and pin holes. The feasible working ranges differ for different tools. The feasible working range for TPP tool less as compared to CPP and SPP tool. The feasible working ranges of aluminium alloys are better than that for other metals because of higher ductility (DebRoy and Bhadeshia 2010; Rai et al. 2011). The maximum and minimum limit of each parameters have been tabulated in chapter 3. Further studies were carried out for those parameters, which produce defect free joints for 3 different tools.

Table 4.1 Macrostructure images of friction stir welded joints of alloys of aluminium Al-10Mg-8Ce-3.5Si and Al-5Mg-8Ce-3.5Si, to identify the feasible working range of welding parameters for TPP, SPP and CPP tools

Tool pin shape	Speed of Tool Rotation (RPM)	Speed of Welding (mm/min)	Macrostructure Image	Defect Type	Reason for Defect
TPP	< 800	<8		Pin Hole	Insufficient heat generation
		>20		Worm Hole	Insufficient heat generation and inadequate metal flow

	>1200	< 10		Worm Hole	Excessive heat generation and inadequate metal flow
		>25		Tunnel Hole	Excessive turbulence in plasticized metal flow
SPP	< 800	<5		Pin Hole	Insufficient heat generation
		>20		Worm Hole	Insufficient heat generation and inadequate metal flow
	>1200	< 10		Tunnel Hole	Excessive heat generation and inadequate metal flow
		>20		Tunnel Hole	Excessive heat generation and excessive metal flow
CPP	< 800	<10		Pin Hole	Insufficient heat generation
		> 30		Pin & Worm Hole	Insufficient heat generation and inadequate metal flow
	>1200	< 10		Pin & Tunnel Hole	Excessive heat generation and inadequate vertical metal flow
		>20		Worm & Tunnel Hole	Excessive heat generation and inadequate vertical metal flow

4.2.3 Effect of Magnesium (Mg) percentage on microstructure of FSW welded material
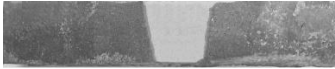
Magnesium (Mg) is usually added to the aluminium alloys as a strengthening additive. Mg additions contribute to appreciable solid solution strengthening, and typically maintain a high degree of ductility/formability. In the quest for improved strength, the trend in aluminium alloys is one of increasing magnesium contents. The difference in % of Mg in alloys Al-10Mg-8Ce-3.5Si and Al-5Mg-8Ce-3.5Si does not lead to a major change in microstructure but leads to increase in strength. Mg addition to the Al-Ce-Mg-Si aluminium alloy does not significantly affect the thermodynamics or phase constitution of the Al-Ce system, but instead, it strengthens the matrix phase by forming the intermetallic Al-Mg precipitates. Intermetallic precipitates are beneficial for increasing the strength of the ductile aluminium matrix without affecting the existing $Al_{11}Ce_3$. The $Al_{11}Ce_3$ intermetallic are present in the form of eutectic lath (plate) microstructure and primary crystals. The increase in Mg in the alloy also appears to suppress the undercooling characteristics of the rapid solidification and force some small amount primary solidification in the $Al_{11}Ce_3$ phase. This leads to a slight growth in $Al_{11}Ce_3$ intermetallic, which is evident from the microstructure of Al-10Mg-8Ce-3.5Si compared to Al-5Mg-8Ce-3.5Si alloy. During FSW these $Al_{11}Ce_3$ intermetallic which are generally hard and brittle, break down into small particles. The bigger crystals break down into smaller particles and get distributed into the matrix uniformly. Higher number of hard particles distributed uniformly as in the case of Al-10Mg-8Ce-3.5Si alloy will lead to better strengthening of the matrix and hence improved strength and other mechanical properties compared to the alloy Al-5Mg-8Ce-3.5Si (Poznak et al. 2018; Rios et al. 2016).
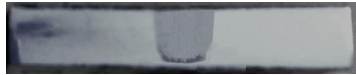
4.3 MACRO OF AND MICROSTRUCTUAL ANALYSIS OF FRICTION STIR WELDED JOINTS OF Al-10Mg-8Ce-3.5Si AND Al-5Mg-8Ce-3.5Si ALUMINIUM ALLOYS, USING TRIANGULAR PIN PROFILE (TPP) TOOL

4.3.1 Macro Analysis of joints Friction stir Welded Al-10Mg-8Ce-3.5Si and Al-5Mg-8Ce-3.5Si aluminium alloys, using Triangular Pin Profile (TPP) tool.

Table 4.2 presents the defect free joints obtained for a TPP tool at different speeds of tool rotation, speeds of welding and weight percentage of magnesium. The FSW experiments were conducted with tool profiles (round, triangular, square), tool rotation speeds (800,1000,1200) and varying welding speeds as 3 different process variables. The defect free welded joints were obtained mainly for welding speeds ranging approximately from 8 mm/min to 23 mm/min for all the cases. Even though the welding speed range changed for each of the cases, the optimum range of speed of welding was considered as 10 mm/min to 20 mm/min for all cases. Defect free joints are attained mainly because of proper material flow and sufficient heat generated due to appropriate selection of process variables. The defect free joints were observed at the weld zone as per the cases listed in are presented in Table 4.1. A Basin shaped nugget zone is observed at lower speeds of tool rotation, and as the speed of tool rotation increases, elliptical shaped nugget zone is observed (Mishra and Ma 2005). This observation is confirmed from the macro images presented in Table 4.2.

Table 4.2 Macrostructural images of Al-5Mg-8Ce-3.5Si and Al-10Mg-8Ce-3.5Si aluminium alloys, Friction Stir welded at various speeds of tool rotation and various speeds of welding using TPP tool.

Exp. No.	Speed of Tool Rotation (RPM)	Speed of Welding (mm/min)	Macro image of FSW region of Al-5Mg-8Ce-3.5Si Aluminium Alloy	Macro image of FSW region of Al-10Mg-8Ce-3.5Si Aluminium Alloy
1.	800	10		

2.		15		
3.		20		
4.		10		
5.	1000	15		
6.		20		
7.		10		
8.	1200	15		
9.		20		

4.3.2 Microstructural Study

Fine grains are produced at the weld center due to the plastic deformation caused by the stirring action of the tool. The weld region showed considerably modified micro-structure when compared to that of the base material. The study of the micro-structure of specimen welded using friction stir welding was carried out using SEM. Figure 4.1 shows the micro image of one such sample. Figure reveals a gradual alteration in the micro-structure from the original coarse undeformed grains of the base material to fine and equiaxed grains at the weld center. Based on the evolution of micro-structure, the weld region could be segregated as three zones or regions as nugget zone/region (NZ), thermo mechanically affected zone/region (TMAZ), heat affected zone/region (HAZ)

(Aydin et al. 2009; Dong et al. 2013; Mishra and Ma 2005; Salih et al. 2015), which is affirmed in this work. The base material region is denoted as BM, and these regions are represented in Figure 4.10 below.

i.) The region where fine equiaxed grains, were developed is named as nugget zone (NZ) (Boonchouytan et al. 2012). This region undergoes high plastic deformation. Frictional heat induced by stirring action of the tool in turn, gives rise to the reorganization of particles from heterogeneous and agglomerated dispersal in the base material to homogeneous dispersal in weld NZ (Hao et al. 2013a; Kallee and Nicholas 2000; Mishra and Ma 2005).

ii.) The NZ is surrounded by highly deformed and elongated grains due to stirring action of the tool (Shettigar and Manjaiah 2017a; Threadgilll et al. 2009). This region is named as thermo-mechanically affected zone (TMAZ). The width of TMAZ region is observed to be very narrow as compared to rest of the zones which is in line with the findings of Dong et al. (2013). Plastic deformation is less in TMAZ region as compared to NZ and therefore recrystallization is incomplete. TMAZ divulges the orientation of α-Al and $Al_{11}Ce_3$ particles and grains in the inclined direction. An elongated grain boundary with parallel band-like distribution of particles is detected in the TMAZ, because of the heat produced due to friction and applied stress induced plastic deformation.

iii.) Heat affected zone (HAZ) is located between TMAZ and Base material. There is no plastic deformation HAZ, and it experiences only thermal cycle. At HAZ, grain size is larger than the base metal due to thermal cycle (Dong et al. 2013; Mishra and Ma 2005).

iv.) Base Material (BM), where there is no change in the micro-structure and mechanical properties as reported by Mishra and Ma (2005).

Interfacial region of NZ and TMAZ

Figure 4.11 depicts the SEM image of interfacial region of NZ and TMAZ of aluminium alloy being welded by FSW. The NZ comprised of numerous small particles as compared to the region of TMAZ. This is due to the striking of hard particles amongst each other and abrasive action of the rotating tool, resulting in numerous small particles.

Stirring action of the tool distributes small particles uniformly in the NZ. The load bearing capacity of the alloy goes up because of uniform distribution of small particles (Alidokht et al. 2012; Li et al. 2015; Starke and Staley 2010). Therefore, the decrease in weight percentage of Mg led to the decline in strength and hardness.
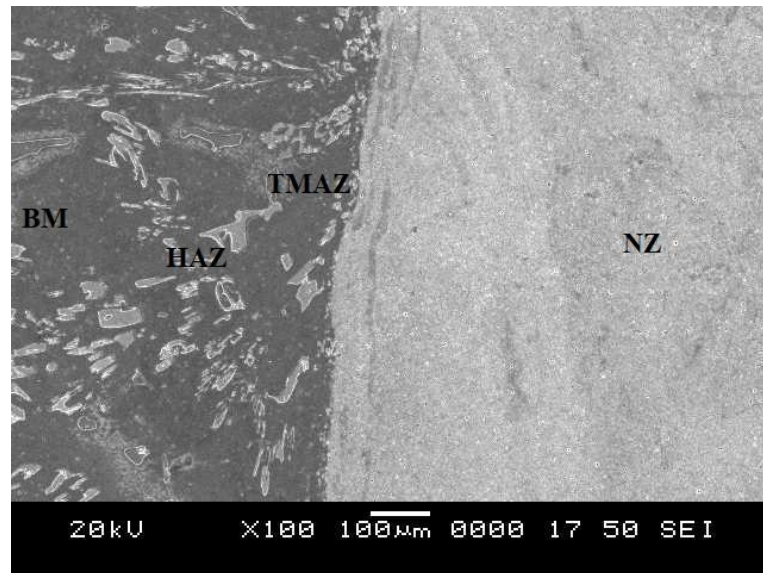
Figure 4.10 Scanning Electron Micrograph showing the advancing side friction stir welded Al-10Mg-8Ce-3.5Si aluminium alloy weld region.
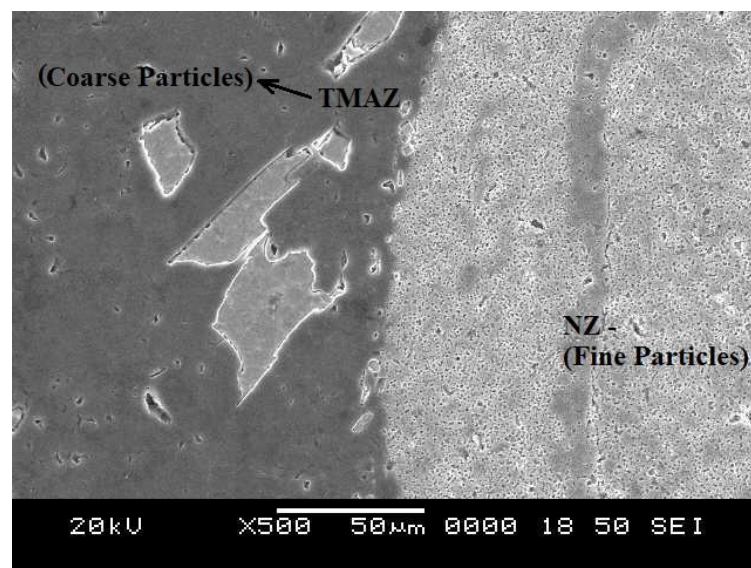
Figure 4.11 Scanning Electron Micrograph showing the advancing side of weld region of friction stir welded Al-10Mg-8Ce-3.5Si alloy of aluminium.

145

Figure 4.12 (a to f) represent distribution of elements in the NZ of a welded Al-10Mg-8Ce-3.5Si aluminium alloy. All the elements are uniformly distributed in the NZ. The stirring action of the tool at the center of the NZ produces fine equiaxed grains. It is observed that, the weld made by the TPP tool revealed finer equiaxed grains when compared to other pins. Similar observation was also found by Elangovan et al. (2008) and Babu et al. (2009). The flow of plasticized material from the front of the tool to the back of the rotating tool is dependent on the relation between dynamic and static volumes. Pin profiles having flat faces associates with eccentricity. This eccentricity permits incompressible material to flow around the profiled pin. The dynamic to static volume ratio is found to be 2.47 for TPP tool, whereas that for the SPP tool is 1.56 and for the CPP tool is 1(Refer Appendix-II). Therefore, the TPP tool sweeps more material than other tools considered in this work. The square and triangle shaped tool pin are associated with eccentricity compared to round and threaded shapes, which allow the incompressible material movement around the pin profile. Because of the eccentricity of the pin, the dynamic orbit is related to the eccentricity of the rotating plasticized material. The path for the flow of plasticized material is identified by the ratio of static volume and dynamic volume. In addition to that, the flat faces of triangular tool generate a pulsating stirring action in the flow of the plasticized material. It in turn leads to the pulsating stirring action in the plasticized flowing material due to flat surfaces. Because of this better plasticizing and pulsating action, the resulting joint is produced with fine grained material which is of relatively better strength and hardness compared to the joints produced with tools of other type of geometries. The TPP tool produces 40, 50 and 60 pulses/sec for a speed of tool rotation of 800, 1000 and 1200 RPM, respectively (Elangovan and Balasubramanian 2008b; Huang et al. 2018b; Palanivel et al. 2012; Shettigar and Manjaiah 2017b).

The stirring action of the tool induces excessive amount of plastic deformation and liberation of frictional heat among the base material and the tool. This leads to dynamic recrystallization (Barcellona et al. 2006; Fratini and Buffa 2007; Murr et al. 1998).

Figure 4.13 (a) and (b) and Figure 4.14 (a) and (b) represent SEM image and EDX spot analysis of friction stir welded Al-10Mg-8Ce-3.5Si and Al-5Mg-8Ce-3.5Si aluminium alloy joints respectively. At NZ, the circular and irregular shaped objects are seen as shown in Figure 4.13 (a) and Figure 4.14 (a), and are analyzed by EDX. Different levels in the peaks of Al, Ce, Si, Mg, Zn, Ti, Fe, and Mn elements have been observed in Figure 4.13 (b) and Figure 4.14 (b). In Al-Cu-Si-Mg alloy, such kinds of precipitates are common (Dong et al. 2019; Nafsin and Rashed 2013; Toschi 2018).
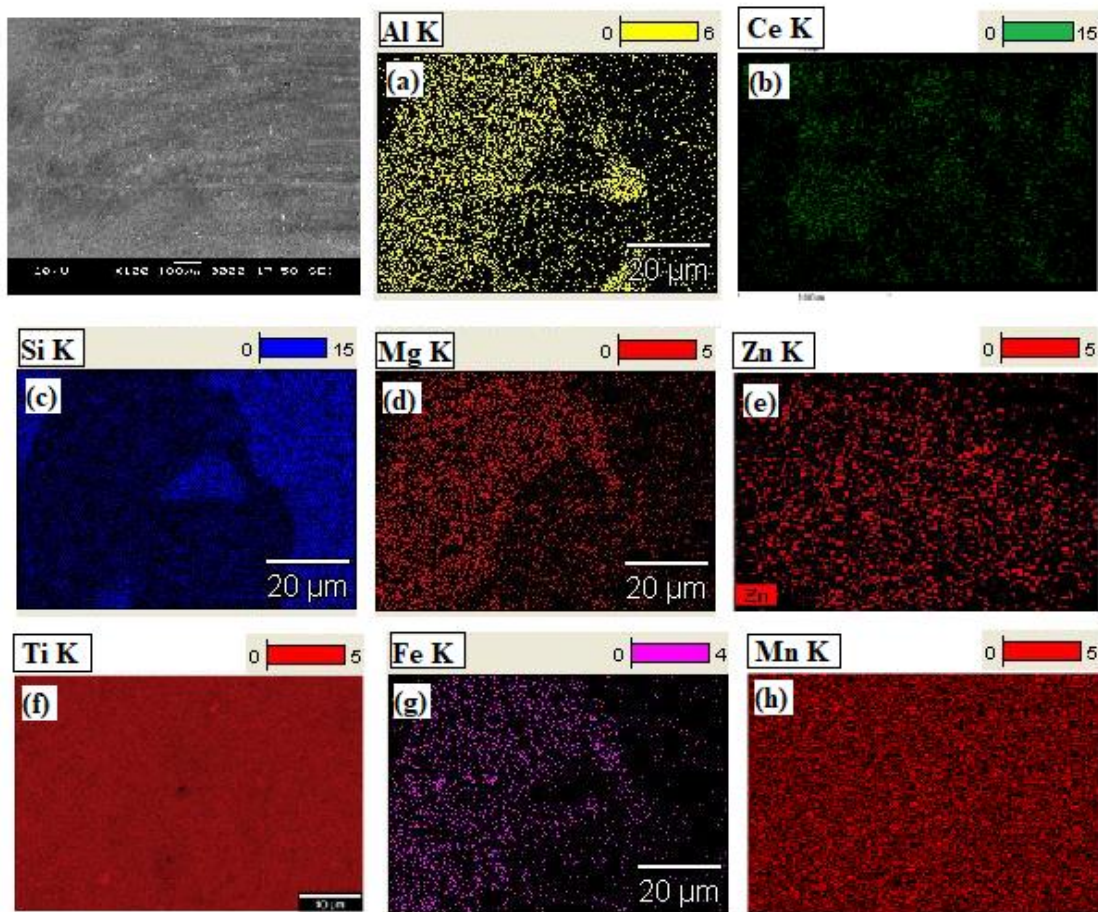
Figure 4.12 Friction Stir Welded Al-10Mg-8Ce-3.5Si aluminium alloy; (a) SEM image of NZ, (b) EDX map of Al, (c) EDX of map of Ce, (d) EDX map of Si, (e) EDX map of Mg, (f) EDX map of Zn, (f) EDX map of Ti, (f) EDX map of Fe and (f) EDX map of Mn elements
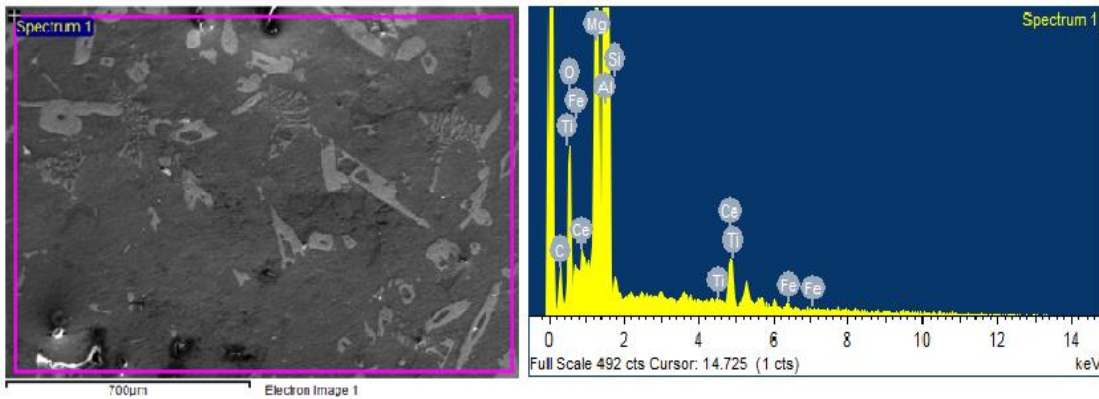
Figure 4.13 Friction Stir Welded Al-10Mg-8Ce-3.5Si aluminium alloy joint; (a) SEM image of the NZ and (b) EDX spectrum showing the presence of individual elemental peaks.
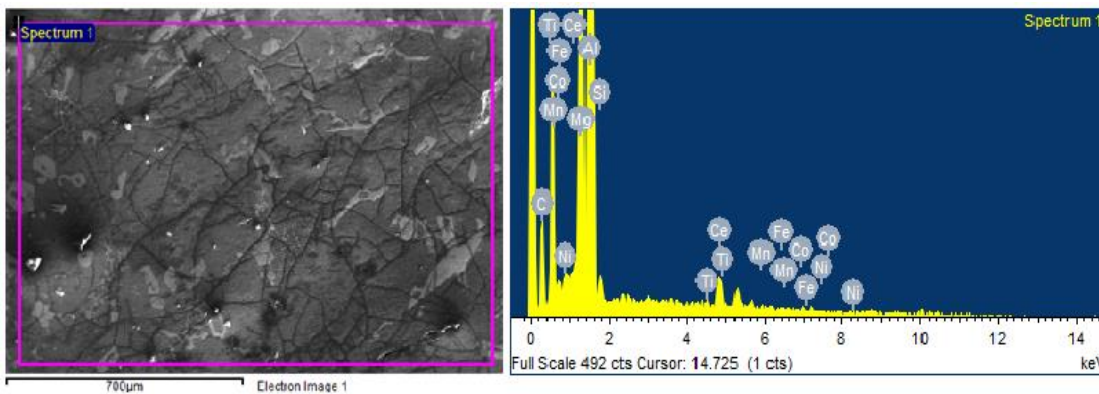
Figure 4.14 Friction Stir Welded Al-5Mg-8Ce-3.5Si aluminium alloy joint; (a) SEM image of the NZ and (b) EDX spectrum showing the presence of individual elemental peaks.

Figure 4.15 (a) depicts SEM image of the NZ and Figure 4.15 (b) depicts plots the EDX spot analysis of friction stir welded Al-10Mg-8Ce-3.5Si aluminium alloy joint. The rectangular shaped objects in Figure 4.15 (a) represent the α-Al, $Al_{11}Ce_3$ and AlSiMg particles which is confirmed by EDX. The peaks present in Figure 4.15 (b) correspond to Al, Ce, Si and Mg. Small cracks have been spotted at the bottom these particles which provided evidence for the breakdown of particles in the stair zone.

148
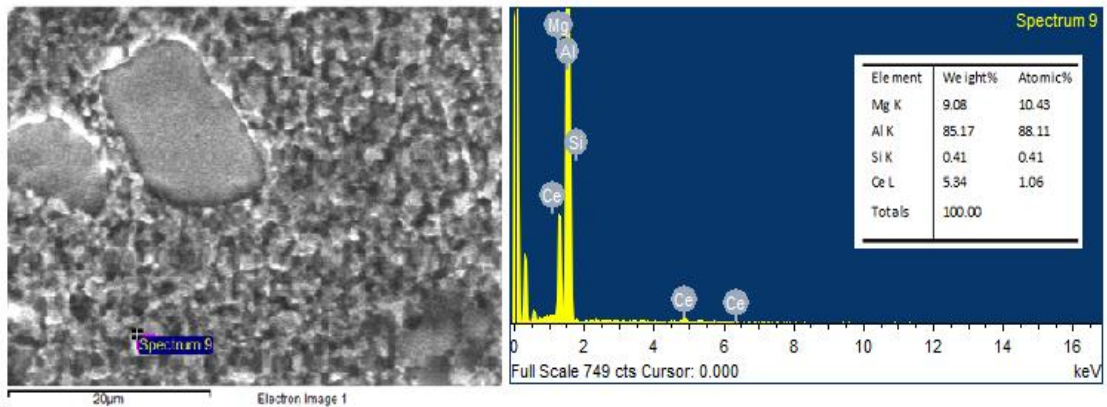
Figure 4.15 Friction Stir Welded Al-10Mg-8Ce-3.5Si aluminium alloy joint; (a) SEM image of NZ showing α-Al, Al$_{11}$Ce$_3$ and AlMgSi particles and (b) EDX spectrum displaying the presence of Al-Ce-Si-Mg peaks.

Figure 4.16 (a) depicts SEM image of the NZ and Figure 4.16 (b) Plots the EDX spot analysis of friction stir welded Al-10Mg-8Ce-3.5Si aluminium alloy joint. The bright spots present in Figure 4.16 (a) are Al and Ce elements, and this is confirmed by the corresponding peaks in EDX map of the stir zone. The coarse precipitates presented in the base material are fragmented by tool action during the welding process. These precipitates are uniformly distributed in the NZ, which were initially present at the grain boundary, in the base material.
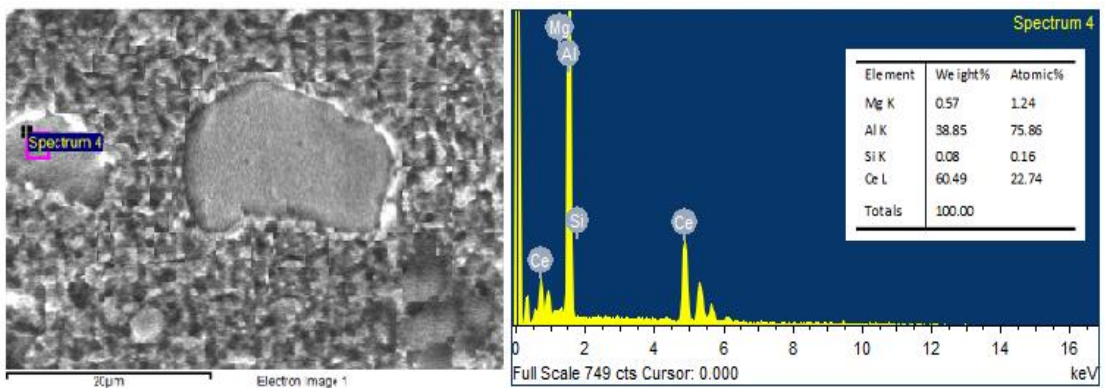
Figure 4.16 Friction Stir Welded Al-10Mg-8Ce-3.5Si aluminium alloy joint; (a) SEM image of NZ showing Al, Ce, Si and Mg and (b) EDX spectrum displaying the presence of Al-Ce-Si-Mg peaks.

149

Figure 4.17 illustrates the SEM image NZ of Al-10Mg-8Ce-3.5Si aluminium alloy obtained by friction stir welding. The image shows the evidence for breaking down of α-Al, $Al_{11}Ce_3$ and AlMgSi particles. The stirring action of the tool makes the hard particles having sharp edges to collide with each other leading to breakage (Balakrishnan et al. 2019; Shettigar and Manjaiah 2017a). The breakage also occurs due to abrasive action of the rotating tool (Murugan and Ashok Kumar 2013).
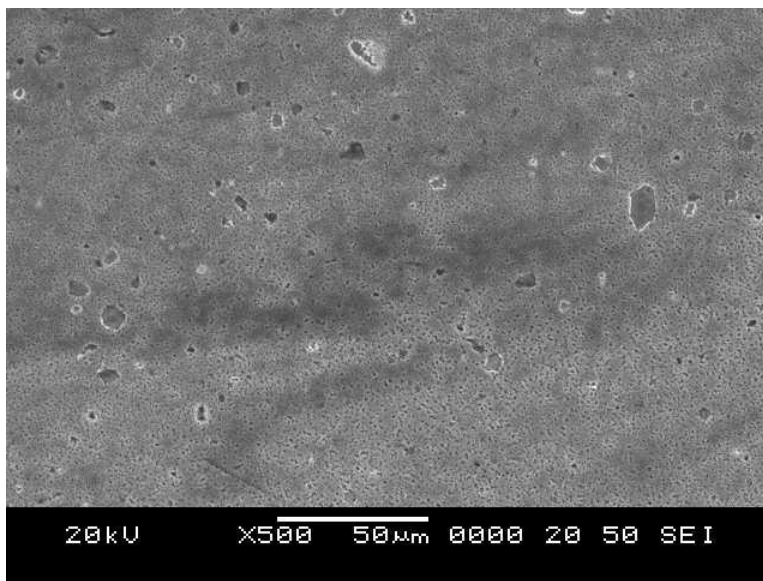
Figure 4.17 SEM image of nugget zone of friction stir welded Al-10Mg-8Ce-3.5Si aluminium alloy, showing the breakage of α-Al, $Al_{11}Ce_3$ and AlMgSi particles.

4.3.3 Micro-structure of Al-10Mg-8Ce-3.5Si aluminium alloy Friction stir welded using TPP tool Study

Figure 4.18 (a to e) represent the SEM images of Al-10Mg-8Ce-3.5Si aluminium alloy, friction stir welded with a speed of tool rotation of 1000 RPM and at a welding speed of 15 mm/min, using TPP tool. Figure 4.19 (a to c) represent the distribution of grain size at top, middle and bottom of the NZ, respectively. The grain distribution at top, middle and bottom of the NZ are tabulated in Table 4.3. The average grain size at the top, middle and bottom regions of the NZ are 9.7±0.23, 7.4±0.17 and 6.8±0.12 µm respectively, got at a speed of tool rotation of 1200 RPM and at a welding speed of 10 mm/min. It is clear that the grain size from the top surface of the weld to the bottom of

150

the weld connection is decreasing. Compared to bottom NZ, The top of the NZ is subjected to centrifugal forces of higher magnitude (Herbert et al. 2016; Mastanaiah et al. 2018). An extrusion crushing force small magnitude will be subjected on metals per unit area during recrystallization, leading to bigger crystal nucleus. In the meantime, a higher temperature is produced by the shoulder which acts as a source of heat. This necessitates an extended cooling time, because of which the growth in grain happens. Also, to avoid the plunged pin of the tool touching the backing plate, the penetration depth of the pin is kept less than the thickness plate being welded. As a consequence, there will be inadequate plasticization and flow of the material at the bottom of the NZ because of dearth of stirring and forging action. The heat travels from the top to bottom by conduction phenomenon of heat transfer and base plate behaves as a heat sink at the root of the weld. In the bottom, the extrusion forming is not completed under peak temperature. Therefore, extrusion takes place because of plastic deformation of the material around the weld root. Because of this whole phenomenon the creation of fine grains takes place at the bottom of the NZ. This is in proved by Aydin et al. (2009), Ji et al. (2016) and Khan et al. (2017) in their findings. The average decrease in the grain size at NZ is 93.2% at a speed of tool rotation of 1200 RPM and a welding speed of 10 mm/min. Figure 4.18 (d and e) represent the grain structure found at TMAZ on both sides of the NZ. A non-homogeneous, coarser, elongated, bent and, highly deformed, grains are found because of the tool's stirring action. One can also notice from Table 4.3 that, as the speed of tool rotation goes up from 800 RPM to 1000 RPM, the grain size decreases. This is because of the rotating tool being accountable for stirring and mixing of softened plasticized material. The flow of plasticized material from the front of the tool to the back of the rotating tool depends on the relation between dynamic and static volume. The dynamic to static volume ratio is found to be 2.3 for TPP tool (Elangovan et al. 2008a).

Considerable increase in temperature around the rotating tool will result in softening of the plasticized material. Thus, in this case, sufficient heat generation and adequate material flow have led to the formation of equiaxed, fine grains at NZ, at a speed of tool rotation of 1000 RPM. Further increase of speed of tool rotation from 1000 RPM to 1200 RPM increased the heat generated at NZ. This effect led to turbulence in the

material flow and the excess heat, causing grain growth. In the case of welding speed, with an increase in welding speed from 10 to 15 mm/min, the grain refinement was proportionally improved. The reason behind improvement in the grain size was due to the rate of heat supplied during the FSW. The increase in welding speed from 10 to 15 mm/min not only reduces the exposure time of frictional heat but also decreases the deformation heat per unit length of weld as cited by Hamilton et al. (2008) and Lakshminarayanan et al. (2011). At a lower welding speed of 10 mm/min, the heat generated is higher because of longer exposure time to frictional heat per unit length of weld. Higher heat at weld area and lower cooling rate causes grain growth and affects the precipitates (Fonda and Bingert 2006; Fu et al. 2013; Hassan et al. 2003a; Sato et al. 2002).
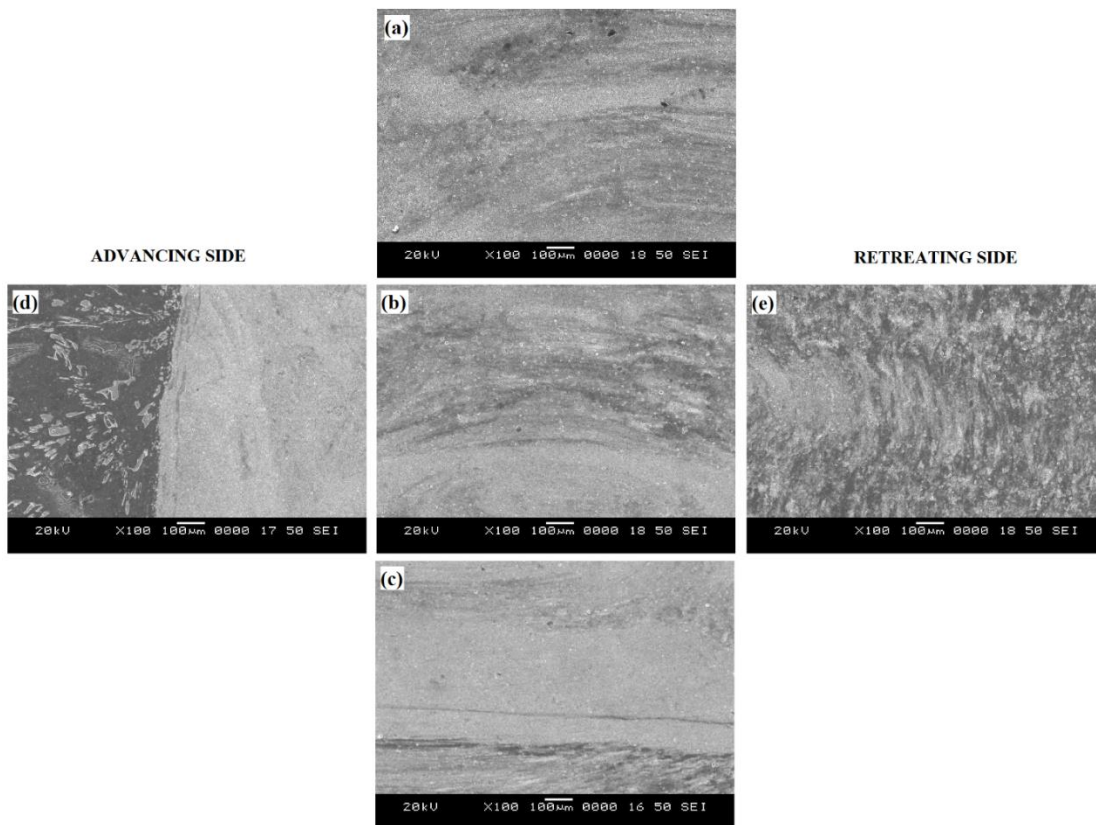
Figure 4.18 Scanning Electron Micrograph of friction stir welded joint of Al-10Mg-8Ce-3.5Si Aluminium alloy using TPP tool at a speed of tool rotation of 1000 RPM and a welding speed 15 mm/min, depicting distribution of grain size at (a) Top of the NZ, (b) Middle of the NZ, (c) Bottom of the NZ, (d) Advancing side of TMAZ and (e) Retreating side of TMAZ.

152

Table 4.3 Average grain size found at top, middle and bottom of the NZ of friction stir welded Al-10Mg-8Ce-3.5Si Aluminium alloy weld connection, fabricated at various speeds of tool rotation and speeds of welding, using TPP tool.

Expt. No.	Speed of Tool Rotation (RPM)	Speed of Welding (mm/min)	Average Grain Size (µm)		
			Top	Middle	Bottom
1.		10	8.8±0.21	6.9±0.2	6.2±0.08
2.	800	15	8.1±0.16	6.1±0.23	5.7±0.19
3.		20	7.7±0.11	5.5±0.2	5.3±0.08
4.		10	6.8±0.21	7.1±0.23	6.4±0.08
5.	1000	15	6.7±0.11	6.6±0.18	5.8±0.16
6.		20	6.5±0.22	5.9±0.17	5.1±0.12
7.		10	9.7±0.17	7.4±0.14	6.8±0.12
8.	1200	15	8.1±0.23	6.7±0.18	6.2±0.19
9.		20	7.3±0.23	6.2±0.16	5.6±0.14

Figure 4.19 illustrates the plots of distribution of average grain size at NZ of weld joint obtained using friction stir welding Al-10Mg-8Ce-3.5Si aluminium alloy plates. The alloys were welded using TPP tool. It is clear from the plots that, the grain size at the top of the NZ is bigger and gets smaller towards the bottom of the weld NZ. The weld connection fabricated at a speed of tool rotation of 1200 RPM and a welding speed of 15 mm/min revealed highest average grain size of 9.7±0.23 µm. Increased heat conditions existing at a lower welding speed (10 mm/min), with decreased cooling rate led to the coarsening of grains in the NZ (Çam 2011; Dong et al. 2013; Feng et al. 2010). On the other hand, the weld connection fabricated at a speed of tool rotation of 1000 RPM and a welding speed of 20 mm/min revealed least average grain size of 5.1±0.12 µm. This is due to the increase in welding speed (20 mm/min) leading to lesser heat input because of shorter availability of time for friction in the process. Also, it seems that, the existing minimized heat condition works as a stimulus for more

strain and strain rate, leading to more dynamic recrystallization which in turn, contributes towards refinement of grains (Fratini and Buffa 2005; McNelley et al. 2008). In addition to this, the pinning effects of AlMgSi particles which are mainly resident at the grain boundaries, thwart the grain growth and due to this the grain size gets reduced (Feng et al. 2006; Robson and Campbell 2010; Yaduwanshi et al. 2014).

Table 4.4 presents the grain structure of friction stir welded aluminium alloy at different process parameters.
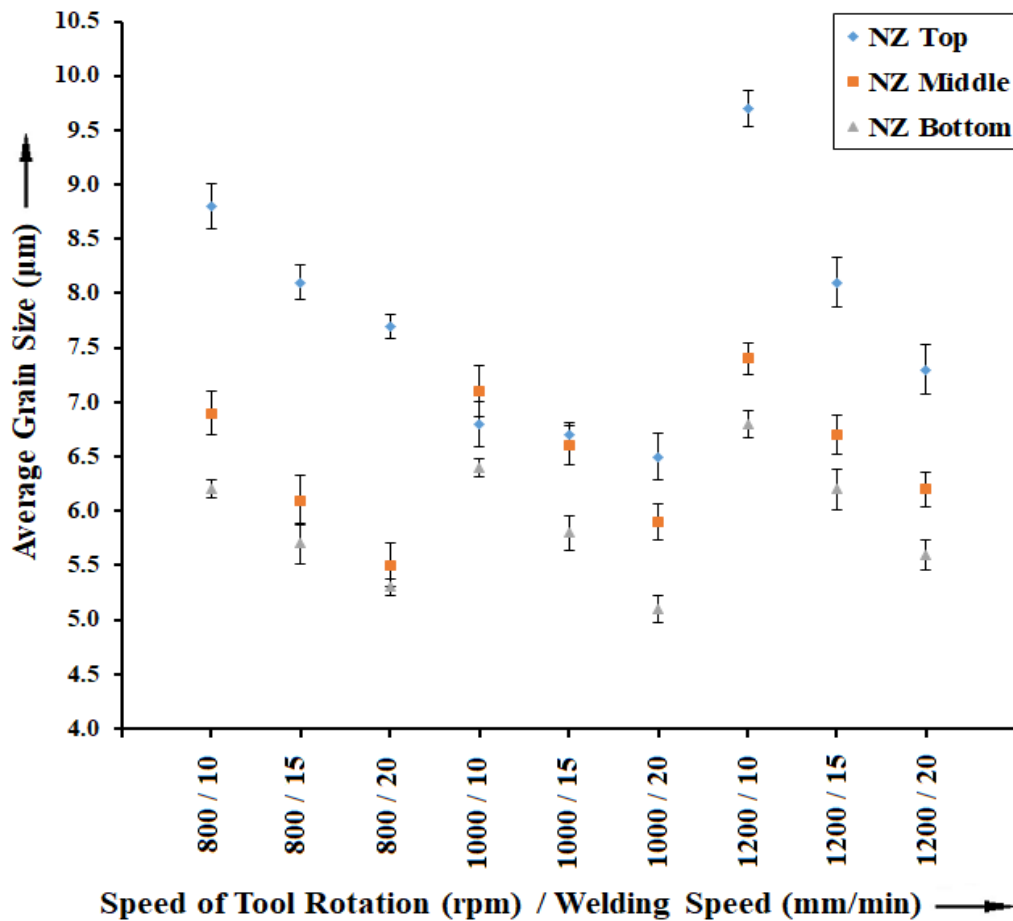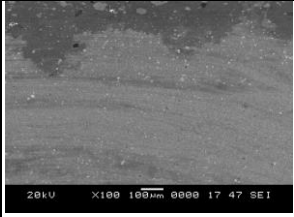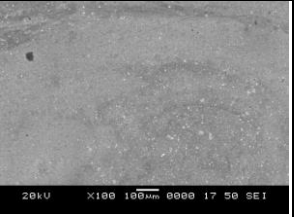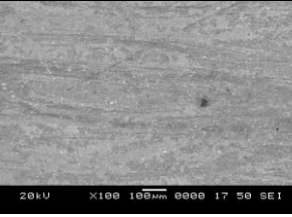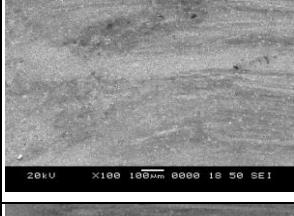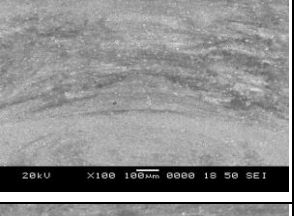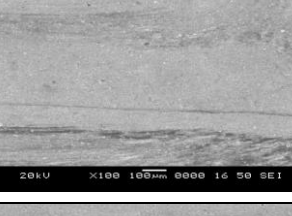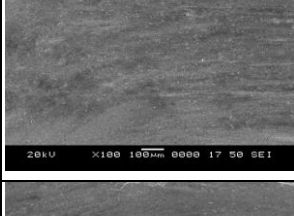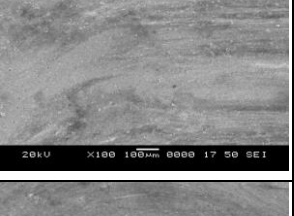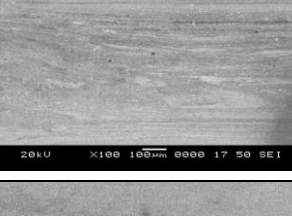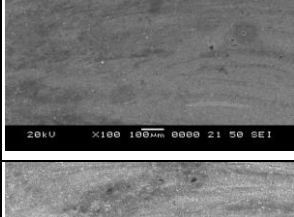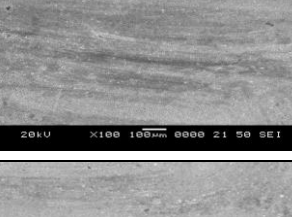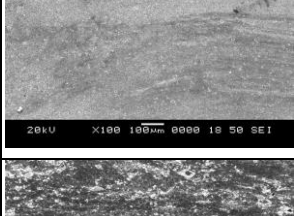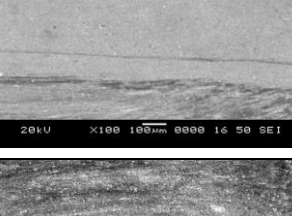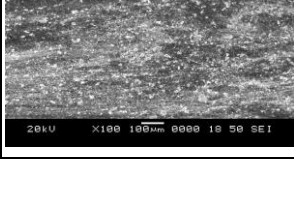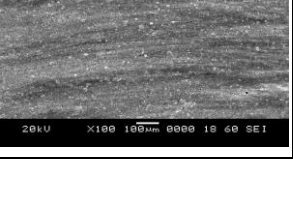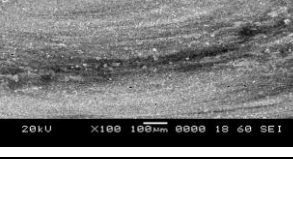
Figure 4.19 Average grain size distribution at NZ of friction stir welded Al-10Mg-8Ce-3.5Si aluminium alloy joint, fabricated through TPP tool.

Table 4.4 Micro-structure images of NZ of friction stir welded Al-10Mg-8Ce-3.5Si aluminium alloy joint, fabricated using TPP tool for different process parameters.

Method variable	Micro-structure image of top of nugget zone	Micro-structure image of middle of nugget zone	Micro-structure image of bottom of nugget zone
800 RPM and 10 mm/min			
800 RPM and 15 mm/min			
800 RPM and 20 mm/min			
1000 RPM and 10 mm/min			
1000 RPM and 15 mm/min			
1000 RPM and 20 mm/min			

1200 RPM and 10 mm/min			
1200 RPM and 15 mm/min			
1200 RPM and 20 mm/min			
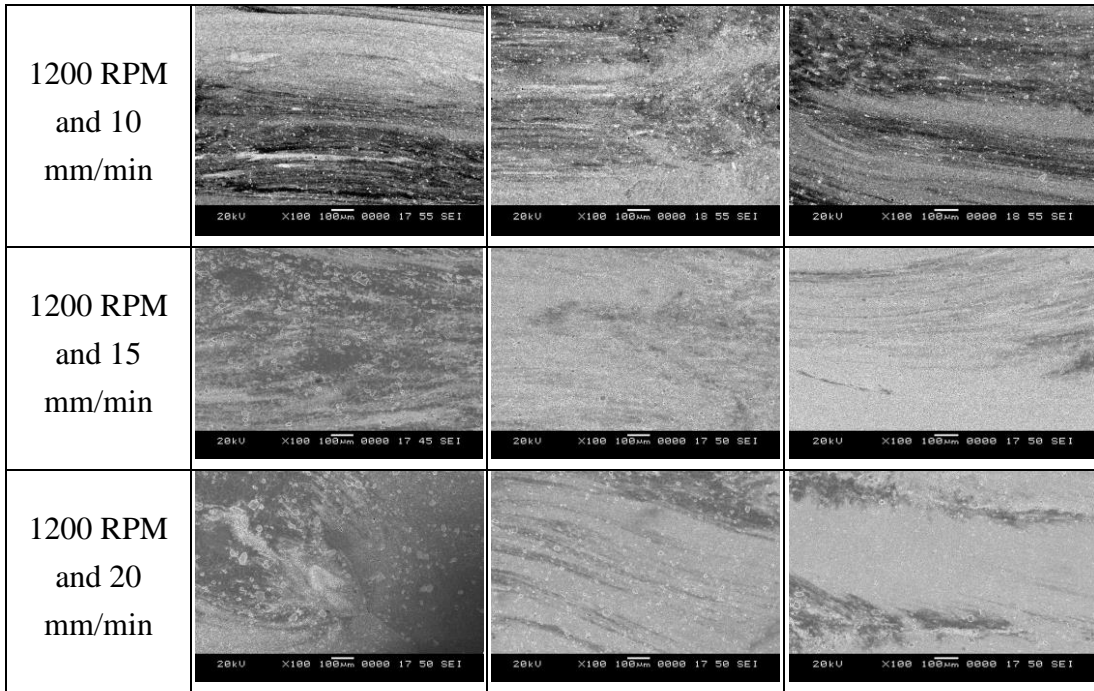
4.3.4 Micro-structure of Al-5Mg-8Ce-3.5Si aluminium alloy friction stir welded using TPP tool Study

Figure 4.20 (a to e) depict the SEM images of Al-5Mg-8Ce-3.5Si aluminium alloy, friction stir welded with TPP tool. The welding of aluminium alloy was done at a speed of tool rotation of 1000 RPM and a welding speed of 20 mm/min. Figure 4.20 (a to c) represent the distribution of grain size at the top, middle and bottom of the NZ, respectively. The measured average grain size for various speeds of tool rotation and speeds of welding have been tabulated in Table 4.5. The average grain size obtained at the top, middle and bottom of the NZ is 12.3±0.15, 9.4±0.18 and 8.3±0.11 µm respectively, with a speed of tool rotation of 1200 RPM and a welding speed of 10 mm/min. The average decrease in the grain size at the NZ is 89.5%. Similar trend of grain size distribution is also found in the Al-10Mg-8Ce-3.5Si aluminium alloy for various speeds of tool rotation and speeds of welding. Figure 4.20 (d) and (e) represent the grain structure evolved at TMAZ on either side of the NZ.
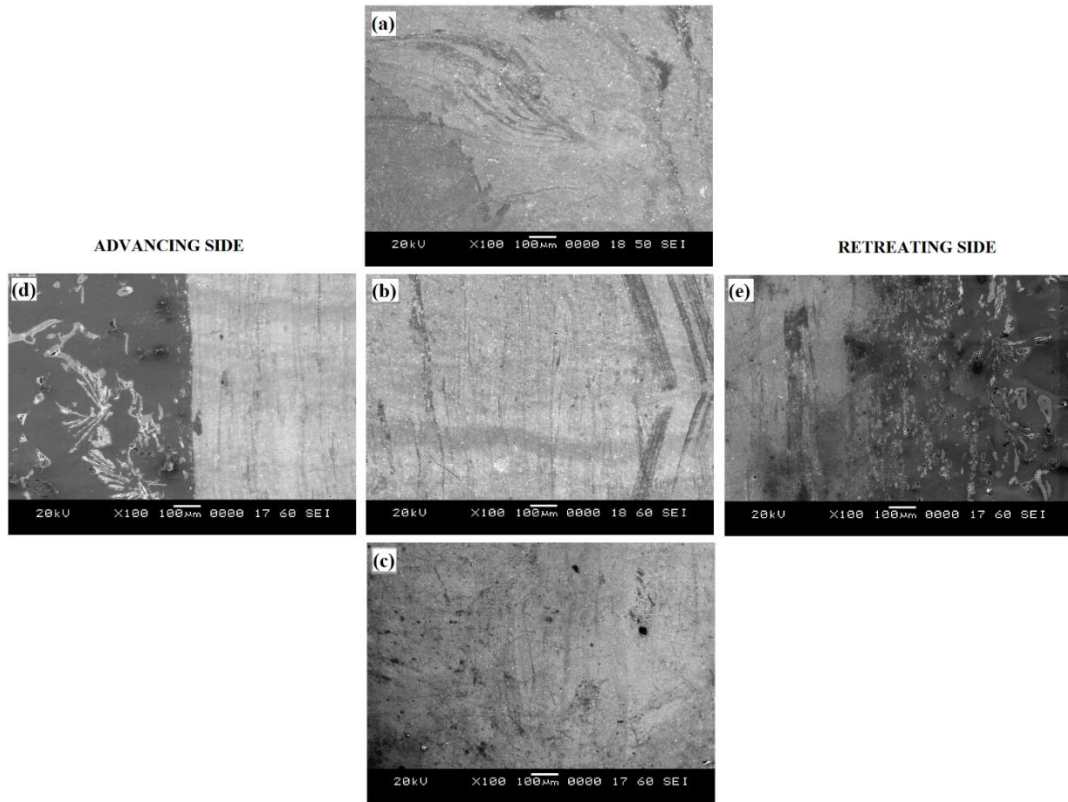
Figure 4.20 Scanning Electron Micrograph of friction stir welded joint of Al-5Mg-8Ce-3.5Si Aluminium alloy weld connection, fabricated using TPP tool at a speed of tool rotation of 1000 RPM and a welding speed 20 mm/min, depicting distribution of grain size at (a) Top of the NZ, (b) Middle of the NZ, (c) Bottom of the NZ, (d) Advancing side of TMAZ and (e) Retreating side of TMAZ.

Table 4.5 Average grain size obtained at top, middle and bottom of the NZ of friction stir welded Al-5Mg-8Ce-3.5Si Aluminium alloy weld connection, fabricated at various speeds of tool rotation and speeds of welding, using TPP tool.

Expt. No.	Speed of Tool Rotation (RPM)	Speed of Welding (mm/min)	Average Grain Size (µm)		
			Top	Middle	Bottom
1.		10	11.2±0.18	8.7±0.21	7.5±0.16
2.	800	15	10.3±0.14	7.9±0.14	7±0.07
3.		20	9.8±0.16	7.2±0.2	6.6±0.19

4.		10	8.6±0.18	8.3±0.21	7.8±0.16
5.	1000	15	8.5±0.23	8.1±0.24	7.4±0.07
6.		20	7.9±0.19	7.5±0.16	6.3±0.13
7.		10	12.3±0.15	9.4±0.18	8.3±0.11
8.	1200	15	10.1±0.19	8.5±0.18	7.6±0.17
9.		20	8.7±0.12	7.5±0.2	6.8±0.09

Figure 4.21 shows graphically, the average grain size distribution formed at NZ of Al-5Mg-8Ce-3.5Si Aluminium alloy during friction stir welding. The alloys were welded using TPP tool for various speeds of tool rotation and speeds of welding. Similar observations were also obtained for friction stir welded Al-5Mg-8Ce-3.5Si Aluminium alloy. Slightly average grain size evolved at NZ due to increase in the weight percentage of Mg particles. The Mg particles restrict the grain growth during recrystallization (Azizieh et al. 2011; Cerri and Leo 2013).
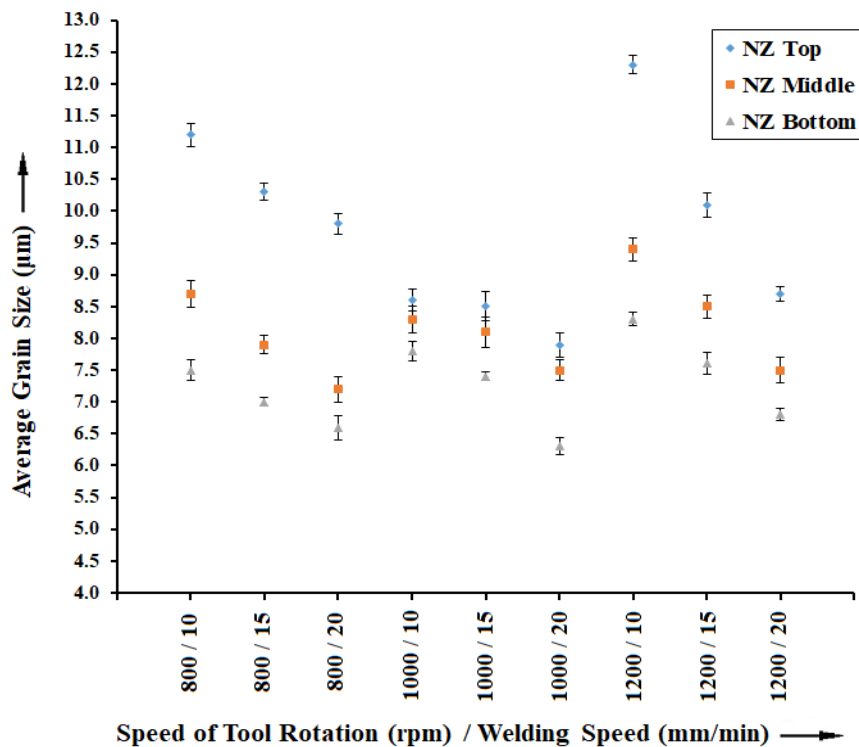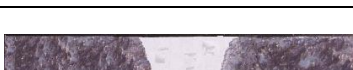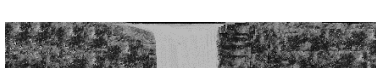
Figure 4.21 Average grain size distribution at NZ of friction stir welded Al-5Mg-8Ce-3.5Si Aluminium alloy weld connection fabricated through TPP tool.

4.4 MACRO AND MICROSTRUCTUAL ANALYSIS OF FRICTION STIR WELDED JOINTS OF Al-10Mg-8Ce-3.5Si AND Al-5Mg-8Ce-3.5Si ALUMINIUM ALLOYS, USING SQUARE PIN PROFILE (SPP) TOOL

4.4.1 Macro Analysis of joints friction stir Welded joints of Al-10Mg-8Ce-3.5Si and Al-5Mg-8Ce-3.5Si aluminium alloys, using Square Pin Profile (SPP) tool.

The macro images of the Al-10Mg-8Ce-3.5Si and Al-5Mg-8Ce-3.5Si aluminium alloys friction stir welded, with different combinations of speeds of welding of 10, 15, 20 mm/min and speeds of tool rotation of 800, 1000 and 1200 RPM, using SPP tool, have been presented in Table 4.6. The NZ exhibited combined basin and elliptical shape for all the cases of welding using SPP tool. The change in the nugget shape is mainly credited to the geometry of the tool (Mishra and Ma 2005; Schneider et al. 1991). The flow of plasticized material from the front of the tool to the back of the rotating tool depends on the relation between dynamic and static volume. Pin profiles having flat faces associates with eccentricity. This eccentricity allows incompressible material to pass around the pin profile. The dynamic to static volume ratio is found to be 1.56 for SPP tool (Elangovan et al. 2008a). Therefore, the SPP tool sweeps less material than triangular profile pin tool and more material than the round profile pin tool considered in this work. In addition to that, the flat faces of square tool produce a pulsating stirring action in the flow of plasticized material. The SPP tool produces 53, 67 and 80 pulses/sec for speeds of tool rotation of 800, 1000 and 1200 RPM, respectively. There is fairly good pulsating effect in the case of the weld connection fabricated using SPP tool (Elangovan and Balasubramanian 2008b; Huang et al. 2018b; Palanivel et al. 2012).

Table 4.6 Macrostructural images of Al-5Mg-8Ce-3.5Si and Al-10Mg-8Ce-3.5Si aluminium alloys, friction Stir welded at various speeds of tool rotation and various speeds of welding using SPP tool.

Expt. No.	Speed of Tool Rotation (RPM)	Speed of Welding (mm/min)	Macro image of FSW region of Al-5Mg-8Ce-3.5Si Aluminium Alloy	Macro image of FSW region of Al-10Mg-8Ce-3.5Si Aluminium Alloy
1.		10		
2.	800	15		
3.		20		
4.		10		
5.	1000	15		
6.		20		
7.		10		
8.	1200	15		
9.		20		

4.4.2 Micro-structure of Al-10Mg-8Ce-3.5Si aluminium alloy, friction stir welded using SPP tool.

Figure 4.22 (a to e) show the SEM images of friction stir welded Al-10Mg-8Ce-3.5Si aluminium alloy joint, fabricated with SPP tool at a speed of tool rotation of 1000 RPM and a welding speed of 15 mm/min. Figure 4.22 (b, c and d) present the average grain size distribution of NZ near the top, middle, and at the bottom. Table 4.7 presents the average grain size measured at different zones of aluminium alloys at different process parameters. The average grain size obtained near the top, middle and near the bottom of the NZ are 11.4±0.15, 8.8±0.23, 7.9±0.18 µm respectively, got at a speed of tool rotation of 1200 RPM and a welding speed of 10 mm/min. The grain size obtained is much smaller than the base material. Also, the size of the grains in the NZ is bigger than the grain sizes in NZ for samples welded by TPP tool, for various combinations of process parameters. This is due to the lower dynamic to static volume ratio of the SPP tool, which influence the stirring effect, thereby causing lesser fragmentation of both the particles and the grains. The percentage of reduction in the grain size is 88.6% as compared to base material as against a value of 93.2% for the weld connection fabricated using TPP tool. Figure 4.22 (a) and (e) represent the advancing side and retreating side of TMAZ, respectively. Rotated and elongated grain structures have been observed on both the sides of the TMAZ.

Figure 4.23 illustrates the plots for distribution of average grain size at the nugget zone of the joint of Al-10Mg-8Ce-3.5Si Aluminium alloy obtained with friction stir welding. The average grain size at NZ of the alloy weld connection friction stir welded using SPP tool is found to be more than the grain size obtained for weld connection fabricated by TPP tool. When square pin used for FSW, the ratio of swept volume to static volume is lower. Hence, SPP tool generates lesser pulsating stirring action in the flow of material than the TPP tool, which leads to the creation of coarser grains. The grain boundaries were the chief obstruction to the dislocation slips and the material with a tinier size of grain had a greater strength as it would levy more restrictions to the movement of dislocations (Chowdhury et al. 2010; Li et al. 2014b; Luo et al. 2016; Prangnell and Heason 2005; Rizi and Kokabi 2014). Therefore, strength of the weld

connection fabricated by square profile pin tool is expected to be lower as compared to the weld connection fabricated using triangular profile pin tool.
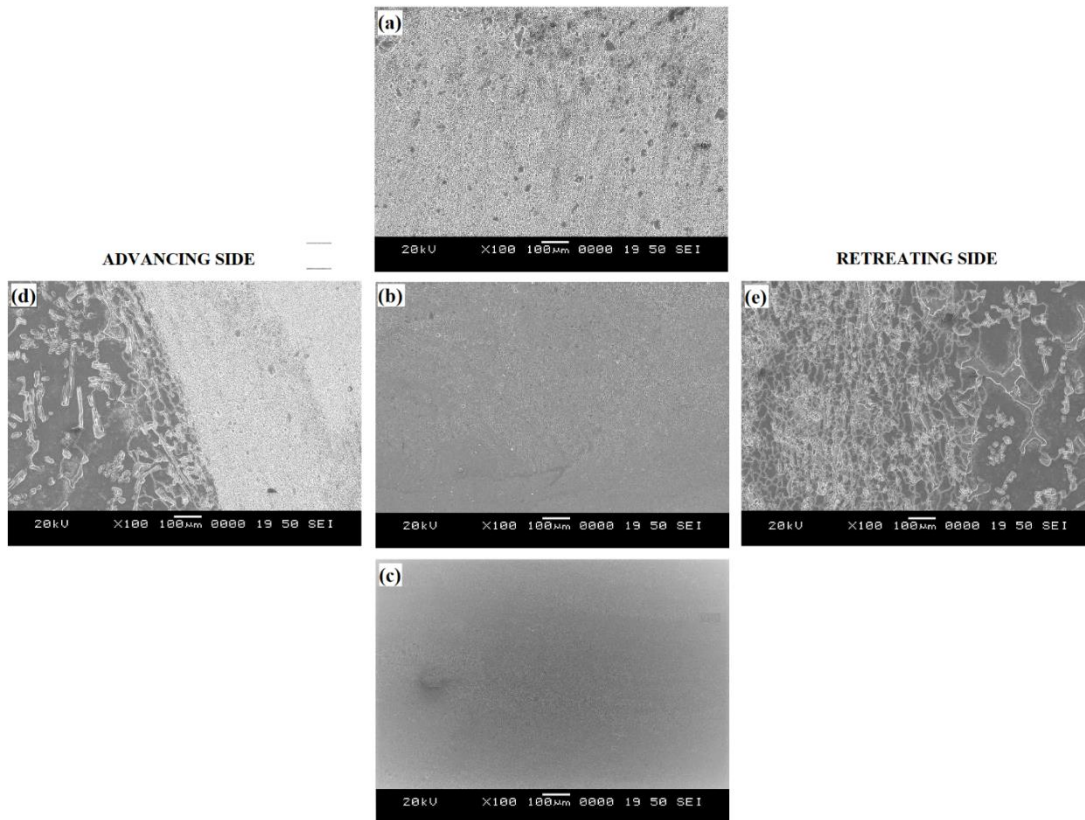
Figure 4.22 Scanning Electron Micrograph of friction stir welded Al-10Mg-8Ce-3.5Si Aluminium alloy joint, fabricated using SPP tool at a speed of tool rotation of 1000 RPM and a welding speed 15 mm/min, showing distribution of grain size at (a) Top of the NZ, (b) Middle of the NZ, (c) Bottom of the NZ, (d) Advancing side of TMAZ and (e) Retreating side of TMAZ.

4.4.3   Micro-structure of Al-5Mg-8Ce-3.5Si aluminium alloy joint, fabricated using friction stir welding with SPP tool.

The SEM images of Al-5Mg-8Ce-3.5Si aluminium alloy joint, fabricated using friction stir welding with SPP tool at a speed of tool rotation of 1000 RPM and a welding speed of 10 mm/min are depicted in the Figure 4.24 (a to e). Figure 4.24 (b, c and d) represent the average grain size distribution of NZ near the top of square pin, at middle of square pin, as well as near the bottom of the square pin. The measured average grain size for

162

various speeds of tool rotation and speeds of welding are listed in the Table 4.8. The average grain size found near the top, at middle, and near the bottom of the NZ are 12.1±0.14, 9.7±0.15, 8.7±0.13 µm, respectively obtained at a speed of tool rotation of 1200 RPM and welding speed of 10 mm/min. The average decrease in the grain size is 87.9% as compared to the base alloy. Similar trend is also observed for Al-10Mg-8Ce-3.5Si aluminium alloy.

Table 4.7 Average grain size found at top, middle and bottom of the NZ of friction stir welded Al-10Mg-8Ce-3.5Si Aluminium alloy weld connection, fabricated at various speeds of tool rotation and speeds of welding, using SPP tool.

Expt. No.	Speed of Tool Rotation (RPM)	Speed of Welding (mm/min)	Average Grain Size (µm)		
			Top	Middle	Bottom
1.		10	10.5±0.14	8.6±0.18	7.7±0.13
2.	800	15	9.6±0.19	7.2±0.24	6.8±0.07
3.		20	9.2±0.17	6.8±0.18	6.4±0.1
4.		10	8.6±0.22	8.7±0.14	7.8±0.07
5.	1000	15	7.9±0.11	8±0.18	7.1±0.17
6.		20	7.3±0.13	6.9±0.23	6.1±0.1
7.		10	11.4±0.15	8.8±0.23	7.9±0.18
8.	1200	15	9.5±0.21	8.2±0.19	7.6±0.15
9.		20	8.4±0.19	7.7±0.2	6.7±0.07
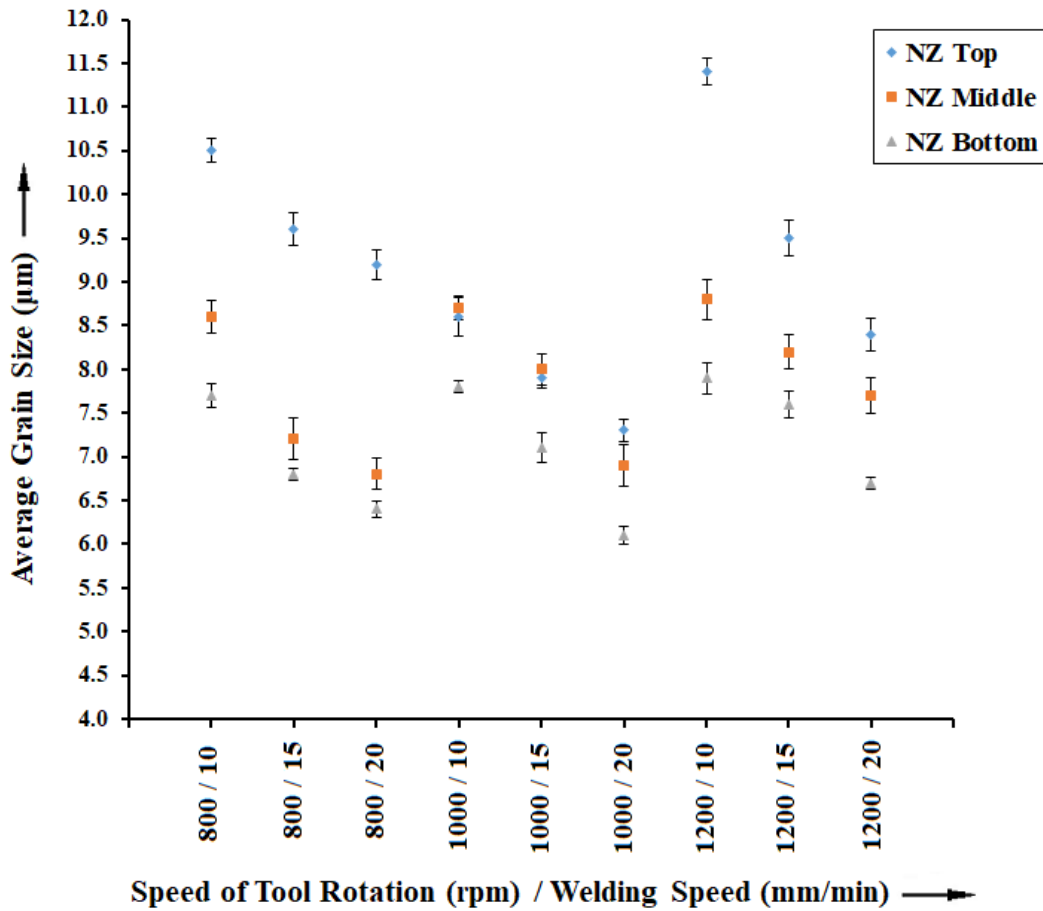
Figure 4.23 Average grain size distribution at NZ of friction stir welded Al-10Mg-8Ce-3.5Si Aluminium alloy weld connection fabricated through SPP tool.

Figure 4.25 shows the distribution of average grain size at the nugget zone of friction stir welded Al-5Mg-8Ce-3.5Si aluminium alloy obtained at different combinations of speeds of tool rotation and speeds of welding. The measured grain size is much smaller than that for the base material and more than the grain size obtained for weld connection fabricated by TPP tool.
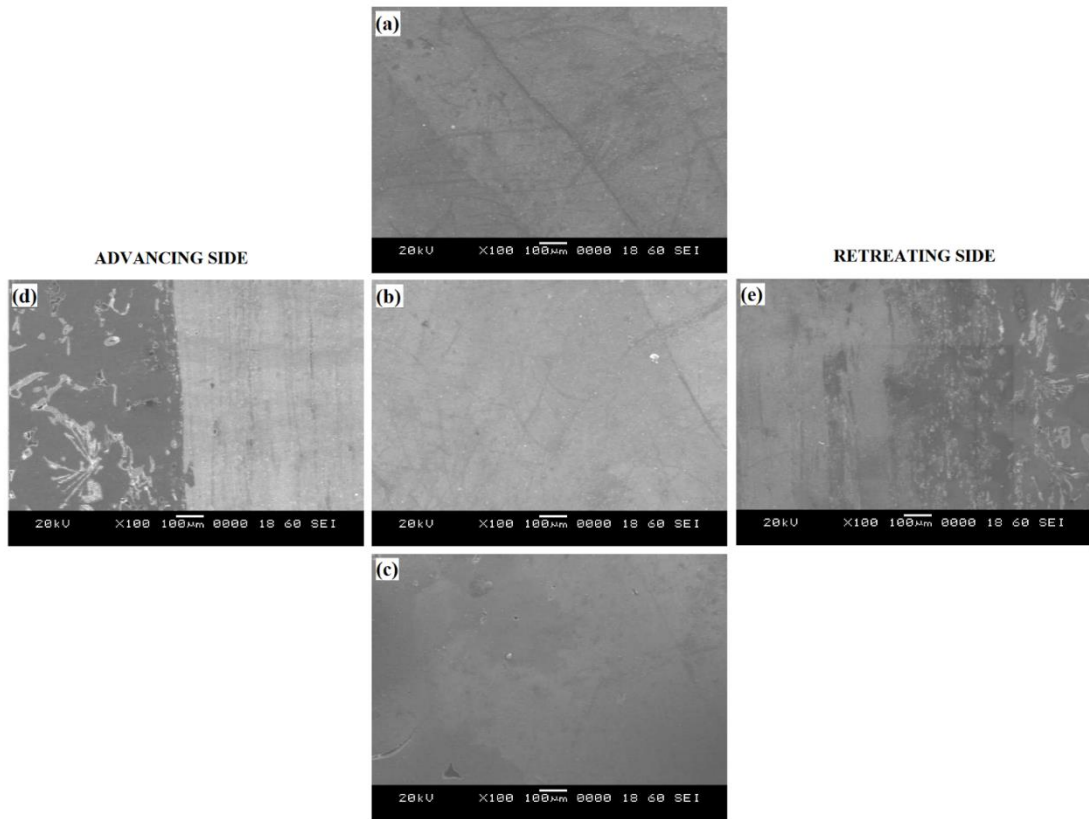
Figure 4.24 Scanning Electron Micrograph of Al-5Mg-8Ce-3.5Si Aluminium alloy joint, fabricated using friction stir welding with SPP tool at a speed of tool rotation of 1000 RPM and a welding speed of 10 mm/min, depicting distribution of grain size at (a) Top of the NZ, (b) Middle of the NZ, (c) Bottom of the NZ, (d) Advancing side of TMAZ and (e) Retreating side of TMAZ.

Table 4.8 Average grain size found at top, middle and bottom of the NZ of friction stir welded Al-5Mg-8Ce-3.5Si Aluminium alloy weld connection, fabricated at various speeds of tool rotation and speeds of welding, using SPP tool.

Expt. No.	Speed of Tool Rotation (RPM)	Speed of Welding (mm/min)	Average Grain Size (μm)		
			Top	Middle	Bottom
1.	800	10	11.4±0.21	9.5±0.2	8.5±0.13
2.		15	10.3±0.22	8.9±0.21	7.5±0.16

3.		20	9.8±0.11	7.5±0.14	7.0±0.08
4.		10	9.0±0.13	9.2±0.24	8.6±0.14
5.	1000	15	8.7±0.13	8.2±0.14	7.8±0.11
6.		20	8.0±0.19	7.6±0.15	6.7±0.09
7.		10	12.1±0.14	9.7±0.15	8.7±0.13
8.	1200	15	10.9±0.2	9.0±0.22	8.4±0.15
9.		20	9.2±0.13	8.5±0.17	7.4±0.15
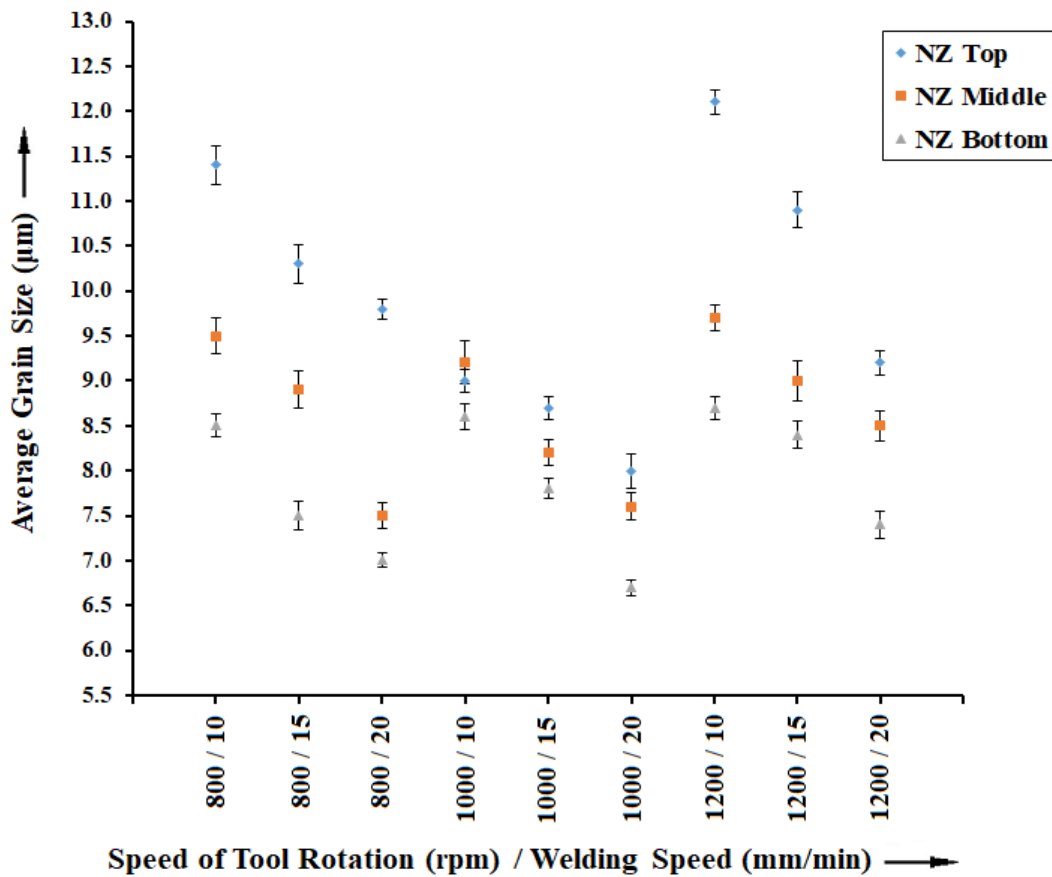
Figure 4.25 Average grain size distribution at NZ of weld joint of Al-5Mg-8Ce-3.5Si Aluminium alloy friction stir welded, fabricated through SPP tool.

4.5 MACRO AND MICROSTRUCTUAL ANALYSIS OF JOINTS OF FRICTION STIR WELDED Al-10Mg-8Ce-3.5Si AND Al-5Mg-8Ce-3.5Si ALUMINIUM ALLOYS, USING CIRCULAR / ROUND PIN PROFILE (CPP) TOOL

4.5.1 Macro Analysis of joints of friction stir Welded Al-10Mg-8Ce-3.5Si and Al-5Mg-8Ce-3.5Si aluminium alloys, using Circular / Round Pin Profile (CPP) tool.
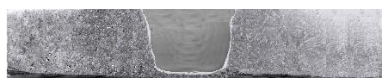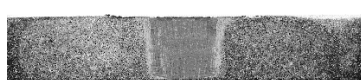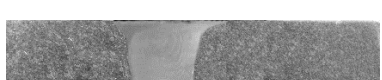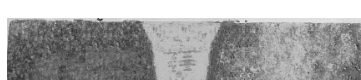
The macro images of the Al-10Mg-8Ce-3.5Si and Al-5Mg-8Ce-3.5Si aluminium alloys, friction stir welded with different combinations of speeds of welding of 10, 15, 20 mm/min and speeds of tool rotation of 800, 1000 and 1200 RPM, using CPP tool have been presented in Table 4.9. The nugget zone exhibited cup shape for the all the cases of welding using CPP tool. The change in the nugget shape is mainly attributed to the geometry of the tool (Mishra and Ma 2005; Schneider et al. 1991). Round Pin profiles in the absence of flat faces does not produce any eccentricity or material flow around pin. The flow of plasticized material from the front of the tool to the back of the rotating tool is dependent on the relation between dynamic and static volumes. The dynamic to static volume ratio is found to be 1.0 for CPP tool Therefore, the CPP tool sweeps very less material than other tools considered in this work. In addition to that, the circular or round profile of the tool does not produce any pulsating stirring action in the flow of the plasticized material (Elangovan and Balasubramanian 2008b; Huang et al. 2018b; Palanivel et al. 2012).

4.5.2 Micro-structure Analysis of joints friction stir Welded joints of Al-10Mg-8Ce-3.5Si aluminium alloys, using CPP tool.

Figure 4.26 (a to e) presents the SEM images of Al-10Mg-8Ce-3.5Si aluminium alloys friction stir welded with CPP tool, with a speed of tool rotation of 800 RPM and a welding speed of 20 mm/min. Figure 4.26 (b, c and d) show the grain distribution at the top, middle and bottom of the nugget region. The measured average grain size for various speeds of tool rotation and speeds of welding are tabulated in the Table 4.10. The average grain size is 13.8±0.23, 11.0±0.24 and 9.9±0.09 µm at the top, middle and bottom of the nugget region, respectively got at a speed of tool rotation of 1200 RPM

and a welding speed of 10 mm/min. Figure 4.26 (a) and (e) represent the retreating side and advancing side of the TMAZ. Bent elongated grains are observed on both sides of the nugget.

Table 4.9 Macrostructural images of Al-5Mg-8Ce-3.5Si and Al-10Mg-8Ce-3.5Si aluminium alloys, friction Stir welded at various speeds of tool rotation and various speeds of welding using CPP tool.

Expt. No.	Speed of Tool Rotation (RPM)	Speed of Welding (mm/min)	Macro image of FSW region of Al-5Mg-8Ce-3.5Si Aluminium Alloy	Macro image of FSW region of Al-10Mg-8Ce-3.5Si Aluminium Alloy
1.		10		
2.	800	15		
3.		20		
4.		10		
5.	1000	15		
6.		20		
7.		10		
8.	1200	15		
9.		20		

Figure 4.26 Scanning Electron Micrograph of Al-10Mg-8Ce-3.5Si Aluminium alloy joints fabricated using friction stir welding with CPP tool at a speed of tool rotation of 800 RPM and a welding speed 20 mm/min, depicting distribution of grain size at (a) Top of the NZ, (b) Middle of the NZ, (c) Bottom of the NZ, (d) Advancing side of TMAZ and (e) Retreating side of TMAZ.

Figure 4.27 shows the plot of grain size distribution at the NZ of weldment fabricated through FSW method using CPP tool. If is obvious from the results obtained from measurement of grain size, that for all joints, the grain size at the top surface of the weld NZ will be larger and a progressive decrease in grain size has been detected moving in the direction of the bottom of the weld NZ. The weld connection fabricated at a speed of tool rotation of 1200 RPM and a welding speed of 10 mm/min exhibited higher average grain size of 13.8±0.23 µm. High heat conditions prevailed at lower welding speed (10 mm/min), with decreased cooling rate resulting in coarsening of the grains in the weld zone. Instead, the smallest average grain size stir welded with a speed of tool rotation of 1000 RPM and a welding speed of 20mm/min. The smaller average grain

size is due to the increased welding speed (20mm/min) which leads to less heat input due to quicker friction time of the process. The prevalent low heat condition also attributed to the stimulus of higher strain and strain rate, leading to higher dynamic recrystallization, which successively contributes to grain refinement (Fratini and Buffa 2005; McNelley et al. 2008). In addition to this, the pinning effects of AlMgSi particles which are mainly resident at the boundaries of the grains, foil the grain growth and hence the grain size becomes tinier (Feng et al. 2006; Robson and Campbell 2010; Yaduwanshi et al. 2014).

Table 4.10 Average grain size found at top, middle and bottom of the NZ of friction stir welded Al-10Mg-8Ce-3.5Si Aluminium alloy weld connection, fabricated at various speeds of tool rotation and speeds of welding, using CPP tool.

Expt. No.	Speed of Tool Rotation (RPM)	Speed of Welding (mm/min)	Average Grain Size (µm)		
			Top	Middle	Bottom
1.		10	13.1±0.13	10.8±0.15	9.8±0.13
2.	800	15	12.4±0.22	9.7±0.21	8.8±0.09
3.		20	11.6±0.12	8.6±0.15	7.9±0.12
4.		10	10.7±0.18	10.2±0.24	9.8±0.17
5.	1000	15	10.3±0.13	9.5±0.21	8.4±0.15
6.		20	9.1±0.12	8.7±0.14	7.2±0.19
7.		10	13.8±0.23	11.0±0.24	9.9±0.09
8.	1200	15	12.3±0.22	10.3±0.14	9.5±0.16
9.		20	10.4±0.17	9.2±0.24	8.1±0.17
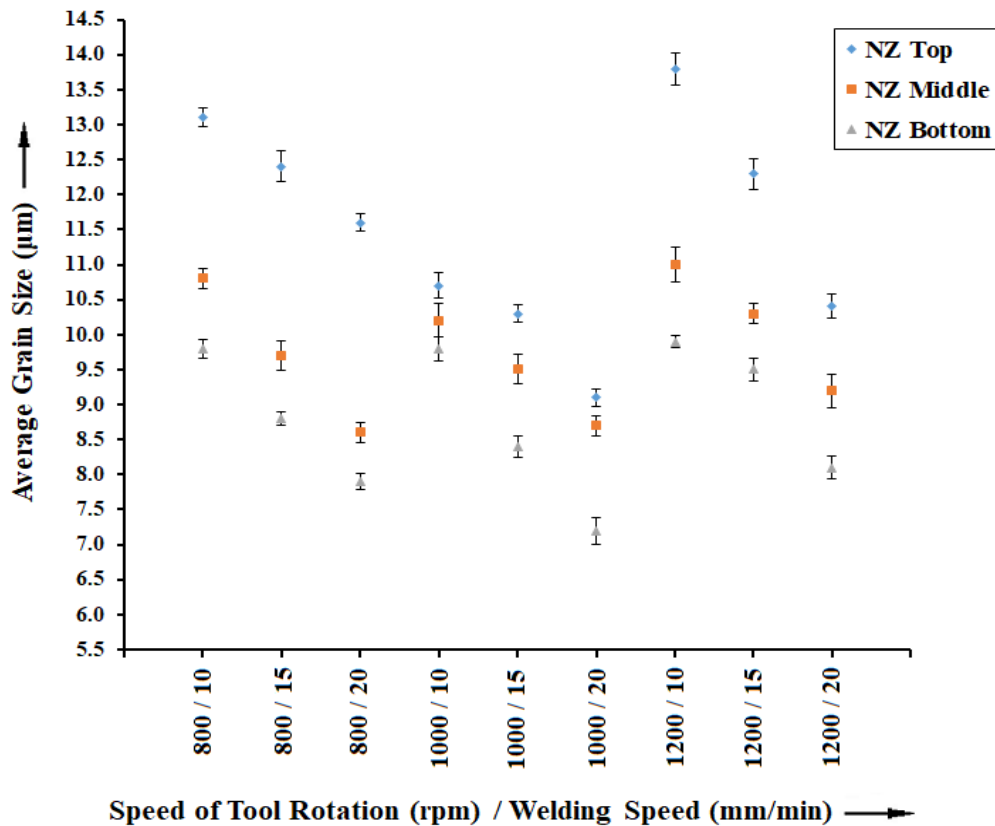
Figure 4.27 Average grain size distribution at NZ of friction stir welded Al-10Mg-8Ce-3.5Si Aluminium alloy weld connection fabricated through CPP tool.

4.5.3 Micro-structure Analysis of friction stir Welded joints of Al-5Mg-8Ce-3.5Si aluminium alloy, using Circular / Round Pin Profile (CPP) tool

The grain structure of Al-5Mg-8Ce-3.5Si aluminium alloy friction stir welded using circular profile pin is shown in the Figure 4.28 (a to e). A speed of tool rotation of 1000 RPM and a welding speed of 10 mm/min were the welding parameters selected for FSW. The measured average grain size for various speeds of tool rotation and speeds of welding are tabulated in Table 4.11. The average grain sizes at the top of the NZ, middle of the NZ and bottom of the NZ are 15.2±0.11, 12.1±0.13 and 10.9±0.13 respectively got at a speed of tool rotation of 1200 RPM and a welding speed of 10 mm/min. The decrease in the grain size is 84.8% over the grain size exhibited by base alloy. Figure 4.28 (a) and (e) represent the retreating side and advancing side of the TMAZ. Bent elongated grains are observed on either side of the nugget zone. The size

of the grains obtained using circular profile pin (CPP) tool is much bigger than the size of the grains obtained with TPP and SPP tool. Since dynamic to static ratio of CPP tool (1.00) is less than the SPP tool (1.56) and TPP tool (2.30), it sweeps less material as compared to SPP and TPP tool. The absence of pulsating effect in the case of CPP tool also affects material flow during welding. No pulsating action due to lower dynamic to static ratio in the case of CPP tool results in less mixing of the material as well as insufficient heat generation for the same process parameters compared to the SPP and TPP tools. The material flow and mixing in the case of CPP tool also is less compared to SPP and TPP tool. Hence the grain size obtained in the case of CPP tool is bigger as compared SPP and TPP tools.
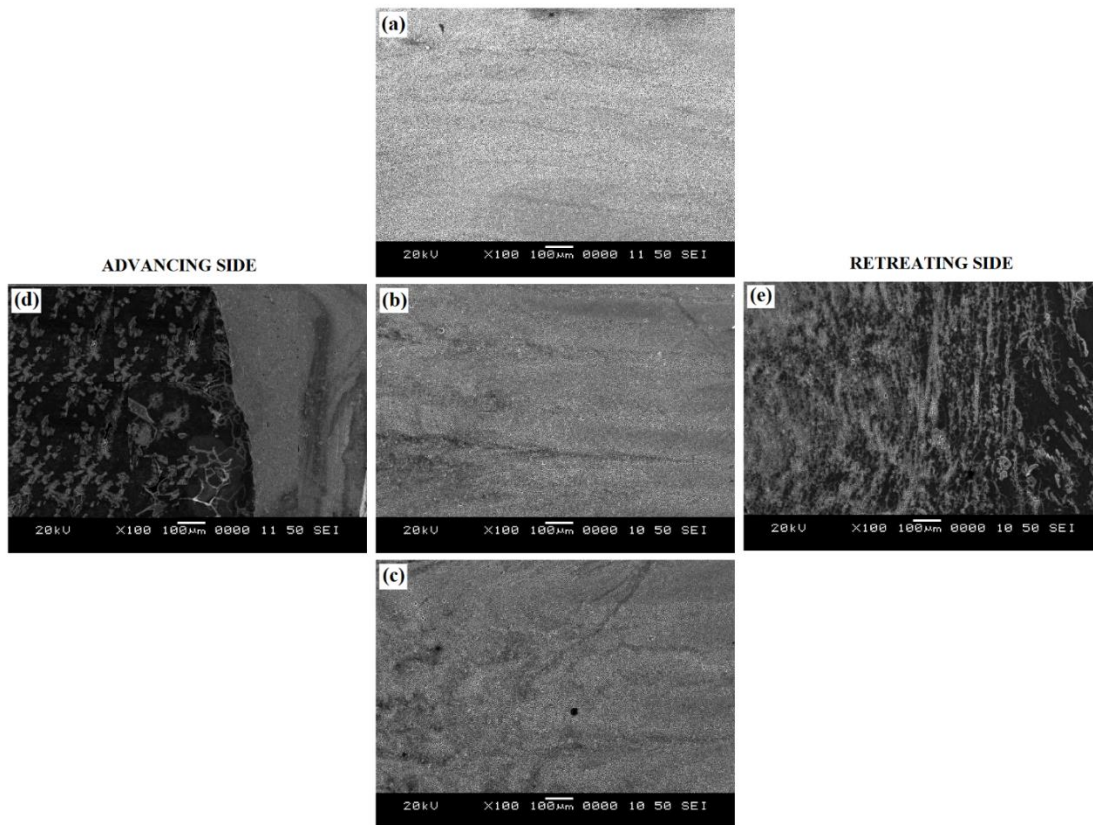
Figure 4.28 Scanning Electron Micrograph of joint of Al-5Mg-8Ce-3.5Si Aluminium alloy fabricated using friction stir welding with CPP tool at a speed of tool rotation of 1000 RPM and a welding speed of 10 mm/min, showing distribution of grain size at (a) Top of the NZ, (b) Middle of the NZ, (c) Bottom of the NZ, (d) Advancing side of TMAZ and (e) Retreating side of TMAZ.

Table 4.11 Average grain size found at top, middle and bottom of the NZ of friction stir welded Al-5Mg-8Ce-3.5Si Aluminium alloy weld connection, fabricated at various speeds of tool rotation and speeds of welding, using CPP tool.

Expt. No.	Speed of Tool Rotation (RPM)	Speed of Welding (mm/min)	Average Grain Size (μm)		
			Top	Middle	Bottom
1.		10	13.8±0.2	11.7±0.15	10.5±0.09
2.	800	15	13.2±0.16	10.9±0.2	9.3±0.1
3.		20	12.1±0.13	9.8±0.14	8.3±0.12
4.		10	11.3±0.16	11.2±0.17	10.8±0.17
5.	1000	15	10.6±0.14	10.5±0.15	9.2±0.19
6.		20	9.6±0.16	8.4±0.18	7.6±0.14
7.		10	15.2±0.11	12.1±0.13	10.9±0.13
8.	1200	15	13.5±0.2	11.3±0.24	10.5±0.09
9.		20	10.8±0.14	9.8±0.15	8.5±0.12

Figure 4.29 shows the plot of grain size distribution at the NZ of weldment fabricated through FSW method using CPP tool at various combinations of speeds of tool rotation and speeds of welding. It is obvious from the results obtained from measurement of grain size, that for all joints, the grain size at the top surface of the weld NZ will be larger and it decreases towards the bottom of the weld NZ. The reason behind the improvement in grain size is already discussed in the previous section 4.5.2.
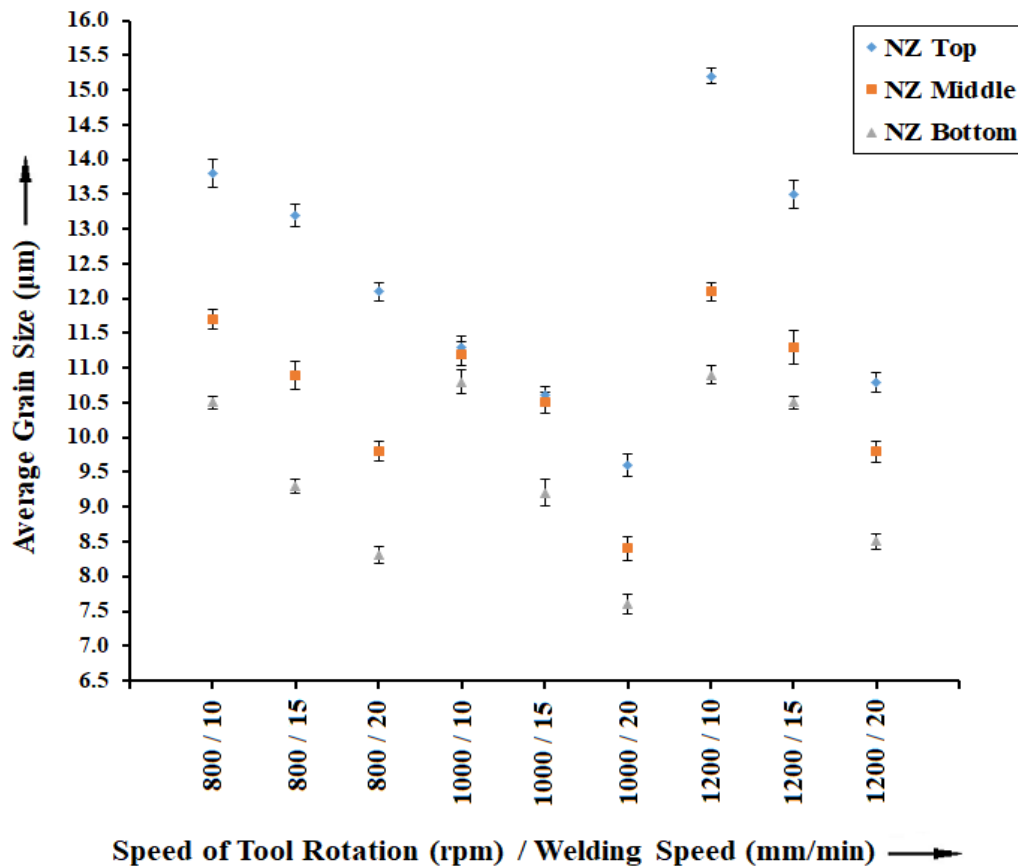
Figure 4.29 Average grain size distribution at NZ of friction stir welded Al-5Mg-8Ce-3.5Si Aluminium alloy weld connection fabricated through CPP tool.

4.6 MECHANICAL PROPERTIES OF FRICTION STIR WELDED JOINTS OF Al-10Mg-8Ce-3.5Si AND Al-5Mg-8Ce-3.5Si ALUMINIUM ALLOYS

The mechanical properties of the aluminium alloys are dependent on chemical composition, weight percentage of hard particles added to the casting mix, processing technique and distribution of hard particles in the casting mix (Dahle et al. 2001; Eskin et al. 2004; Rao et al. 2016; Sabatino and Arnberg 2009; Sims et al. 2016). The tensile stress of the Al-10Mg-8Ce-3.5Si and Al-5Mg-8Ce-3.5Si aluminium alloy friction stir welded joints is influenced by several factors like distribution of Ce, Mg & Si particles and precipitates in the weld region, grain morphology, formation of intermetallic phases

and processing temperature. Mg particles are usually used in the preparation of aluminium alloys to enhance the mechanical and wear properties of the aluminium alloys. Higher volume fraction of Mg particles in mix enhances the strength because of increase in the brittleness at the expense of ductility of the alloy. Mg does not significantly affect the thermodynamics or phase constitution of the Al-Ce binary system, but instead, it strengthens the matrix phase by forming intermetallic Al-Mg precipitates and metastable clusters. Intermetallic precipitates are beneficial for increasing the strength of the ductile aluminium matrix without affecting the existing $Al_{11}Ce_3$ (Davis 2001; Kaufman and Rooy 2014; Sims et al. 2016). Silicon has two effects when added to conventional aluminium alloys: Silicon works to increase alloy castability, and silicon, when combined with Mg normally precipitates an Mg_2Si strengthening phase (Bergsma et al. 1998; Chakrabarti and Laughlin 2004; Sims et al. 2016). The mechanical properties like hardness depends not only on fine grain size, but also on % volume of phases present in the nugget zone (NZ). The increase in hardness of Al alloys can also be attributed to the increase in size and volume fraction of intermetallics present in the material at nugget zone (particularly β-phase). (Darvishi et al. 2010). Mechanical tests have been conducted to evaluate the performance of the weld connection and expand the possible application of FSW for joining aluminium alloys.

4.6.1 Hardness test

4.6.1.1 Hardness test of friction stir welded weld connection of Al-10Mg-8Ce-3.5Si and Al-5Mg-8Ce-3.5Si aluminium alloys using Triangular Profile Pin (TPP) Tool

4.6.1.1.1 Hardness distribution of Al-10Mg-8Ce-3.5Si aluminium alloy weld connection friction stir welded using TPP tool

In FSW process, the tool rotational speed is one of the most predominant process parameters. Plastic deformation of the material is caused by force of friction between the contact surfaces of rotating tool (pin and shoulder) and the substrate material. It is responsible for stirring and mixing of the plasticized material around the pin (Casalino

et al. 2014; Elangovan and Balasubramanian 2008a; Selamat et al. 2016). The nucleation sites are increased with the presence of the precipitates, which lead to the reduction of grain size in the base material (Carlone and Palazzo 2013; El-Rayes and El-Danaf 2012; Gallais et al. 2008; Kamp et al. 2007; Sato et al. 2002).

The hardness is measured on either side of the weld line. Friction stir welded samples show highest hardness in the NZ than the parent material due to the finer grain size (Dong et al. 2013; Hao et al. 2013b; Hu et al. 2012b; Khan et al. 2017). Stirring Action of the tool causes a high plastic flow which leads to rearrangement of particles from agglomerated and heterogeneous distribution in the base metal to a homogeneous distribution in the NZ (Huang et al. 2018a; Ma et al. 2018; Tamadon et al. 2019). This phenomenon has been noticed in all the samples at various combinations of speeds of tool rotation of 800, 1000 and 1200 RPM, and welding speed of 10, 15 and 20 mm/min. Reduction in hardness was noticed as the distance increases from the center, on both sides of NZ (Dong et al. 2013; Kumar et al. 2015b; Trimble et al. 2015a; Yeni et al. 2008). Lesser hardness value has been noticed between the base material and NZ, termed as Heat affected zone (HAZ). This is largely because of grain softening induced by the thermal effect while stirring of the material by the tool. Slightly higher hardness value has been noticed on the advancing side when compared with the retreating side (Aval 2015b; Jones et al. 2005; Khan et al. 2017; Koilraj et al. 2012; Scialpi et al. 2007; Xie et al. 2008). This hardness distribution is due to non-uniform field of plastic flow on the two sides of the welded joint, as advancing side experiences more plastic strain than the retreating side. This results in more deformation heat causing higher temperature close to the weld center on advancing side. Higher peak temperature on advancing side causes better dissolution of strengthening precipitates leading to higher hardness on the advancing side when compared to the retreating side as reported. At low welding speed, NZ is more homogenous than at high welding speed because high heat input per unit weld results in more homogenous temperature distribution. At a constant welding speed of 10 mm/min, as the speed of tool rotation is increased from 1000 RPM to 1200 RPM, the hardness value was found to increase. This was mainly because of the increase in the heat input. The higher heat input makes the weld material to experience higher temperature and higher strain rate (Cavaliere and Squillace 2005;

Charit and Mishra 2003). During FSW process, if adequate heat is generated, work material gets plasticized in front of the tool and is transported from the advancing side to the retreating side. At the back of the tool, the transported material cools down and gets consolidated by the forging method (Allen 2005; Arora et al. 2011; Balasubramanian et al. 2009; Dwivedi 2014; Ghosh et al. 2010).

Figure 4.30 shows the plot illustrating the variation of hardness across the mid thickness of FSW joints of Al-10Mg-8Ce-3.5Si aluminium alloy, being fabricated using TPP tool at various speeds of tool rotation of 800, 1000 and 1200 RPM, respectively, with welding speed (transverse speed) being held constant at 10 mm/min. The highest hardness value of 166.6 VHN was exhibited in the weld connection fabricated with speed of tool rotation of 1200 RPM and welding speed of 15 mm/min. Lowest hardness value of 151.8 VHN was observed in the weld connection fabricated with a speed of tool rotation of 1200, and a welding speed of 10 mm/min. It is to be noted that for the cases under consideration, the smallest grain size obtained at 800 RPM was 6.2 µm, at 1000 RPM was 6.4 µm and at 1200 RPM was 6.8 µm. The gain sizes obtained with 800 RPM, 1000 RPM and 1200 RPM were more or less in the same range and accordingly the hardness values recorded were also in the same order. The welding speed determines the exposure time of frictional heat per unit length of the weld which influences the heat transfer rate and consequently affects the grain growth (Babu et al. 2017; Guo et al. 2014; Threadgilll et al. 2009). Thus, the rate of heating in a thermal cycle during FSW is a strong function of the welding speed. The weld connection fabricated with 1200 RPM speed of tool rotation and 10 mm/min welding speed showed lower hardness. At low speed of tool rotation, the heat produced is less irrespective of welding speed and as a result, the heat input to the base material is very less. This leads to inadequate plasticization and incomplete flow of material in stir zone. But as the speed of tool rotation rises slightly to 1000 RPM, the heat generation also increases due to increased heat of friction, irrespective of welding speed. This results in more rigorous stirring and correct mixing of materials, which results in formation of fine grains. But the hardness declines as the speed of tool rotation is further raised up to 1200 RPM. High speed of tool rotation leads to higher heat generation and causes the stirred material to flow to the upper surface producing voids in the nugget region.

Similarly, a higher heat input reduces the cooling rate, thus giving enough time for the growth of the grains. Furthermore, at higher speed of tool rotation, due to improper flow of material, the accumulation of hard particles takes place. As a combined effect, hardness value decreases (Elangovan et al. 2008a; Lakshminarayanan et al. 2011; Trimble et al. 2015b).
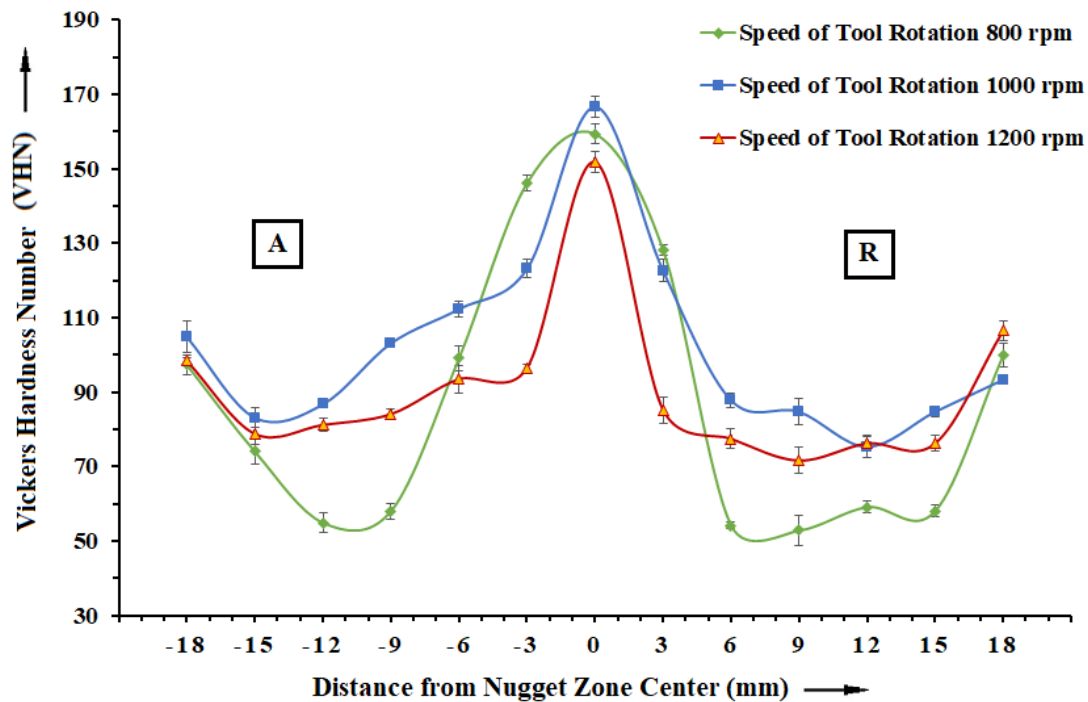
Figure 4.30 Hardness distribution across NZ of Al-10Mg-8Ce-3.5Si aluminium alloy, friction stir welded using TPP tool at various speeds of tool rotation of 800, 1000 and 1200 RPM with constant welding speed of 10 mm/min (A- Advancing side and R- Retreating side)

Figure 4.31 shows the plots illustrating the variation of hardness across the friction stir welded weld connection of Al-10Mg-8Ce-3.5Si aluminium alloy, fabricated using TPP tool at various speeds of tool rotation of 800, 1000, 1200 RPM, respectively, with a constant welding speed of 15 mm/min. The translation of the rotating tool moves the stirred material from the front to back of the tool pin. The welding speed determines the exposure time of frictional heat per unit length of the weld, which influences the heat transfer rate and consequently affects the grain growth (Babu et al. 2017; Guo et

al. 2014; Threadgilll et al. 2009). Thus, the rate of heating in a thermal cycle during FSW is a strong function of the welding speed. When the welding speed increases from 10 mm/min to 15 mm/min, the heat per unit length decreases which results in an increase in the hardness value. When the speed of tool rotation is increased from l000 to 1200 RPM with welding speed being held constant at 15 mm/min, the hardness decreased considerably. This was because of the increased heat input and reduced cooling rate at higher speed of tool rotation, leading to the formation of large sized grains (Hassan et al. 2003a; Mehdi and Mishra 2016). The peak hardness value of 167.7 VHN was exhibited in the weld connection fabricated with speed of tool rotation of 1000 RPM and welding speed of 15 mm/min. The lowest hardness value of 151.3 VHN was observed in the weld connection fabricated with speed of tool rotation of 1200 RPM and welding speed 15 mm/min.

Figure 4.31 Hardness distribution across NZ of Al-10Mg-8Ce-3.5Si aluminium alloy, friction stir welded using TPP tool at various speeds of tool rotation of 800, 1000 and 1200 RPM with constant welding speed of 15 mm/min

Figure 4.32 shows the plots illustrating the hardness distribution across the friction stir welded Al-10Mg-8Ce-3.5Si aluminium alloy joint, produced using TPP tool at

various speeds of tool rotation of 800, 1000, 1200 RPM respectively with a constant welding speed of 20 mm/min. Highest hardness value 158.9 VHN was observed for a rotational speed of 1000 RPM and welding speed of 20 mm/min. A speed of tool rotation of 800 RPM and welding speed of 20 mm/min led to a lower hardness value of 149.4 VHN. Similarly, a speed of tool rotation of 1200 RPM and welding speed 20 mm/min, produced lowest hardness of 138.6 VHN. However, the stirring effect of the welding tool becomes relatively weaker when the welding speed was increased with the increase in speed of tool rotation. As a result, the weld flaws were observed at these speeds. Higher welding speed reduces the hardness value. This was due to the non-uniform accumulation of the AlSiMg and other hard particles, due to the high speed of tool rotation and high welding speed. Figure 4.33 showing the non-uniform accumulation of AlSiMg particles and other hard particles, in the measurement region, at higher speed of tool rotation (1200 RPM) and higher welding speed (20 mm/min) which leads to lower hardness values.

Figure 4.32 Hardness distribution across NZ of Al-10Mg-8Ce-3.5Si aluminium alloy, friction stir welded using TPP tool at various speeds of tool rotation of 800, 1000 and 1200 RPM with constant welding speed of 20 mm/min

4.6.1.1.2 Hardness distribution of Al-5Mg-8Ce-3.5Si aluminium alloy weld connection friction stir welded using TPP tool

Figure 4.34 shows the plots illustrating the variation of hardness across the mid thickness of FSW weld connection of Al-5Mg-8Ce-3.5Si aluminium alloy, being fabricated using TPP tool at different rotational speeds of 800, 1000 and 1200 RPM, respectively, with welding speed of 10 mm/min being held constant. The hardness of the NZ was found to increase by 22.0%, 33.1% and 15.6%, respectively, for speeds of tool rotation of 800, 1000 and 1200 RPM, as compared to the hardness of the base material (99.3 VHN). The increase in the hardness was due to the fine grain structure and uniform distribution of hard particles. As seen from the graph, hardness goes up with increase in the speed of tool rotation. Higher speed of tool rotation and lower welding speed leads to higher heat generation and constant rate of cooling, results in grain refinement in the weld zone and even distribution of precipitates and other hard particles resulting in an increase in hardness (Aval 2015a; Golezani et al. 2015; Ma 2008; Uday et al. 2016). The hardness distribution trend obtained for friction stir welded weld connection of Al-5Mg-8Ce-3.5Si aluminium alloy is like the one obtained for Al-10Mg-8Ce-3.5Si aluminium alloy.
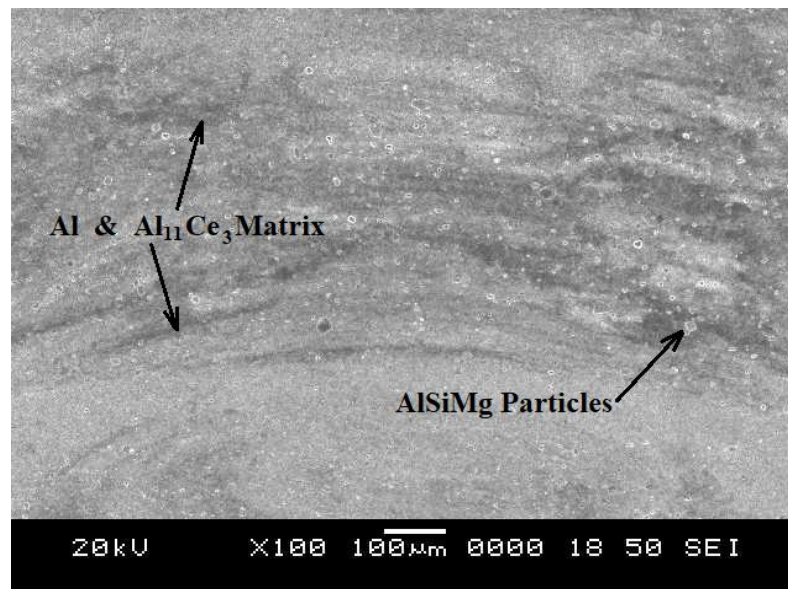
Figure 4.33 Non-Uniform dispersion of AlSiMg particles in weld zone

181

The variation of hardness across the mid thickness of FSW weld connection of Al-5Mg-8Ce-3.5Si aluminium alloy, being fabricated using TPP tool at various speeds of tool rotation of 800, 1000 and 1200 RPM, respectively, with welding speed 15 mm/min being held constant is as shown in Figure 4.35. The increase in the percentage of hardness was 26.1%, 37.7% and 22.1%, respectively, for speed of tool rotation of 800, 1000 and 1200 RPM, as compared to hardness of base alloy material. The trend of hardness variation is like that of friction stir welded aluminium alloy Al-10Mg-8Ce-3.5Si. It can be observed that the highest hardness of 143.3 VHN at NZ was obtained at speed of tool rotation of 1000 RPM and welding speed of 15 mm/min. The lowest hardness observed at NZ was 127.1 VHN for speed of tool rotation of 1200 RPM and welding speed of 15 mm/min.
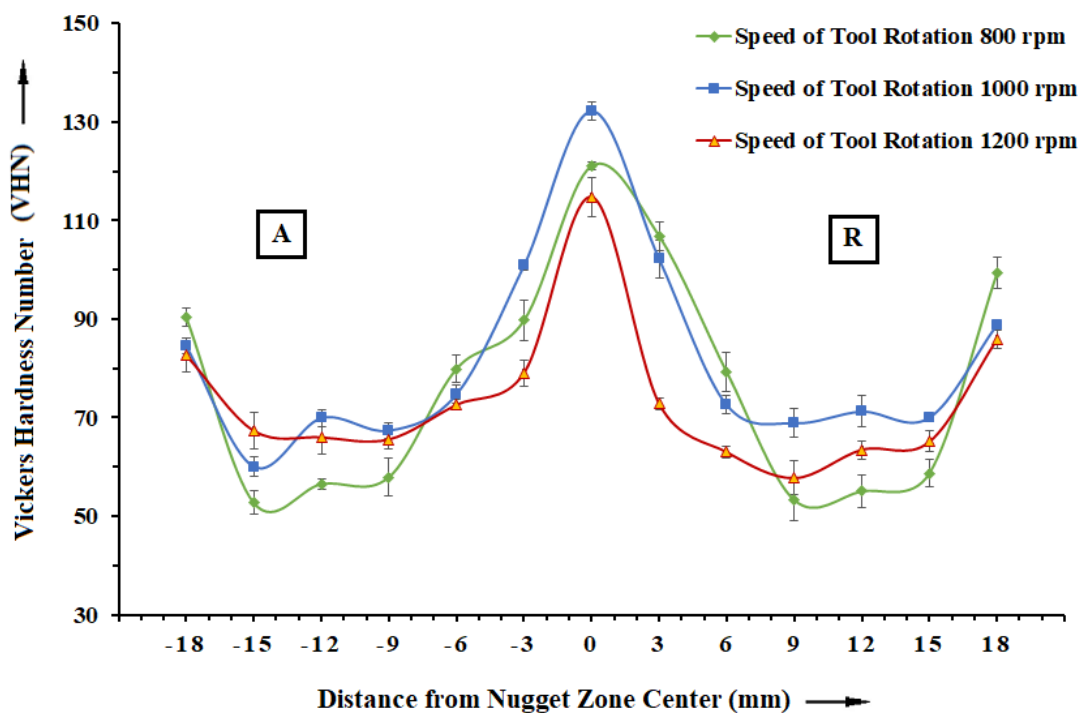
Figure 4.34 Hardness distribution across NZ of Al-5Mg-8Ce-3.5Si aluminium alloy, friction stir welded using TPP tool at various speeds of tool rotation of 800, 1000 and 1200 RPM with constant welding speed of 10 mm/min

The variation of hardness across the mid thickness of FSW weld connection of Al-5Mg-8Ce-3.5Si aluminium alloy, being fabricated using TPP tool at various speeds of tool rotation of 800, 1000 and 1200 RPM, respectively, with welding speed at 20 mm/min was held constant as shown in Figure 4.36. The hardness profile is very similar to the previous Figure 4.35. The variation in the hardness at NZ of the three welded joints (800, 1000 and 1200 RPM) is significant. This is attributed to speed of tool rotation. A speed of tool rotation of 1000 RPM generates sufficient heat to plasticize the material and adequate material flow results in higher hardness of 129.2 VHN. Further increase in the speed of tool rotation results in higher heat and produces turbulence in material flow. This excess heat and lower cooling rate results in grain growth (Refer Table 4.10) with lower hardness of l16.4 VHN.
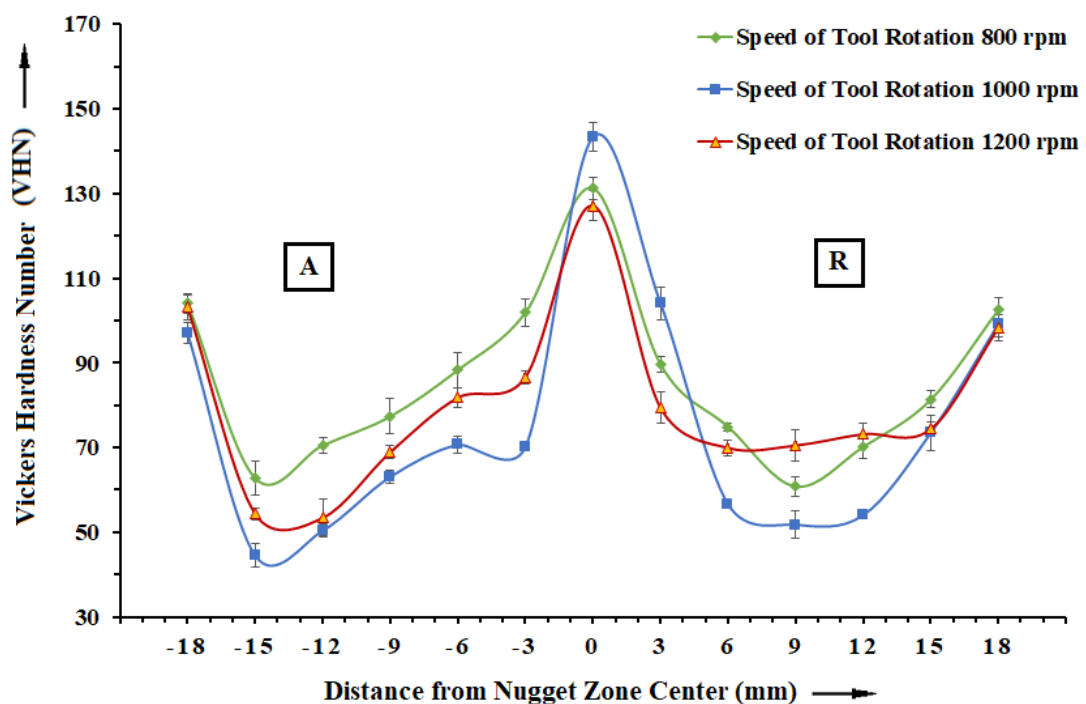
Figure 4.35 Hardness distribution across NZ of Al-5Mg-8Ce-3.5Si aluminium alloy, friction stir welded using TPP tool at various speeds of tool rotation of 800, 1000 and 1200 RPM with constant welding speed of 15 mm/min

4.6.1.2 **Hardness test of friction stir welded weld connection of Al-10Mg-8Ce-3.5Si and Al-5Mg-8Ce-3.5Si aluminium alloys using Square Profile Pin (SPP) Tool**

4.6.1.2.1 **Hardness distribution across Al-10Mg-8Ce-3.5Si aluminium alloy weld connection friction Stir Welded using SPP tool**

Figure 4.37 depicts the hardness variation across the friction stir welded Al-10Mg-8Ce-3.5Si aluminium alloy weld connection fabricated using a SPP tool at various speeds of tool rotation of 800, 1000, 1200RPM respectively, with welding speed 10 mm/min being held constant. It can be noticed that, the hardness of the NZ was significantly more than that of the base metal irrespective of the speed of tool rotation. The reasons behind the increase in the hardness at NZ are:
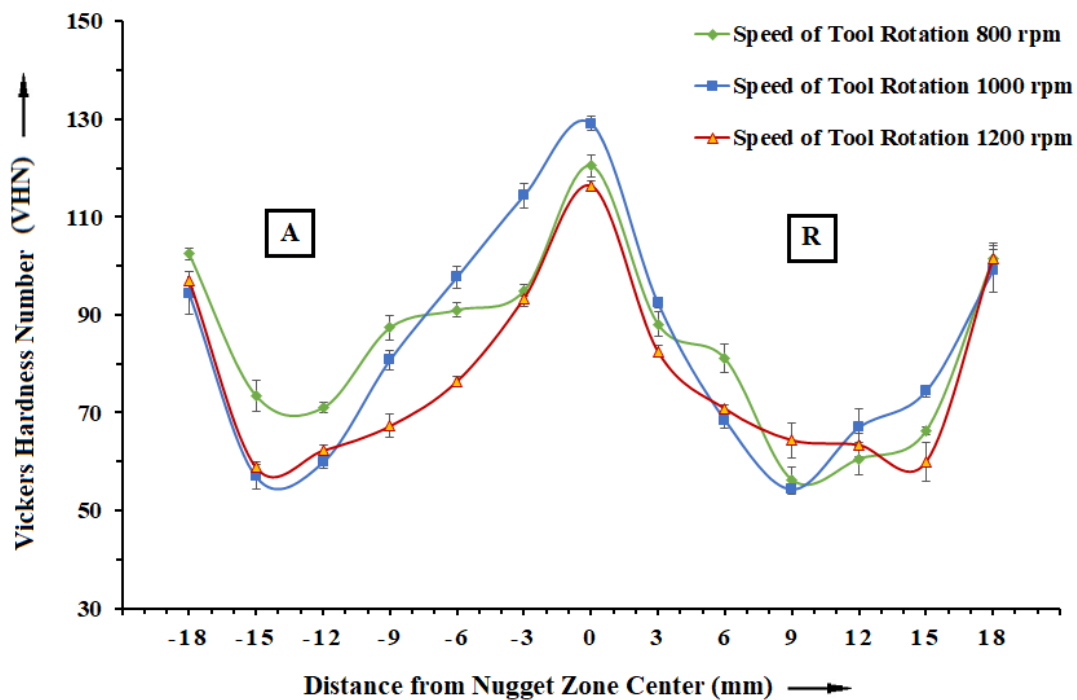
Figure 4.36 Hardness distribution across NZ of Al-5Mg-8Ce-3.5Si aluminium alloy, friction stir welded using TPP tool at various speeds of tool rotation of 800, 1000 and 1200 RPM with constant welding speed of 20 mm/min

(i)   The grain size of NZ is much finer than that of base metal; grain refinement plays a vital part in strengthening of the material. According to the Hall-Petch equation, hardness goes up as the grain size reduces.

(ii)   Uniform distribution of Mg particles as well as intermetallic particles in the NZ which assists the increase in hardness.

The variation in hardness among the HAZ and NZ is ascribed to superior stirring by the FSW tool in the NZ, which produces high plastic strain which leads to rearrangement of particles from heterogeneous and agglomerated distribution in the base material to homogeneous distribution in the nugget zone (Guerra et al. 2003; Ji et al. 2016a). Further, the homogeneous distribution of Mg particles as well as spheroidization of silicon needles and their spreading through the base metal matrix were the dominant reasons for property improvement in the NZ. Band-like arrangement of Al-Mg-Si particles and silicon needles lead to an surge in hardness in the nugget zone (Dong et al. 2013; Feng et al. 2009; Li et al. 2014a). The boundary between the NZ and TMAZ is very clearly visible. TMAZ reveals the alignment of Al-Mg-Si particles and grains in the inclined direction. An elongated grain boundary with distribution of parallel band-like particles is observed (Figures 4.10 and 4.11), due to frictional heat generated and plastic deformation induced by the applied stresses in TMAZ (Commin et al. 2012; Kalemba-Rec et al. 2016; Tao et al. 2017). For all the joints fabricated, the minimum hardness was observed in the HAZ. Hardness of the advancing side was lower than the retreating side. This hardness distribution is due to the non-uniform field of plastic flow on the two sides of the welded joint. Advancing side experiences more plastic strain than the retreating side, which in turn results in more deformation heat. This causes higher temperature close to the weld center on the advancing side than that on the retreating side. Higher peak temperatures on the advancing side causes more dissolution of strengthening precipitates and fine grain formation. This leads to higher hardness on the advancing side as compared to the retreating side (Aval 2015b; Koilraj et al. 2012). It is observed that, as speed of tool rotation increases from 1000 to 1200 RPM, the nugget zone hardness is reduced due to increase in the heat generation. The highest hardness of 132.2 VHN was obtained for the weld connection fabricated with speed of tool rotation of 1000 RPM and welding

speed of 10 mm/min. Conversely, the lowest hardness obtained was 114.8 VHN, for the weld connection fabricated at speed of tool rotation of 1200 RPM and welding speed of 10 mm/min.
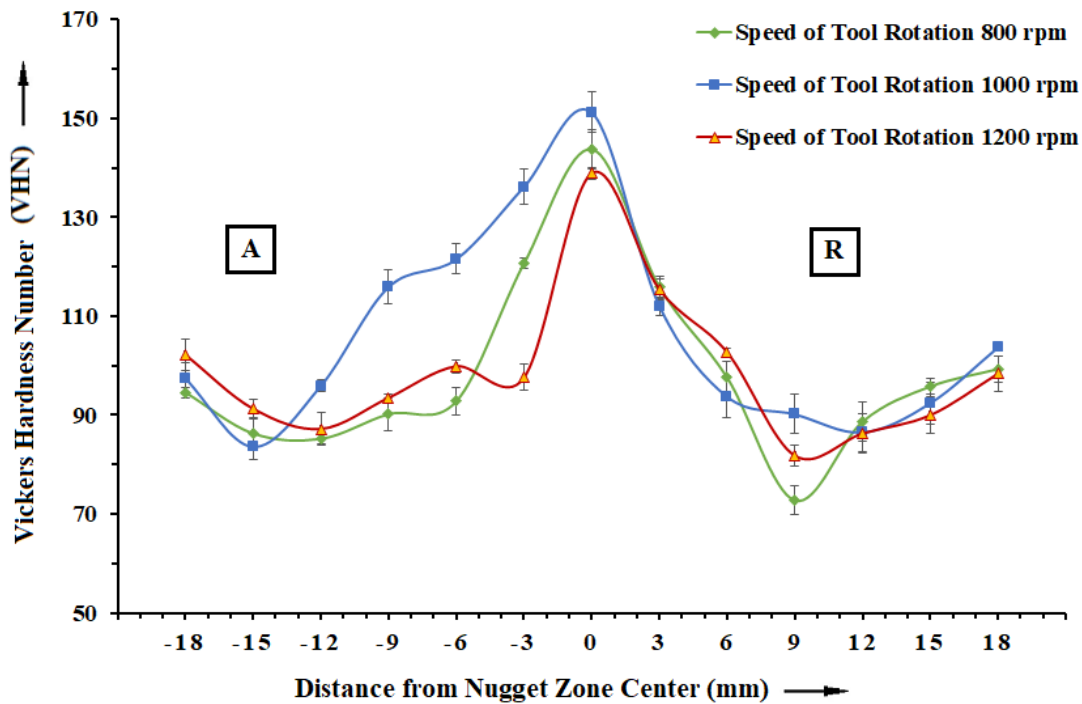
Figure 4.37 Hardness distribution across NZ of friction stir welded Al-10Mg-8Ce-3.5Si aluminium alloy, with SPP tool at various speeds of tool rotation of 800, 1000 and 1200 RPM with constant welding speed of 10 mm/min

Figure 4.38 plots the hardness distribution across the friction stir welded Al-10Mg-3.5Si aluminium alloy weld connection produced with a SPP tool at various speeds of tool rotation of 800, 1000, 1200 RPM respectively, with welding speed (transverse speed) 15 mm/min being held constant. The highest hardness of 145.9 VHN was exhibited in the specimen of the weld connection fabricated with speed of tool rotation of 1000 RPM and welding speed of 15 mm/min. Conversely, the lowest hardness obtained was 132.1 VHN which is for the weld connection fabricated at a speed of tool rotation of 1200 RPM and a welding speed of 15 mm/min. The lowest hardness in the hardness distribution plot would represent the HAZ, where some grain softening could have taken place. The highest hardness obtained is at NZ. The hardness obtained for

constant welding speed of 15 mm/min is more than the hardness found for constant welding speed of 10 mm/min. This is because as the welding speed increases from 10 to 15 mm/min, the quantity of heat exposed per unit area of weld region decreased. This is due to the stirring of FSW tool causing a high plastic strain which resulted in rearrangement of particles from heterogeneous and accumulated distribution in the base metal to homogeneous distribution in the nugget zone (Guerra et al. 2003; Ji et al. 2016a). A slightly higher hardness was observed on either side of the NZ (known as TMAZ) in the hardness distribution plot, where the material is plastically deformed and thermally affected. TMAZ is characterized by the elongated grains. The hardness obtained from all the samples exhibited slightly higher hardness values in the TMAZ than the HAZ region. This increase in the hardness in the TMAZ is attributed to the second phase particle dissolution and work hardening due to intense plastic deformation (Grujicic et al. 2010; Leitão et al. 2012; Rao et al. 2013).
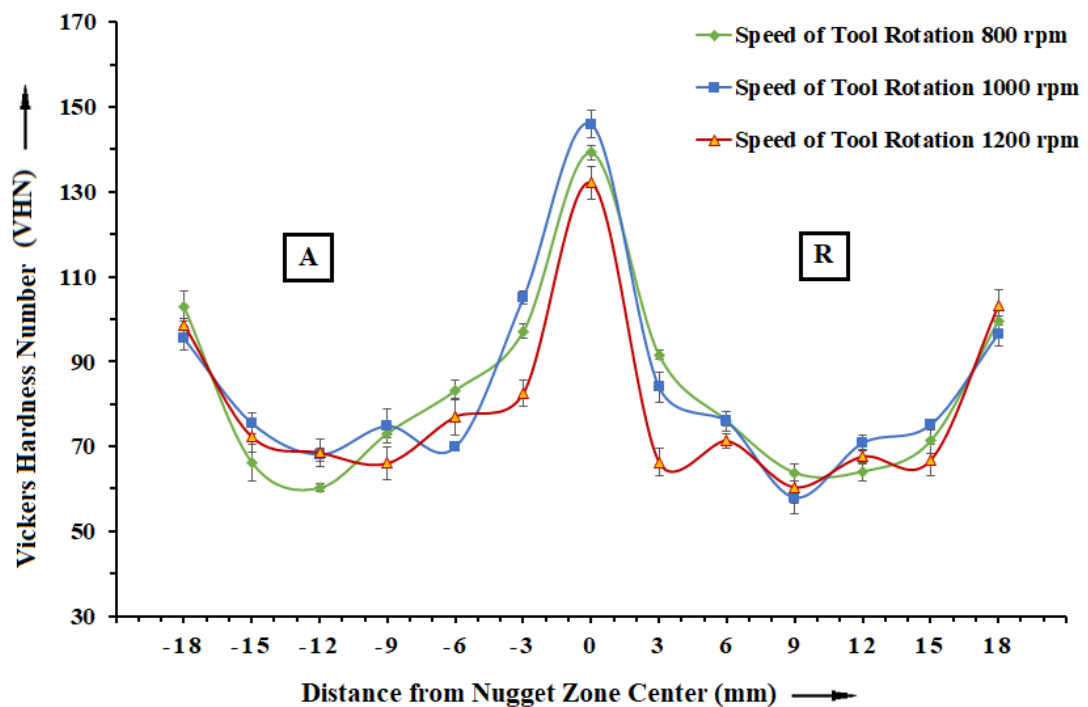
Figure 4.38 Hardness distribution across NZ of friction stir welded Al-10Mg-8Ce-3.5Si aluminium alloy, with SPP tool at various speeds of tool rotation of 800, 1000 and 1200 RPM with constant welding speed of 15 mm/min

Figure 4.39 shows the plots of distribution of hardness across the friction stir welded joints of Al-10Mg-8Ce-3.5Si aluminium alloy, produced with a SPP tool at various speeds of tool rotation of 800, 1000, 1200RPM, respectively, and with constant welding speed of 20 mm/min. A peak hardness value of 151.1 VHN was exhibited in the weld connection fabricated with speed of tool rotation of 1000 RPM and welding speed of 20 mm/min. The lowest hardness value of 126.9 VHN was observed in the weld connection fabricated with a speed of tool rotation of 1200 RPM and a welding speed of 20 mm/min. At higher speed of tool rotation (1200 RPM) and higher welding speed (20 mm/min), the hardness obtained was comparatively less. The reasons for this phenomenon were the same as discussed in section 4.6.1.1.2 earlier.
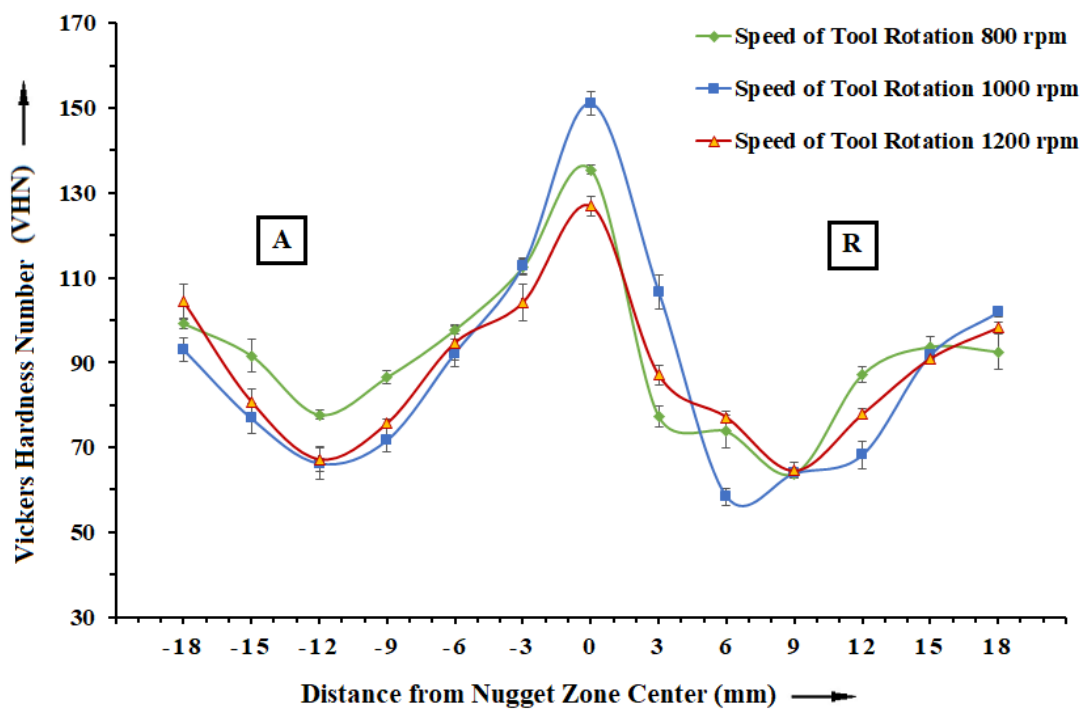
Figure 4.39 Hardness distribution across NZ of friction stir welded Al-10Mg-8Ce-3.5Si aluminium alloy, with SPP tool at various speeds of tool rotation of 800, 1000 and 1200 RPM with constant welding speed of 20 mm/min

4.6.1.2.2   Hardness distribution across Al-5Mg-8Ce-3.5Si aluminium alloy weld connection friction Stir Welded using SPP tool

The hardness of the Al-5Mg-8Ce-3.5Si aluminium alloy, welded by FSW method using SPP tool, is a function of grain size, hard reinforcing particles, dislocation density, and welding process parameters. According to Hall-Petch theory, finer grain sizes result in higher hardness (Heidarzadeh et al. 2015; Jones et al. 2005; Yuqing et al. 2017). Usually, hard particles in aluminium alloy have double effect on the hardness. One arises from its hard nature and second one relates to the role of AlSiMg particles in grain boundary pinning (El-Rayes and El-Danaf 2012; Hassan et al. 2003a; Ma et al. 2018; Starke and Staley 2010). Hardness distribution in specimens welded at speed of tool rotation of 800, 1000 and 1200 RPM and at constant welding speed 10 mm/min is illustrated in Figure 4.40. All the aluminium alloy joints revealed higher hardness at NZ when compared to the base material. However, the pattern of distribution of hardness along the weld region is "W" shaped. This is because of the variation in the grain size and distribution of hard particles. Highest average hardness obtained was 125.6 VHN for an aluminium alloy weld connection welded with speed of tool rotation of 1000 RPM and welding speed of 10 mm/min. A lowest average hardness value of 112.9 VHN was obtained for a speed of tool rotation of 1200 RPM and a welding speed of 10 mm/min. This result confirms that the speed of tool rotation is one of the most significant process parameters in the welding of aluminium alloy by FSW method.

Figure 4.41 depicts the distribution of hardness attained across the transverse cross-section of an aluminium alloy weld connection welded at speed of tool rotation of 800, 1000 and 1200 RPM with welding speed of 15 mm/min being held constant. An increase in the hardness at NZ is noted for all the specimens. The maximum increment in the NZ was 31.5% (136.1 VHN) as compared to the base material for an aluminium alloy weld connection welded at a speed of tool rotation of 1000 RPM and a welding speed of 15 mm/min. The minimum increment in the NZ was 20.8% (125 VHN) for an aluminium alloy welded at a speed of tool rotation of 1200 RPM and a welding speed of 15 mm/min.
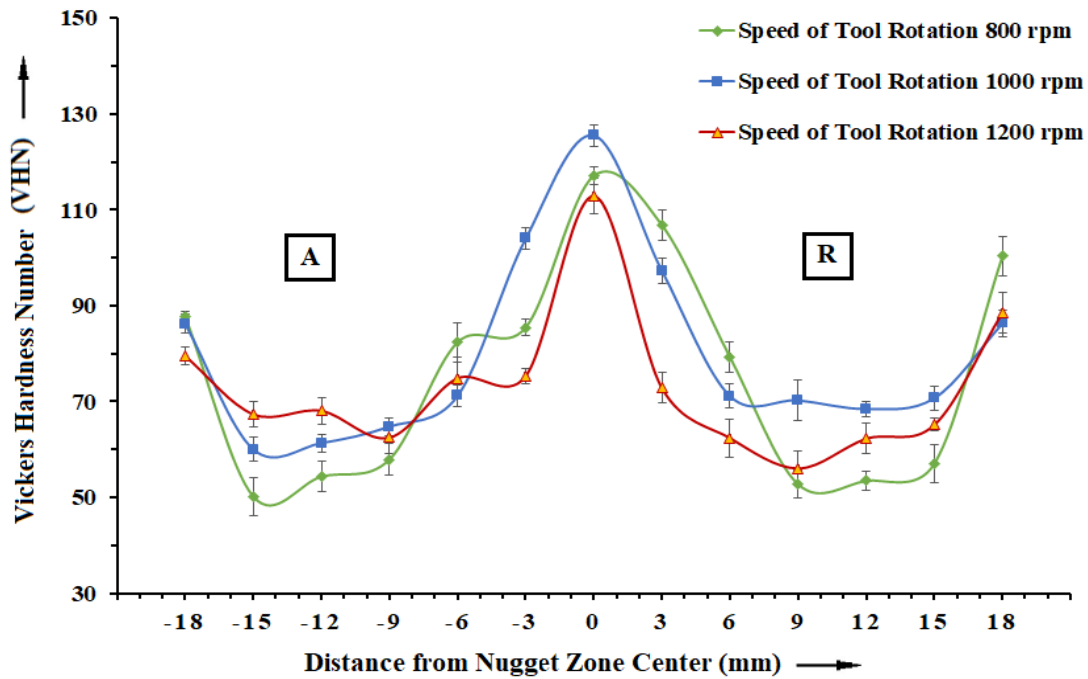
Figure 4.40 Hardness distribution across NZ of friction stir welded Al-5Mg-8Ce-3.5Si aluminium alloy, with SPP tool at various speeds of tool rotation of 800, 1000 and 1200 RPM with constant welding speed of 10 mm/min
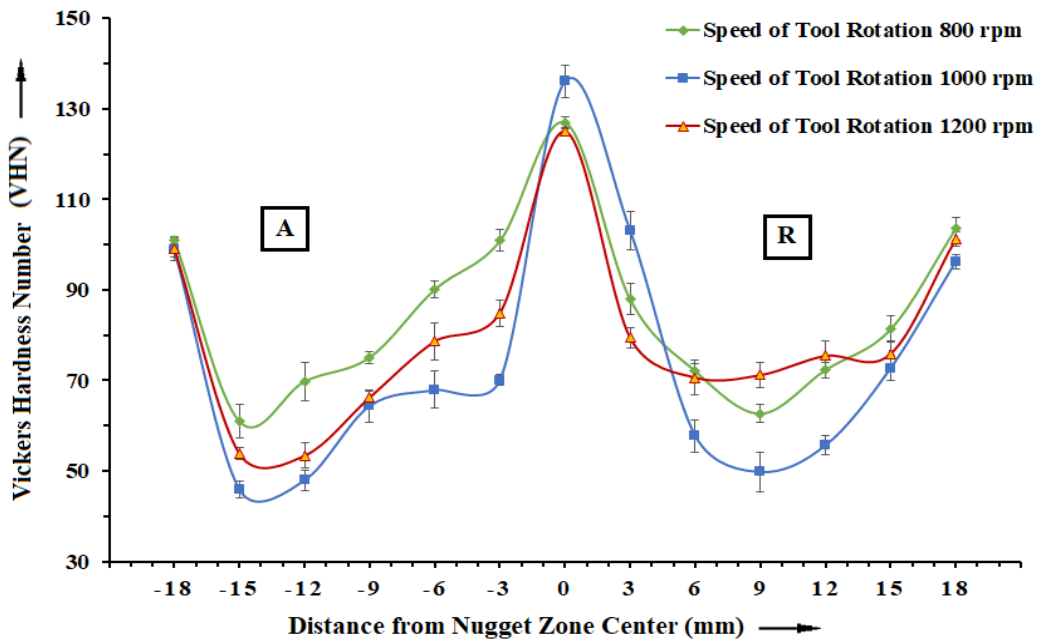
Figure 4.41 Hardness distribution across NZ of friction stir welded Al-5Mg-8Ce-3.5Si aluminium alloy, with SPP tool at various speeds of tool rotation of 800, 1000 and 1200 RPM with constant welding speed of 15 mm/min.

Figure 4.42 depicts the plot of the distribution of hardness over the cross-section of aluminium alloy weld connection welded at speed of tool rotation of 810, 1000 and 1200 RPM and welding speed of 20 mm/min. The temperatures at different positions have different intensities. So, the hardness distribution at the weld region is uneven. The region where highest hardness obtained is at NZ. The increase in the hardness is observed for all the aluminium alloy joints. The maximum increase in the hardness over base material is found to be 11.2% (122.7 VHN) for a speed of tool rotation of 1000 RPM and welding speed of 20 mm/min. Similarly, the minimum increase in hardness is 9.4% (114.5VHN) for speed of tool rotation of 1200 RPM and welding speed of 20 mm/min.
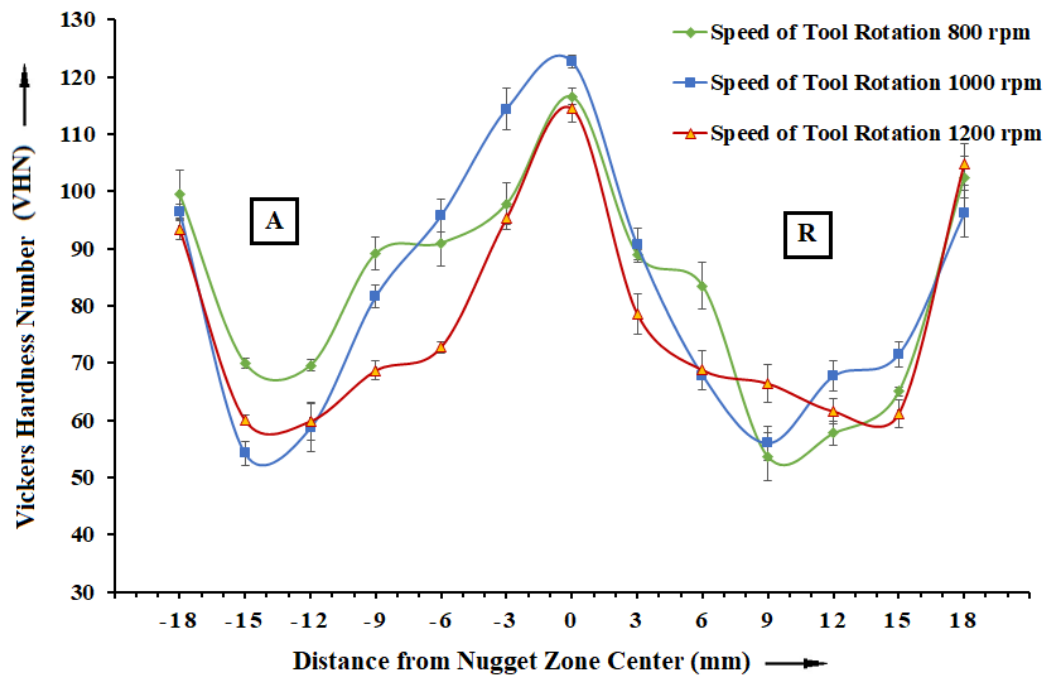
Figure 4.42 Hardness distribution across NZ of friction stir welded Al-5Mg-8Ce-3.5Si aluminium alloy, with SPP tool at various speeds of tool rotation of 800, 1000 and 1200 RPM with constant welding speed of 20 mm/min.

4.6.1.3 Hardness test of friction stir welded weld connection of Al-10Mg-8Ce-3.5Si and Al-5Mg-8Ce-3.5Si aluminium alloys using Circular / Round Profile Pin (CPP) Tool

4.6.1.3.1 Hardness distribution across Al-10Mg-8Ce-3.5Si aluminium alloy joints friction Stir Welded using Circular / Round Profile Pin (CPP) Tool

Figure 4.43 shows the plots illustrating the variation of hardness across the mid thickness offriction stir welded weld connection of Al-10Mg-8Ce-3.5Si aluminium alloy being fabricated u s i n g CPP tool at various speeds of tool rotation of 810, 1000, 1200 RPM, respectively, with a welding speed (transverse speed) of 10 mm/min being held constant. The hardness is measured on either side of the weld line. The relative velocity between the tool and the material is influenced mainly by the speed of tool rotation. Therefore, the heat generation rate is not significantly affected by the welding speed. High traverse speeds tend to reduce the heat input rate and temperatures (Elangovan et al. 2008a; Sharma et al. 2012a; Threadgilll et al. 2009). Lower welding speed leads to greater amount of heat input to materials and therefore, it improves plastic deformation of the material and the formation of the effective weld connection (Jayaraman et al. 2010; Khorrami et al. 2012). Friction stir welded samples show greater hardness in the NZ than the parent material because of increased effect of dynamic recrystallization, homogeneous distribution of AlSiMg particles, numerous small rounded particles and reduced grain size (Prapas et al. 2017). The small particle produced due to stirring effect of the tool, which abrades the surface of the particles and shapes the particles to be spherical, due to collision of particles with each other (Ceschini et al. 2007; Sato et al. 2003; Svensson et al. 2000b). When the speed of tool rotation was increased from 1000 RPM to 1200 RPM, the hardness was found to decrease. As the speed of tool rotation increases, the heat generated is also increases which results in grain coarsening and decrease in hardness. At TMAZ, which is adjacent to the weld nugget on either side, i.e., on the advancing and the retreating side, the hardness obtained was lower than nugget zone but higher than the base material. The region between TMAZ and base material

known as HAZ is affected by the thermal cycle but is not subjected to any plastic deformation. As a result, coarse grain size has been observed in HAZ and hence the hardness obtained was less than that of the base material (Dong et al. 2013; Zhang et al. 2011). The highest hardness value of 131.5 VHN was exhibited in the weld connection fabricated with speed of tool rotation of 1000 RPM and welding speed of 10 mm/min. The lowest hardness value of 120.8 VHN was observed in the weld connection fabricated with speed of tool rotation of 1200 RPM and welding speed of 10 mm/min.
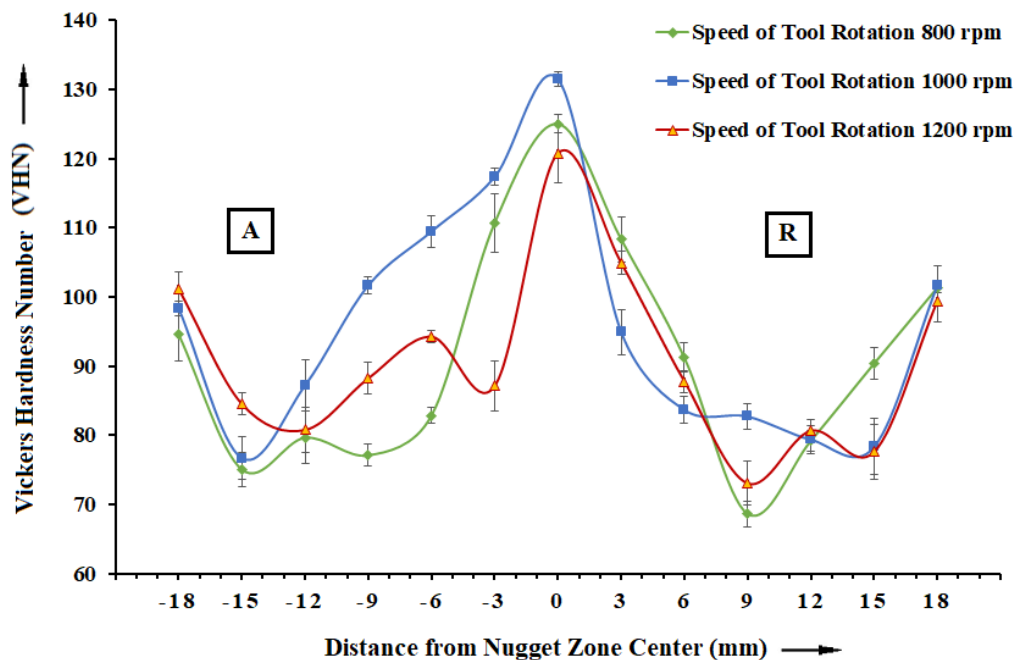
Figure 4.43 Hardness distribution across NZ of friction stir welded Al-10Mg-8Ce-3.5Si aluminium alloy, with CPP tool at various speeds of tool rotation of 800, 1000 and 1200 RPM with constant welding speed of 10 mm/min.

Figure 4.44 represents the hardness variation across the Al-10Mg-8Ce-3.5Si aluminium alloy friction stir welded with various combinations of speed of tool rotation and welding speed. The hardness distribution plot showed the higher value of hardness at the NZ when compared to the base aluminium alloy, irrespective of speed of tool rotation and welding speed. The reasons behind the increase in the hardness at NZ are.

(i)　Refined and decreased grain size as compared to base metal: The size of the grain plays a major role in increasing or decreasing the strength of the material. As per Hall-Petch equation, the grain size is inversely proportional to the hardness of the material (Heidarzadeh et al. 2015; Heurtier et al. 2006; Ilangovan et al. 2015a; Kamp et al. 2007).

(ii)　Uniform distribution of AlSiMg particles as well as intermetallic particles in the NZ assists the increase in hardness (Goel et al. 2018; Sajadifar et al. 2019).

The stirring effect of the tool at NZ resulted in high plastic deformation due to which fine grains were formed. Striking of hard particles with each other resulted in rounding and breaking of AlSiMg particles. These particles were uniformly distributed with decrease in size and increase in the quantity at NZ (Hu et al. 2015; Li et al. 2015). Slightly lesser hardness value was observed on either side of the NZ representing TMAZ, where the material is plastically deformed and thermally affected. TMAZ is characterized by elongated grains. The hardness obtained in all the samples exhibited slightly higher hardness values in the TMAZ than HAZ region. The increase in the hardness in the TMAZ is attributed to the second phase particle dissolution and work hardening due to intense plastic deformation (Grujicic et al. 2010; Leitão et al. 2012; Rao et al. 2013). Lower hardness is obtained in HAZ. The decrease in the hardness in HAZ is mainly due to thermal cycle, which resulted in grain growth and softening (Dong et al. 2013; Zhang et al. 2011). The maximum hardness value of 126.9 VHN was exhibited in the weld connection fabricated with speed of tool rotation of 1000 RPM and welding speed of 15 mm/min. The lowest hardness value of 114.9 VHN was observed in the weld connection fabricated with speed of tool rotation of 1200 RPM and welding speed of 20 mm/min.

Figure 4.45 shows the plots illustrating the hardness distribution across the friction stir welded weld connection of Al-10Mg-8Ce-3.5Si aluminium alloy, fabricated using CPP tool at various speeds of tool rotation of 800, 1000 and 1200 RPM, respectively, with welding speed 20 mm/min being held constant. The highest hardness value was attained for a speed of tool rotation of 1000 RPM and welding speed of 20 mm/min. As the speed increases from 1000 to 1200 RPM, the hardness value reduces due to increase

in the heat generation. Higher welding speed reduces the hardness value. This is mainly due to agglomeration or accumulation of AlSiMg particles in the NZ due to high rotary speed and high welding speed. Therefore, the non-uniform dispersion of AlSiMg particles in the measurement region would give rise to unsatisfactory results at higher speed of tool rotation (1200 RPM) and higher welding speed (20 mm/min). The highest hardness value of 121.4 VHN was exhibited in the weld connection fabricated with speed of tool rotation of 1000 RPM and welding speed of 20 mm/min. The lowest value of hardness observed was 114.3 VHN in the weld connection fabricated with speed of tool rotation of 1200 RPM, and welding speed of 20 mm/min.
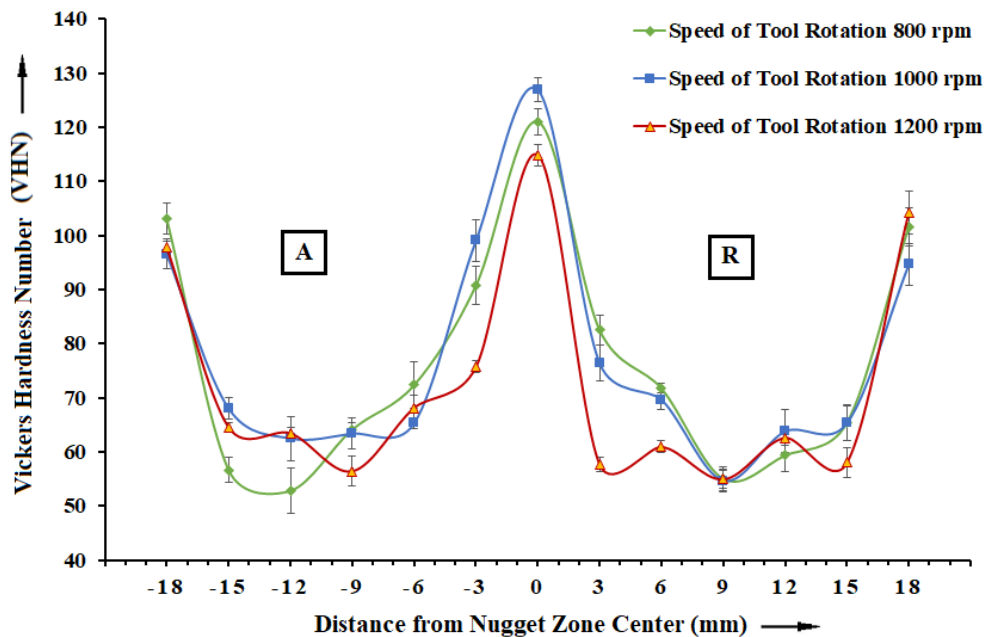
Figure 4.44 Hardness distribution across NZ of friction stir welded Al-10Mg-8Ce-3.5Si aluminium alloy, with CPP tool at various speeds of tool rotation of 800, 1000 and 1200 RPM with constant welding speed of 15 mm/min.
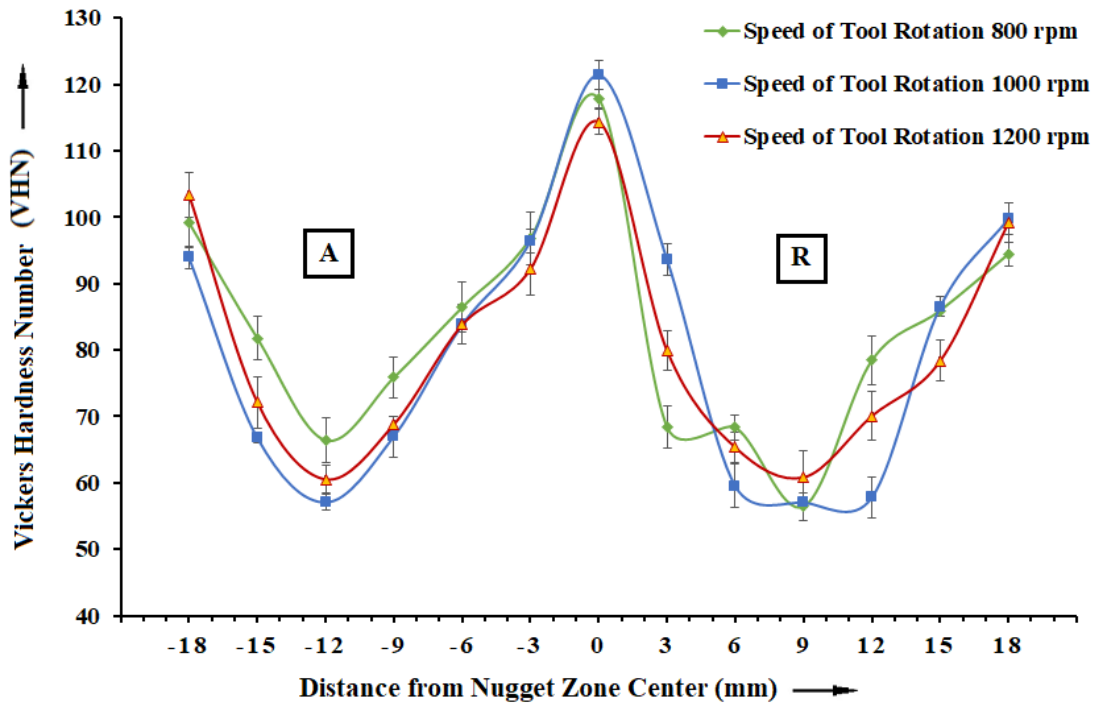
Figure 4.45 Hardness distribution across NZ of friction stir welded Al-10Mg-8Ce-3.5Si aluminium alloy, with CPP tool at various speeds of tool rotation of 800, 1000 and 1200 RPM with constant welding speed of 20 mm/min.

4.6.1.3.2 Hardness distribution across Al-5Mg-8Ce-3.5Si aluminium alloy joints friction Stir Welded using Circular / Round Profile Pin (CPP) Tool

Figure 4.46 depicts the plot illustrating the distribution of hardness values across the FSW welded aluminium alloy specimen at various speeds of tool rotation of 800, 1000 and 1200 RPM with welding speed being held constant at 10 mm/min. Hardness profiles exhibited W-shape for all the cases studied. It has been found that the hardness of the nugget zone was higher than the base material for all the cases (Cerri and Leo 2013; Ji et al. 2016b). The hardness value increase in the in the nugget zone is largely because of the stirring action of the pin, which results in recrystallization, leading to break up of AlSiMg particles, and formation of fine equiaxed grains. The breakage of AlSiMg particles is because of the abrasive effect of tool and collision of particles (having sharp comers) among themselves. Also, the broken AlSiMg particles get

196

uniformly distributed within the nugget zone due to the stirring action of the tool, which eventually leads to increase in hardness. According to the Hall-Petch equation, hardness is inversely proportional to grain size. Sato et al. (2002) reported that, the higher hardness in the nugget zone could be elucidated by higher density of sub-grains and small size of the grains. The overall behavior is because of the contribution from substructure, particle redistribution and grain boundaries. However, it has been observed from Figure 4.46 that, as the speed of tool rotation goes up from 800 RPM to 1000 RPM, the nugget zone hardness also goes up. At low speed of tool rotation, the heat produced is less irrespective of welding speed, due to this the heat input to the base material is reduced. This causes inadequate plasticization and insufficient flow of material in the stir zone. But as the speed of tool rotation goes up, the heat generation also goes up because of higher frictional heat, irrespective of welding speed. This results in more powerful stirring action and good mixing of materials, due to this the fine grains were created (Kang et al. 2009; Kumar et al. 2008). But, when the speed of tool rotation was further increased to 1200 RPM, the hardness decreased. High speed of tool rotation results in higher heat creation and causes the stirred material to move towards the top surface producing voids in nugget region. Also higher heat input causes slower rates of cooling, thereby providing enough time for the growth of the grains (Banik et al. 2019; Ma et al. 2018). In addition, at higher speed of tool rotation, accumulation of AlSiMg particles occurs due to inappropriate flow of material. As a cascading effect, hardness value comes down (Asadi et al. 2012; Heinz and Skrotzki 2002; Svensson et al. 2000b). The maximum value of hardness exhibited in the weld connection was 119.2 VHN, fabricated with a speed of tool rotation of 1000 RPM and welding speed of 10 mm/min. The lowest hardness value of 111.2 VHN was observed in the weld connection fabricated with speed of tool rotation of 1200 RPM, and welding speed of 10 mm/min.
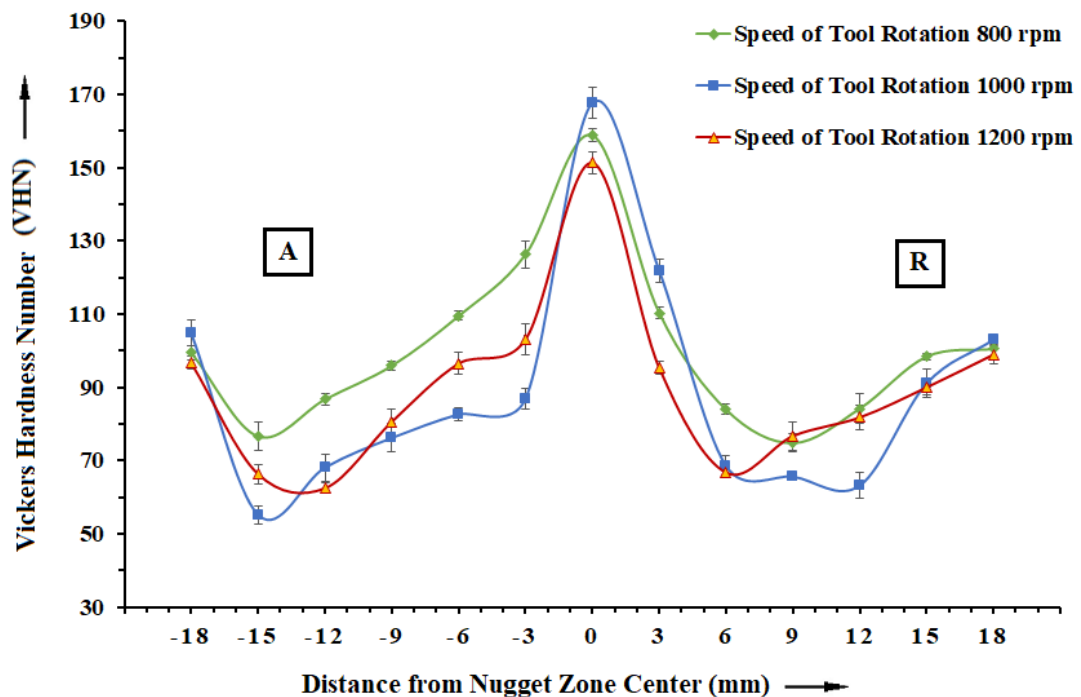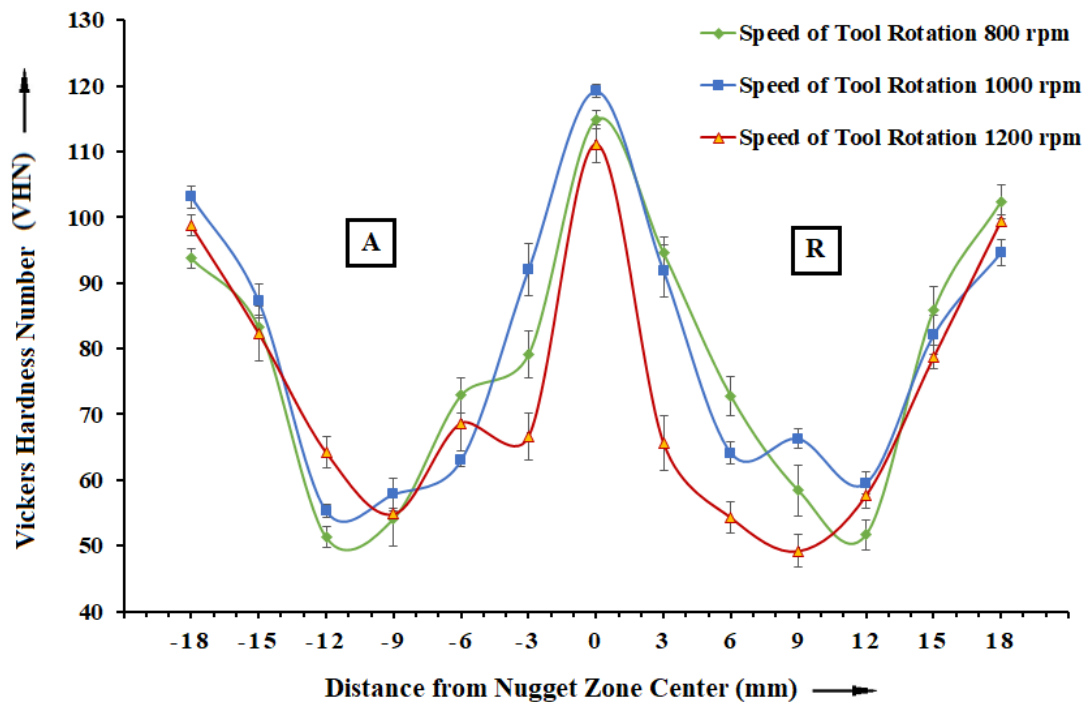
Figure 4.46 Hardness distribution across NZ of friction stir welded Al-5Mg-8Ce-3.5Si aluminium alloy, with CPP tool at various speeds of tool rotation of 800, 1000 and 1200 RPM with constant welding speed of 10 mm/min.

Figure 4.47 illustrates the hardness plots of Al-5Mg-8Ce-3.5Si aluminium alloy, weld connection being welded with rotational speeds of 800, 1000 and 1200 RPM and at a constant welding speed of 15 mm/min. In both the cases, as seen from Figure 4.46 and Figure 4.47, the hardness distribution plots were similar. However, it has been observed from Figure 4.46 and Figure 4.47 that, as the welding speed was increased from 10 mm/min to 15 mm/min, the hardness of the nugget zone also increased. Initially, the welding speed is low due to which high temperature is obtained. The rate of cooling of the friction stir processing region is low and hence more time is available for the growth of the grains resulting in considerable grain growth. This leads to lower value of hardness (Banik et al. 2019; Cole et al. 2014; Ma et al. 2018). When the welding speed is increases, the temperature reached in the weld region is reduces. Due to swifter movement of the tool, there is decrease in the friction time and hence the weld material experiences lower processing temperature. As a result of this, the friction stir welded

specimen will cool faster generating finer grains, which in turn lead to higher hardness values (Kang et al. 2009; Kumar et al. 2008). The maximum value of hardness exhibited in the weld connection was 129.2 VHN, fabricated with speed of tool rotation of 1000 RPM and welding speed of 15 mm/min. The lowest hardness value of 118.9 VHN was observed in the weld connection fabricated with speed of tool rotation of 1200 RPM, and welding speed of 15 mm/min.
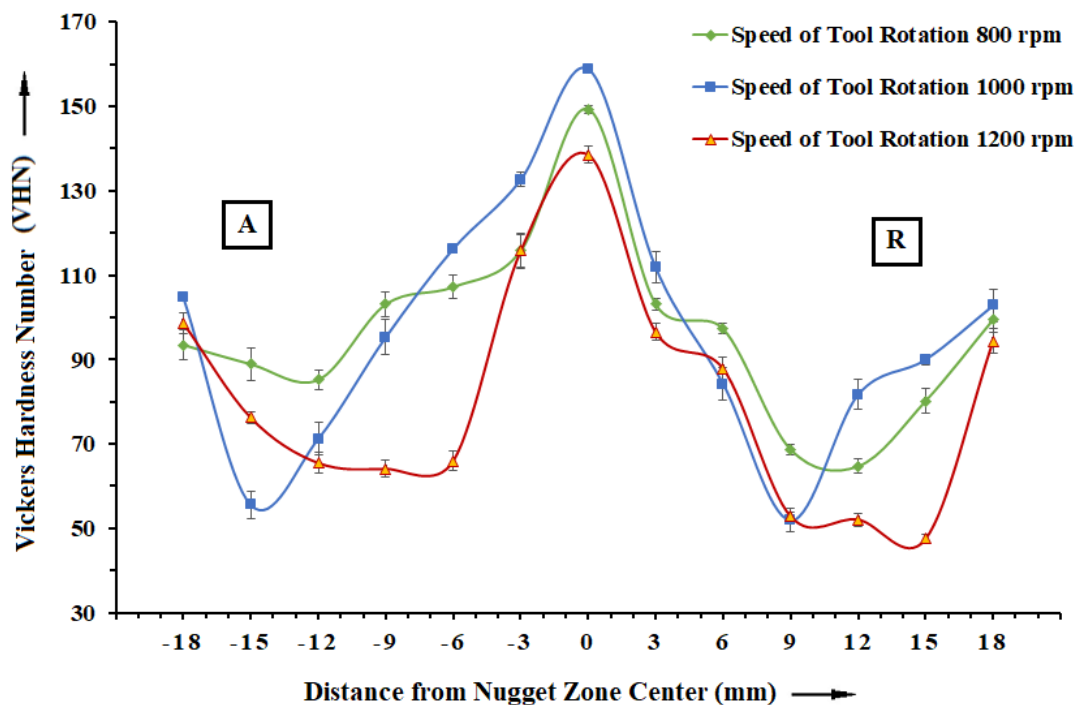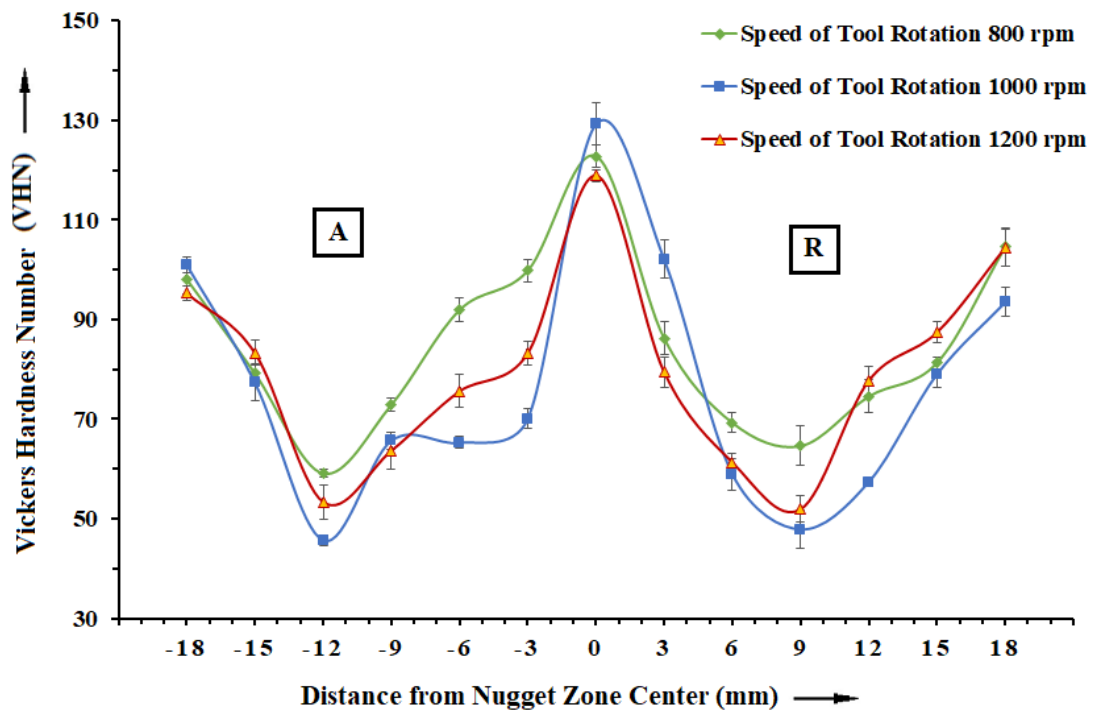

Figure 4.47 Hardness distribution across NZ of Al-5Mg-8Ce-3.5Si aluminium alloy, friction stir welded using CPP tool at various speeds of tool rotation of 800, 1000 and 1200 RPM with constant welding speed of 15 mm/min.

Figure 4.48 shows the plots illustrating the variation of hardness across the mid thickness of friction stir welded weld connection of Al-5Mg-8Ce-3.5Si aluminium alloy being fabricated using CPP tool at various speeds of tool rotation of 800, 1000, 1200 RPM, respectively, with welding speed 20 mm/min being held constant. Similar trend has been observed as in Figure 4.47. The maximum hardness value obtained was 124.5 VHN for a speed of tool rotation of 1000 RPM and welding speed of 20 mm/min. The minimum hardness obtained was 113.5 VHN for a speed of tool rotation of 1200

RPM and welding speed of 20 mm/min. The reasons for the variation in hardness have already been discussed in previous section.
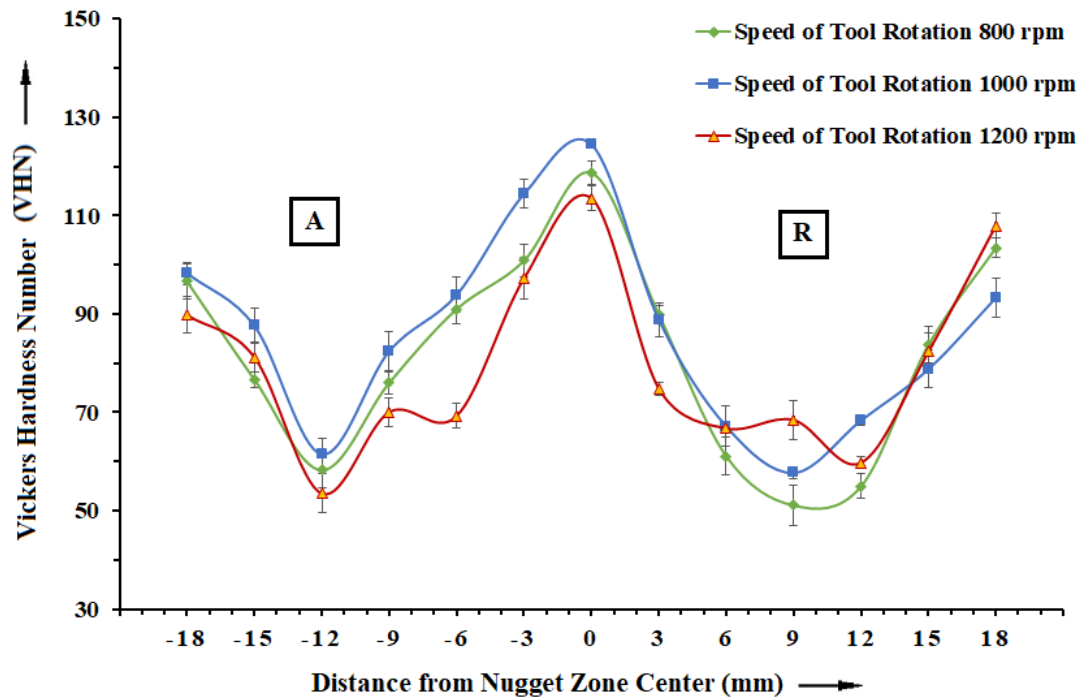
Figure 4.48 Hardness distribution across NZ of Al-5Mg-8Ce-3.5Si aluminium alloy, friction stir welded using CPP tool at various speeds of tool rotation of 800, 1000 and 1200 RPM with constant welding speed of 20 mm/min.

4.6.2   Tensile stress test

4.6.2.1   Tensile stress test of friction stir welded weld connection of Al-10Mg-8Ce-3.5Si aluminium alloys using Triangular Profile Pin (TPP) Tool, Square Profile Pin (SPP) Tool and Round/Circular Profile Pin (CPP) Tools

4.6.2.1.1   Tensile stress test of friction stir welded weld connection of Al-10Mg-8Ce-3.5Si aluminium alloy using Triangular Profile Pin (TPP) Tool

Table 4.12 presents the tensile test results of Al-10Mg-8Ce-3.5Si aluminium alloy joints friction stir welded using TPP tool, at different combinations of speeds of tool rotation and speeds of welding. The UTS of the joints fabricated using TPP tool

200

increases with increase in the welding speed from 10 to 20 mm/min and reaches to a maximum value at a speed of 20 mm/min. For the samples welded at welding speed less than 20 mm/min, the specimen fracture at HAZ, near to the base material (Cavaliere and Cerri 2005; Huang et al. 2017; Kadlec et al. 2015; Zhao et al. 2017a). Further increase in the welding speed beyond 20 mm/min leads to formation of pin holes, worn hole and tunnel hole defects. Therefore, these specimens fracture at NZ (Kadlec et al. 2015; Khan et al. 2015b; Moreira et al. 2009). This results in the decrease in tensile strength. The forward movement of the rotating tool makes the stirred material to move from the front to the back of the tool pin. The rate of heat input depends on the welding speed (Li et al. 2014b; Sharma et al. 2012a; Waheed et al. 2017). The welding speed regulates the exposure time of frictional heat per unit length of the weld which impacts the heat transfer rate and consequently affects the grain growth (Bisadi et al. 2013; Long et al. 2007; Singh 2012; Yadav and Bauri 2012). At high welding speed, the amount of heat input to the weld region is less, and this results in higher cooling rate of the material. As the speed of tool rotation is increased from 800 RPM to 1000 RPM the UTS also increases. Further increase in the speed of tool rotation leads to reduction in UTS (Babu et al. 2009; Bisadi et al. 2013; Palanivel et al. 2012). Highest weld connection efficiency of 81.2% was attained for a speed of tool rotation of 1000 RPM and welding speed of 20 mm/min. Weld connection efficiency (defined in Chapter 3 - Research methodology section) decreases with further increase in the speed of tool rotation (Carlone and Palazzo 2013; Rezaei et al. 2011). Speed of tool rotation of 1000 RPM and welding speed of 20 mm/min were decided as the optimal method variable values for FSW using TPP tool.

Table 4.12 Tensile test results of Al-10Mg-8Ce-3.5Si aluminium alloy joints, friction stir welded using Triangular Profile Pin (TPP) tool.

Speed of tool rotation (RPM)	Welding speed (mm/min)	Yield stress (N/mm^2)	Ultimate Tensile stress (UTS) (N/mm^2)	Elongation (%)	Weld connection Efficiency (%)
800	10	54 ± 1	95 ± 3	5.6 ± 0.3	71.5

800	15	67 ± 3	104 ± 3	5.5 ± 0.2	78.2
800	20	63 ± 3	107 ± 3	5.4 ± 0.3	80.5
1000	10	62 ± 3	101 ± 4	5.8 ± 0.3	76.0
1000	15	63 ± 2	102 ± 4	5.2 ± 0.1	76.7
1000	20	72 ± 3	108 ± 4	5.6 ± 0.1	81.2
1200	10	62 ± 3	99 ± 4	4.9 ± 0.2	74.5
1200	15	58 ± 1	96 ± 2	5.6 ± 0.3	72.2
1200	20	55 ± 3	87 ± 3	4.9 ± 0.2	65.4

4.6.2.1.2   Tensile stress test of friction stir welded weld connection of Al-10Mg-8Ce-3.5Si aluminium alloy using Square Profile Pin (SPP) Tool

Table 4.13 presents the tensile properties of the Al-10Mg-8Ce-3.5Si aluminium alloy, friction stir welded at various speeds of tool rotation and speeds of welding using SPP tool. It can be seen from Table 4.13 that the tensile properties of each of the weld connection were less than that of the base material. Weld connection strength of FSW joints is mainly influenced by the welding defects and hardness distributions at the joints, which are functions of the welding parameters. When joints are free from defects, their weld connection strengths are affected dominantly by hardness distributions (Han et al. 2013; Khodir and Shibayanagi 2008; Rajakumar and Balasubramanian 2012a). When a tensile load is applied to the joint, the stress and strain concentration take place in the lowest-strength part or region in the joint, and consequently the weld connection is fractured in this region. It is to be noted that the HAZ region of the weldment exhibited the lowest hardness due to thermal cycle which leads to grain growth. The hardness at HAZ was much less than that of the base material and the tensile specimens failed at this region of the lower strength (Cavaliere and Cerri 2005; Huang et al. 2017; Kadlec et al. 2015; Zhao et al. 2017a). The maximum UTS of the weld connection fabricated using SPP tool was 99 ± 3 N/mm^2 with a speed of

tool rotation of 1000 RPM and a welding speed 20 mm/min. Minimum UTS of the weld connection fabricated using SPP tool was 66 ± 3 N/mm^2 with a speed of tool rotation of 1200 RPM and a welding speed of 10 mm/min. UTS decreases with further increase in the speed of tool rotation (Carlone and Palazzo 2013; Rezaei et al. 2011). A speed of tool rotation of 1000 RPM and a welding speed of 20 mm/min were decided as the optimal method variable values for FSW using SPP tool.

4.6.2.1.3 Tensile stress test of friction stir welded weld connection of Al-10Mg-8Ce-3.5Si aluminium alloy using Round/Circular Profile Pin (CPP) Tool

Table 4.14 presents the tensile test results of Al-10Mg-8Ce-3.5Si aluminium alloy joints, friction stir welded using CPP tool. Maximum weld connection efficiency of 66.9% was obtained at a speed of tool rotation of 1000 RPM and a welding speed of 20 mm/min. At lower speed of tool rotation (800 RPM) and higher speed of tool rotation (1200 RPM), the weld connection efficiency was poor. When the speed of tool rotation was increased from 800 RPM to 1000 RPM, the weld connection efficiency also increased and reached a highest value (Adamowski et al. 2007; Babu et al. 2017). The weld connection efficiency reduced with further increase in the speed of tool rotation. At lower speed of tool rotation, poor stirring action ensues, and lower heat condition of the tool results in inappropriate consolidation of base material. Hence, lower weld connection efficiency was attained (Khaled 2005; Nami et al. 2011; Prabhu et al. 2016). Increase in the speed of tool rotation improves the stirring effect and heat condition, resulting in uniform grain refinement. It results in enhanced weld connection efficiency. A substantial increase in the speed of tool rotation creates excessive stirring, increased heat, and reduced cooling rate, resulting in grain growth. Hence lower ultimate tensile stress was attained at a higher speed of tool rotation (Carlone and Palazzo 2013; Rezaei et al. 2011). From Table 4.12, Table 4.13 and Table 4.14, it is evident that the strength of the weld connection fabricated using TPP tool is about 10% greater than SPP tool and about 21% greater than CPP tool. This is because of the increase in the dynamic to

static volume ratio for the TPP tool (Elangovan et al. 2008b; Marzbanrad et al. 2014; Zhang et al. 2012), which sweeps more material than SPP and CPP tools.

Table 4.13 Tensile test results of Al-10Mg-8Ce-3.5Si aluminium alloy friction stir welded using Square profile pin (SPP) tool

Speed of tool rotation (RPM)	Welding speed (mm/min)	Yield stress (N/mm^2)	Ultimate Tensile stress (UTS) (N/mm^2)	Elongation (%)	Weld connection Efficiency (%)
800	10	42 ± 3	81 ± 3	4.9 ± 0.3	60.9
800	15	45 ± 3	85 ± 4	5.6 ± 0.1	63.9
800	20	55 ± 1	93 ± 4	5.2 ± 0.2	69.9
1000	10	45 ± 3	77 ± 2	5.5 ± 0.3	57.9
1000	15	49 ± 1	88 ± 3	5.2 ± 0.1	66.2
1000	20	61 ± 3	99 ± 3	5.2 ± 0.3	74.5
1200	10	45 ± 3	66 ± 3	5.7 ± 0.2	49.6
1200	15	46 ± 1	79 ± 2	5.4 ± 0.3	59.4
1200	20	50 ± 2	83 ± 3	5.1 ± 0.1	62.4

Table 4.14 Tensile test results of Al-10Mg-8Ce-3.5Si aluminium alloy weld connection friction stir welded using Circular/Round profile pin (CPP) tool

Speed of tool rotation (RPM)	Welding speed (mm/min)	Yield stress (N/mm^2)	Ultimate Tensile stress (UTS) (N/mm^2)	Elongation (%)	Weld connection Efficiency (%)
800	10	35 ± 2	55 ± 3	4.9 ± 0.3	41.4

800	15	37 ± 2	69 ± 4	5.6 ± 0.1	51.9
800	20	52 ± 3	88 ± 2	5.2 ± 0.3	66.2
1000	10	41 ± 2	68 ± 4	5.5 ± 0.1	51.1
1000	15	50 ± 3	78 ± 3	5.2 ± 0.3	58.7
1000	20	56 ± 1	89 ± 3	5.2 ± 0.2	66.9
1200	10	43 ± 2	72 ± 2	5.7 ± 0.3	54.2
1200	15	43 ± 1	79 ± 2	5.4 ± 0.2	59.4
1200	20	45 ± 1	80 ± 4	5.1 ± 0.2	60.2

4.6.2.2 Tensile stress test of friction stir welded weld connection of Al-5Mg-8Ce-3.5Si aluminium alloys using Triangular Profile Pin (TPP) Tool, Square Profile Pin (SPP) Tool and Round/Circular Profile Pin (CPP) Tools

4.6.2.2.1 Tensile stress test of friction stir welded weld connection of Al-5Mg-8Ce-3.5Si aluminium alloy using Triangular Profile Pin (TPP) Tool

Table 4.15 presents the tensile properties of friction stir welded Al-5Mg-8Ce-3.5Si aluminium alloy joints produced with TPP tool. The nature of tensile properties of the FSW joints of Al-5Mg-8Ce-3.5Si aluminium alloy is like the joints of Al-10Mg-8Ce-3.5Si aluminium alloy. However, decrease in the UTS was observed as compared to Al-10Mg-8Ce-3.5Si aluminium alloy. This is mainly because of the presence of less quantity of hard AlSiMg particles which impart strength to the matrix, thereby providing reduced resistance to tensile stress. There is an surge in the interspatial distance between the hard AlSiMg particles as the volume fraction of AlSiMg particles increases, which results in decrease of dislocation pile-up as the particulate content is decreased (Guo et al. 2014; Ma et al. 2018; Tao et al. 2017). The variation in the thermal expansion coefficient between aluminium matrix and AlSiMg particles increases the dislocation density. Higher dislocation density resists the propagation of the cracks during the tensile test (Starke and Staleyt 1996; Xie et al. 2017). Also, the presence of

numerous small particles increases the load bearing capacity of the aluminium alloy (Svensson et al. 2000b; Threadgilll et al. 2009). Maximum UTS was 91 ± 4 N/mm^2 for a speed of tool rotation of 1000 RPM and a welding speed of 20 mm/min. Minimum UTS was 73 ± 2 N/mm^2 for a speed of tool rotation of 1200 RPM and a welding speed of 20 mm/min.

Table 4.15 Tensile test results of Al-5Mg-8Ce-3.5Si aluminium alloy joints friction stir welded using Triangular Profile Pin (TPP) Tool.

Speed of tool rotation (RPM)	Welding speed (mm/min)	Yield stress (N/mm^2)	Ultimate Tensile stress (UTS) (N/mm^2)	Elongation (%)	Weld connection Efficiency (%)
800	10	49 ± 1	85 ± 2	5.6 ± 0.1	63.9
800	15	54 ± 2	90 ± 2	6.1 ± 0.3	67.7
800	20	53 ± 3	79 ± 3	5.6 ± 0.3	59.4
1000	10	58 ± 1	86 ± 3	5.7 ± 0.3	64.7
1000	15	51 ± 3	85 ± 3	6 ± 0.2	63.9
1000	20	58 ± 2	91 ± 4	5.9 ± 0.1	68.4
1200	10	45 ± 3	78 ± 2	5.8 ± 0.2	58.7
1200	15	52 ± 3	82 ± 4	5.6 ± 0.1	61.7
1200	20	46 ± 2	73 ± 2	6.1 ± 0.3	54.9

4.6.2.2.2 **Tensile stress test of friction stir welded weld connection of Al-5Mg-8Ce-3.5Si aluminium alloy using Square Profile Pin (SPP) Tool**

Table 4.16 presents the tensile test results of Al-5Mg-8Ce-3.5Si aluminium alloy joints, friction stir welded using SPP tool. Maximum weld connection efficiency was attained at a speed of tool rotation of 1000 RPM and a welding speed of 20 mm/min. When the speed of tool rotation raised from 800 RPM to 1000 RPM, the weld connection efficiency also improved and reached a peak value of 63.2%. The weld connection efficiency declined with further rise in the speed of tool rotation. It is evident from the Table 4.15 and Table 4.16 that, the tensile property of the aluminium alloy weld connection friction stir welded using TPP tool is higher than that for the joints friction stir welded using SPP. This may be due to the pulsating effect and higher dynamic to static volume ratio of material swept by the TPP tool compared to the SPP tool (Elangovan et al. 2008b; Marzbanrad et al. 2014; Zhang et al. 2012).

Table 4.16 Tensile test results of Al-5Mg-8Ce-3.5Si aluminium alloy joints friction stir welded using Square Profile Pin (SPP) Tool.

Speed of tool rotation (RPM)	Welding speed (mm/min)	Yield stress (N/mm^2)	Ultimate Tensile stress (UTS) (N/mm^2)	Elongation (%)	Weld connection Efficiency (%)
800	10	37 ± 1	67 ± 4	5.6 ± 0.2	50.4
800	15	40 ± 1	71 ± 2	6 ± 0.1	53.4
800	20	48 ± 2	78 ± 4	5.7 ± 0.3	58.7
1000	10	34 ± 3	64 ± 3	5.8 ± 0.2	48.1
1000	15	44 ± 2	74 ± 4	5.5 ± 0.1	55.7
1000	20	48 ± 1	84 ± 4	5.9 ± 0.2	63.2
1200	10	31 ± 1	55 ± 2	6.1 ± 0.3	41.4
1200	15	40 ± 2	67 ± 3	5.9 ± 0.2	50.4
1200	20	41 ± 3	70 ± 4	5.8 ± 0.1	52.6

4.6.2.2.3 **Tensile stress test of friction stir welded weld connection of Al-5Mg-8Ce-3.5Si aluminium alloy using Circular / Round Profile Pin (CPP) Tool**

The tensile behavior of Al-5Mg-8Ce-3.5Si aluminium alloy joints, friction stir welded using CPP tool is tabulated in the Table 4.17. The UTS of the aluminium weld connection is significantly low compared to the joints fabricated using other pin profile tools. This is because of the absence of any pulsating effect and lower dynamic to static volume ratio of material swept by the CPP tool compared to the TPP and SPP tool (Elangovan et al. 2008b; Marzbanrad et al. 2014; Zhang et al. 2012). It can be observed from Table 4.17 that, the weld connection efficiency of the Al-5Mg-8Ce-3.5Si aluminium alloy was close to 50%, when compared to that of the base material. Maximum percentage of weld connection efficiency was 56.4% for a speed of tool rotation of 1000 RPM and a welding speed of 20 mm/min with a peak UTS of 75 ± 4 N/mm^2. Minimum UTS was 47 N/mm^2 for a speed of tool rotation of 1200 RPM and a welding speed of 10 mm/min.

4.6.2.3 **Comparative study of tensile properties of Al-10Mg-8Ce-3.5Si aluminium alloy joints friction stir welded using different tool pin shapes.**

Figure 4.49 represents the bar chart showing UTS of the joints of friction stir welded Al-10Mg-8Ce-3.5Si aluminium alloy, obtained with various combinations of speeds of tool rotation, speeds of welding and tool pin shapes. As the speed of tool rotation is raised from 800 RPM to 1000 RPM the UTS of the friction stir welded aluminium weld connection increases and reaches a maximum value. Further increase in the speed of tool rotation from 1000 RPM to 1200 RPM results in reduced UTS. Speed of tool rotation the most predominant factor which brings the material to plastic state by generating sufficient heat between the contacting surfaces of the rotating tool pin and the substrate material. Speed of tool rotation is also responsible for mixing of the material around the tool. At low speed of tool rotation, stirring of plasticized material is less owing to insufficient heat generation. As the speed of tool rotation is increased from 800 RPM to 1000 RPM, the heat generated in the NZ also increases due to increase

in the relative velocity between rotating tool pin and material. This results in proper mixing of the material. At higher speed of tool rotation, the heat generation is also higher which results in turbulence in material flow. It is clearly noticeable that among the tools studied, the TPP tool has shown maximum ultimate tensile stress at speed of tool rotation of 1000 RPM and welding speed of 20 mm/min. The increase in the strength may probably be due to pulsating effect of the flat faces of the TPP tool, resulting in sufficient heat generation and proper mixing of the material (Elangovan and Balasubramanian 2008b; Kadaganchi et al. 2015; Marzbanrad et al. 2014; Trimble et al. 2015b). The weld connection fabricated using CPP tool has shown lower UTS.

Table 4.17 Tensile test results of Al-5Mg-8Ce-3.5Si aluminium alloy joints friction stir welded using Circular / Round Profile Pin (CPP) Tool.

Speed of tool rotation (RPM)	Welding speed (mm/min)	Yield stress (N/mm^2)	Ultimate Tensile stress (UTS) (N/mm^2)	Elongation (%)	Weld connection Efficiency (%)
800	10	32 ± 3	60 ± 4	5.5 ± 0.3	45.1
800	15	39 ± 1	65 ± 2	5.9 ± 0.2	48.9
800	20	46 ± 3	73 ± 2	5.5 ± 0.3	54.9
1000	10	32 ± 1	56 ± 4	5.5 ± 0.3	42.1
1000	15	40 ± 1	64 ± 4	6.1 ± 0.1	48.1
1000	20	50 ± 1	75 ± 2	5.5 ± 0.2	56.4
1200	10	30 ± 2	47 ± 2	5.8 ± 0.3	35.3
1200	15	34 ± 3	58 ± 3	6.1 ± 0.1	43.6
1200	20	44 ± 1	67 ± 2	6 ± 0.3	50.4
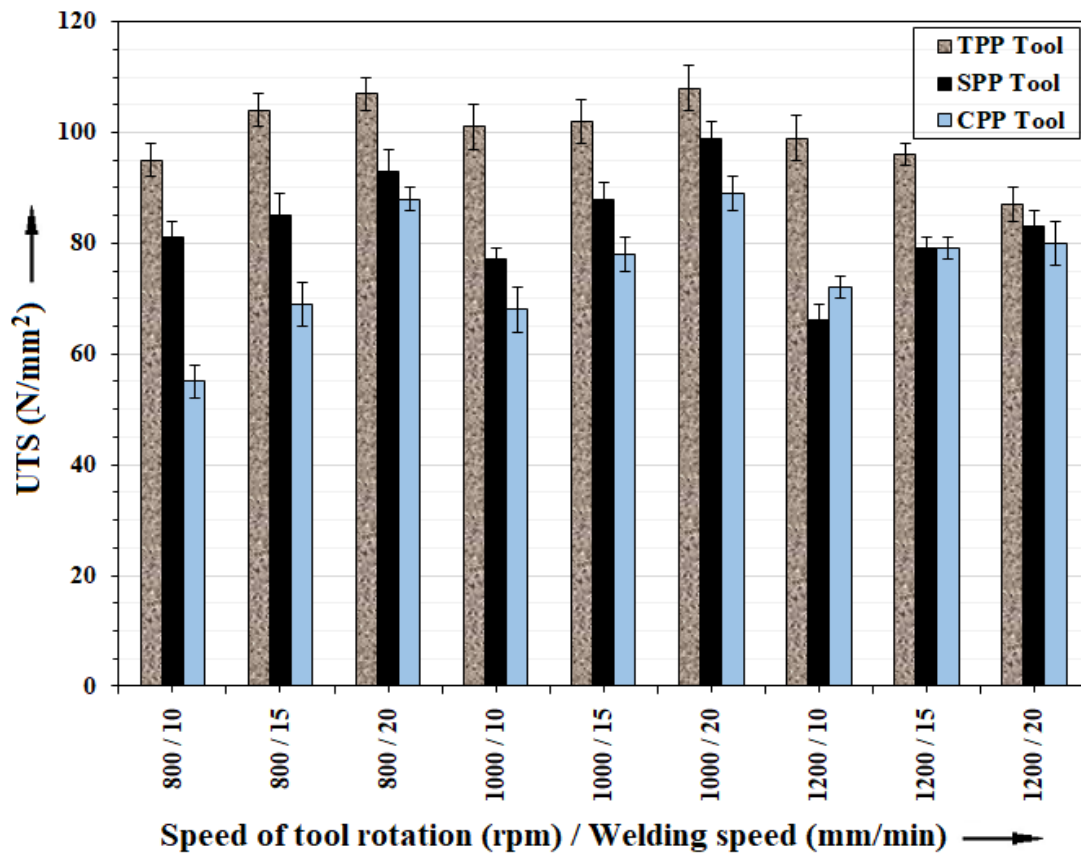
Figure 4.49 UTS of the Al-10Mg-8Ce-3.5Si aluminium alloy joints friction stir welded using Triangular, Square and Circular profile pin tool.

4.6.2.4 Comparative study of tensile properties of Al-5Mg-8Ce-3.5Si aluminium alloy joints friction stir welded using different tool pin shapes.

Figure 4.50 displays the bar chart showing UTS of Al-5Mg-8Ce-3.5Si aluminium alloy joints, friction stir welded with different combinations of speeds of tool rotation, speeds of welding and tool pin shapes. The trend of variation of UTS for friction stir welded Al-5Mg-8Ce-3.5Si aluminium alloy joints was similar to that of Al-10Mg-8Ce-3.5Si aluminium alloy joints.
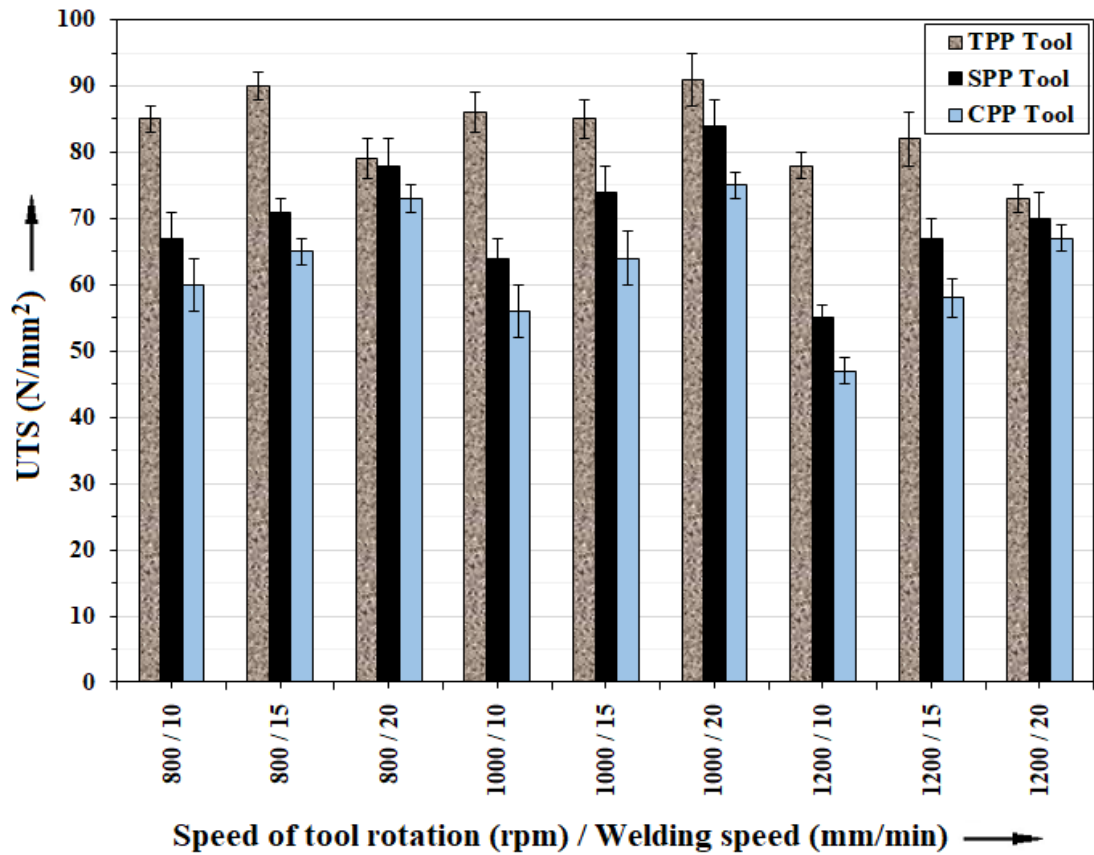
Figure 4.50 UTS of the Al-5Mg-8Ce-3.5Si aluminium alloy joints friction stir welded using Triangular, Square and Circular profile pin tool.

4.6.2.5 Tensile properties in the direction of weld of Al-10Mg-8Ce-3.5Si and Al-5Mg-8Ce-3.5Si aluminium alloy joints friction stir welded using different tool pin shapes.

Table 4.18 to Table 4.20 show the tensile properties of aluminium alloy joints friction stir welded using various speeds of tool rotation, speeds of welding and tool pin shapes. The ultimate tensile stress of the aluminium alloy weld connection is more than the base material irrespective of tool pin shape and process parameters. For a threaded profile pin tool, Table 4.18 exhibited increase in the ultimate tensile stress as the welding speed is increased from 10 mm/min to 20 mm/min for a constant speed of tool rotation of 1000 RPM. The increase in the ultimate tensile stress over that of the base material was 21.3% for Al-10Mg-8Ce-3.5Si aluminium alloy and 18.7% for Al-5Mg-8Ce-3.5Si aluminium alloy, with a speed of tool rotation of 1000 RPM and a welding

speed of 20 mm/min respectively. Table 4.19 shows the ultimate tensile stress of aluminium alloy, friction stir welded using SPP tool. The ultimate tensile stress was found to increase with an increase in the speed of welding from 10 mm/min to 20 mm/min. The increase in ultimate tensile stress over that of the base material was 15.2% for Al-10Mg-8Ce-3.5Si aluminium alloy and 13.1% for Al-5Mg-8Ce-3.5Si aluminium alloy, with a speed of tool rotation of 1000 RPM and a welding speed of 20 mm/min respectively.

Table 4.20 shows the ultimate tensile stress for the joints fabricated using a CPP tool. The ultimate tensile stress was found to be increasing with an increase in the welding speed from 10 mm/min to 20 mm/min. The increase in ultimate tensile stress over that of the base material was 10.1% for Al-10Mg-8Ce-3.5Si aluminium alloy and 8.0% for Al-5Mg-8Ce-3.5Si aluminium alloy, with a speed of tool rotation of 1000 RPM and a welding speed of 20 mm/min respectively.   The increase in the UTS is because of the formation of fine grains and even distribution of AlSiMg particles (El-Rayes and El-Danaf 2012; Yang et al. 2014).

Table 4.18 Tensile properties in the direction of weld of aluminium alloy joints, friction stir welded using TPP tool

Process parameters		Triangular profile pin tool (TPP)					
		Al-10Mg-8Ce-3.5Si			Al-5Mg-8Ce-3.5Si		
Speed of tool rotation (RPM)	Speed od welding (mm/min)	Ultimate Tensile stress (UTS) (N/mm^2)	Elongation (%)	Increase in strength (%)	Ultimate Tensile stress (UTS) (N/mm2)	Elongation (%)	Increase in strength (%)
1000	10	121 ± 3	8.9 ± 1	19.8	98 ± 2	8.7 ± 2	14
1000	15	123 ± 4	9 ± 2	20.6	97 ± 2	10.4 ± 1	14.1
1000	20	131 ± 2	9.5 ± 2	21.3	108 ± 4	9.2 ± 1	18.7

Table 4.19 Tensile properties in the direction of weld of aluminium alloy joints, friction stir welded using SPP tool

Process parameters		Triangular profile pin tool (SPP)					
		Al-10Mg-8Ce-3.5Si			Al-5Mg-8Ce-3.5Si		
Speed of tool rotation (RPM)	Speed od welding (mm/min)	Ultimate Tensile stress (UTS) (N/mm^2)	Elongation (%)	Increase in strength (%)	Ultimate Tensile stress (UTS) (N/mm2)	Elongation (%)	Increase in strength (%)
1000	10	87 ± 4	9.9 ± 2	13	71 ± 3	9 ± 2	10.9
1000	15	101 ± 2	9.8 ± 1	14.8	83 ± 4	8.7 ± 1	12.2
1000	20	114 ± 3	8.8 ± 1	15.2	95 ± 2	9.6 ± 2	13.1

Table 4.20 Tensile properties in the direction of weld of aluminium alloy joints, friction stir welded using CPP tool

Process parameters		Triangular profile pin tool (CPP)					
		Al-10Mg-8Ce-3.5Si			Al-5Mg-8Ce-3.5Si		
Speed of tool rotation (RPM)	Speed od welding (mm/min)	Ultimate Tensile stress (UTS) (N/mm^2)	Elongation (%)	Increase in strength (%)	Ultimate Tensile stress (UTS) (N/mm2)	Elongation (%)	Increase in strength (%)
1000	10	74 ± 4	8.7 ± 1	8.8	60 ± 4	9.3 ± 2	7.1
1000	15	85 ± 3	8.8 ± 2	9.0	69 ± 3	9.2 ± 2	7.8
1000	20	98 ± 2	10 ± 2	10.1	81 ± 2	9.2 ± 2	8.0

4.7   REPEATABILITY TEST FOR PROCESS PARAMETERS

The repeatability test for mechanical properties of friction stir welded aluminium alloys is carried out and the results are tabulated in the Table 4.21. A small variation between average values of the tested components and repeated test component has been observed. The speed of tool rotation is held constant at 1000 RPM for all the friction stir welded joints.

Table 4.21 Repeatability tests of aluminium alloy joints, friction Stir welded using TPP, SPP and CPP tool

Sl. No.	Aluminium Alloy	Tool pin shape	Welding speed (mm / min)	Vickers Hardness Values (VHN)		Ultimate Tensile stress – UTS (N/mm^2)	
				Average	Repeatability	Average	Repeatability
1	Al-10Mg-8Ce-3.5Si	TPP	10	167 ± 3	166	101 ± 4	99
2		TPP	15	168 ± 4	167	102 ± 4	101
3			20	159 ± 1	157	108 ± 4	110
4		SPP	10	151 ± 4	152	77 ± 2	81
5		SPP	15	146 ± 3	148	88 ± 3	90
6			20	151 ± 3	149	99 ± 3	101
7		CPP	10	132 ± 1	130	68 ± 4	70
8		CPP	15	127 ± 2	125	78 ± 3	76
9			20	121 ± 2	121	89 ± 3	93
10	Al-5Mg-8Ce-3.5Si	TPP	10	132 ± 2	131	86 ± 3	83
11		TPP	15	143 ± 3	141	85 ± 3	87
12			20	129 ± 1	131	91 ± 4	94
13		SPP	10	126 ± 3	128	64 ± 3	61
14		SPP	15	136 ± 4	135	74 ± 4	76
15			20	123 ± 1	124	84 ± 4	82
16		CPP	10	119 ± 1	120	56 ± 4	54
17		CPP	15	129 ± 4	128	64 ± 4	62
18			20	125 ± 1	123	75 ± 2	74

4.8 FRACTURE ANALYSIS OF TENSILE TEST SPECIMENS OF FRICTION STIR WELDED ALUMINIUM ALLOYS

4.8.1 Analysis of fractured tensile test specimens of Al-10Mg-8Ce-3.5Si aluminium alloy joints friction Stir Welded using TPP, SPP, and CPP tools

The fracture surfaces of tensile test specimens are helpful in interpreting the microstructural effects on the ductility / brittleness and fracture properties of the aluminium alloy. It is well known that fracture in aluminium alloys is controlled by three main mechanisms: (1) Cracking of the hard particles, (2) Interfacial de-cohesion at the particle and metal matrix interface resulting in the nucleation of voids, (3) Growth and coalescence of voids in the aluminium matrix (Johari et al. 1973; Kubit et al. 2018a; Schwerdt et al. 2010). Figure 4.51 represents the macro images of fractured tensile test specimens of friction stir welded aluminium alloy joints fabricated with speeds of welding of 10, 15 and 20 mm/min, respectively, at a constant rotational speed of 1000 RPM using triangular profiled pin tool. The macroscopic examination of the fractured surface has revealed ductile failure (Li et al. 2014a; Palanivel et al. 2014; Sajadifar et al. 2019). All the samples, irrespective of process parameters and tool profile, were broken at HAZ, where minimum hardness was found during hardness measurement, in a direction normal to the tensile stress axis. As reported in section 4.4.2, the tensile specimens in the transverse orientation cover four different microstructural regions, i.e., BM, HAZ, TMAZ, and NZ. The observed ductility is an average strain over the gage length including various zones. The different zones have different resistances to deformation due to differences in grain size and precipitate size and distribution. The HAZ has the lowest strength due to significantly coarsened precipitates. It should also be noted that the HAZ region is subjected to thermal cycle which leads to grain growth. However, the HAZ was not subjected to plastic deformation. Thus, the HAZ recorded lowest hardness and was the weakest section. Thus, during tension, strain occurs mainly in the HAZ. The low-strength HAZ had locally elongated to high levels of strain, eventually resulting in necking and fracture, whereas the nugget zone experiences lesser strain. Therefore, fracture always occurred in the HAZ, resulting in a low strength and ductility along transverse orientation of the weld (Jannet et al. 2014; Mosleh et al. 2016).
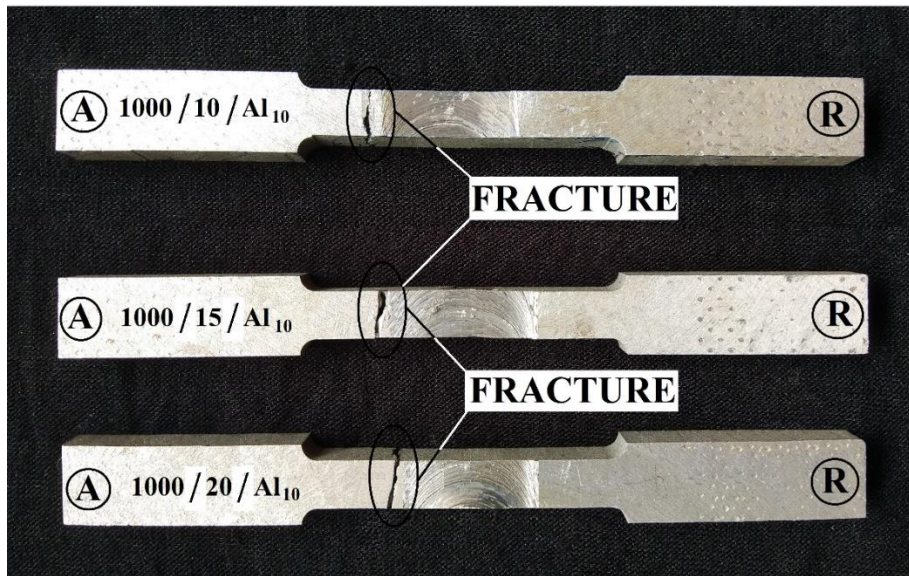
Figure 4.51 Macro image of fractured tensile test specimen of friction stir welded Al-10Mg-8Ce-3.5Si aluminium alloy joint

Figure 4.52 (a-c) shows the fractured surface of aluminium alloy joints, friction stir welded using TPP, SPP, and CPP tools, respectively. Figure 4.52 (a) shows the fractured surface of aluminium alloy weld connection friction stir welded at speed of tool rotation of 1000 RPM and welding speed of 20 mm/min using TPP tool. The microscopic examination of the fractured surface, at high magnification, revealed ductile mechanisms (Li et al. 2014a; Palanivel et al. 2014; Sajadifar et al. 2019). It is characterized by large and shallow dimples with tear edges. There were no cracked particles in the fractured surface. Cracking of the particles is more in the region where agglomeration or clusters are present due to high stress. De-cohesion of metal matrix and hard particles occurs due to strain difference between the hard particle and the matrix metal. Figure 4.52 (b) shows the fractured   surface of aluminium alloy weld connection friction stir welded at a speed of tool rotation of 1000 RPM and a welding speed of 20 mm/min using SPP tool. The dimples tear edges and cracks have been observed on the fractured surface. Figure 4.52 (c) shows SEM image of fracture surface of the aluminium alloy weld connection friction stir welded at a speed of tool rotation of 1000 RPM and a welding speed of 20 mm/min using SPP tool. The welded aluminium alloys are fractured near HAZ. There were dimples, tear edges and cracks on the fractured surface.

216
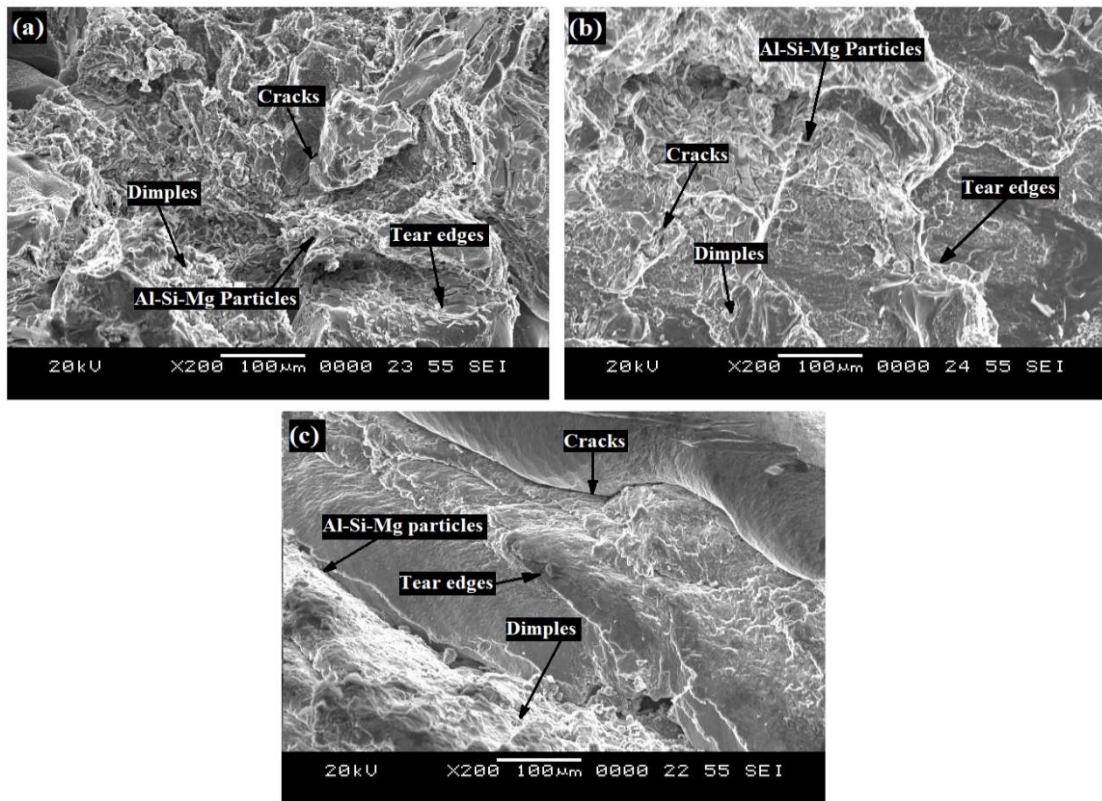
Figure 4.52 SEM images of tensile fracture surface of Al-10Mg-8Ce-3.5Si aluminium alloy joints friction stir welded at a speed of tool rotation of 1000 RPM and a welding speed of 20 mm/min using; (a) Triangular profile pin (TPP) tool, (b) Square profile pin (SPP) tool and (c) Circular / Round profile pin (CPP) tool.

4.8.2 Analysis of fractured tensile test specimens of Al-5Mg-8Ce-3.5Si aluminium alloy joints friction Stir Welded using TPP, SPP, and CPP tools

Figure 4.53 (a-c) present the fracture surface of Al-5Mg-8Ce-3.5Si aluminium alloy weld connection friction stir welded using TPP, SPP and CPP tools, respectively. The macroscopic examination of the fracture surface has revealed ductile failure. All the samples, irrespective of process parameters and tool profile, were broken at HAZ where minimum hardness was found during hardness measurement, in a direction normal to the tensile stress axis. However, microscopic examination of the fractured surfaces, at high magnification, revealed features similar to locally ductile and brittle mechanisms (Li et al. 2014a; Palanivel et al. 2014; Sajadifar et al. 2019). It is characterized by large and deep dimples with tearing edges.
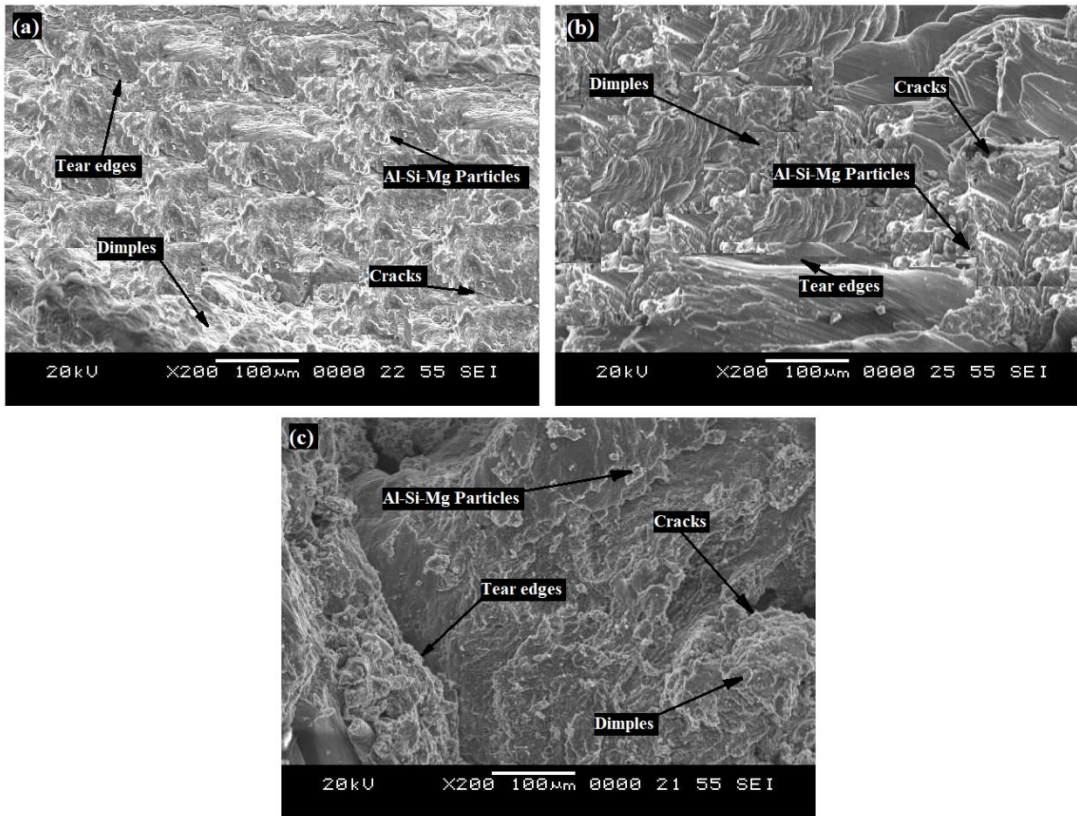
Figure 4.53 SEM images of tensile fracture surface of Al-5Mg-8Ce-3.5Si aluminium alloy joints friction stir welded at a speed of tool rotation of 1000 RPM and a welding speed of 20 mm/min using; a) Triangular profile pin (TPP) tool, b) Square profile pin (SPP) tool and c) Circular / Round profile pin (CPP) tool.

4.8.3 Analysis of fractured tensile test specimens of Al-10Mg-8Ce-3.5Si aluminium alloy joints friction Stir Welded using TPP, SPP, and CPP tools and tensile tested in the direction of weld.

The macroscopic view of the fractured tensile test specimen of the friction stir welded Al-10Mg-8Ce-3.5Si aluminium alloy weld connection is shown in Figure 4.54. Tensile testing of the specimen was carried out along the direction of weld. It was observed that the crack propagates in a direction of 45° angle to the tensile test axis. This is the typical feature of the shear fracture pattern. Figure 4.55 (a - f) reveal the tensile facture surface of friction stir welded Al-10Mg-8Ce-3.5Si aluminium alloy joint, at a various speeds of welding of 10, 15 and 20 mm/min with the speed of tool rotation being held constant at 1000 RPM and tensile tested along the direction of weld. Welding is carried out using

TPP tool. In all the cases, there was breakage of hard particles and breakdown of metal matrix. Hence, two distinct failure mechanisms are acting in combination. Firstly, there is a cracking of hard particle inside the large dimple produced by plastic deformation of the surrounded matrix. The cracking of AlSiMg hard particles is due to the stress transferred to AlSiMg particles during the test, which results in interfacial shearing. Since the value of the stress is high, the cracks nucleated in particulates grow and proceed through the matrix and thus connect with the adjacent particulates (Li et al. 2014a; Mishra et al. 2007). Secondly, the fracture surface is dominated by small and shallow dimples with thinner tearing edges. Fine dimples were observed due to finer grains in the weld nugget (Guo et al. 2014; Ji et al. 2017; Xu et al. 2009). Cracked, broken particles and pull-out particles were observed. The mode of failure was ductile in nature. Comparing the facture surfaces of the base material with that of welded aluminium alloy, the latter exhibited fine and equiaxed dimples. Figure 4.55 (a - c), presents the fracture surface characteristics of tensile specimens welded at speeds of welding of 10 mm/min, 15 mm/min and 20 mm/min, respectively, with constant speed of tool rotation of 1000 RPM. The presence of dimples in the fracture surface shows evidence of ductile fracture. A network of fine dimples is observed on the fracture surface of the friction stir welded aluminium because of the existence of fine equiaxed grains in the NZ. Figure 4.55 (d) shows the dimples, pull-out, decohesion and cracked AlSiMg particles. Figure 4.55 (e) represent the AlSiMg particle which is confirmed by EDAX. The peaks present in Figure 4.55 (f) correspond to Si and Mg.
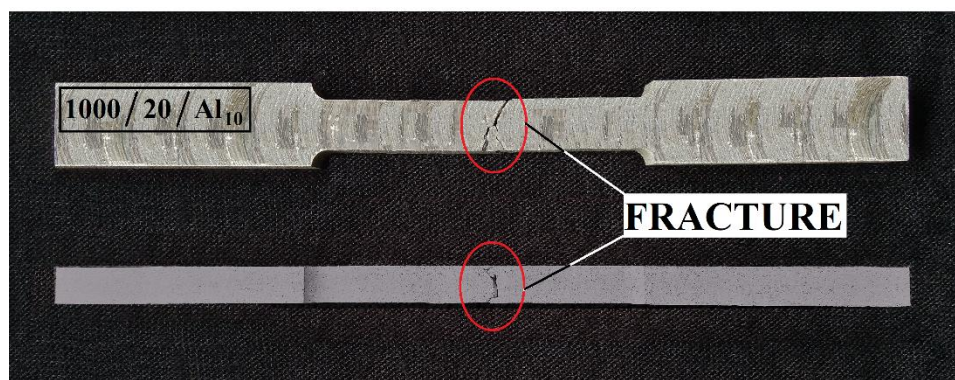
Figure 4.54 Macro image of fractured tensile test specimen of aluminium alloy plate with friction stir welded joint, and tensile tested in the direction of weld.

Figure 4.56 (a - d) depict the tensile fracture surface of Al-10Mg-8Ce-3.5Si aluminium alloy weld connection friction stir welded using SPP tool at various speeds of welding of 10, 15 and 20 mm/min with the speed of tool rotation being held constant at 1000 RPM and tensile tested along the direction of weld. The fracture surface of the tensile specimen of the weld connection fabricated using SPP tool was identical to the fracture surface of the tensile specimen of the weld connection fabricated with TPP tool. The mode of fracture was ductile in nature. Fine dimples were observed with small particles existing at the bottom of these dimples. Broken particles were also detected at the bottom of the dimple. Figure 4.56 (a - c) presents the SEM image of fracture surface of failed tensile specimens of the weld connection friction stir welded at speeds of welding of 10, 15 and 20 mm/min, respectively, with a speed of tool rotation being held constant at 1000 RPM. A network of fine dimples is observed on the fracture surface of the friction stir welded aluminium alloy, because of the presence of equiaxed fine grains in the NZ. Figure 4.56 (d) presents the magnified view of fracture surface showing the dimples, pullout, decohesion and cracked AlSiMg particles.
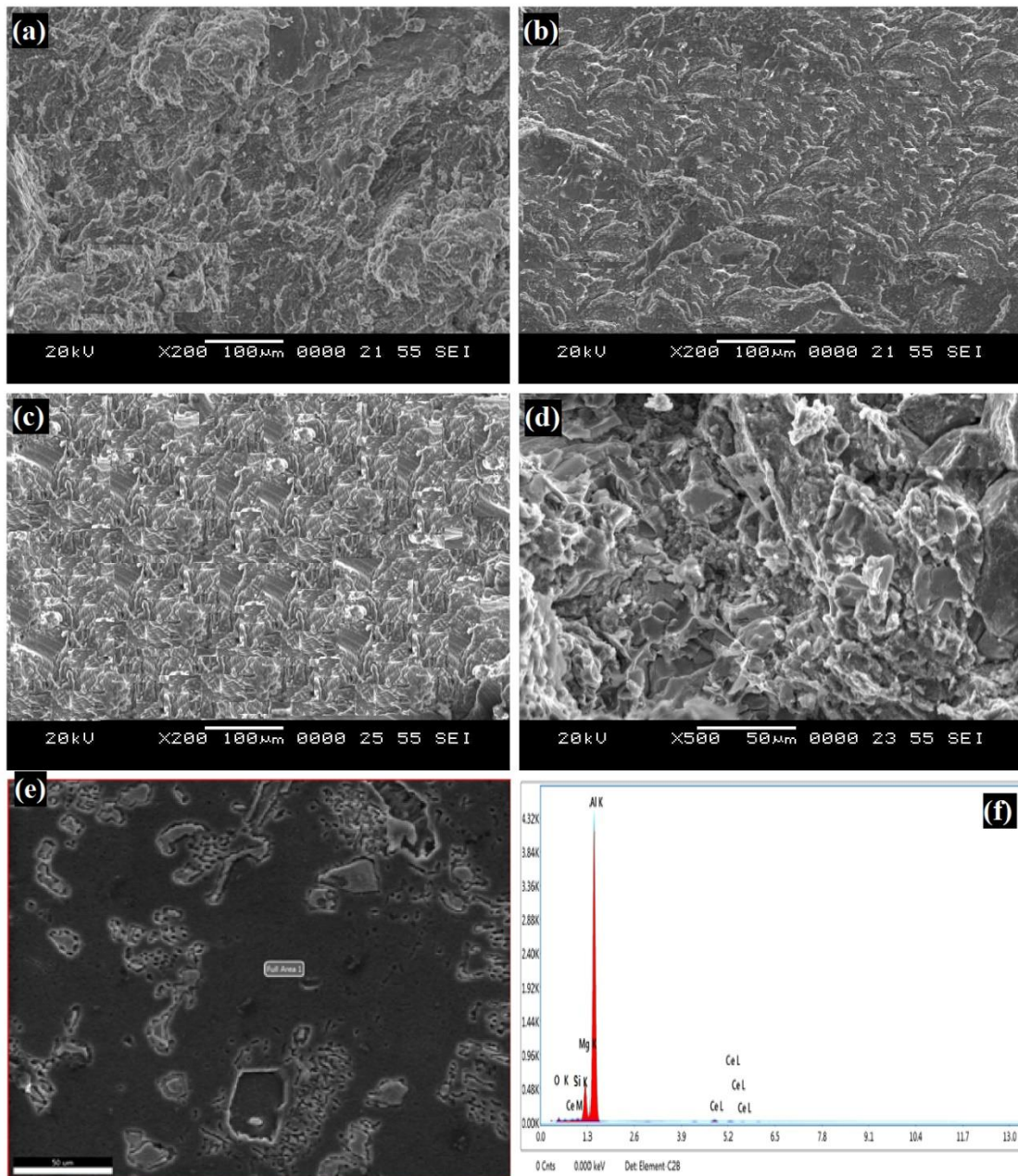
Figure 4.55 SEM images of tensile fracture surface (tested in the direction of weld) of Al-10Mg-8Ce-3.5Si aluminium alloy joints friction stir welded with TPP tool, at (a) Speed of tool rotation of 1000 RPM and welding speed of 10 mm/min, (b) Speed of tool rotation of l000 RPM and welding speed of 15 mm/min, (c) Speed of tool rotation of l000 RPM and welding speed of 20 mm/min, (d) Higher magnification image showing the dimples, pullout, decohesion and cracked AlSiMg particles, (e) Spot EDAX image and (f) EDX spectrum showing the presence of Si. Mg and Ce peaks.
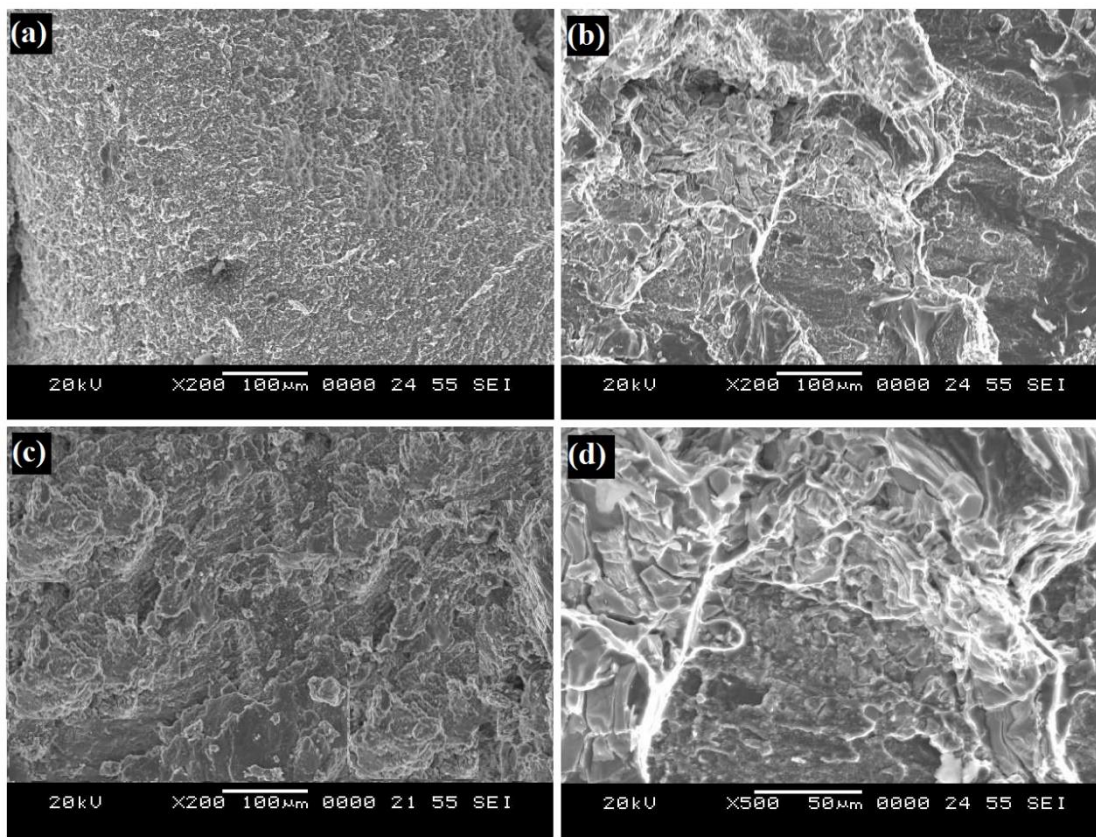
Figure 4.56 SEM images of tensile fracture surface (tested in the direction of weld) of Al-10Mg-8Ce-3.5Si aluminium alloy joints friction stir welded using SPP tool, at (a) Speed of tool rotation of 1000 RPM and welding speed of 10 mm/min, (b) Speed of tool rotation of l000 RPM and welding speed of 15 mm/min, (c) Speed of tool rotation of l000 pm and welding speed of 20 mm/min, (d) Higher magnification image showing the dimples, pullout, decohesion and cracked AlSiMg particles.

Figure 4.57 (a - d) depicts the SEM images of tensile fracture surface of friction stir welded Al-10Mg-8Ce-3.5Si aluminium alloy joint, produced using CPP tool at various speeds of welding of 10, 15 and 20 mm/min with the speed of tool rotation being held constant at 1000 RPM and tensile tested along the direction of weld. The analysis of the tensile fracture surface showed the presence of tear ridges, large dimples, large voids linked with hard particle and matrix metal decohesion, and occurrence of small dimples inside the large dimples because of the ductile failure of the matrix. Figure 4.57 (a - c) presents the SEM image of fracture surface of failed tensile specimens of the weld connection friction stir welded at speeds of welding of 10, 15 and 20 mm/min

222

respectively, with the speed of tool rotation being held constant at 1000 RPM. A network of fine dimples is observed on the fracture surface of the friction stir welded aluminium alloy because of the presence of equiaxed fine grains in the NZ. Figure 4.57 (d) presents the magnified view of fracture surface showing the dimples, pullout, decohesion and cracked AlSiMg particles. The presence of deeper dimples indicates maximum plastic deformation.
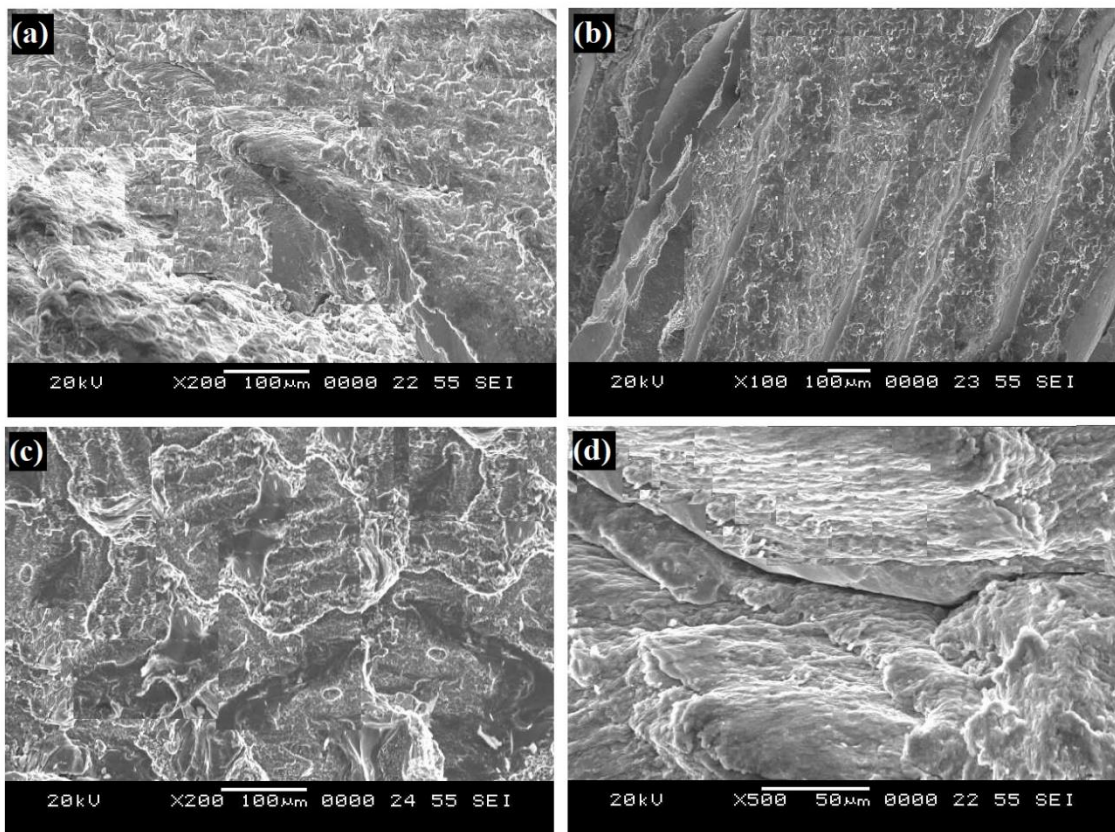
Figure 4.57 SEM images of tensile fracture surface (tested in the direction of weld) of Al-10Mg-8Ce-3.5Si aluminium alloy joints friction stir welded with CPP tool, at (a) Speed of tool rotation of 1000 RPM and welding speed of 10 mm/min, (b) Speed of tool rotation of l000 RPM and welding speed of 15 mm/min, (c) Speed of tool rotation of l000 RPM and welding speed of 20 mm/min, (d) Higher magnification image showing the dimples, pullout, decohesion and cracked AlSiMg particles.

4.8.4 Analysis of fractured tensile test specimens of Al-5Mg-8Ce-3.5Si aluminium alloy joints friction Stir Welded using TPP, SPP, and CPP tools and tensile tested in the direction of weld.

The fracture surface of Al-5Mg-8Ce-3.5Si aluminium alloy friction stir welded joints is shown in Figure 4.58 (a - d). The joints were fabricated with TPP tool at a constant speed of tool rotation of 1000 RPM and speeds of welding of 10, 15 and 20 mm/min and tensile tested in the direction of weld. Fracture surfaces of all the joints exhibit a mixed fracture mechanism (Li et al. 2014a; Palanivel et al. 2014; Sajadifar et al. 2019), brittle fracture of the hard particles and ductile tearing of the metal matrix. All fracture surfaces necessarily comprise of dimples. The fracture surface of the joints shows fine dimples than the base material. Figure 4.58 (a-c), presents the fracture surface characteristic of tensile specimens welded at speeds of welding of 50 mm/min, 63 mm/min and 80 mm/min, respectively, with a constant speed of tool rotation of 1000 RPM. The presence of dimples in the fracture surface shows evidence of dimple fracture. Figure 4.58 (d) shows the higher magnification image showing the dimples and AlSiMg particles.

Figure 4.59 (a - d) shows the tensile fracture surface of Al-5Mg-8Ce-3.5Si aluminium alloy weld connection friction stir welded with SPP tool at various speeds of welding of 10, 15 and 20 mm/min with the speed of tool rotation being held constant at 1000 RPM. The mode of fracture was ductile in nature. Fine dimples were observed with small particles prevailing at the bottom of these dimples. Broken particles were also noticed at the bottom of the dimple. Figure 4.59 (a - c) presents the SEM images of fractured surface of failed tensile specimens of the weld connection friction stir welded at speeds of welding of 10, 15 and 20 mm/min respectively, with the speed of tool rotation being held constant at 1000 RPM. Figure 4.59 (d) presents the magnified view of fracture surface showing the dimples.

Figure 4.60 (a - d) illustrates the SEM image of tensile fracture surface of Al-5Mg-8Ce-3.5Si aluminium alloy joint, friction stir welded, at various speeds of welding of 10, 15 and 20 mm/min with the rotational speed being held constant at 1000 RPM, using CPP tool. The analysis of the tensile fracture reveals the presence of tear ridges, large dimples, large voids associated with particle- matrix decohesion, and occurrence of

small dimples inside the large dimples because of the ductile-brittle failure of the matrix. Figure 4.60 (a - c) presents the SEM image of the fractured surface of failed tensile specimens of the weld connection FS welded at speeds of welding of 10, 15 and 20 mm/min, respectively, with the rotational speed being held constant at 1000 RPM. A network of fine dimples is observed on the fracture surface of the friction stir welded aluminium alloy because of the presence of equiaxed fine grains in the NZ. Figure 4.60 (d) presents the magnified view of fracture surface showing the dimples, decohesion and cracked AlSiMg hard particles. The deeper dimples indicate maximum plastic deformation.
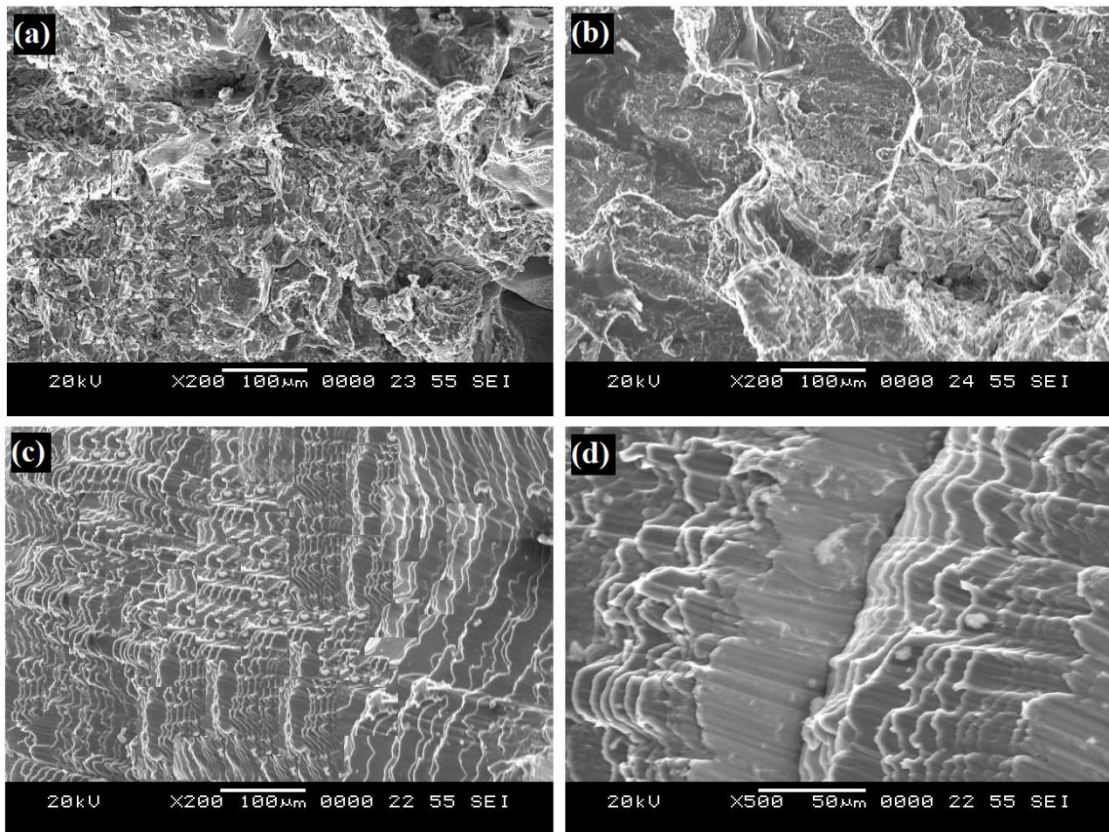
Figure 4.58 SEM images of tensile fracture surface (tested in the direction of weld) of Al-5Mg-8Ce-3.5Si aluminium alloy joints friction stir welded with TPP tool, at (a) Speed of tool rotation of 1000 RPM and welding speed of 10 mm/min, (b) Speed of tool rotation of l000 RPM and welding speed of 15 mm/min, (c) Speed of tool rotation of l000 RPM and welding speed of 20 mm/min, (d) Higher magnification image showing the dimples, pullout, decohesion and cracked AlSiMg particles.
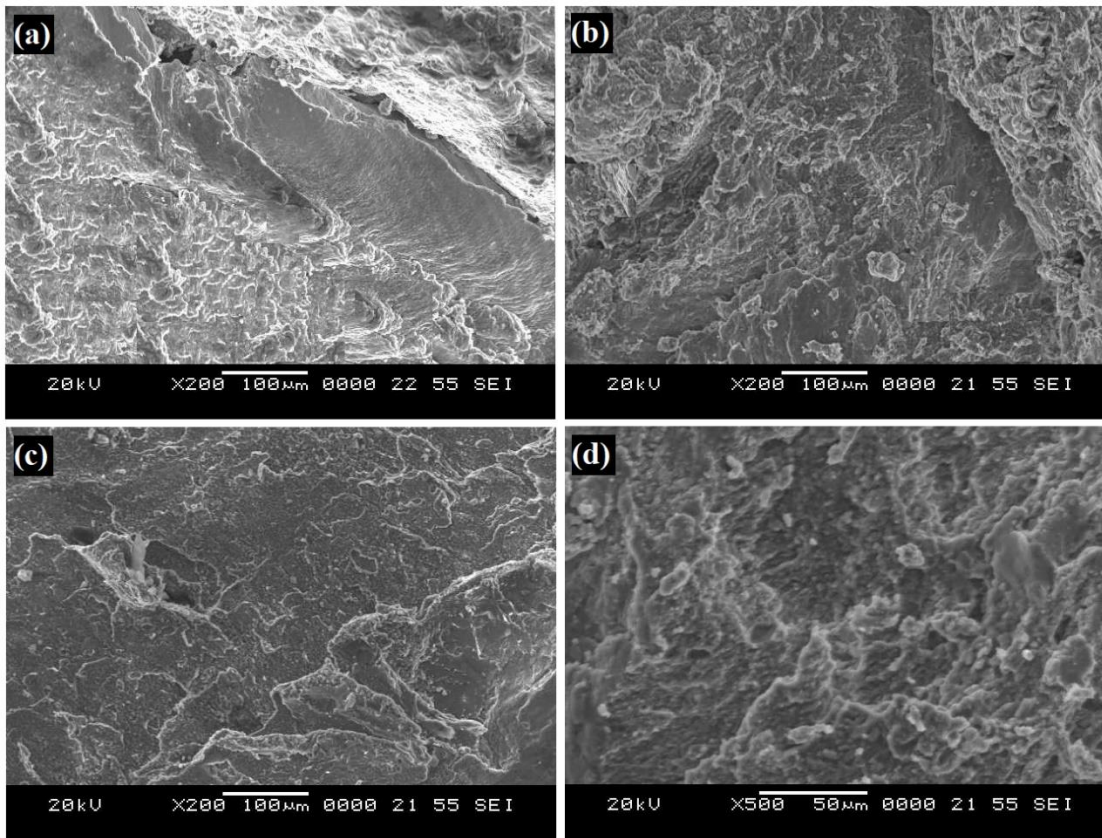
Figure 4.59 SEM images of tensile fracture surface (tested in the direction of weld) of Al-5Mg-8Ce-3.5Si aluminium alloy joints friction stir welded with SPP tool, at (a) Speed of tool rotation of 1000 RPM and welding speed of 10 mm/min, (b) Speed of tool rotation of l000 RPM and welding speed of 15 mm/min, (c) Speed of tool rotation of l000 RPM and welding speed of 20 mm/min, (d) Higher magnification image showing the dimples, pullout, decohesion and cracked AlSiMg particles.
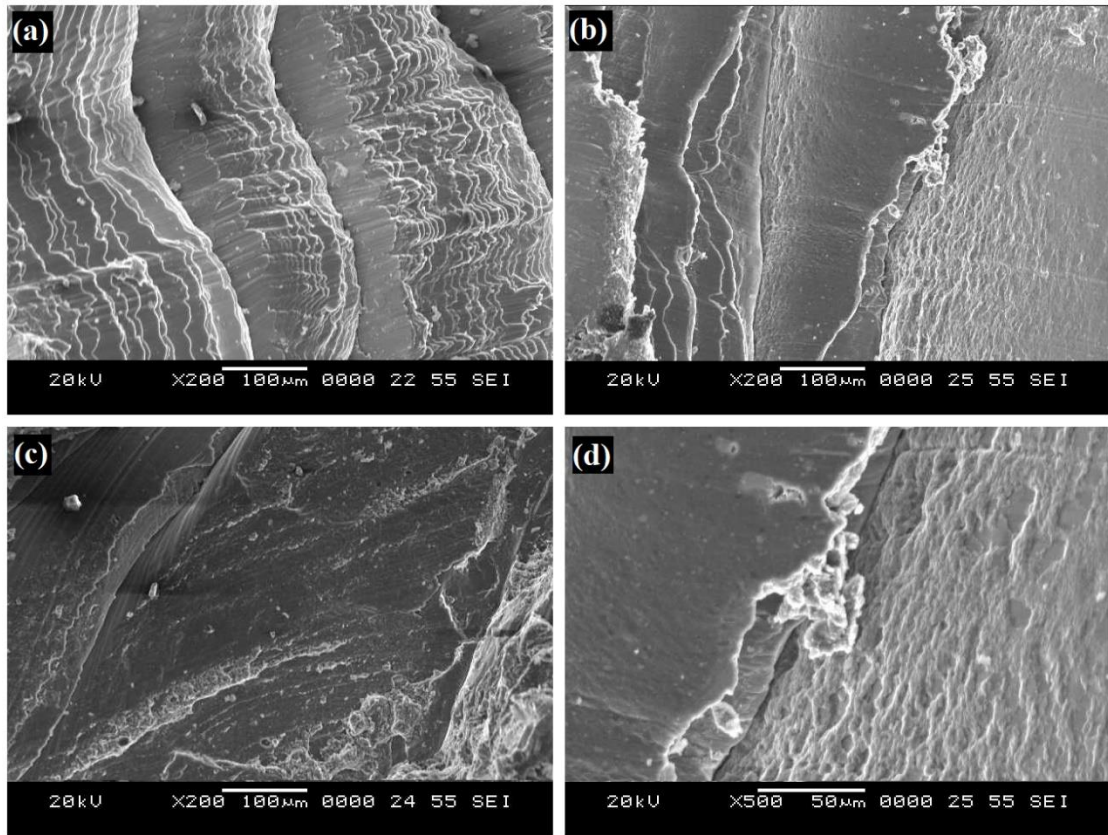
Figure 4.60 SEM images of tensile fracture surface (tested in the direction of weld) of Al-5Mg-8Ce-3.5Si aluminium alloy joints friction stir welded with CPP tool, at (a) Speed of tool rotation of 1000 RPM and welding speed of 10 mm/min, (b) Speed of tool rotation of l000 RPM and welding speed of 15 mm/min, (c) Speed of tool rotation of l000 RPM and welding speed of 20 mm/min, (d) Higher magnification image showing the dimples, pullout, decohesion and cracked AlSiMg particles.

4.9   ANALYSIS OF HARDNESS AND GRAIN SIZE OF FRICTION STIR WELDED ALUMINIUM ALLOYS

Figure 4.61 illustrates the relationship between the average grain size and hardness measured at the center of NZ of Al-10Mg-8Ce-3.5Si aluminium alloy friction stir welded using TPP tool, at different process parameters. From the Figure 4.61, it is clear that process parameters, like speed of tool rotation and welding speed affect the grain size and hardness of the joint of aluminium alloy prepared using friction stir welded. When the speed of tool rotation is high (1200 RPM) and the welding speed is low (10

mm/min), coarse grains were formed at NZ. This effect results in lower hardness at NZ. Similarly, when both the speed of tool rotation (800 RPM) and welding speed are low, the hardness is minimum. This is because of the annealing (softening) effect (Bisadi et al. 2013; Palanivel et al. 2012; Xie et al. 2008). The minimum grain size and maximum hardness are attained for a speed of tool rotation of 1000 RPM and a welding speed of 20 mm/min. The improvement in fine grain strengthening effect which overrides the annealing effect leads to an increase in the hardness at nugget zone (Xie et al. 2007; Zhou et al. 2016). In all the cases, as the grain size decreases the hardness increases. Also, it can be observed that the maximum value of hardness measuring 167.7 VHN corresponds to joints fabricated with TPP tool.
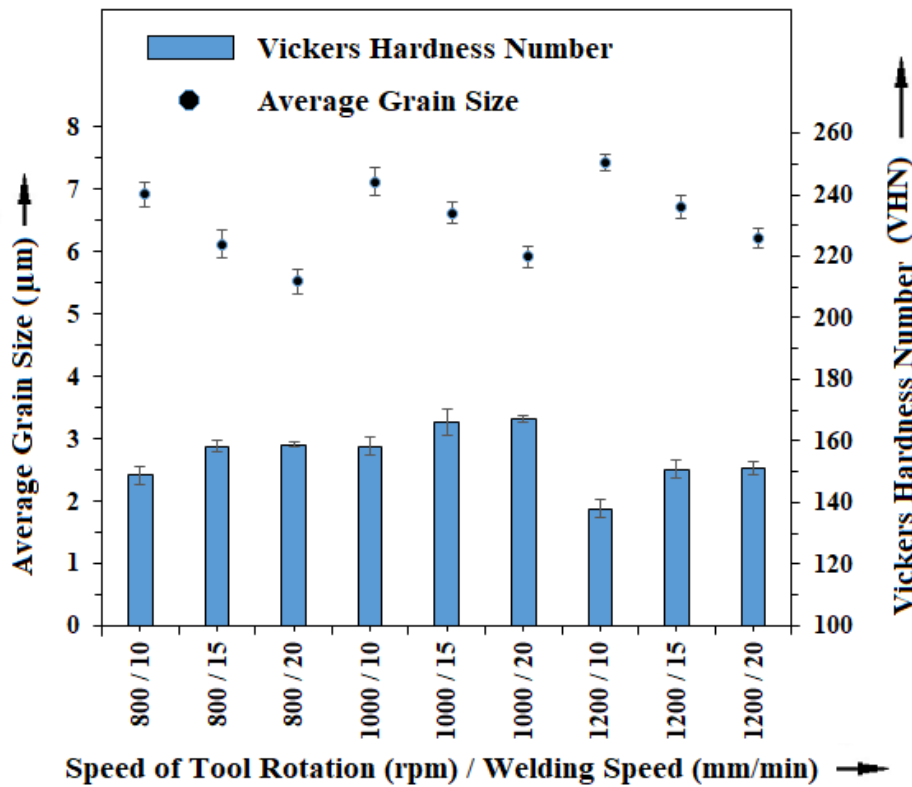
Figure 4.61 Comparison of average grain size with hardness at the center of NZ of the Al-10Mg-8Ce-3.5Si aluminium alloy friction stir welded using TPP tool

The correlation between the average grain size and hardness at the NZ of Al-10Mg-8Ce-3.5Si aluminium alloy friction stir welded using SPP tool has been shown

in Figure 4.62. It is clear from the Figure 4.62 that, the grain size and hardness at the NZ is dependent on the process parameters. As the speed of tool rotation rises from 800 RPM to 1000 RPM the grain size decreases with increase in hardness. Further increase in speed of tool rotation from l 000 RPM to 1200 RPM, the grain size increases with decrease in the hardness. The minimum hardness with coarse grained structure is attained at a rotational speed of 1200 RPM and a welding speed of 10 mm/min. Maximum hardness and fine grain sizes were attained at a speed of tool rotation of 1000 RPM and a welding speed of 20 mm/min. The reason behind this was described in the previous section. The hardness observed in NZ of the aluminium alloy welded using SPP tool is less than that of the hardness observed at NZ of aluminium alloy being welded using TPP tool.
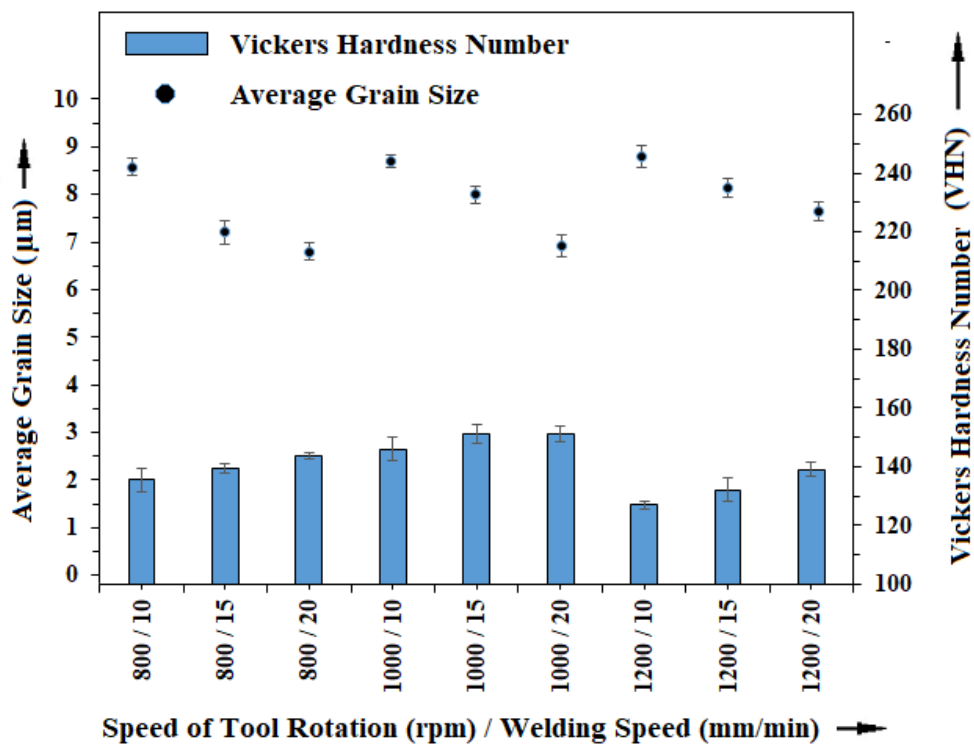
Figure 4.62 Comparison of average grain size with hardness at the center of NZ of the Al-10Mg-8Ce-3.5Si aluminium alloy friction stir welded using SPP tool.

Figure 4.63 shows the plot depicting the variation of average grain size with hardness of friction stir welded Al-10Mg-8Ce-3.5Si aluminium alloy samples using CPP tool.

The plot depicting the variation of average grain size with hardness at NZ for different process parameters are shown in Figure 4.63 for comparison. A rise in hardness was observed as the welding speed increases from 10 to 20 mm/min for a constant speed of tool rotation of 800 RPM, along with a fall in the average grain size. When comparing various speeds of tool rotation with constant welding speed (experiment no 1, 4 and 7) the hardness was found to increase with the increase in speed of tool rotation. A decrease in the average grain size was observed when the speed of tool rotation increases from 800 RPM to 1000 RPM. With further rise in the welding speed, the hardness decreases. The temperature developed at a higher speed of tool rotation of 1200 RPM is more than that at 1000 RPM and consequently the material softens. This resulted in coarse grain structure. Hence, the hardness of the NZ was found to decrease. The fine grain with highest hardness was obtained for a speed of tool rotation of 1000 RPM and a welding speed of 20 mm/min.
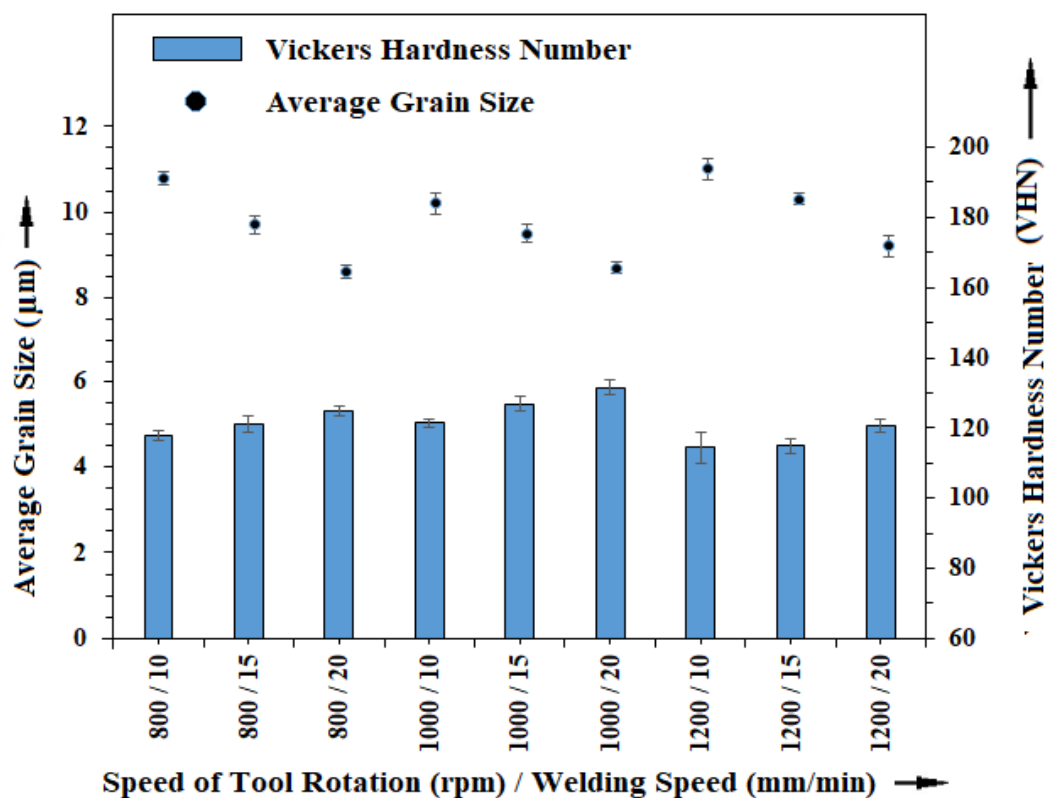
Figure 4.63 Comparison of average grain size with hardness at the center of NZ of the Al-10Mg-8Ce-3.5Si aluminium alloy friction stir welded using CPP tool.

Plot in Figure 4.64 (a - c) shows the variation of average grain size and hardness at NZ of Al-5Mg-8Ce-3.5Si aluminium alloy, friction stir welded with various speeds of tool rotation and speeds of welding, with TPP, SPP and CPP tools respectively. It can be seen from the plots that both, the grain sizes, and hardness have inverse relationship with each other. The hardness of Al-5Mg-8Ce-3.5Si aluminium alloy at NZ is found to have lower hardness in comparison to the hardness of the Al-10Mg-8Ce-3.5Si aluminium alloy at the NZ. The improvement in hardness is due to the increase in the weight percentage of hard particles which enhances the pinning effect (El-Rayes and El-Danaf 2012; Hassan et al. 2003a; Ma et al. 2018; Starke and Staley 2010). In all the plots, fine grains with maximum hardness correspond to a speed of tool rotation of 1000 RPM and a welding speed of 20 mm/min. This is quite anticipated because the grain refinement influences the hardness. In addition to this, high strength of the AlSiMg hard particles significantly increases the hardness at NZ. The coarse grain sizes with minimum hardness were observed for a speed of tool rotation of 1200 RPM and a welding speed of 10 mm/min. High rotational speed induces higher frictional heat with turbulence in the material flow which results in increase in the heat generation. This causes grain growth (Dong et al. 2013; Zhang et al. 2011).
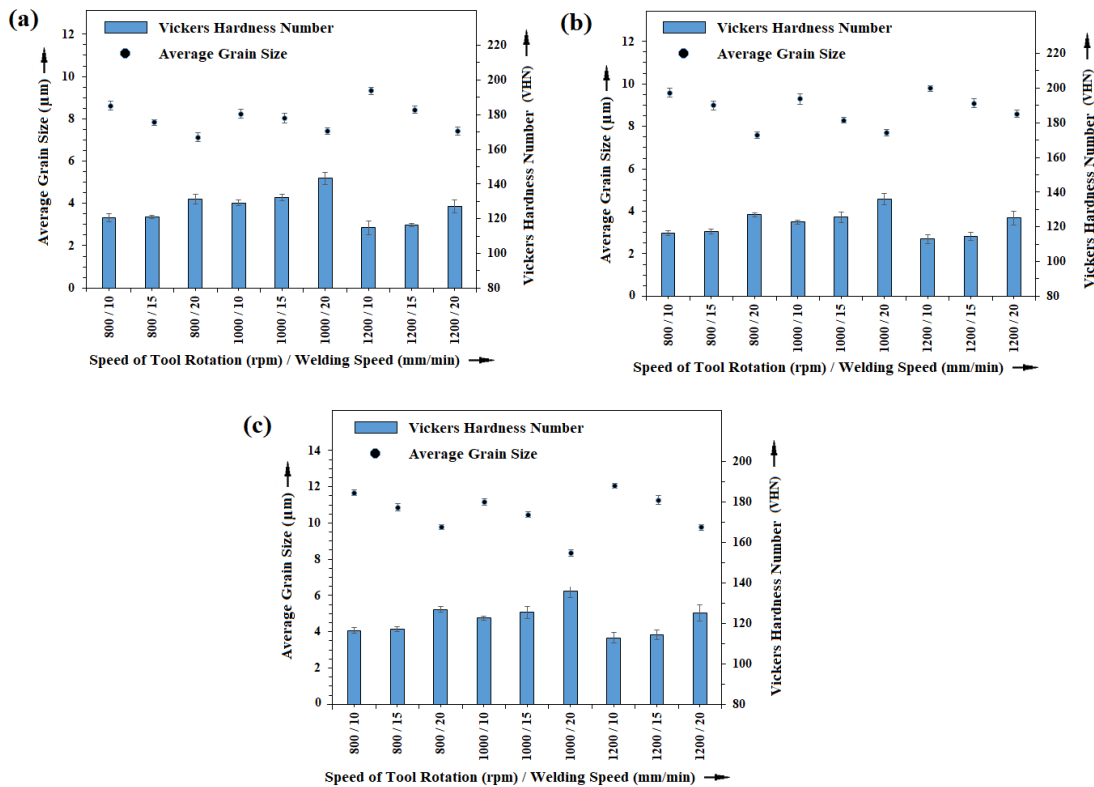
Figure 4.64 Comparison of average grain size with hardness at the center of NZ of the Al-5Mg-8Ce-3.5Si aluminium alloy friction stir welded using (a) TPP tool, (b) SPP tool and (c) CPP tool.

4.10 CORRELATION BETWEEN ULTIMATE TENSILE STRESS AND NUGGET ZONE HARDNESS OF FRICTION STIR WELDED ALUMINIUM ALLOYS

Figure 4.65 illustrates the variation between the UTS and hardness of Al-10Mg-8Ce-3.5Si aluminium alloy friction stir welded with various speeds of tool rotation and speeds of welding using TPP tool. It is observed from Figure 4.65 that hardness and UTS have direct relationship. The poor UTS and hardness observed at a speed of tool rotation of 800 and 1000 RPM when welded with a constant welding speed of 10 mm/min. The welding speed is responsible for quantity of heat supplied to the material, while the speed of tool rotation is responsible for the generation of heat. If the generation of heat is less, then the heat supplied is also less. Adequate heat is required

232

to form a weld connection possessing good strength. Lower speeds of tool rotation resulting in lesser heat generation cause improper mixing, and therefore reduce the UTS and hardness of the joint. Similarly, lower welding speed results in higher quantity of heat supplied, while slower cooling rate results in grain growth. A speed of tool rotation of 1000 RPM and a welding speed of 20 mm/min has shown the strength of the weld connection quite close to the strength of the base material. A triangular pin profile tool has higher dynamic to static volume ratio of 2.3 compared to square pin profile tool (dynamic to static volume ratio of 1.56) and round pin profile tool (dynamic to static volume ratio of 1.0). Hence it sweeps greater amount of material during welding method (Elangovan and Balasubramanian 2008b; Huang et al. 2018b; Palanivel et al. 2012; Vijayavel and Balasubramanian 2018). Goel et al. (2018) reported that the square faces of the tool pin help in producing pulsating effect which leads to better weld connection strength.
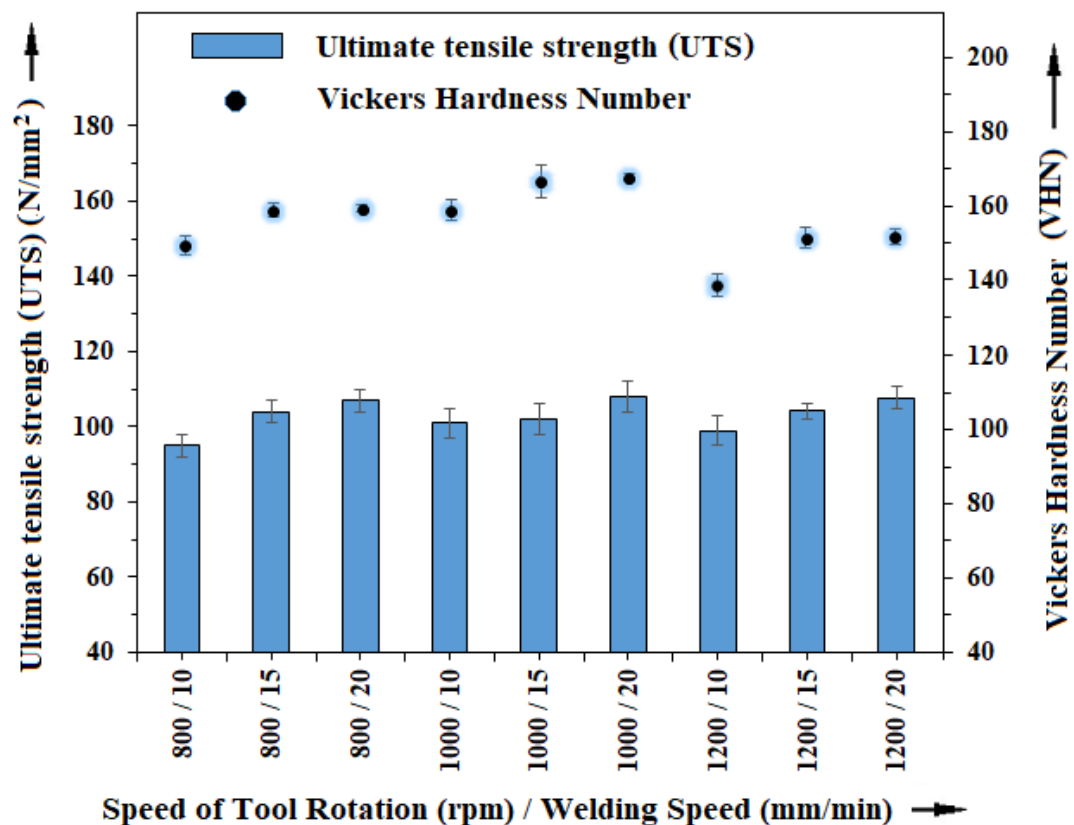
Figure 4.65 Comparison of hardness and UTS of Al-10Mg-8Ce-3.5Si aluminium alloy friction stir welded using TPP tool.

Figure 4.66 shows the effect of speed of tool rotation and welding speed on UTS and Hardness of the Al-10Mg-8Ce-3.5Si aluminium alloy friction stir welded using SPP tool. It is evident from the figure that as the hardness of the aluminium alloy increases, UTS of the aluminium alloy also increases. The hardness and UTS of the aluminium alloy, welded using SPP tool is lower than that of the aluminium alloy welded using TPP tool. Tang et al. (2015) reported that the volume of material being stirred during welding method is directly dependent on the pin diameter. If the pin profile changes then it leads to the change in dynamic to static volume ratio of the material stirred. SPP tool has lower dynamic to static volume ratio than TPP tool (Elangovan and Balasubramanian 2008b; Huang et al. 2018b; Palanivel et al. 2012). Hence, a lower UTS value was observed in the case of SPP tool compared to TPP tool.
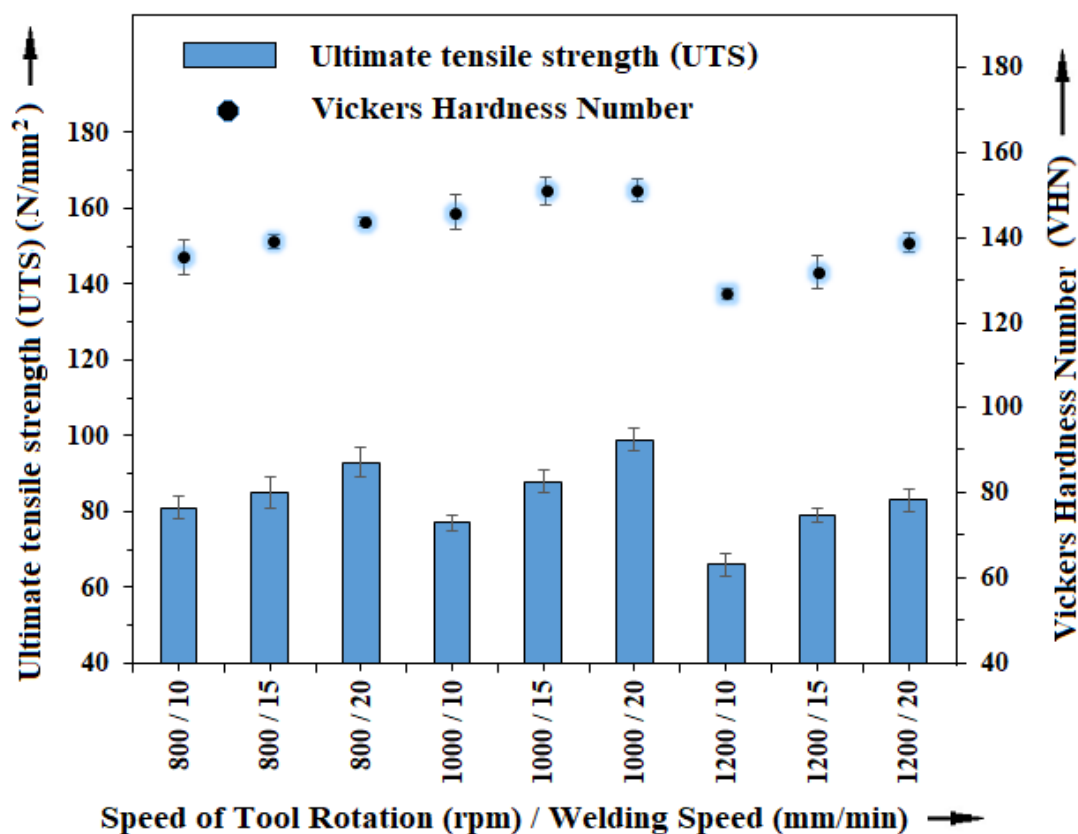
Figure 4.66 Comparison of hardness and UTS of Al-10Mg-8Ce-3.5Si aluminium alloy friction stir welded using SPP tool.

Figure 4.67 indicates the variation in the UTS and hardness of the friction stir welded Al-10Mg-8Ce-3.5Si aluminium alloy, fabricated with various speeds of tool rotation and speeds of welding using CPP tool. The hardness and UTS values of the welded aluminium alloy are seen to be lower than those of the aluminium alloy being welded using TPP and SPP tool. Tang et al. (2015) reported that the volume of material being stirred during welding method is directly dependent on the pin diameter. If the pin profile changes then it leads to the change in dynamic to static volume ratio of the material stirred. It can be noticed from the Figure 4.67 that, greater weld connection strength and higher hardness is found for a speed of tool rotation of 1000 RPM and a welding speed of 20 mm/min. The adequate heat generation and proper stirring of the tool led to increase in the weld connection strength.
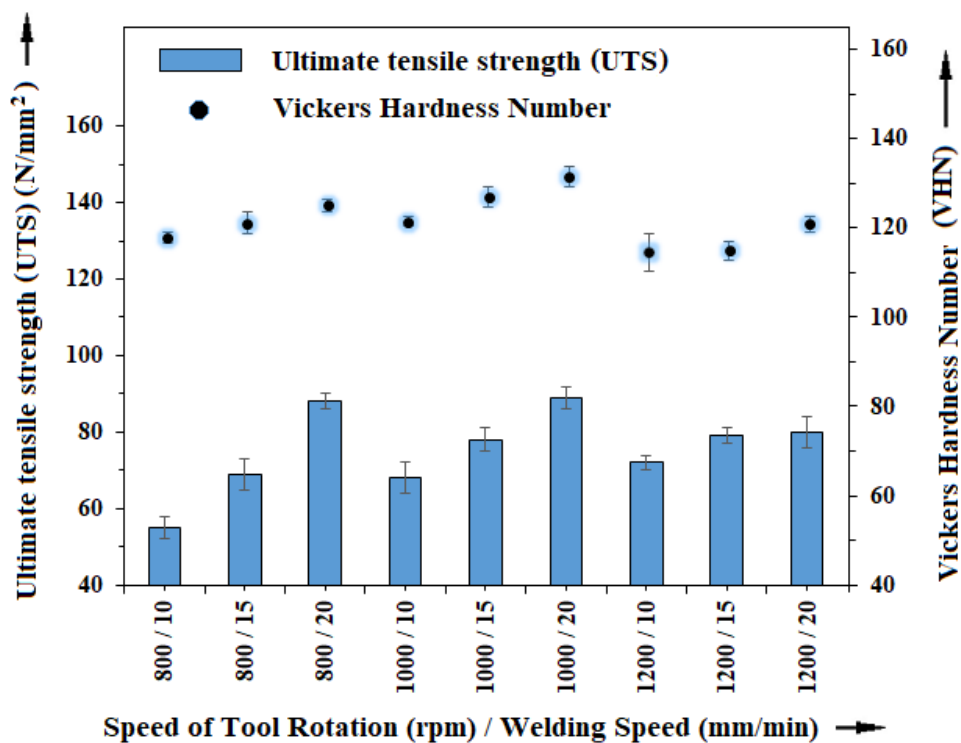
Figure 4.67 Comparison of hardness and UTS of Al-10Mg-8Ce-3.5Si aluminium alloy friction stir welded using CPP tool.

Figure 4.68 (a - c) represents the variation in the UTS and Hardness of the Al-5Mg-8Ce-3.5Si aluminium alloy, friction stir welded with different speeds of tool rotation, speeds of welding, and using TPP, SPP and CPP tools respectively. The UTS and hardness at NZ shows direct relationship. The UTS and NZ hardness values of the

friction stir welded Al-5Mg-8Ce-3.5Si aluminium alloy are lower than that of the friction stir welded Al-10Mg-8Ce-3.5Si aluminium alloy. Zhao et al. (2017) reported that the dislocation density around the AlSiMg hard particles increases with increase in weight percentage of Si and Mg particles during solidification. Hence, degree of resistance increases in the matrix which results in increased UTS. From Figure 4.68 (a - c), it is observed that, for a speed of tool rotation of 1000 RPM and a welding speed of 20 mm/min, the weld connection strength is the highest. A sufficient heat generation and adequate mixing of the softened material led to increase in the strength. Higher dynamic to static ratio obtained by using TPP tool causes more sweeping of material as compared to other tools (Elangovan and Balasubramanian 2008b; Huang et al. 2018b; Palanivel et al. 2012; Vijayavel and Balasubramanian 2018). Therefore, highest value of UTS and hardness values have been obtained for weld connection fabricated using TPP tool.
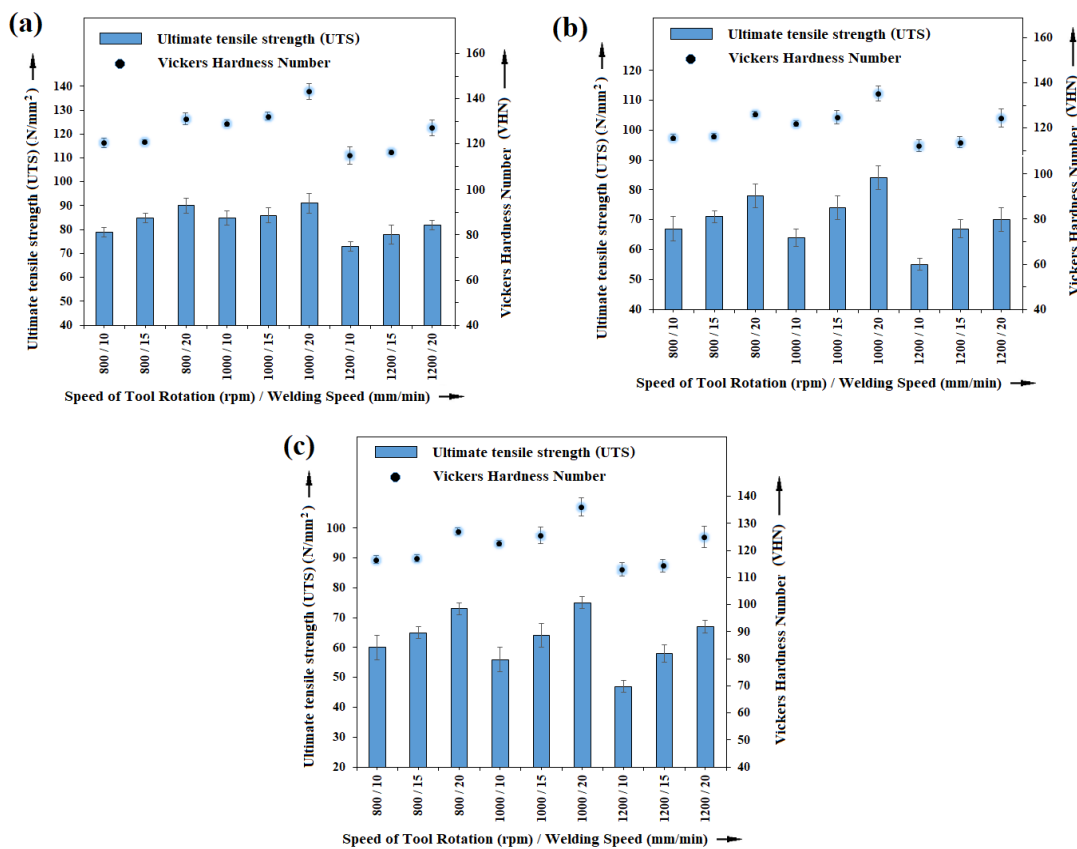
Figure 4.68 Comparison of hardness and UTS of Al-5Mg-8Ce-3.5Si aluminium alloy friction stir welded using (a) TPP tool, (b) SPP tool and (c) CPP tool.

236

4.11 ANALYSIS OF PROCESS PARAMETERS USING TAGUCHI DESIGN OF EXPERIMENT TECHNIQUE

4.11.1 Analysis of process parameters using Taguchi Method

To analyze the influence of design factors namely, speed of tool rotation, welding speed, tool pin shape and weight percentage of "Mg" particles, and the interactions on the experimental data. Analysis of variance is performed at 95% confidence level. Table 4.22 and Table 4.23 represent the ranking of each welding method variable with the help of Taguchi Design of Experiment (DOE) and Analysis for S/N ratio, and means (Larger is better) obtained at different method variable levels. The term 'delta' in Table 4.22 and Table 4.23 represents that the response is highly significant with respect to the factors under consideration. From Table 4.22 and Table 4.23, it could be understood that, the Tool pin shape is the most significant factor influencing UTS. The next significant factor is welding speed followed by Material composition. Speed of tool rotation has shown minimal effect on UTS response in FSW of aluminium alloys.

Table 4.22 Response Table for Signal to Noise Ratios of UTS

Level	Alloy Composition (A)	Speed of Tool rotation (RPM) (B)	Welding speed (mm/min) (C)	Tool pin shape (D)
1	38.60	37.95	36.92	39.18
2	37.04	38.22	37.88	37.61
3		37.28	38.66	36.67
Delta	1.57	0.94	1.74	2.51
Rank	3	4	2	1

Table 4.23 Response Table for Means of UTS

Level	Alloy Composition (A)	Speed of Tool rotation (RPM) (B)	Welding speed (mm/min) (C)	Tool pin shape (D)
1	86.22	80.28	71.56	91.56
2	72.00	82.72	79.33	76.72
3		74.33	86.44	69.06
Delta	14.22	8.39	14.89	22.50
Rank	3	4	2	1

The relative emphasis of the factor effects is further analyzed using analysis of variance (ANOVA). The ANOVA is carried out for means. Table 4.24 and Table 4.25 present the result of ANOVA for S/N ratio and means of the UTS responses, respectively. The most influencing factor on the mean and variations can be identified from Table 4.24 and Table 4.25. The results stipulate that alloy composition, speed of tool rotation, welding speed, and tool pin shape are the important parameters, which affect the UTS response. The interaction between the material composition and the speed of tool rotation does not have remarkable effect on the UTS of aluminium alloy weld connection fabricated using friction stir welding. From evaluation of the percentage of contribution (P%) of the different factors for UTS, it can be observed that tool pin shape factor has the highest contribution of 43.23%. Alloy composition has the second highest contribution of 25.06%. The contribution of the third factor, the welding speed is 18.32%. Finally, the contribution of speed of tool rotation is 6.25%. The error is seen to be 5.89%. Thus, tool pin shape is a vital factor to be taken into consideration in FSW of aluminium alloys; followed by the alloy composition, welding speed and speed of tool rotation.

Based on the above analysis, the optimum welding parameters for maximization of UTS could be calculated by using the following equation.

Predicted S/N Ratio   = Alloy Composition at level 1 + Speed of Tool Rotation
(maximization of UTS)   at level 2 + Welding speed   at level 3 + Tool pin

$$\text{shape at level } 1 - (3 \times N) \qquad \text{...Equation (9)}$$

$$= 38.60 + 38.22 + 38.66 + 39.18 - (3 \times 37.82)$$

$$= \underline{\mathbf{41.2}}$$

Predicted UTS Mean
(maximization of UTS)

$$= 86.22 + 82.72 + 86.44 + 91.56 - (3 \times 79.11)$$

$$= 109.61 \text{ N/mm}^2$$

$$= \underline{\mathbf{110}} \text{ N/mm}^2$$

Where "N" represents average value of "S/N Ratios" and "UTS Means".

The above combination of experimental conditions is compared with the experimental results (108 N/mm^2) and a relative error is 1.8%. The confidence interval for the UTS means is within the range.

Table 4.24 ANOVA for S/N Ratio of UTS of Aluminium alloy joint obtained using FSW.

Source	DF	Seq SS	Adj SS	Adj MS	F	P Value	% Contribution
Alloy Composition(A)	1	33.083	33.083	33.0831	147.79	0.000	23.67
Speed of Tool rotation (RPM) (B)	2	8.427	8.427	4.2136	18.82	0.000	6.03
Welding speed (mm/min) (C)	2	27.279	27.279	13.6396	60.93	0.000	19.52
Tool pin shape (D)	2	57.936	57.936	28.9679	129.41	0.000	41.46
C*D	4	3.619	3.619	0.9048	4.04	0.007	2.59
Residual Error	42	9.401	9.401	0.2238			6.73
Total	53	139.746					100

Legend: DF-Degrees of freedom, Seq MS- Sequential mean of squares, Adj SS-Adjusted sum of squares, Adj MS-Adjusted mean squares, F-Fischer ratio, P-Probability that 95% confidence level exceeds.

Figure 4.69 illustrates the main effect plot of factors that affect UTS of the aluminium alloys joint made through friction stir welding. The data mean value is used to analyze each factor effect. Figure 4.69 shows that composition, speed of tool rotation, welding speed and tool pin shape have dominant effect on UTS of the friction stir welded aluminium alloy. In addition, from the Figure 4.69, it can be observed that an increase in composition of Mg from 5% to 10% results in an increase of UTS. The increase in UTS may be because of the Mg particles preventing the movement of dislocations in the micro-structure. This dislocation decreases the dislocation density, which provides for strength of the aluminium alloys. There is a decrease in the inter-particle distance between the reinforcement particles, which results in increased resistance to dislocation motion as the particulate content is increased. During deformation, either the matrix material has to push the hard particulate further or it has to bypass the particles for deformation. During the process, the dislocations pile up. This restriction in the plastic flow in the matrix provides enhanced strength to the aluminium alloy (Cao 2005; McNelley et al. 2008). The increase in the number of hard particles results in increase of dislocation density and increase in UTS. The increase in the speed of tool rotation from 800 RPM to 1000 RPM results in expansion of the ultimate tensile stress region. With further increase in the speed of tool rotation the ultimate tensile stress decreases. Jayaraman and Balasubramanian (2013) reported that the heat generation due to friction is principally dependent on the speed of tool rotation. Lower speed of tool rotation yields less heat generation, irrespective of welding speed. Subsequently, heat supplied to the base material is reduced. This effect causes insufficient material flow and less plasticization in the stir zone. Hence, ultimate tensile stress is low. The higher speed of tool rotation yields high heat generation, irrespective of welding speed. Subsequently, the heat supplied to the base material is higher. This effect causes turbulence in material flow and grain coarsening in the stir zone. Hence, ultimate tensile stress is found to be low. Thus, it can be concluded that a moderate heat input during FSW is desirable for optimum strength. The significant increase in the welding speed leads to an increase in ultimate tensile strength. The softened area is diminished as the welding speed is increased (Heidarzadeh et al. 2012; Li et al. 2014a; Radisavljevic 2014; Shen et al. 2010). Thus, ultimate tensile stress has proportional relationship with welding speed. Lower speeds of welding are associated with higher heat input, which result in lower

cooling rate of welded joint. This can significantly increase the size of grains. Hence ultimate tensile stress is less. When the welding speed is less than the critical value, the FSW generally, produce defect-free joints. When the welding speed is higher than the critical value, weld defects tend to creep in to the joint. These defects act as crack initiation sites during tensile test. The tool profile analysis showed that, the TPP profiled pin is better than SPP and CPP pins. This is attributed to dynamic volume (DV) to static volume (SV) ratio which results in grain refinement and annealing during the welding method and more number of pulsating actions (60 pulses/sec) of the tool (Elangovan and Balasubramanian 2008b; Huang et al. 2018b; Palanivel et al. 2012). Triangular profile tool sweeps larger amount of material as compared to other types of tool. The weld connection fabricated by SPP tool showed UTS results slightly better to that of CPP tool. This is due to their less SV/DV ratio. The ultimate tensile stress obtained with the CPP tool is lesser than that obtained with other tools. This is due to the fact that, the frictional heat produced by the CPP tool is much lesser than that produced by other tools. This is because of lesser contact area and due to the absence of pulsating effect.

Table 4.25 ANOVA for Means of UTS of Aluminium alloy joined through FSW.

Source	DF	Seq SS	Adj SS	Adj MS	F	P Value	% Contribution
Alloy Composition(A)	1	2730.7	2730.7	2730.67	178.67	0.000	25.06
Speed of Tool rotation (RPM) (B)	2	670.1	670.1	335.06	21.92	0.000	6.15
Welding speed (mm/min) (C)	2	1996.4	1996.4	998.22	65.32	0.000	18.32
Tool pin shape (D)	2	4710.3	4710.3	2355.17	154.10	0.000	43.23
C*D	4	145.9	145.9	36.47	2.39	0.066	1.34
Residual Error	42	641.9	641.9	15.28			5.89
Total	53	10895.3					100

Legend: DF-Degrees of freedom, Seq MS- Sequential mean of squares, Adj SS-Adjusted sum of squares, Adj MS-Adjusted mean squares, F-Fischer ratio, P-Probability that 95% confidence level exceeds.

It is inappropriate to analyze how the process parameters might influence the properties of aluminium alloy joint produced by friction stir welding, without considering the effect / variation plot of each of the process parameters. Thus, to get more insight into the interactive mechanics of various process parameters, the effects of the process parameters were examined using the interaction plot. In the interaction plot, the intersection on the graph implied high interactions among the three parameters. Thus, the graph 'With an intersection coordinate was analyzed. As shown in Figure 4.70, the interactions between the three fixing parameters had an influence over the UTS. The interactions between the parameters showed that the alloy composition, speed of tool rotation, welding speed, and tool pin shape tend to affect the UTS. As shown in Figure 4.70 UTS increases as welding speed increases. But the UTS increases initially when the speed of tool rotation increases from 800 to 1000 RPM and then decreases from 1000 to 1200 RPM. The interaction of rotational speed and welding speed has shown higher UTS at a welding speed of 20 mm/min. The tool profiles (1, 2 and 3) have shown higher UTS for a speed of tool rotation of 1000 RPM. The TPP tool has shown highest value in all the cases of alloy composition, speed of tool rotation and welding speed. In all the cases, the UTS increased as the composition of the aluminium alloy is increased from 5% Mg to 10% Mg.
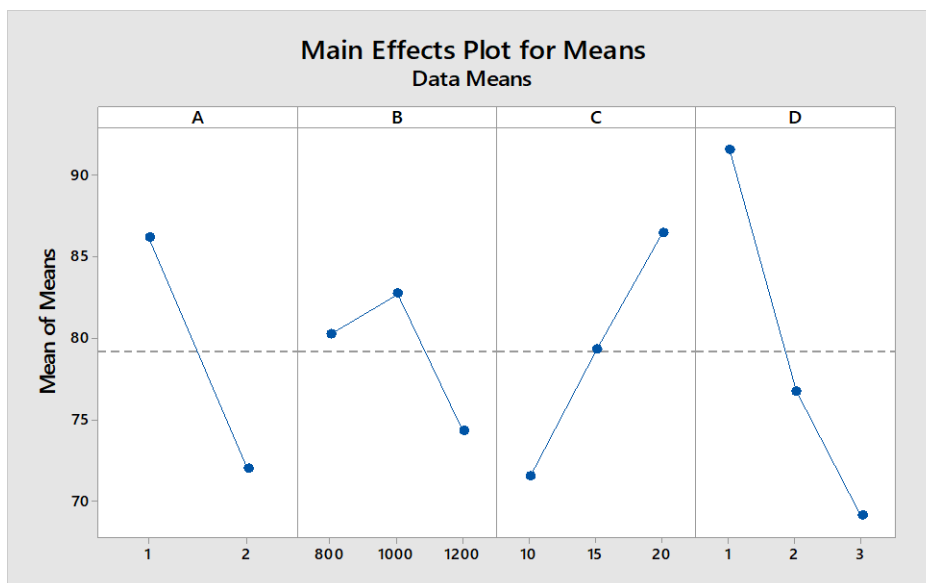
Figure 4.69 Main effects plot for UTS means of joint of friction Stir Welded alloy of aluminium. ("A" – Material; "B" – Speed of tool rotation; "C"- Welding speed; "D" – Tool pin profile)

Optimum values of speed of tool rotation and welding speed are analyzed by using the contour plot. Figure 4.71 shows the contour plot for the UTS response in terms of the process parameters, speed of tool rotation and welding speed. It is relatively easy to identify on examining from Figure 4.71 that the optimum values were near to 20 mm/min (welding speed) and 940 RPM (speed of tool rotation) and the response UTS is maximum at this point. From the Figure 4.71, it can be inferred that the method may be slightly more sensitive to change in speed of tool rotation than to change in welding speed.
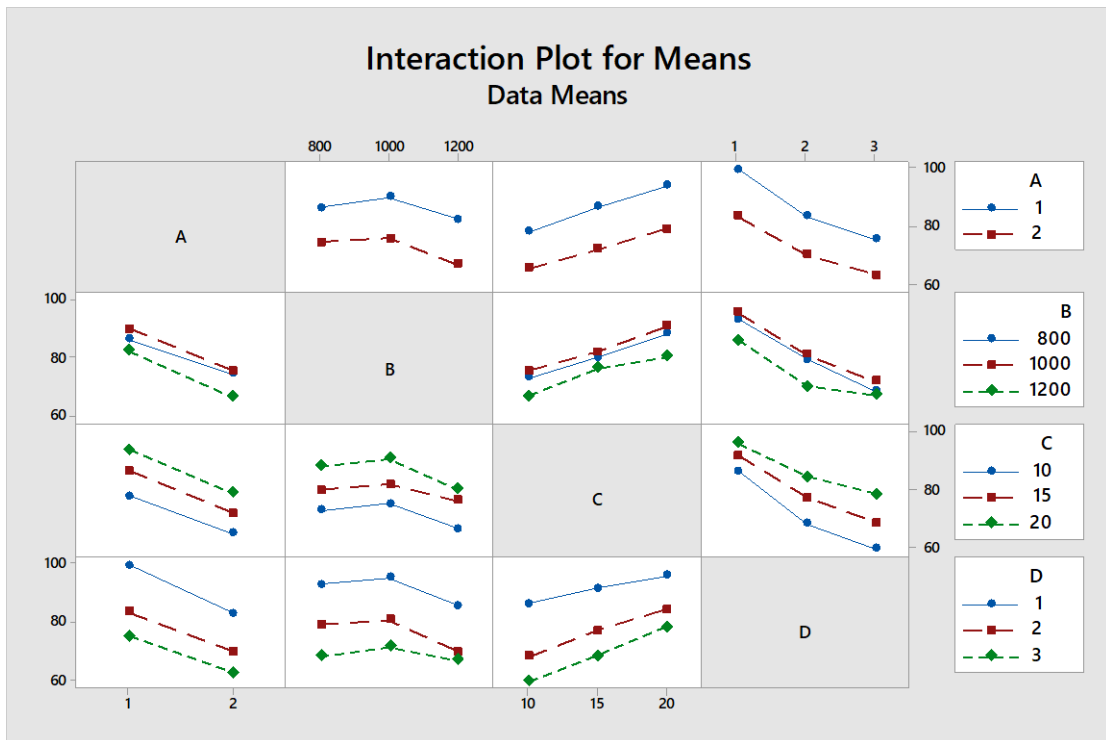
Figure 4.70 Interaction plot for means of UTS of joint of friction Stir Welded alloy of aluminium. ("A" – Material; "B" – Speed of tool rotation; "C"- Welding speed; "D" – Tool pin profile)

4.11.2   Prediction of response UTS using Taguchi Method

The predicted values of the UTS obtained using Taguchi Orthogonal Array Technique are compared with the experimentally obtained values and the same are presented in the Table 4.26. It can be noticed from the Table 4.26 that, the minimum percentage of

relative error is -0.05%, obtained for Al-5Mg-8Ce-3.5Si aluminium alloy friction stir welded at a speed of tool rotation of 1000 RPM, a welding speed of 20 mm/min using a triangular pin profile (TPP) tool. The maximum percentage of relative error is -5.52%, obtained for Al-10Mg-8Ce-3.5Si aluminium alloy joint obtained by friction stir welding process, at a speed of tool rotation of 1200 RPM and a welding speed of 10 mm/min using a SPP tool.
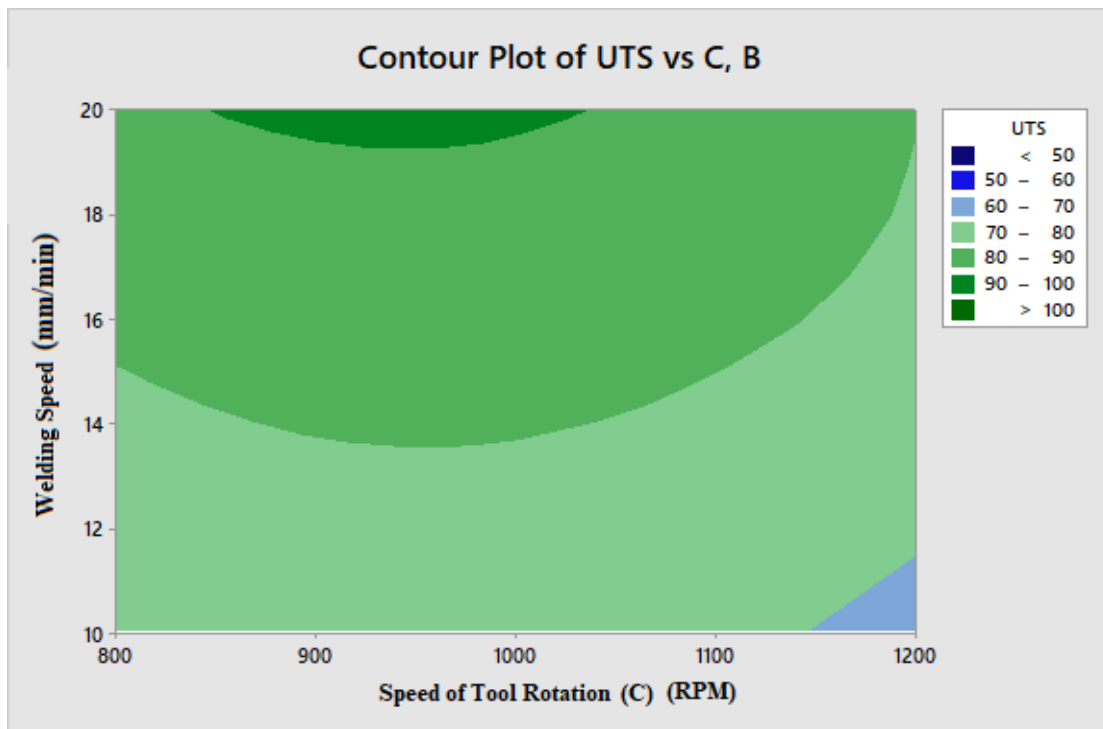
Figure 4.71 Contour plot UTS v/s Speed of tool rotation and Welding speed of friction stir welded Aluminium alloys

Figure 4.72 represents the plot of experimental and predicted UTS of joint of aluminium alloy created by friction stir welding, using Taguchi orthogonal array method. It can be observed from Figure 4.72 that, there is a close arrangement between the experimental and predicted UTS of the weld connection for different weight percentage of Mg particles, speed of tool rotation, welding speed and tool pin shape. The minimum and maximum percentage of relative errors have been tabulated in Table 4.26.

The developed model is utilized to predict the UTS of the joint of aluminium alloy obtained by friction stir welding. In the remaining 36 experiments, input parameters

and their corresponding results are utilized to predict the UTS of the joint. The obtained values are listed in Table 4.27. There is a good correlation among the experimental and predicted UTS of the joint of aluminium alloy obtained by friction stir welding. The maximum percentage of relative error is 10.26% for a speed of tool rotation of 1200 RPM, a welding speed of 10 mm/min, CPP tool pin shape and Al-10Mg-8Ce-3.5Si aluminium alloy. The minimum percentage of relative error is -0.06% for a speed of tool rotation of 1000 RPM, a welding speed of 20 mm/min, TPP tool pin shape and Al-10Mg-8Ce-3.5Si aluminium alloy.

Table 4.26 Comparison of Ultimate Tensile stress predicted by Taguchi orthogonal array Technique with the experimentally obtained values of UTS of the aluminium alloy joints

Sl. No.	Material Composition (Al-10 / Al-5)	Speed of Tool rotation (RPM)	Welding speed (mm/min)	Tool pin shape (T / S / C)	UTS (Experimental) (N/mm^2)	UTS (Predicted) (N/mm^2)	Relative Error in UTS (%)
1	1	800	10	1	95	96	-1.33
2	1	1000	10	1	101	96	4.50
3	1	1200	20	1	99	99	0.31
4	2	800	15	1	85	86	-1.39
5	2	1000	20	1	91	91	0.05
6	2	1200	15	1	78	77	1.39
7	1	800	15	2	85	85	0.50
8	1	1000	15	2	88	86	2.03
9	1	1200	10	2	66	70	-5.52
10	2	800	20	2	78	75	3.59
11	2	1000	10	2	64	63	1.95
12	2	1200	20	2	70	69	1.66
13	1	800	20	3	88	87	0.94
14	1	1000	20	3	89	90	-1.42
15	1	1200	15	3	79	75	5.44
16	2	800	10	3	60	59	2.03
17	2	1000	15	3	64	67	-4.12
18	2	1200	10	3	47	45	3.23
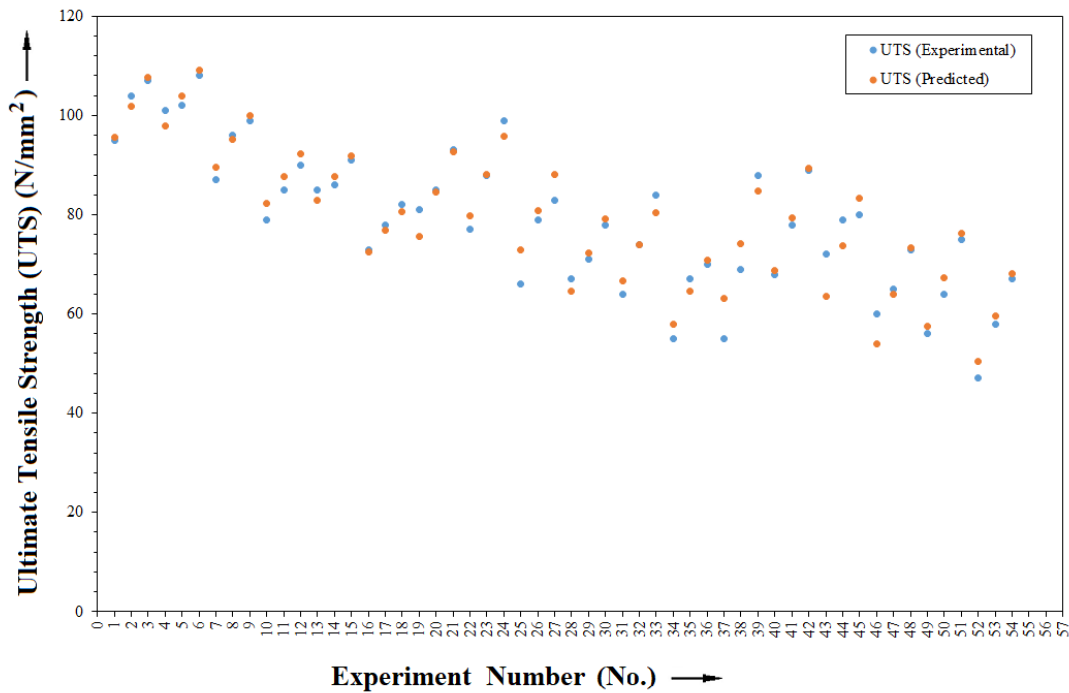
Figure 4.72 Plots showing comparison of UTS values obtained experimentally and values of UTS predicted by Taguchi orthogonal array model.

Figure 4.73 represents the plot of experimental and predicted UTS of friction stir welded aluminium alloys using Regression equation obtained by Response surface method of Design of Experiments. It can be observed from the Figure 4.73 that, there is a good agreement among the predicted and experimental UTS values for the weld connection fabricated with different weight percentage of Mg particles, speed of tool rotation, welding speed and tool pin shape. The minimum and maximum percentage of relative errors is listed in Table 4.27.

Table 4.27 Comparison of Ultimate Tensile stress predicted by Taguchi Technique with the experimentally obtained values of UTS of the aluminium alloy joints for other experiments.

Sl. No.	Material Composition (Al-10 / Al-5)	Speed of Tool rotation (RPM)	Welding speed (mm/min)	Tool pin shape (T / S / C)	UTS (Experimental) (N/mm^2)	UTS (Predicted) (N/mm^2)	Relative Error in UTS (%)

246

1	1	800	15	1	104	102	2.39
2	1	800	20	1	107	108	-0.53
3	1	1000	15	1	102	103	-1.20
4	1	1000	20	1	108	108	-0.06
5	1	1200	10	1	87	90	-3.16
6	1	1200	15	1	96	94	2.60
7	2	800	10	1	79	81	-2.58
8	2	800	20	1	90	94	-4.31
9	2	1000	10	1	85	82	3.62
10	2	1000	15	1	86	87	-1.39
11	2	1200	10	1	73	71	2.24
12	2	1200	20	1	82	79	3.30
13	1	800	10	2	81	76	6.54
14	1	800	20	2	93	92	0.93
15	1	1000	10	2	77	81	-5.34
16	1	1000	20	2	99	95	3.95
17	1	1200	15	2	79	81	-2.43
18	1	1200	20	2	83	87	-4.34
19	2	800	10	2	67	64	4.53
20	2	800	15	2	71	73	-2.17
21	2	1000	15	2	74	75	-0.90
22	2	1000	20	2	84	82	2.55
23	2	1200	10	2	55	59	-7.67
24	2	1200	15	2	67	65	2.47
25	1	800	10	3	55	60	-9.65
26	1	800	15	3	69	71	-2.44
27	1	1000	10	3	68	68	-0.26
28	1	1000	15	3	78	77	0.86
29	1	1200	10	3	72	65	10.26
30	1	1200	20	3	80	80	-0.37
31	2	800	15	3	65	62	5.00
32	2	800	20	3	73	72	1.02
33	2	1000	10	3	56	57	-1.61
34	2	1000	20	3	75	76	-0.81
35	2	1200	15	3	58	59	-2.55
36	2	1200	20	3	67	68	-0.79
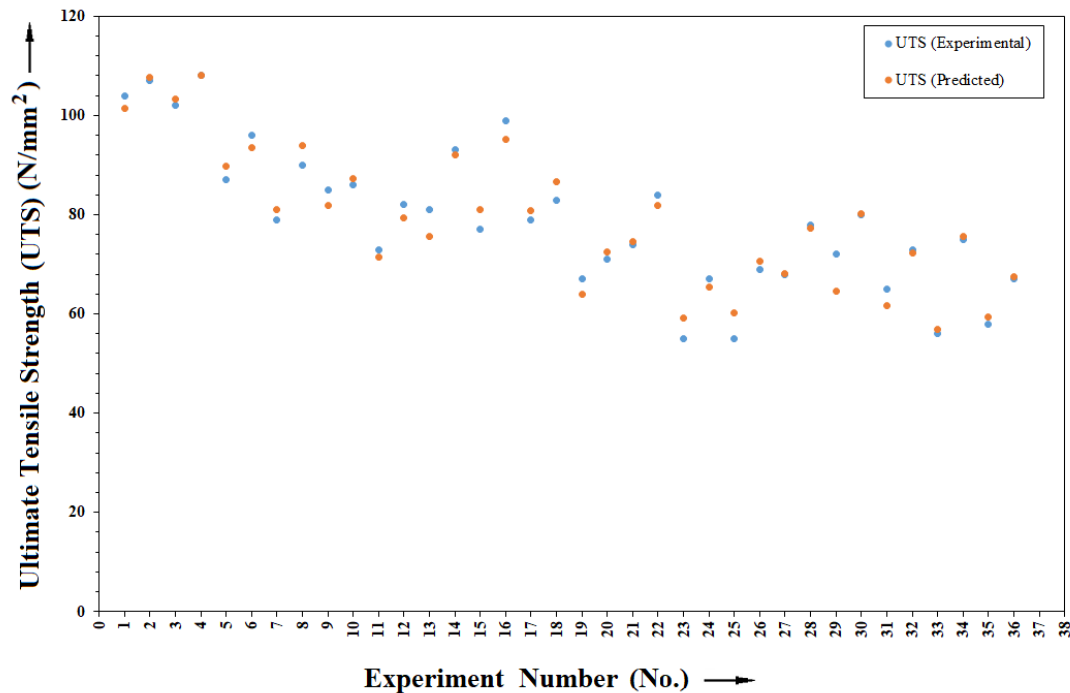
Figure 4.73 Plots showing comparison of UTS values obtained experimentally and values of UTS predicted by Taguchi model for other experiments based on confirmation tests.

4.11.3   Relationship between Grain size and hardness

Figure 4.74 to Figure 4.76 show the plots depicting the variation of hardness with grain size at nugget zone of the aluminium alloy weld connection made by friction stir welding at various speeds of tool rotation, speeds of welding, tool pin shapes and compositions of the alloy material. The data fitted with a best fit line with the regression equation as [198.5 – 7.87 × (grain size)]. The linear regression coefficient, R^2 for the best fit line has been found to be 66.5%. The grain size decreases more or less linearly with increasing hardness. Similarly, in Figure 4.75, the data follows simple square regression and R^2 for the best fit is 75.4%. The equation is [323.3 – 37.24 × (grain size) + 1.674 × (grain size)^2]. Whereas, in the Figure 4.76, the data follows simple cubic regression and R^2 for the best fit is 75.4 and the equation is [330.5 – 39.82 × (grain size) + 1.976 × (grain size)^2 - 0.0115 × (grain size)^3]. The best fit curve is cubic regression.

248
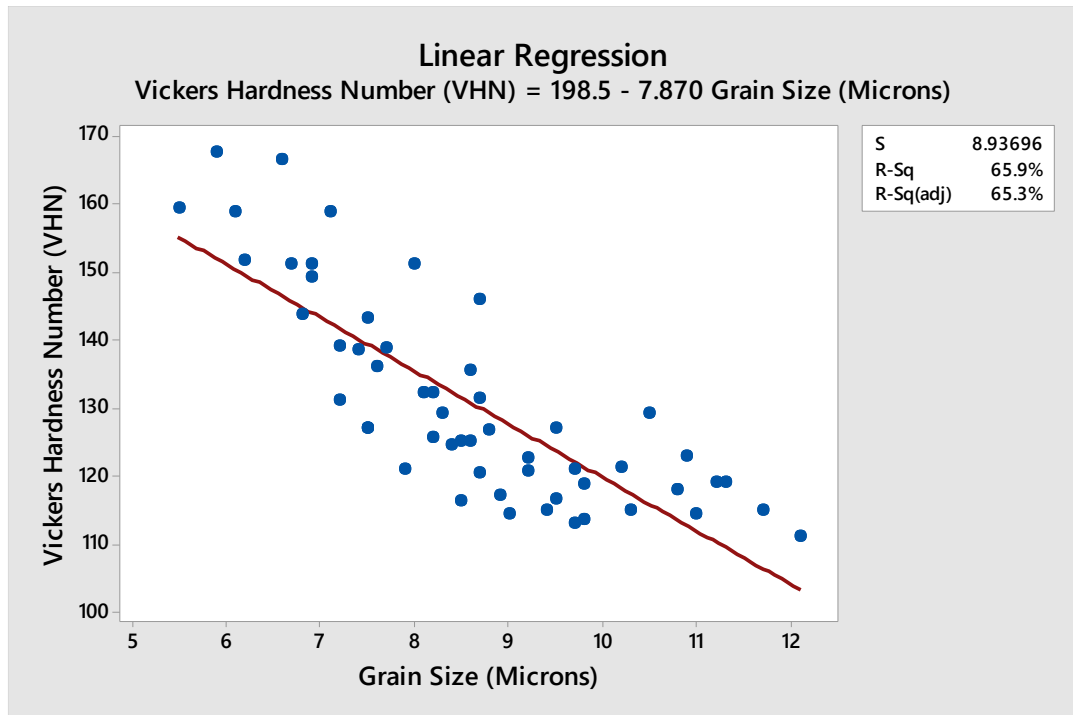
Figure 4.74 Plots showing the variation of grain size with hardness at NZ of aluminium alloys at different combinations of process parameters using Linear regression.
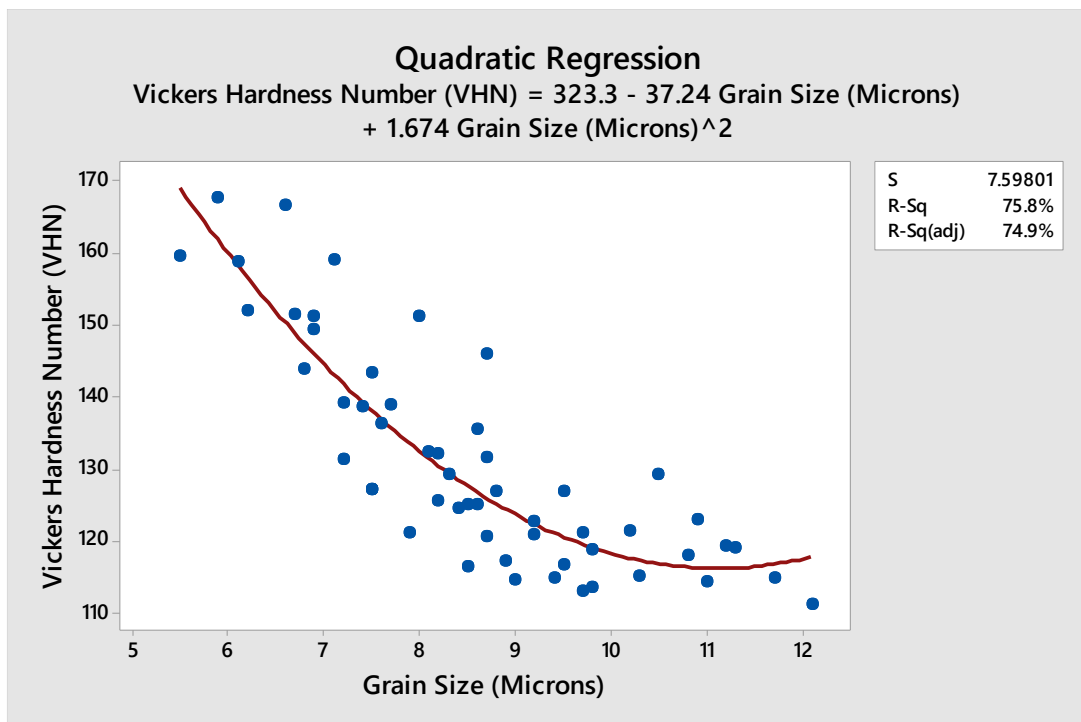
Figure 4.75 Plots showing the variation of grain size with hardness at NZ of aluminium alloys at different combinations of process parameters using Quadratic regression
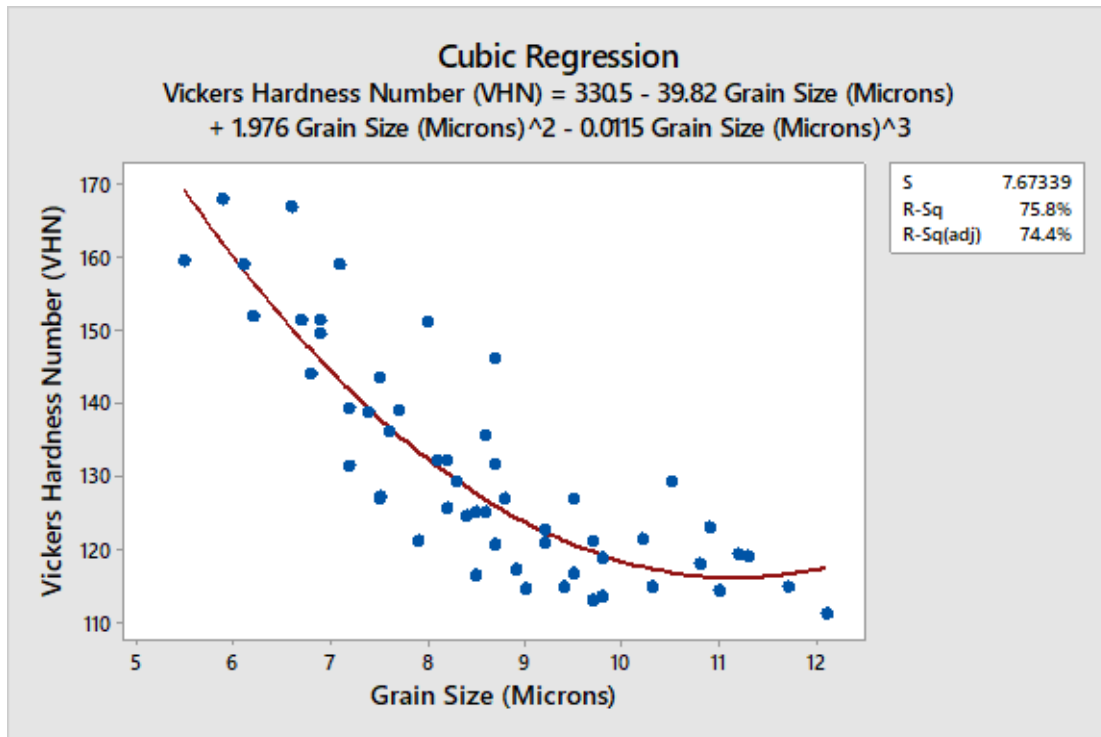
Figure 4.76 Plots showing the variation of grain size with hardness at NZ of aluminium alloys at different combinations of process parameters using Cubic regression

4.11.4 Relationship between Nugget zone hardness and Ultimate Tensile stress (UTS)

From the relationship between grain size and hardness, regression images of the aluminium alloy weld connection friction stir welded at different process parameters, it is concluded that the best fit is obtained for cubic regression. Hence, further analysis for hardness and UTS of the aluminium alloy weld connection is carried out using cubic regression. Figure 4.77 shows plot depicting the relationship between the UTS and hardness at NZ of the aluminium alloy joints. The cubic regression coefficient, R^2 for the best fit line has been found to be 72.4%. The cubic regression equation is [395.2 + 8.51 × (VHN) - 0.0530 × (VHN)^2 + 0. 000120 × (VHN)^3].
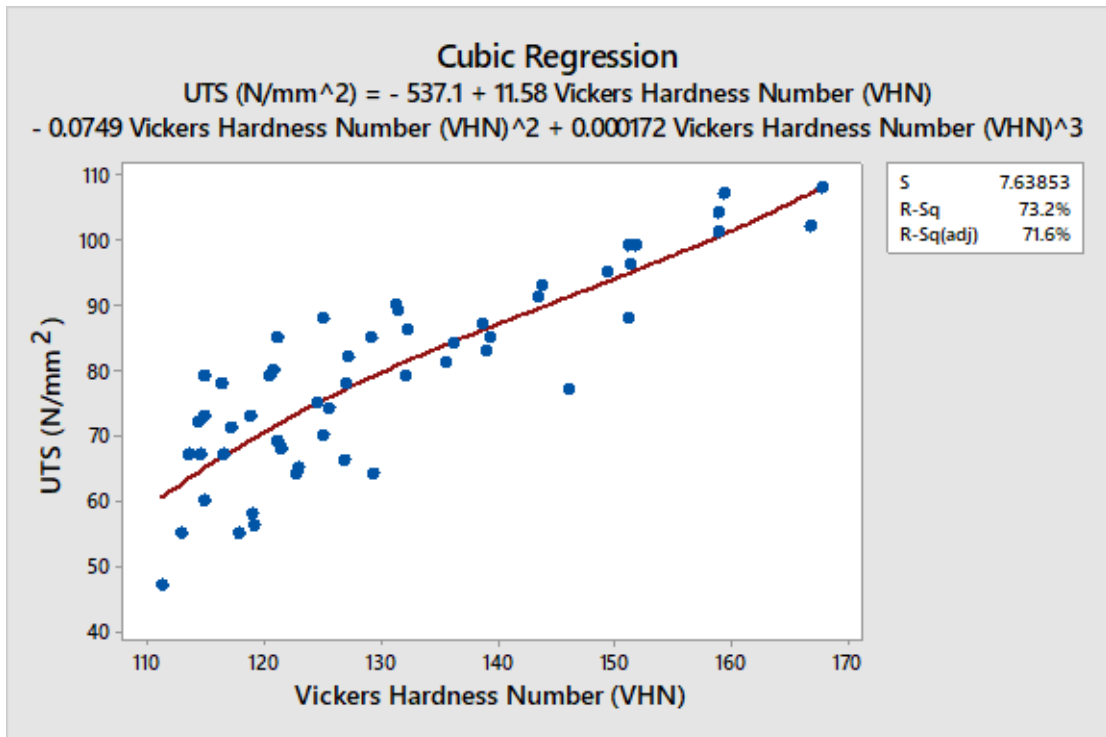
Figure 4.77 Plots showing the variation of hardness with UTS at NZ of aluminium alloys at different combinations of process parameters using Cubic regression

4.12 ANN MODEL TO PREDICT MECHANICAL PROPERTIES OF Al-10Mg-8Ce-3.5Si AND Al-5Mg-8Ce-3.5Si ALUMINIUM ALLOY JOINTS FABRICATED BY FSW PROCESS

4.12.1 ANN model for hardness prediction

The conception of ANN model for prediction of hardness at NZ of Al-10Mg-8Ce-3.5Si and Al-5Mg-8Ce-3.5Si aluminium alloys joined through FSW is discussed in this section. The microstructural characterization of FS welded aluminium alloys was discussed in the previous chapter. It is observed that the original dendritic structure present in the as-cast aluminium alloy gets recrystallized because of the frictional heat and plastic deformation produced by the rotating tool at the weld connection interface. It was also observed that the small and broken AlSiMg and $Al_{11}Ce_3$ hard particles at

NZ, because of the presence of sharp corners of hard particles collide with each other. It is quite well known that the hardness is mainly dependent on grain morphology and grain distribution. In general, the presence of small grains of hard particles and fine recrystallized grain structure in comparison to the base material leads to an increase in hardness of the aluminium alloy at NZ. This chapter deals with formulation of an ANN model for hardness prediction, which is treated as a function of speed of tool rotation, welding speed, tool pin contour and composition of the alloy. The chapter also includes the results of the experiments performed to validate the ANN model for hardness predicted.

Resistance to plastic deformation by indentation refers to hardness of the material. Therefore, it can be correlated to yield stress of the material. Generally, the hardness of the material provides approximate assessment of tensile stress of the material. Thus, hardness provides a means for comparative assessment of strength of material in absence of data on strength properties of material (E. Taban 2013; Kumbhar et al. 2011a).

Table 4.28 depicts the experimentally found values of hardness at NZ and those predicted by ANN model for Al-10Mg-8Ce-3.5Si and Al-5Mg-8Ce-3.5Si aluminium alloys joined with FSW method by altering speed of tool rotation, welding speed, tool pin contour and composition of the alloy, for a set of input parameters used for training the ANN program. Table 4.29 provides a comparison of hardness values predicted by ANN and experimentally obtained values for a set of input parameters used for validation of the ANN program. From Table 4.28, it can be noticed that the percentage of relative error between the ANN predicted values and corresponding experimental values range from -5.71% and +5.41%. Maximum error corresponds to a combination of process parameters of speed of tool rotation of 800 RPM, welding speed of 15 mm/min, TPP tool pin profile and Al-5Mg-8Ce-3.5Si aluminium alloy. Minimum relative error was attained for a speed of tool rotation of 1000 RPM, welding speed of 15 mm/min, SPP tool pin profile and Al-10Mg-8Ce-3.5Si aluminium alloy. Similarly, from Table 4.29, the percentages of minimum and maximum error predicted for validation results are -5.29% and +0.71%, respectively.

The percentage of error between ANN predicted and experimental results at different welding method variable values for the complete range of data are within 5.71%. This shows that the model has attained enough knowledge regarding relationship among the input parameters and output response. Hence, this model can be made use of to predict the hardness of the FSW weld connection of aluminium alloys. Further, this model can also be used for predicting the hardness of aluminium alloys, processed using friction stir processing technique.

Table 4.28 Comparison of Hardness at NZ predicted by trained ANN Model with the experimentally obtained values of Hardness of the aluminium alloy joints.

Sl. No.	* Tool pin contour	Material Composition	Speed of Tool rotation (RPM)	Welding speed (mm/min)	Experimental Hardness (VHN)	Predicted Hardness (VHN)	Relative Error (%)
1	1	1	800	10	149	152	-1.80
2	1	1	800	15	159	161	-1.18
3	1	1	800	20	159	166	-4.03
4	1	1	1000	10	159	160	-0.97
5	1	1	1000	15	167	162	2.92
6	1	1	1000	20	168	166	1.21
7	1	1	1200	15	151	148	2.14
8	1	1	1200	20	152	155	-1.81
9	1	2	800	15	121	128	-5.71
10	1	2	800	20	131	136	-3.40
11	1	2	1000	10	129	134	-3.81
12	1	2	1000	15	132	135	-2.44
13	1	2	1000	20	143	139	2.84
14	1	2	1200	15	116	121	-4.06
15	1	2	1200	20	127	125	1.51
16	2	1	800	10	135	129	4.71
17	2	1	800	15	139	140	-0.32
18	2	1	1000	10	146	139	4.76

19	2	1	1000	15	151	143	5.47
20	2	1	1000	20	151	149	1.23
21	2	1	1200	10	127	121	4.98
22	2	1	1200	15	132	130	1.86
23	2	2	800	10	117	118	-1.10
24	2	2	800	15	117	121	-2.91
25	2	2	800	20	127	126	1.03
26	2	2	1000	10	123	126	-2.68
27	2	2	1000	15	126	129	-3.01
28	2	2	1000	20	136	134	1.34
29	2	2	1200	15	114	118	-3.27
30	2	2	1200	20	125	123	1.75
31	3	1	800	10	118	117	0.60
32	3	1	800	15	121	123	-1.55
33	3	1	1000	10	121	125	-3.37
34	3	1	1000	15	127	129	-1.81
35	3	1	1000	20	131	135	-2.37
36	3	1	1200	10	114	114	0.25
37	3	1	1200	15	115	119	-3.58
38	3	1	1200	20	121	126	-4.08
39	3	2	800	10	117	115	1.42
40	3	2	800	20	127	120	5.20
41	3	2	1000	10	123	122	0.56
42	3	2	1000	15	126	124	1.40
43	3	2	1000	20	136	131	3.54
44	3	2	1200	10	113	109	3.09
45	3	2	1200	15	114	116	-0.92
46	3	2	1200	20	125	122	2.14

* Legend: 1 = TPP, 2 = SPP, 3 = CPP → Tool pin contours.

The model testing is done to provide a direct comparison among the experimental values and the corresponding predicted values. Figure 4.78 represents the linear fit plot of experimental UTS versus the predicted UTS obtained using ANN model. The straight line in Figure 4.78 represents the perfect fit between the experimental and

predicted values of UTS. The round dots represent the predicted UTS values. The distance between the dot and the line reports the deviation of predicted values from the corresponding experimental values. The standard deviation for the predicted UTS is 3.82573 and adjusted R square value is 0.935. A value of regression coefficient close to '1' represents proximity of the predicted values with the target values.

Table 4.29 Comparison of Hardness at NZ predicted by trained ANN Model with the experimentally obtained values of Hardness of the aluminium alloy joints.

Sl. No.	* Tool pin contour	Material Composition	Speed of Tool rotation (RPM)	Welding speed (mm/min)	Experimental Hardness (VHN)	Predicted Hardness (VHN)	Relative Error (%)
1	1	1	1200	10	139	138	0.71
2	1	2	800	10	120	123	-1.94
3	1	2	1200	10	115	116	-0.91
4	2	1	800	20	144	149	-3.71
5	2	1	1200	20	139	139	0.15
6	2	2	1200	10	113	113	0.07
7	3	1	800	20	125	132	-5.29
8	3	2	800	15	117	117	0.07

* Legend: 1 = TPP, 2 = SPP, 3 = CPP → Tool pin contours.

Figure 4.79 represents the linear fit plot of experimental and predicted UTS for data used for validation of ANN model. The variation shows a similar pattern as in the case of training data predictions, discussed in previous paragraph, for which similar reasoning holds good.
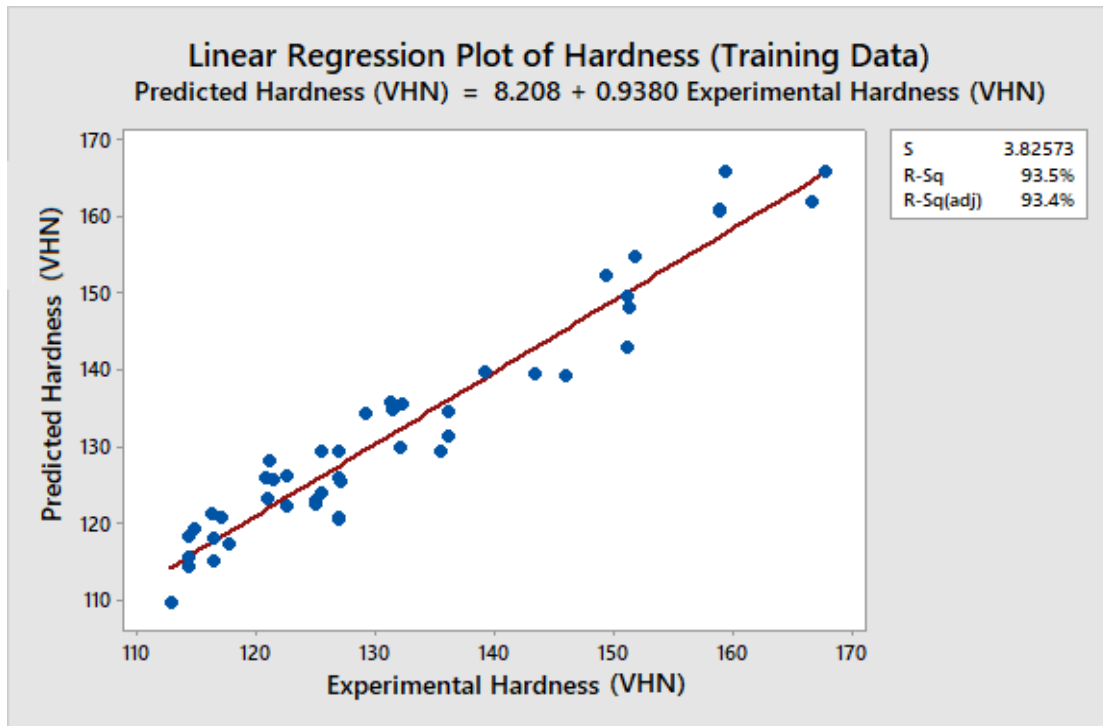
Figure 4.78 Scatter plot showing the variation of hardness for experimental and predicted values for the training data, using ANN model
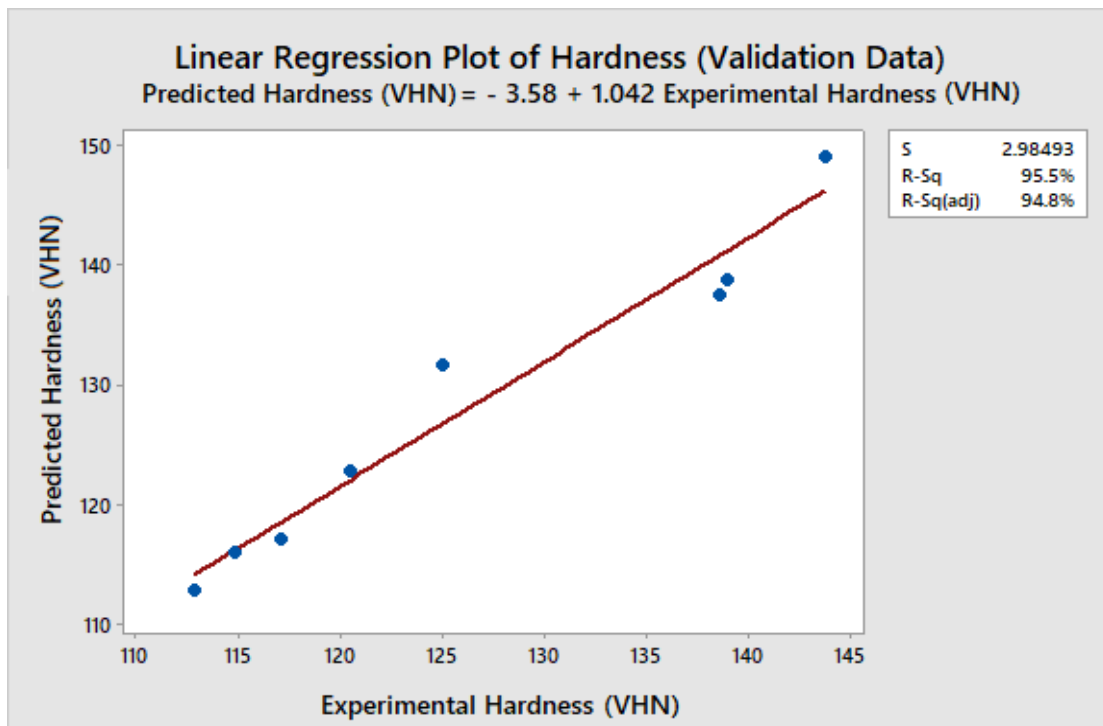
Figure 4.79 Scatter plot showing the variation of hardness for experimental and predicted values for the validation data, using ANN model

4.12.2 ANN model for Ultimate Tensile stress prediction

Ultimate tensile stress of Al-10Mg-8Ce-3.5Si and Al-5Mg-8Ce-3.5Si aluminium alloys joined through FSW, predicted using ANN model are discussed in this section. Welding of aluminium alloys is carried out at various speed of tool rotation, welding speeds, tool pin contours and composition of material. The model is trained with 85% of data collected from the single approach method and rest of the data is utilized to test and validate the model. Table 4.30 represents the experimental and predicted values of UTS and elongation percentage of aluminium alloys joints, produced by FSW, using ANN model. The mean square error was fixed at $1x10^{-3}$. The maximum percentage of relative error got for trained data was + 6.6% at speed of tool rotation of 1000 RPM, welding speed of 20 mm/min, SPP tool and Al-5Mg-8Ce-3.5Si. The minimum percentage of relative error obtained for trained data was -7.94. The maximum relative error for percent elongation was 7.37% and minimum relative error was -7.96%. The error obtained for predicting UTS by making use of ANN model was much less than that of Taguchi OA prediction. Therefore, it can be presumed that this model gives superior results in comparison to the OA.

Table 4.31 represents the predicted and experimental UTS and percent elongation of the welded joint in aluminium alloy plates produced by FSW process. The minimum relative error for UTS is -7.34% and maximum error was +8.09%. Similarly, the minimum relative error is -4.58 and maximum relative error for percentage elongation is +7.45%. The maximum relative error for UTS values obtained using ANN model is far better than that obtained using Taguchi model (+10.26 & -9.65. Refer Table 4.27) and suggests its superiority over Taguchi method in this application.

Figure 4.80 shows the plot depicting the direct comparison between the predicted values from ANN model and experimentally observed values of UTS. The red color line represents the perfect fit line and round dots represent the predicted UTS from ANN model. From the Figure 4.80 it is confirmed that the predicted values are closer to the experimental values with standard deviation of 3.08907 and adjusted R square value is 0.954. The R value close to '1' indicates an excellent generalization of input output relationship.

Table 4.30 Comparison of Ultimate Tensile stress and Percentage Elongation predicted by trained ANN Model, with the experimentally obtained UTS and Percentage Elongation values of aluminium alloy joints

Sl. No.	* Tool pin contour	Material Composition	Speed of Tool rotation (RPM)	Welding speed (mm/min)	Ultimate Tensile stress (N/mm^2)			Percentage Elongation (%)		
					Experimental	Predicted	Relative Error (%)	Experimental	Predicted	Relative Error (%)
1	1	1	800	10	95	98	-2.71	5.6	5.4	3.12
2	1	1	800	15	104	104	0.40	5.5	5.5	-0.19
3	1	1	800	20	107	108	-1.01	5.4	5.7	-4.98
4	1	1	1000	10	101	94	6.52	5.8	5.6	2.88
5	1	1	1000	15	102	101	0.85	5.2	5.3	-2.24
6	1	1	1000	20	108	106	1.59	5.6	5.3	5.42
7	1	1	1200	15	96	98	-2.47	5.6	5.2	7.15
8	1	1	1200	20	99	104	-5.27	4.9	5.3	-7.96
9	1	2	800	15	85	86	-0.67	5.6	5.8	-3.84
10	1	2	800	20	90	88	2.08	6.1	5.9	3.65
11	1	2	1000	10	85	80	6.07	6	5.6	7.21
12	1	2	1000	15	86	84	2.22	5.7	5.9	-4.08
13	1	2	1000	20	91	87	4.29	5.9	5.9	-0.58
14	1	2	1200	15	78	82	-5.58	5.8	5.7	2.50
15	1	2	1200	20	82	86	-4.74	5.6	5.7	-1.16
16	2	1	800	10	81	79	1.98	4.9	5.2	-5.56
17	2	1	800	15	85	89	-4.37	5.6	5.5	2.29
18	2	1	1000	10	77	75	2.40	5.5	5.5	0.17
19	2	1	1000	15	88	85	3.86	5.2	5.5	-6.25
20	2	1	1000	20	99	94	5.52	5.2	5.1	2.26
21	2	1	1200	10	66	71	-7.56	5.7	5.5	3.18

22	2	1	1200	15	79	80	-1.75	5.4	5.3	1.38
23	2	2	800	10	67	67	-0.01	5.6	6.0	-7.38
24	2	2	800	15	71	75	-5.33	6	5.7	5.27
25	2	2	800	20	78	81	-3.88	5.7	5.7	-0.53
26	2	2	1000	10	64	63	1.38	5.8	5.8	-0.57
27	2	2	1000	15	74	72	3.37	5.5	5.9	-7.46
28	2	2	1000	20	84	78	6.60	5.9	5.9	-0.45
29	2	2	1200	15	67	68	-1.39	5.9	6.2	-4.74
30	2	2	1200	20	70	76	-7.94	5.8	5.8	0.08
31	3	1	800	10	55	57	-2.90	4.9	5.1	-3.93
32	3	1	800	15	69	68	1.98	5.6	5.2	6.83
33	3	1	1000	10	68	69	-1.24	5.5	5.6	-1.94
34	3	1	1000	15	78	79	-1.82	5.2	5.4	-4.71
35	3	1	1000	20	89	88	1.27	5.2	5.2	0.51
36	3	1	1200	10	72	70	2.69	5.7	5.6	1.34
37	3	1	1200	15	79	76	3.48	5.4	5.2	4.26
38	3	1	1200	20	80	84	-4.97	5.1	5.1	0.32
39	3	2	800	10	60	58	4.12	5.5	5.3	4.44
40	3	2	800	20	73	77	-4.84	5.5	5.1	7.37
41	3	2	1000	10	56	54	4.22	5.5	5.6	-1.54
42	3	2	1000	15	64	63	1.95	6.1	5.8	5.53
43	3	2	1000	20	75	72	3.51	5.5	5.8	-6.19
44	3	2	1200	10	47	50	-6.37	5.8	5.9	-0.99
45	3	2	1200	15	58	59	-1.10	6.1	5.8	5.44
46	3	2	1200	20	67	68	-1.70	6	6.1	-2.21

* Legend: 1 = TPP, 2 = SPP, 3 = CPP → Tool pin contours.

Table 4.31 Comparison of Ultimate Tensile stress and Percentage Elongation predicted by trained ANN Model with the experimentally obtained UTS and Percentage Elongation values of aluminium alloy joints

Sl. No.	* Tool pin contour	Material Composition	Speed of Tool rotation (RPM)	Welding speed (mm/min)	Ultimate Tensile stress (N/mm^2)			Percentage Elongation (%)		
					Experimental	Predicted	Relative Error (%)	Experimental	Predicted	Relative Error (%)
1	1	1	800	10	87	91	-4.55	4.9	5.1	-4.58
2	1	1	800	15	79	82	-3.69	5.6	5.7	-2.41
3	1	1	800	20	73	77	-6.12	6.1	5.6	7.45
4	1	1	1000	10	93	97	-4.48	5.2	5.3	-2.78
5	1	1	1000	15	83	90	-8.09	5.1	5.2	-1.50
6	1	1	1000	20	55	59	-7.34	6.1	5.7	6.11
7	1	1	1200	15	88	90	-2.42	5.2	5.0	2.92
8	1	1	1200	20	65	67	-3.03	5.9	5.5	7.39

* Legend: 1 = TPP, 2 = SPP, 3 = CPP → Tool pin contours.

Figure 4.81 depicts the plot showing the UTS values of experimental and predicted UTS form the ANN model. From Figure 4.81 it is confirmed that the predicted values using prediction model is in decent agreement with corresponding experimentally measured values. The closeness of the R value of regression line to unity indicates very high accuracy of the predicted data (X) for the predictions carried out on the training, testing and validation data. This further confirms the potential of ANN modelling as an efficient prediction tool for generalizing the complex input output co-relationship.
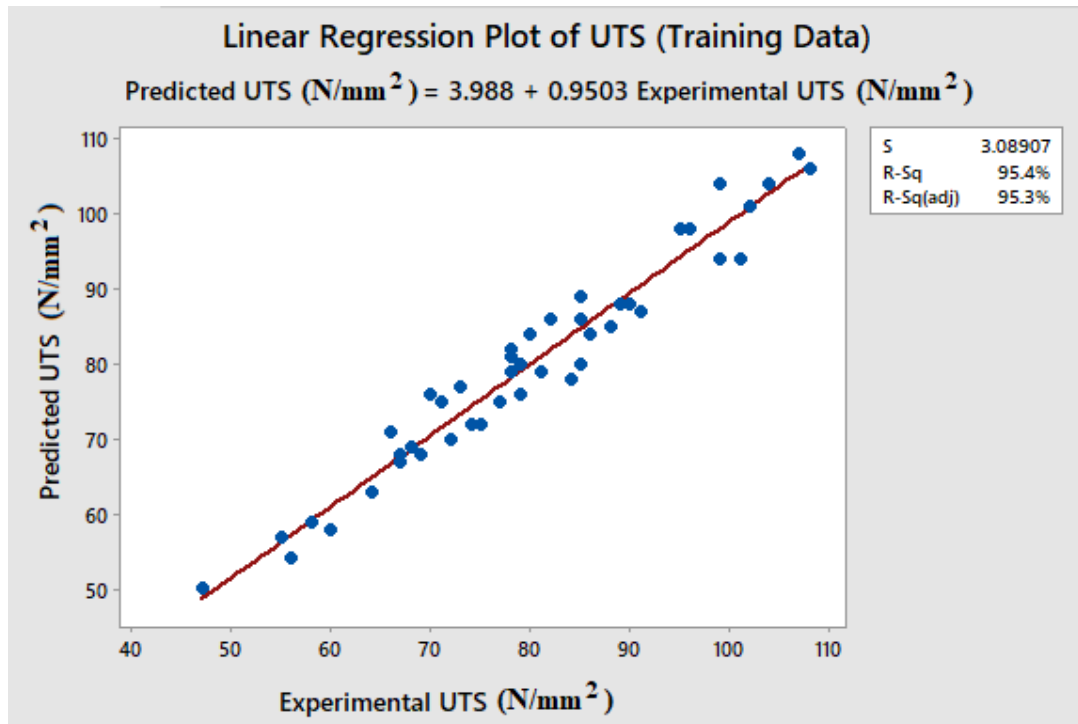
Figure 4.80 Scatter plot showing the variation of UTS for experimental and predicted values using ANN model
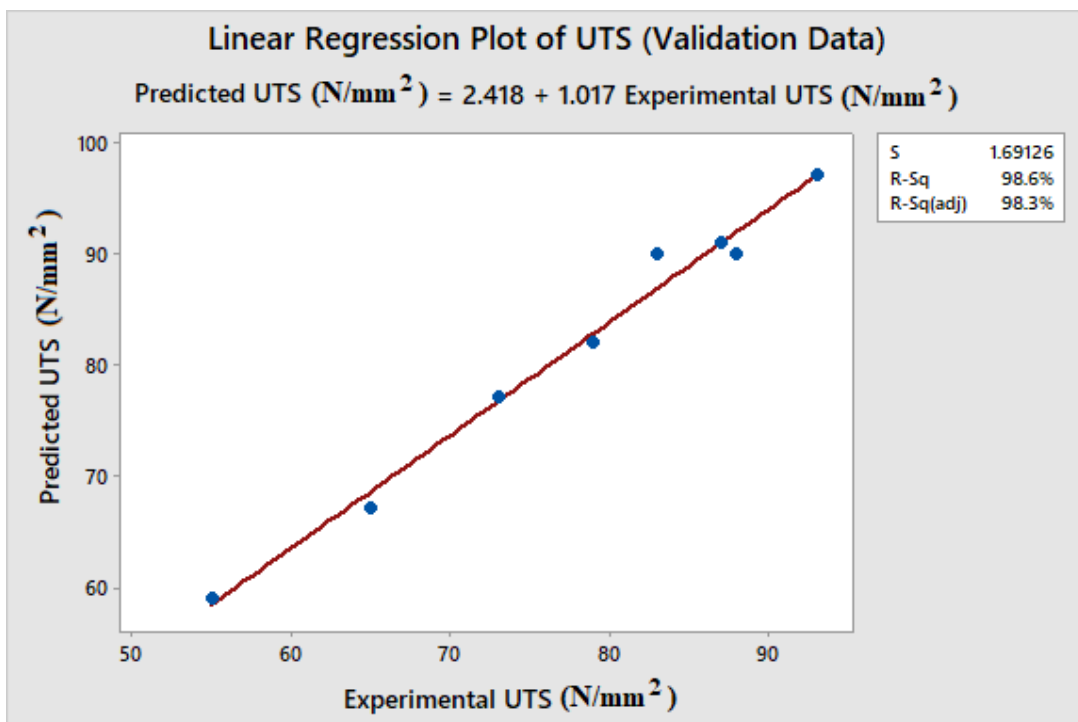
Figure 4.81 Scatter plot showing the variation of UTS for experimental and predicted values using ANN model

4.13   SUMMARY OF RESULTS

4.13.1   Microstructural and Mechanical Characterization of As-cast Al-Mg-Ce-Si aluminium alloys (Al-10Mg-8Ce-3.5Si and Al-5Mg-8Ce-3.5Si aluminium alloys)

1. The XRD analysis of as-cast Al-10Mg-8Ce-3.5Si aluminium alloy revealed the α-Al cells with intercellular α-$Al_{11}Ce_3$, that indicates amorphous phase which gives the alloy required castability and ductility to make it ideal material for welding.

2. The SEM examination of as cast Al-10Mg-8Ce-3.5Si alloy of aluminium exhibited characteristic primary α-Al dendrites with inter-dendritic α-Al/α-$Al_{11}Ce_3$ eutectic. An average grain size of 100.0±0.25 μm, Vickers hardness value of 98±1 VHN, Yield tensile stress of 101.7±4 N/mm^2, Ultimate tensile stress of 154±4.5 N/mm^2 and percentage elongation of 4.66±0.3 % were observed from SEM analysis, Vickers hardness measurements and tensile tests respectively.

3. The as-cast Al-5Mg-8Ce-3.5Si aluminium alloy revealed typical dendritic structure with average grain size of 117.6±2.3 μm. The grain size of aluminium alloy was reduced by 17.6% as compared to Al-5Mg-8Ce-3.5Si aluminium alloy. The Vickers hardness value was 81.6±1.8 VHN, yield tensile stress was 88.0±3 N/mm^2, Ultimate tensile stress 135.8±2 N/mm^2 and percentage elongation was 5.5±0.4 %.

4. The fracture surfaces of the Al-10Mg-8Ce-3.5Si and Al-5Mg-8Ce-3.5Si aluminium alloy exhibit dimples and tear ridges confirming to a mixture of the ductile-brittle fracture.

4.13.2   FSW of Al-10Mg-8Ce-3.5Si and Al-5Mg-8Ce-3.5Si aluminium alloy

FSW of Al-10Mg-8Ce-3.5Si and Al-5Mg-8Ce-3.5Si aluminium alloys were conducted for various combinations of speeds of tool rotational and welding, using three types of tools. The welded specimens were investigated for micro-structure and mechanical

properties of joints produced by friction stir welding to study the effect of process parameters. The following conclusions were derived.

4.13.2.1 Macrostructural and microstructural characterization of welded joints of Al-10Mg-8Ce-3.5Si and Al-5Mg-8Ce-3.5Si aluminium alloy plates prepared by friction stir welding process

The influence of process parameters on the defect free weld joints of Al-10Mg-8Ce-3.5Si and Al-5Mg-8Ce-3.5Si aluminium alloy during FSW have been studied based on macrostructural and microstructural investigations.

1. The macro image analysis of the aluminium alloy joints friction stir welded using circular shape pin tool (CPP) have revealed defects. Similar defects were observed for the speed of tool rotation less than 800 RPM and more than 1200 RPM. Similarly, defects were observed when the welding speed was below 10 mm/min and above 20 mm/min.

2. The macro image analysis of the aluminium alloy welded using a tool with Triangular shape pin have revealed the following results.
   a. When the speed of tool rotation was below 800 RPM and the welding speed was below 8 mm/min, pinhole defects were observed. For a welding speed above 20 mm/min and a speed of tool rotation below 800 RPM, wormhole defects were observed.
   b. When the speed of tool rotation was above 1200 RPM, and welding speed was below n 10 mm/min, wormhole defects were found and when the welding speed was more than 25 mm/min, tunnel hole defects have been observed. A remarkable improvement in defect free welds has been observed due to the change in the shape of the pin as compared to those obtained with the CPP tool.

3. The macro image analysis of the aluminium alloy welded using square pin shape has revealed the following results.
   a. When the speed of tool rotation was below 800 RPM and the welding speed was below 5 mm/min, pinhole defects were observed. For speed of tool rotation 800 RPM and welding speed more than 20 mm/min, wormhole defects were observed.

b. When the speed of tool rotation was above 1200 RPM and welding speed was below 10 mm/min, tunnel hole defects were observed. When the speed of tool rotation was above 1200 RPM and welding speed was below 20 mm/min, tunnel hole defects have been observed. The extent of defect free welds obtained from the SPP tool was same as the defect free welds obtained with the TPP tool.

4. The microstructural observations of welded region of the aluminium alloy friction stir welded using TPP, SPP and CPP have led to the following conclusions.

   a. Recrystallized structure has been observed at the weld connection interface of the FSW joint.

   b. The micro-structure of welded region of the aluminium alloy obtained by friction stir welding is segregated into four zones. Namely (i) NZ, (ii) TMAZ, (iii) HAZ and (vi) Base material.

   c. The micro-structure at the NZ revealed recrystallized and equiaxed fine grains of size spanning from 5.5 to 12.1 µm. Homogeneous distribution of all elements was observed in the NZ. The size of the particles was reduced due to stirring action of the tool and striking of hard particles with each other.

   d. Coarse grains have been obtained at HAZ due to the annealing process.

   e. The grain structure at TMAZ has shown parallel band like distribution of α-Al and $Al_{11}Ce_3$ particles and elongated grains.

   f. The grain size obtained at the top region of the NZ was higher in comparison to the bottom region of the NZ.

   g. The grain size obtained at NZ using triangular shape pin tool is lesser than that obtained with other tools.

5. The analysis of XRD showed the peaks of α-Al and $α-Al_{11}Ce_3$. No evidence of any chemical reaction between matrix alloy and hard particles was detected. No harmful intermetallic phases were detected.

4.13.2.2   Mechanical properties of the joint of Al-10Mg-8Ce-3.5Si and Al-5Mg-8Ce-3.5Si aluminium alloys, welded by friction stir welding process

4.13.2.2.1   Hardness

1. "W" shaped hardness distribution pattern was observed across the cross section of the welded joint.

2. Highest hardness was obtained at the NZ irrespective of the speed of tool rotation, welding speed, tool pin shapes and composition of the aluminium alloy.

3. The maximum hardness of the aluminium alloy at NZ was attained at a speed of tool rotation of 1000 RPM and a welding speed of 20 mm/min irrespective of the tool pin shapes. Similarly, the minimum hardness of the aluminium alloys at NZ was attained at a speed of tool rotation of 1200 RPM and a welding speed of 10 mm/min irrespective of the tool pin shapes. The hardness attained for different tool pin shapes is as discussed below.

   a) **TPP tool**
      i. The maximum hardness at NZ of Al-10Mg-8Ce-3.5Si aluminium alloy was 167.7 VHN and the minimum hardness was 138.6 VHN.
      ii. The maximum hardness at NZ of Al-5Mg-8Ce-3.5Si aluminium alloy was 143.3 VHN and the minimum hardness was 114.8 VHN.

   b) **SPP tool**
      i. The maximum hardness at NZ of Al-10Mg-8Ce-3.5Si aluminium alloy was 151.2 VHN and the minimum hardness was 126.9 VHN.
      ii. The maximum hardness at NZ of Al-5Mg-8Ce-3.5Si aluminium alloy was 136.1 VHN and the minimum hardness was 112.9 VHN.

   c) **CPP tool**
      i. The maximum hardness at NZ of Al-10Mg-8Ce-3.5Si aluminium alloy was 131.5 VHN and the minimum hardness was 114.3 VHN.

ii. The maximum hardness at NZ of Al-5Mg-8Ce-3.5Si aluminium alloy was 129.2 VHN and the minimum hardness was 111.2 VHN.

4. Lowest hardness in the hardness distribution shape of welded aluminium alloy was obtained at HAZ due to annealing effect.

5. The specimens welded with the TPP tool revealed higher hardness as compared to that produced with SPP and CPP tool.

4.13.2.2.2 Tensile strength

The tensile test of Al-10Mg-8Ce-3.5Si and Al-5Mg-8Ce-3.5Si aluminium alloy friction stir welded exhibited following characteristics.

1. The tensile test of the weld connection of aluminium alloy plates, prepared by friction stir welding, exhibited fracture along the interface between the FSW region and base material on the advancing side, normal to the tensile stress axis, where lowest hardness was noticed, irrespective of the speed of tool rotation, welding speed, tool pin shape and composition.

2. The microscopic examination of the fracture surfaces demonstrated combined ductile and brittle fracture. It is distinguished by the formation of large dimples with tear ridges and partially smooth and shiny surface on fracture surface.

3. The fracture surface of aluminium alloys tested along the direction of weld revealed fine dimples and AlSiMg and other hard particles were located at the bottom of the dimple.

4. Maximum UTS has been attained for a speed of tool rotation of 1000 RPM and a welding speed of 20 mm/min irrespective of tool pin shape and composition of the alloy.

   a) **TPP tool**

   i. As the welding speed is increased from 10 to 20 mm/min, with the speed of tool rotation held constant, the UTS of the specimen welded using TPP tool increases and reaches a maximum value. Further increase in

the welding speed beyond 20 mm/min resulted in a decrease in the tensile strength.

ii. For a constant welding speed of 10 or 15 or 20 mm/min and an increase in the speed of tool rotation from 800 RPM to 1000 RPM, an increase in the tensile stress was observed. As the speed of tool rotation increases to 1200 RPM, the tensile stress decreases.

iii. The maximum weld connection efficiency of friction stir welded Al-10Mg-8Ce-3.5Si aluminium alloy was 81.2 % for a speed of tool rotation of 1000 RPM and a welding speed of 20 mm/min. The maximum weld connection efficiency of friction stir welded Al-5Mg-8Ce-3.5Si was 68.4 % for a speed of tool rotation of 1000 RPM and a welding speed of 20 mm/min.

iv. The weld connection efficiency increased by 21.3 % for an Al-10Mg-8Ce-3.5Si aluminium alloy and by 18.7 % for an Al-5Mg-8Ce-3.5Si aluminium alloy, when the tensile test was performed in the direction of weld.

b) SPP tool

i. Tensile stress increased when the speed of tool rotation was held constant and the welding speed was increased from 10 to 20 mm/min.

ii. With the welding speed being held constant and the speed of tool rotation being increased from 800 RPM to 1000 RPM, an increase in the tensile stress was noticed. Further increase in the speed of tool rotation to 1200 RPM, resulted in a decrease in the tensile strength.

iii. The maximum weld connection efficiency of friction stir welded Al-10Mg-8Ce-3.5Si aluminium alloy was 74.5 % for a speed of tool rotation of 1000 RPM and a welding speed of 20 mm/min. The maximum weld connection efficiency of friction stir welded Al-5Mg-8Ce-3.5Si aluminium alloy was 63.2 % for a speed of tool rotation of 1000 RPM and a welding speed of 20 mm/min.

iv. The weld connection efficiency increased by 15.2 % for an Al-10Mg-8Ce-3.5Si aluminium alloy and by 13.1 % for an Al-5Mg-8Ce-3.5Si

aluminium alloy, when the tensile test was performed in the direction of weld.

c) CPP tool

i. Maintaining a constant speed of tool rotation and varying the welding speed from 10 mm/min to 20 mm/min, the tensile stress increased.

ii. When the welding speed was held constant and the speed of tool rotation was raised from 800 RPM to 1000 RPM, the tensile stress increased. Further increase in the speed of tool rotation to 1200 RPM, resulted in the reduction of tensile strength.

iii. The maximum weld connection efficiency of friction stir welded Al-10Mg-8Ce-3.5Si aluminium alloy was 66.9 % for a speed of tool rotation of 1000 RPM and the welding speed of 20 mm/min. The maximum weld connection efficiency of friction stir welded Al-5Mg-8Ce-3.5Si aluminium alloy was 56.4 % for a speed of tool rotation of 1000 RPM and a welding speed of 20 mm/min.

iv. The weld connection efficiency increased by 10.1 % for Al-10Mg-8Ce-3.5Si aluminium alloy and by 8.0 % for an Al-5Mg-8Ce-3.5Si aluminium alloy when the tensile test was performed in the weld direction.

v. The fracture surface of the welded joints obtained with friction stir welding process along the weld direction showed smaller dimples. Fractured AlSiMg and $Al_{11}Ce_3$ hard particles were also observed.

Within the scope of the experimental work carried out, it has been found that the optimal condition to obtain best weld connection strength using FSW method is, a speed of tool rotation of 1000 RPM, welding speed of 20 mm/min, tool with square pin shape and Al-10Mg-8Ce-3.5Si aluminium alloy.

4.13.2.3 Analysis of process parameters using Taguchi design of experiment technique

1. Taguchi design of experiment technique is a systematic procedure. It is successfully adapted for analyzing the output of aluminium alloy joints of FSW.

2. It is an efficient and precise methodology of determining the welding process parameters. It is inferred that the Tool pin shape, Welding speed, Material composition and Speed of tool rotation have a substantial impact on the weld connection strength in that order.

3. An optimum combination of process parameters for the maximum UTS was obtained by making use of the Analysis of Variance (ANOVA) technique. A speed of tool rotation 1000RPM, a welding speed 20 mm/min, TPP tool and Al-10Mg-8Ce-3.5Si aluminium alloy were obtained as the optimum parameters of the process.

4. The experimental results confirm the validity test experiment with a maximum error of 5.89 %.

4.13.2.4 Prediction of mechanical properties using ANN model

4.13.2.4.1 ANN modelling for hardness prediction

1. The developed Artificial Neural Network model predicted successfully, the UTS, percentage elongation, and hardness of friction stir welded Al-10Mg-8Ce-3.5Si and Al-5Mg-8Ce-3.5Si aluminium alloy joints.

2. The relative percentage error for hardness ranges from -5.71% to +5.41% for the trained data.

3. The percentage of error for hardness for the validation data ranges from -5.29% to 0.71%.

4.13.2.4.2   ANN modelling for UTS and Percentage elongation prediction

1. Most of the predictions put forward by the ANN model for UTS are within the range of -7.34% to 8.09%.

2. The percentage of relative error predicted by ANN model for percentage elongation is within the range of 4.58% to 7.45%.

3. The developed ANN model accurately represents the correlation between the FSW process parameters and the mechanical properties.

The distinctive feature of the current research is the development of an ANN model which presents more accurate results as compared to the Taguchi technique. The prediction model revealed that the optimal condition to attain best weld connection strength using FSW method is obtained with Al-10Mg-8Ce-3.5Si aluminium alloy using TPP tool.

<div align="center">

* * * * * * *

</div>

CHAPTER 5

CONCLUSIONS AND SCOPE FOR FUTURE WORK

The Aluminium-Cerium-Silicon-Magnesium (Al-Ce-Si-Mg) alloy based aluminium alloys have gained extreme attention for their higher strength to weight ratio. But the welding of Al-Ce-Si-Mg alloys faced serious issues due to poor weldability and machinability. Friction stir welding (FSW) is found to be a viable alternative to conventional welding due to its solid-state welding. However very little information is available on FSW of Al-Ce-Si-Mg aluminium alloys. The present study elucidates on microstructural evolution, mechanical properties of aluminium alloy joints, and investigation on the effect of process parameters on mechanical properties. Taguchi Design of Experiments technique was adopted for arriving at an optimum level of input process parameters for maximization of output UTS of the process. Analysis of Variance (ANOVA) technique was used to predict the mechanical properties of the friction stir welded aluminium alloy for various combinations of the process parameters. The primary objective was to carry out the comparative analysis of structural and mechanical properties and to identify their relationship in aluminium alloy joints through friction stir welding. The secondary objective was to obtain defect free joints of aluminium alloys using different combination of rotational speed, welding speed and tool pin shapes. The aluminium alloys Al-10Mg-8Ce-3.5Si and Al-10Mg-8Ce-3.5Si were prepared by using stir casting process. The welding of these aluminium alloys was carried out on CNC vertical Machining Center with suitable attachments to perform the FSW operation.

5.1 CONCLUSIONS

1. It could be concluded from the FSW studies on Al-Ce-Si-Mg alloys that, the defect free joints are obtained by means of the FSW tool having concave shoulder with diameter equal to two and half times of base material thickness and diameter of the pin approximately equal to the base material thickness. It is found that, the increase in the dynamic to static ratio of pin profile leads to improvement in weld joint strength of the base material. It was also noticed that the tool pin shapes, speeds of tool rotation and speeds of welding have a bearing on the extent of defect free joints in friction stir welded aluminium alloys. It was also proved that the grain size at NZ is dependent on the speed of tool rotation, welding speed, tool pin shape and composition of the aluminium alloy.

2. From the micro-structure studies, it was asserted that the better equiaxed fine grain structure was formed at the NZ due to dynamic recrystallization, as compared to the grain size obtained for as-cast aluminium alloy. The grain size at the bottom of the NZ was found to be decreasing as compared to the top of the NZ, due to variation in the heat input condition. Numerous small broken AlSiMg and $Al_{11}Ce_3$ hard particles were found at the NZ due to stirring and abrasive action of the tool. During the study of mechanical properties of the FSW weld joint of Al-Ce-Si-Mg alloys, a variation in hardness shape was observed on the welded joint. Maximum hardness was found at NZ due to fine grain structure and smaller AlSiMg and $Al_{11}Ce_3$ particles. Minimum hardness was obtained at HAZ due to thermal effect during welding. During the tensile property analysis, it was found that, all the tensile specimens fractured at HAZ, where minimum hardness was obtained during hardness measurement. Also it was noticed that, the optimal weld joint strength was obtained for a speed of tool rotation of 1000 RPM, welding speed of 20 mm/min, tool of triangular pin shape and 10% (wt%) of Mg (Al-10Mg-8Ce-3.5Si) aluminium alloy.

3. The Taguchi orthogonal array-based design has shown that the tool pin shape has greater significance in increasing the weld joint strength, followed by welding speed, material composition and speed of tool rotation. The optimized weld parameters obtained from the Taguchi orthogonal array-based design have resulted

in relatively small percentage of error during validation test. An optimum combination of process parameters for the maximum UTS was attained by using the Analysis of Variance (ANOVA) technique. A speed of tool rotation 1000RPM, welding speed 20 mm/min, TPP tool and Al-10Mg-8Ce3.5Si aluminium alloy were identified as the optimum parameters of the process. The percentage contribution of each of the input process parameters on optimum output quality characteristics, i.e., Ultimate tensile stress (UTS) of the FSW weld joint was found to be maximum for tool pin shape at 43.23 %, followed by composition of the alloy at 25.06 %, welding speed at 18.32 % and speed of tool rotation at 6.15 %. The combined interaction effects among these input process parameters also had a small contribution of 1.34 % on the output UTS. The results obtained by the prediction model using regression equation showed that the value of UTS means predicted for maximization of UTS was about 110 MPa, whereas the UTS obtained from confirmation experiments was around 108.0 MPa, with a relative error of 1.8%, which lies well within the confidence interval of 95% suggested by the Taguchi design.

4. The developed ANN model seems to be very useful model to predict the mechanical properties of aluminium alloy joints produced by friction stir welding. The present work has shown that the prediction results with ANN are more superior to those predicted using statistical methods like Taguchi Techniques. ANN model has a better prediction accuracy compared to statistical prediction methods.

5.2 DIRECTIONS FOR FUTURE RESEARCH

The present research has revealed that the FSW can be efficiently adopted for joining of aluminium alloys, without affecting the chemical homogenization in the alloy. FSW produces less heat at weld region as compared to conventional welding process. Therefore, it eliminates defects related to solidification. The strength of weld joint is entirely dependent on the process parameters. Therefore, optimum values can be

deduced by statistical techniques. Further optimization of the method can also be achieved by ANN models.

The present study has given rise to following avenues for future work.

1. The improved tool pin shapes like threaded round, combined threaded with pin shapes like triangle, square, round etc., fluted pins with threads can be tried on present test materials to study the weld joint strength of the material. Changing the material of the present tools can also be analysed for the changed properties of the FSW weld joint produced. By varying the hardness of the tool, the quality of the weld joint can be studied. By varying the shoulder to pin diameter ratio, the performance of the weld joint can be evaluated. The developed tool can be used to modify the mechanical properties of the aluminium alloy using FSW technique for changing thickness of the material.

2. The developed ANN model can be used to predict the surface hardness of friction stir processed aluminium alloy. Online prediction of the weld joint strength can be achieved by incorporating intelligence through ANN technique with the help of data collection sensors.

3. Damping characteristics and wear behavior of the welded aluminium alloys also can be evaluated.

* * * * * * * *

REFERENCES

Abbas, A. A., and Abdulkadhum, H. H. (2019). "Optimization of Friction Stir Welding Process Parameters to joint 7075-T6 Aluminium Alloy by Utilizing Taguchi Technique." *J Eng*, 25(5), 1–15.

Adamowski, J., Gambaro, C., Lertora, E., Ponte, M., and Szkodo, M. (2007). "Analysis of FSW welds made of aluminium alloy AW6082-T6." *Arch Mater Sci Eng*, 28(8), 453–460.

Afrin, N., Chen, D. L., Cao, X., and Jahazi, M. (2008). "Microstructure and tensile properties of friction stir welded AZ31B magnesium alloy." *Mater Sci Eng A*, 472(1–2), 179–186.

Ahmed, M. M. Z., Ataya, S., El-Sayed, M. M. S., Ammar, H. R., and Ahmed, E. (2017). "Friction stir welding of similar and dissimilar AA7075 and AA5083." *J Mater Process Technol*, 242, 77–91.

Alidokht, S. A., Amir, A.-Z., Soleymani, S., Saeid, T., and Assadi, H. (2012). "Evaluation of microstructure and wear behavior of friction stir processed cast aluminum alloy." *Mater Charact*, 63, 90–97.

Allen, W. A. (2005). *Evaluation of friction spot welds in aluminum alloys. Trans SAE*.

Altenkirch, J., Steuwer, A., Peel, M. J., Withers, P. J., Williams, S. W., and Poad, M. (2008a). "Mechanical tensioning of high-strength aluminum alloy friction stir welds." *Metall Mater Trans A Phys Metall Mater Sci*, Springer, 3246–3259.

Altenkirch, J., Steuwer, A., Peel, M., Richards, D. G., and Withers, P. J. (2008b). "The effect of tensioning and sectioning on residual stresses in aluminium AA7749 friction stir welds." *Mater Sci Eng A*, 488(1–2), 16–24.

Amini, S., Amiri, M. R., and Barani, A. (2014). "Investigation of the effect of tool geometry on friction stir welding of 5083-O aluminum alloy." *Int J Adv Manuf Technol*, 76(1–4), 255–261.

Anjaneya, P. B., and Prasanna, P. (2013). "Experimental comparison of the MIG and

friction stir welding processes for AA 6061 (Al Mg Si Cu) aluminium alloy." *Int J Mining, Metall Mech Eng*, 1(2), 137–140.

Arbegast, W. J. (2008). "A flow-partitioned deformation zone model for defect formation during friction stir welding." *Scr Mater*, 58(5), 372–376.

Arora, A., Debroy, T., and Bhadeshia, H. K. D. H. (2011). "Back-of-the-envelope calculations in friction stir welding - Velocities, peak temperature, torque, and hardness." *Acta Mater*, 59(5), 2020–2028.

Arora, A., Mehta, M., De, A., and Debroy, T. (2012). "Load bearing capacity of tool pin during friction stir welding." *Int J Adv Manuf Technol*, 61(9–12), 911–920.

Asadi, P., Givi, M. K. B., Parvin, N., Araei, A., Taheri, M. S., and Tutunchilar, S. (2012). "On the role of cooling and tool rotational direction on microstructure and mechanical properties of friction stir processed AZ91." *Int J Adv Manuf Technol*, 63(9–12), 987–997.

ASM_Handbook_Vol-16. (1995). *ASM Handbook-Vol 16-Machining*. ASM International.

ASM. (2013). *ASM Handbook-Volume 4A Steel Heat Treating Fundamentals and Processes*. *ASM Int*.

ASM International. (1993a). *ASM handbook*.

ASM International. (1993b). *Aluminum and Aluminum Alloys - Handbook*. *ASM Int*.

ASTM_E112-12. (2012). *E112-12 : Standard Test Methods for Determining Average Grain Size*. *ASTM Int*, 1–27.

ASTM E8-04. (2013). *Standard Test Methods for Tension Testing of Metallic Materials*. *ASTM Int*, E8-04.

Atharifar, H., Lin, D., and Kovacevic, R. (2009). "Numerical and experimental investigations on the loads carried by the tool during friction stir welding." *J Mater Eng Perform*, 18(4), 339–350.

Atxaga, G., Pelayo, A., and Irisarri, A. M. (2001). "Effect of microstructure on fatigue

behaviour of cast Al-7Si-Mg alloy." *Mater Sci Technol*, 17(4), 446–450.

Aval, H. J. (2015a). "Influences of pin profile on the mechanical and microstructural behaviors in dissimilar friction stir welded AA6082-AA7075 butt Joint." *Mater Des*, 67, 413–421.

Aval, H. J. (2015b). "Microstructure and residual stress distributions in friction stir welding of dissimilar aluminium alloys." *Mater Des*, 87, 405–413.

Aydin, H., Bayram, A., Uğuz, A., and Akay, K. S. (2009). "Tensile properties of friction stir welded joints of 2024 aluminum alloys in different heat-treated-state." *Mater Des*, 30(6), 2211–2221.

Aydin, H., Tutar, M., Durmuş, A., Bayram, A., and Sayaca, T. (2012). "Effect of welding parameters on tensile properties and fatigue behavior of friction stir welded 2014-T6 aluminum alloy." *Trans Indian Inst Met*, 65(1), 21–30.

Azizieh, M., Kokabi, A. H., and Abachi, P. (2011). "Effect of rotational speed and probe profile on microstructure and hardness of AZ31/Al2O3 nanocomposites fabricated by friction stir processing." *Mater Des*, 32(4), 2034–2041.

Babu, K. K., Panneerselvam, K., Sathiya, P., Noorul, A. H., Sundarrajan, S., Mastanaiah, P., Murthy, S., and Chunduri, V. (2018). "Effects of various tool pin profiles on mechanical and metallurgical properties of friction stir welded joints of cryorolled AA2219 aluminium alloy." *Metall Res Technol*, 115(2), 14.

Babu, N., Karunakaran, N., and Balasubramanian, V. (2017). "A study to estimate the tensile strength of friction stir welded AA 5059 aluminium alloy joints." *Int J Adv Manuf Technol*, 93(1–4), 1–9.

Babu, S., Elangovan, K., Balasubramanian, V., Balasubramanian, M., Babu, S., and Balasubramanian, M. (2009). "Optimizing friction stir welding parameters to maximize tensile strength of AA2219 aluminum alloy joints." *Met Mater Int*, 15(2), 321–330.

Badarinarayan, H., Shi, Y., Li, X., and Okamoto, K. (2009). "Effect of tool geometry on hook formation and static strength of friction stir spot welded aluminum 5754-O sheets." *Int J Mach Tools Manuf*, 49(11), 814–823.

Bakavos, D., and Prangnell, P. B. (2009). "Effect of reduced or zero pin length and anvil insulation on friction stir spot welding thin gauge 6111 automotive sheet." *Sci Technol Weld Join*, 14(5), 443–456.

Balakrishnan, M., Dinaharan, I., Palanivel, R., and Sathiskumar, R. (2019). "In fluence of friction stir processing on microstructure and tensile behavior of AA6061 / Al3Zr cast aluminum matrix composites." *J Manuf Process*, 38(September 2018), 148–157.

Balasubramanian, N., Gattu, B., and Mishra, R. S. (2009). "Process forces during friction stir welding of aluminium alloys." *Sci Technol Weld Join*, 14(2), 141–145.

Balasubramanian, V. (2008). "Relationship between base metal properties and friction stir welding process parameters." *Mater Sci Eng A*, 480(1–2), 397–403.

Balasubramanian, V., and Lakshminarayanan, A. K. (2008). "The mechanical properties of the GMAW, GTAW and FSW joints of the RDE-40 aluminium alloy." *Int J Microstruct Mater Prop*, 3(6), 837–853.

Banik, A., Deb Barma, J., and Saha, S. C. (2019). "Effect of Threaded Pin Tool for Friction Stir Welding of AA6061-T6 at Varying Traverse Speeds: Torque and Force Analysis." *Iran J Sci Technol Trans Mech Eng*, 1–16.

Barcellona, A., Buffa, G., Fratini, L., and Palmeri, D. (2006). "On microstructural phenomena occurring in friction stir welding of aluminium alloys." *J Mater Process Technol*, 177(1–3), 340–343.

Barnes, T. A., and Pashby, I. R. (2000). "Joining techniques for aluminum spaceframes used in automobiles. Part I - solid and liquid phase welding." *J Mater Process Technol*, 99(1), 62–71.

Barnhisel, R., and Bertsch, P. M. (1982). *Aluminium-Methods of Soil Analysis. Part 2. Chemical and Microbiological Properties-Agronomy Monograph*.

Bassett, J. C., and Birley, S. S. (2000). "Friction stir welding of aluminium armour." *2nd Int Symp Frict Stir Weld (Gothenburg, Sweden)*.

Bergsma, S. C., Kassner, M. E., Li, X., and Wall, M. A. (1998). "Strengthening in the new aluminum alloy AA 6069." *Mater Sci Eng A*, 254(1–2), 112–118.

Besterfield, D. H., Besterfield, M. C., Besterfield, G., and Besterfield, M. S. (2011). *Total Quality Management*. Prentice Hall.

Bisadi, H., Tavakoli, A., Tour Sangsaraki, M., and Tour Sangsaraki, K. (2013). "The influences of rotational and welding speeds on microstructures and mechanical properties of friction stir welded Al5083 and commercially pure copper sheets lap joints." *Mater Des*, 43, 80–88.

Boonchouytan, W., Ratanawilai, T., and Muangjunburee, P. (2012). "Effect of pre/post heat treatment on the friction stir welded SSM 356 aluminum alloys." *Adv Mater Res*, 488–489, 328–334.

Boz, M., and Kurt, A. (2004). "The influence of stirrer geometry on bonding and mechanical properties in friction stir welding process." *Mater Des*, 25(4), 343–347.

Broek, D. (1973). "The role of inclusions in ductile fracture and fracture toughness." *Eng Fract Mech*, 5(1), 55–66.

Buffa, G., Fratini, L., and Micari, F. (2009). "A neural network based approach for the design of FSW processes." *Key Eng Mater*, 410–411(2009), 413–420.

Buffa, G., Hua, J., Shivpuri, R., and Fratini, L. (2006). "Design of the friction stir welding tool using the continuum based FEM model." *Mater Sci Eng A*, 419(2006), 381–388.

Çam, G. (2011). "Friction stir welded structural materials: Beyond Al-alloys." *Int Mater Rev*, 56(1), 1–48.

Çam, G., and İpekoğlu, G. (2017). "Recent developments in joining of aluminum alloys." *Int J Adv Manuf Technol*, 91(5–8), 1851–1866.

Çam, G., and Mistikoglu, S. (2014). "Recent developments in friction stir welding of al-Alloys." *J Mater Eng Perform*, 23(6), 1936–1953.

Çam, G., and Ventzke, V. (2000). "Characterization of laser and electron beam welded Al alloys." *Prakt Metallogr pascal-francisinist*, 37(2), 59-89.

Campbell, G., and Stotler, T. (1999). "Friction stir welding of armor grade aluminum

plate." *Weld J*, 78(12), 45–47.

Campbell, L. C. . J. (2006). *Manufacturing Technology for Aerospace Structural Materials*.

Canaby, J., Blazy, F., Fries, J., and Traverse, J. (1991). "Effects of high temperature surface reaction of aluminum-lithium alloy on the porosity of welded areas." *Mater Sci Eng A*, 136(1991), 131-139.

Cao, G. (2005). "Friction Stir Welding of 2219 Aluminum: Behavior of q (Al2Cu) particles." *J Am Soc Nav Eng*, 84(1), 1-S-8-S.

Carlone, P., and Palazzo, G. S. (2013). "Influence of Process Parameters on Microstructure and Mechanical Properties in AA2024-T3 Friction Stir Welding." *Metallogr Microstruct Anal*, 2(4), 213–222.

Casalino, G., Campanelli, S., and Mortello, M. (2014). "Influence of shoulder geometry and coating of the tool on the friction stir welding of aluminium alloy plates." *Procedia Eng*, 69(2014), 1541–1548.

Cavaliere, P., and Cerri, E. (2005). "Mechanical response of 2024-7075 aluminium alloys joined by Friction Stir Welding." *J Mater Sci*, 40(2005), 3669–3676.

Cavaliere, P., Nobile, R., Panella, F. W., and Squillace, A. (2006). "Mechanical and microstructural behaviour of 2024-7075 aluminium alloy sheets joined by friction stir welding." *Int J Mach Tools Manuf*, 46(6), 588–594.

Cavaliere, P., and Squillace, A. (2005). "High temperature deformation of friction stir processed 7075 aluminium alloy." *Mater Charact*, 55(2), 136–142.

Cederqvist, L., and Reynolds, A. P. (2001). "Factors affecting the properties of friction stir welded aluminum lap joints." *Weld J (Miami, Fla)*, 80(12).

Cerri, E., and Leo, P. (2013). "Influence of high temperature thermal treatment on grain stability and mechanical properties of medium strength aluminium alloy friction stir welds." *J Mater Process Technol*, 213(1), 75–83.

Ceschini, L., Boromei, I., Minak, G., Morri, A., and Tarterini, F. (2007). "Effect of

friction stir welding on microstructure, tensile and fatigue properties of the AA7005/10 vol.%Al2O3p composite." *Compos Sci Technol*, 67(3–4), 605–615.

Chakrabarti, D. J., and Laughlin, D. E. (2004). "Phase relations and precipitation in Al-Mg-Si alloys with Cu additions." *Prog Mater Sci*, 49(3–4), 389–410.

Charit, I., and Mishra, R. S. (2003). "High strain rate superplasticity in a commercial 2024 Al alloy via friction stir processing." *Mater Sci Eng A*, 359(1–2), 290–296.

Chauhan, K. P. S. (2017). "Influence of Heat Treatment on the Mechanical Properties of Aluminium Alloys (6xxx Series): A Literature Review." *Int J Eng Res*, 6(3), 386–389.

Chauhan, P., Jain, R., Pal, S. K., and Singh, S. B. (2018). "Modeling of defects in friction stir welding using coupled Eulerian and Lagrangian method." *J Manuf Process*, 34(1), 158–166.

Chen, G., Li, H., Wang, G., Guo, Z., Zhang, S., Dai, Q., Wang, X., Zhang, G., and Shi, Q. (2018). "Effects of pin thread on the in-process material flow behavior during friction stir welding: A computational fluid dynamics study." *Int J Mach Tools Manuf*, 124, 12–21.

Chen, G. Q., Shi, Q. Y., Li, Y. J., Sun, Y. J., Dai, Q. L., Jia, J. Y., Zhu, Y. C., and Wu, J. J. (2013). "Computational fluid dynamics studies on heat generation during friction stir welding of aluminum alloy." *Comput Mater Sci*, 79, 540–546.

Chen, H. Bin, Yan, K., Lin, T., Chen, S. Ben, Jiang, C. Y., and Zhao, Y. (2006). "The investigation of typical welding defects for 5456 aluminum alloy friction stir welds." *Mater Sci Eng A*, 433(1–2), 64–69.

Chen, Y., Li, H., Wang, X., Ding, H., and Zhang, F. (2019). "A Comparative Investigation on Conventional and Stationary Shoulder Friction Stir Welding of Al-7075 Butt-Lap Structure." *Metals (Basel)*, 9(12), 1264.

Chen, Z. W., Cui, S., and Z W Chen and S Cui. (2009). "Strain and strain rate during friction stir welding/processing of Al-7Si-0.3Mg alloy." *IOP Conf Ser Mater Sci Eng*, 4(1), 6.

Chien, C. H., Lin, W. B., and Chen, T. (2011). "Optimal FSW process parameters for aluminum alloys AA5083." *J Chinese Inst Eng Trans Chinese Inst Eng A*, 34(1), 99–105.

Chionopoulos, S. K., Sarafoglou, C. H. I., and Pantelis, D. I. (2008). "Effect of tool pin and welding parameters on friction stir welded (FSW) marine aluminum alloys." *Proc 3rd Int Conf Manuf Eng*, 1–3.

Chiteka, K. (2013). "Friction Stir Welding/Processing Tool Materials and Selection." *Int J Eng Res Technol*, 2(11), 8–18.

Chiteka, K. (2014). "Artificial Neural Networks in Tensile Strength and Input Parameter Prediction." *Int J Mech Eng Rob Res*, 3(1), 8.

Choi, D., Lee, C., Ahn, B., Choi, J., Yeon, Y., Song, K., Hong, S., Lee, W., Kang, K., and Jung, S. (2011). "Hybrid Friction Stir Welding of High-carbon Steel." *J Mater Sci Technol*, 27(2), 127–130.

Chowdhury, S. M., Chen, D. L., Bhole, S. D., and Cao, X. (2010). "Tensile properties of a friction stir welded magnesium alloy: Effect of pin tool thread orientation and weld pitch." *Mater Sci Eng A*, 527(21–22), 6064–6075.

Cole, E. G., Fehrenbacher, A., Duffie, N. A., Zinn, M. R., Pfefferkorn, F. E., and Ferrier, N. J. (2014). "Weld temperature effects during friction stir welding of dissimilar aluminum alloys 6061-t6 and 7075-t6." *Int J Adv Manuf Technol*, 71(1–4), 643–652.

Colegrove, P. A., and Shercliff, H. R. (2003). "Experimental and numerical analysis of aluminium alloy 7075-T7351 friction stir welds." *Sci Technol Weld Join*, 8(5), ISSN: 1362-1718 (Print) 1743-2936 (Online) Journal.

Colegrove, P. A., and Shercliff, H. R. (2004). "Two-dimensional CFD modelling of flow round profiled FSW tooling." *Sci Technol Weld Join*, 9(6), 483–492.

Colegrove, P. A., and Shercliff, H. R. (2005). "3-Dimensional CFD modelling of flow round a threaded friction stir welding tool profile." *J Mater Process Technol*, 169(2), 320–327.

Colegrove, P. A., and Shercliff, H. R. (2017). "Development of Trivex friction stir welding tool Part 2 – three-dimensional flow modelling Development of Trivex friction stir welding tool Part 2 – three-dimensional flow modelling." *Sci Technol Weld Join*, 9(4), 352–361.

Colegrove, P. A., Shercliff, H. R., Colegrove, P. A., and Shercliff, H. R. (2006). "CFD modelling of friction stir welding of thick plate 7449 aluminium alloy CFD modelling of friction stir welding of thick plate 7449 aluminium alloy." *Sci Technol Weld Join*, 11(4), 429–441.

Colligan, K. (1999). "Material flow behavior during friction stir welding of aluminum." *Weld J (Miami, Fla)*, 78(7), 229-s.

Collins, J. (1993). *Failure of materials in mechanical design: analysis, prediction, prevention*.

Commin, L., Dumont, M., Rotinat, R., Pierron, F., Masse, J. E., and Barrallier, L. (2012). "Influence of the microstructural changes and induced residual stresses on tensile properties of wrought magnesium alloy friction stir welds." *Mater Sci Eng A*, 551, 288–292.

Coniglio, N., Cross, C. E., Michael, T., and Lammers, M. (2008). "Defining a critical weld dilution to avoid solidification cracking in aluminum." *Weld J (Miami, Fla)*, 87(9), 12.

Cotell, C. M., Sprague, J. A., and Smidt, F. A. J. (1994). *ASM Handbook - Surface Engineering*. (C. M. Cotell, J. A. Sprague, and F. A. Smidt, eds.), ASM International.

Cramer, S. D., and Covino, B. S. J. (2003). *ASM Handbook-Corrosion: Fundamentals, Testing, and Protection Volume 13A. ASM Int Handb Comm Stephen*.

D'Souza, A. D., Rao, S. S., and Herbert, M. A. (2019a). "Evaluation of Microstructure, Hardness and Mechanical Properties of Friction Stir Welded Al–Ce–Si–Mg Aluminium Alloy." *Met Mater Int*, 26(9), 10.

D'Souza, A. D., Rao, S. S., and Herbert, M. A. (2019b). "Assessment of influence of process parameters on properties of friction stir welded Al-Ce-Si-Mg aluminium alloy."

Mater Res Express, 6(8), 13.

Dahle, A. K., Lee, Y. C., Nave, M. D., Schaffer, P. L., and StJohn, D. H. (2001). "Development of the as-cast microstructure in magnesium-aluminium alloys." *J Light Met*, 1(1), 61–72.

Darvishi, A., Maleki, A., Mazar Atabaki, M., and Zargami, M. (2010). "The mutual effect of iron and manganese on microstructure and mechanical properties of aluminium –silicon alloy." *Metal Metall*, 16(1), 11–24.

Das, B., Pal, S., and Bag, S. (2015). "Monitoring of Weld Quality in Friction Stir Welding Based on Spindle Speed and Motor Current Signals." *Adv Mater Form Join*, 233–253.

Das, D., Pal, A. R., Das, A. K., Pratihar, D. K., and Roy, G. G. (2019). "Nature-Inspired Optimization Algorithm-Tuned Feed-Forward and Recurrent Neural Networks Using CFD-Based Phenomenological Model-Generated Data to Model the EBW Process." *Arab J Sci Eng*, 19.

Davis, J. R. (2001). *Aluminum and Aluminum Alloys*. ASM International.

Dawes, C. J. (1996). "Friction stir process welds aluminium alloys: The process produces low-distortion, high-quality, low-cost welds on aluminium." *Weld J*, 75(3), 41–45.

Dawes, M. G., Karger, S. A., and Dickerson, T. L. (2000). "Strength and fracture toughness of friction stir welds in aluminum alloys." *Proc 2nd Int Frict Stir Weld Symp 2000 Jun*.

DebRoy, T., and Bhadeshia, H. K. D. H. D. H. (2010). "Friction stir welding of dissimilar alloys - A perspective." *Sci Technol Weld Join*, 15(4), 266–270.

Debroy, T., De, A., Bhadeshia, H. K. D. H., Manvatkar, V. D., and Arora, A. (2012). "Tool durability maps for friction stir welding of an aluminium alloy." *Proc R Soc A Math Phys Eng Sci*, 468(2147), 3552–3570.

Defalco, J. (2009). "Friction Stir Process-Now Welds Steel Pipe." *Weld J*, (May), 44–48.

284

Dehnad, K. (1990). *Quality Control, Robust Design and the Taguchi Method.* (A. &T B. L. Khosrow Dehnad, ed.), Wadsworth & Brooks/Cole Advanced Books & Software, Pacific Grove, California.

Denquin, A., Allehaux, D., Campagnac, M. H., and Lapasset, G. (2002). "Influence of the initial ageing condition on microstructure and properties of a Friction Stir Welded 6056 alloy." *Mater Sci Forum*, 396–402(2), 1199–1204.

Derry, C. G., and Robson, J. D. (2008). "Characterisation and modelling of toughness in 6013-T6 aerospace aluminium alloy friction stir welds." *Mater Sci Eng A*, 490(1–2), 328–334.

Dewan, M. W., Huggett, D. J., Warren Liao, T., Wahab, M. A., and Okeil, A. M. (2016). "Prediction of tensile strength of friction stir weld joints with adaptive neuro-fuzzy inference system (ANFIS) and neural network." *Mater Des*, 92, 288–299.

Dickerson, T. L., and Przydatek, J. (2003). "Fatigue of friction stir welds in aluminium alloys that contain root flaws." *Int J Fatigue*, 25(12), 1399–1409.

Din, T., and Campbell, J. (1996). "High strength aerospace aluminium casting alloys: A comparative study." *Mater Sci Technol*, 12(8), 644–650.

Dinaharan, I., Kalaiselvan, K., Vijay, S. J., and Raja, P. (2012). "Effect of material location and tool rotational speed on microstructure and tensile strength of dissimilar friction stir welded aluminum alloys." *Arch Civ Mech Eng*, 12(4), 446–454.

Dong, P., Li, H., Sun, D., Gong, W., and Liu, J. (2013). "Effects of welding speed on the microstructure and hardness in friction stir welding joints of 6005A-T6 aluminum alloy." *Mater Des*, 45(1), 524–531.

Dong, X., Amirkhanlou, S., and Ji, S. (2019). "Formation of strength platform in cast Al – Si – Mg – Cu alloys." *Sci Rep*, 1–11.

Donne, C., Biallas, G., Ghidini, T., and Sveden, G. R. (2000). "Effect of weld imperfections and residual stresses on the fatigue crack propagation in friction stir welded joints." *Second Int Conf Frict stir Weld*, 26–28.

Doude, H. R., Schneider, J. A., and Nunes, A. C. (2014). "Influence of the tool shoulder

contact conditions on the material flow during friction stir welding." *Metall Mater Trans A Phys Metall Mater Sci*, 45(10), 4411–4422.

Doude, H., Schneider, J., Patton, B., Stafford, S., Waters, T., and Varner, C. (2015). "Optimizing weld quality of a friction stir welded aluminum alloy." *J Mater Process Technol*, 222(2015), 188–196.

Dracup, B. J., and Arbegast, W. J. (1999). "Friction stir welding as a rivet replacement technology." *SAE Tech Pap*, (724).

Dursun, T., and Soutis, C. (2014). "Recent developments in advanced aircraft aluminium alloys." *Mater Des*, 56(2014), 862–871.

Dwivedi, S. P. (2014). "Effect of process parameters on tensile strength of friction stir welding A356/C355 aluminium alloys joint." *J Mech Sci Technol*, 28(1), 285–291.

E. Taban, E. K. (2013). "Comparison between microstructure characteristics and joint performance of AZ31 magnesium alloy welded by TIG and friction stir welding (FSW) processes." *Kov Mater*, 51(3), 197–203.

El-Rayes, M. M., and El-Danaf, E. A. (2012). "The influence of multi-pass friction stir processing on the microstructural and mechanical properties of Aluminum Alloy 6082." *J Mater Process Technol*, 212(5), 1157–1168.

Elangovan, K., and Balasubramanian, V. (2008a). "Influences of tool pin profile and tool shoulder diameter on the formation of friction stir processing zone in AA6061 aluminium alloy." *Mater Des*, 29(2), 362–373.

Elangovan, K., and Balasubramanian, V. (2008b). "Influences of tool pin profile and welding speed on the formation of friction stir processing zone in AA2219 aluminium alloy." *J Mater Process Technol*, 200(1–3), 163–175.

Elangovan, K., Balasubramanian, V., and Babu, S. (2009). "Predicting tensile strength of friction stir welded AA6061 aluminium alloy joints by a mathematical model." *Mater Des*, 30(1), 188–193.

Elangovan, K., Balasubramanian, V., and Valliappan, M. (2008a). "Effect of Tool Pin Profile and Tool Rotational Speed on Mechanical Properties of Friction Stir Welded

AA6061 Aluminium Alloy." *Mater Manuf Process*, 23(3), 251–260.

Elangovan, K., Balasubramanian, V., and Valliappan, M. (2008b). "Influences of tool pin profile and axial force on the formation of friction stir processing zone in AA6061 aluminium alloy." *Int J Adv Manuf Technol*, 38(3–4), 285–295.

Elatharasan, G., and Kumar, V. S. S. (2013). "An Experimental Analysis and Optimization of Process Parameter on Friction Stir Welding of AA 6061-T6 Aluminum Alloy using RSM." *Procedia Eng*, 64(2013), 1227–1234.

Enjo, T., and Kuroda, T. (1982). "Title Microstructure in Weld Heat Affected Zone of Al-Mg-Si Alloy (Materials Metallurgy and Weldability)." *Trans JWRI*, 11(1), 61–66.

Enright, P. G. (1987). "Casting aluminium alloys."

Eskin, D. G., Suyitno, and Katgerman, L. (2004). "Mechanical properties in the semi-solid state and hot tearing of aluminium alloys." *Prog Mater Sci*, 49(5), 629–711.

Feng, A. H., Chen, D. L., and Ma, Z. Y. (2009). "Effect of welding parameters on microstructure and tensile properties of friction stir welded 6061 AL joints." *Mater Sci Forum*, 618 619, 41–44.

Feng, A. H., Chen, D. L., and Ma, Z. Y. (2010). "Microstructure and cyclic deformation behavior of a friction-stir-welded 7075 al alloy." *Metall Mater Trans A Phys Metall Mater Sci*, 41(4), 957–971.

Feng, J. C., Chen, Y. C., and Liu, H. J. (2006). "Effects of post-weld heat treatment on microstructure and mechanical properties of friction stir welded joints of 2219-O aluminium alloy." *Mater Sci Technol*, 22(1), 86–90.

Fernandez et al. (2010). "Friction stir welding (FSW) methods and systems and friction stir welded components made thereby."

Field, D. J., and Moran, G. (1985). "Heat treatment of aluminium alloys."

Filippis, D. L. A. C., Serio, L. M., Facchini, F., Mummolo, G., and Ludovico, A. D. (2016). "Prediction of the vickers microhardness and ultimate tensile strength of AA5754 H111 friction stir welding butt joints using artificial neural network."

Materials (Basel), 9(11), 17.

Flemings, M. C., Niyama, E., and Taylor, H. F. (1961). "Fluidity of Aluminum Alloys: An Experimental and Quantitative Evaluation." *Trans Am Foundrymen's Soc*, 69, 625–635.

Fonda, R. W., and Bingert, J. F. (2006). "Precipitation and grain refinement in a 2195 Al friction stir weld." *Metall Mater Trans A Phys Metall Mater Sci*, 37(12), 3593–3604.

Fonda, R. W., Bingert, J. F., and Colligan, K. J. (2004). "Development of grain structure during friction stir welding." *Scr Mater*, 51(3), 243–248.

Fratini, L., and Buffa, G. (2005). "CDRX modelling in friction stir welding of aluminium alloys." *Int J Mach Tools Manuf*, 45(10), 1188–1194.

Fratini, L., and Buffa, G. (2007). "Continuous dynamic recrystallization phenomena modelling in friction stir welding of aluminium alloys: A neural-network-based approach." *Proc Inst Mech Eng Part B J Eng Manuf*, 221(5), 857–864.

Fratini, L., Buffa, G., and Palmeri, D. (2009). "Using a neural network for predicting the average grain size in friction stir welding processes." *Comput Struct*, 87(17–18), 1166–1174.

Fu, R. D., Zhang, J. F., Li, Y. J., Kang, J., Liu, H. J., and Zhang, F. C. (2013). "Effect of welding heat input and post-welding natural aging on hardness of stir zone for friction stir-welded 2024-T3 aluminum alloy thin-sheet." *Mater Sci Eng A*, 559, 319–324.

Fujii, H., Cui, L., Maeda, M., and Nogi, K. (2006). "Effect of tool shape on mechanical properties and microstructure of friction stir welded aluminum alloys." *Mater Sci Eng A*, 419, 25–31.

Fukuda, T. (2000). "Friction stir welding (FSW) process." *J Japan Weld Soc*, 69(7), 6–10.

Gallais, C., Denquin, A., Bréchet, Y., and Lapasset, G. (2008). "Precipitation microstructures in an AA6056 aluminium alloy after friction stir welding: Characterisation and modelling." *Mater Sci Eng A*, 496(1–2), 77–89.

288

Ghanem, M. M., Bahaitham, H., and El-Morsy, A.-W. (2018). "Effect of Friction Stir Welding Parameters on the Microstructure and Mechanical Properties of AA2024-T4 Aluminum Alloy." *Eng Technol Appl Sci Res*, 8(1), 2493–2498.

Gharaibeh, N., Al-Jarrah, J. A., and Sawalha, S. A. (2016). "Effect of Pin Profile on Mechanical Properties of 6061 Al Alloy Welded Joints Prepared by Friction Stir Welding." *Int J Mech Appl*, 6(August), 39–42.

Ghazanfar, B., Awang, M., Khan, S. R., and Fawad, H. (2013). "Development of a new approach for incorporating tool tilting in friction stir welding." *Adv Mater Res*, 701, 378–381.

Ghetiya, N. D., and Patel, K. M. (2014). "Prediction of Tensile Strength in Friction Stir Welded Aluminium Alloy Using Artificial Neural Network." *Procedia Technol*, 14(October), 274–281.

Ghetiya, N. D., Patel, K. M., and Kavar, A. J. (2016). "Multi-objective Optimization of FSW Process Parameters of Aluminium Alloy Using Taguchi-Based Grey Relational Analysis." *Trans Indian Inst Met*, 69(4), 917–923.

Ghosh, M., Kumar, K., Kailas, S. V., and Ray, A. K. (2010). "Optimization of friction stir welding parameters for dissimilar aluminum alloys." *Mater Des*, 31(6), 3033–3037.

Gibson, B. T., Lammlein, D. H., Prater, T. J., Longhurst, W. R., Cox, C. D., Ballun, M. C., Dharmaraj, K. J., Cook, G. E., and Strauss, A. M. (2014). "Friction stir welding: Process, automation, and control." *J Manuf Process*, 16(1), 56–73.

Gittos, N. F., and Scott, M. H. (1981). *Heat affected zone cracking of Al-Mg-Si alloys. Pascal-francis.inist.fr*.

Goel, P., Siddiquee, A. N., Khan, N. Z., Hussain, M. A., Khan, Z. A., Abidi, M. H., and Al-Ahmari, A. (2018). "Investigation on the effect of tool pin profiles on mechanical and microstructural properties of friction stir butt and scarf welded aluminium alloy 6063." *Metals (Basel)*, 8(1), 1–15.

Golezani, A. S., Barenji, R. V., Heidarzadeh, A., and Pouraliakbar, H. (2015). "Elucidating of tool rotational speed in friction stir welding of 7020-T6 aluminum

alloy." *Int J Adv Manuf Technol*, 81(5–8), 1155–1164.

Gori, Y., and Uniyal, S. (2015). "Study of Al Alloys Weldability for Higher Strength and Low Heat Affected." *Status Weld Res Adv Anal Welded Struct*, (Feb.), 6.

Gratecap, F., Girard, M., Marya, S., and Racineux, G. (2012). "Exploring material flow in friction stir welding: Tool eccentricity and formation of banded structures." *Int J Mater Form*, 5(2), 99–107.

Grjotheim, K., Krohn, C., Malinovsky, M., and Matiasovsky, K. (1977). *Aluminum Electrolysis. The Chemistry of the Hall-Heroult Process*.

Grujicic, M., Arakere, G., Yalavarthy, H. V., He, T., Yen, C. F., and Cheeseman, B. A. (2010). "Modeling of AA5083 material-microstructure evolution during butt friction-stir welding." *J Mater Eng Perform*, 19(5), 672–684.

Guangzong, X., Xingwu, L., Bin, Z., Suyong, W., Hongchang, Z., and Wenxue, C. (2010). "Artificial Neural Network and Genetic Algorithm." *Springer Comput Sci*, (May 2015).

Guerdoux, S., and Fourment, L. (2009). "A 3D numerical simulation of different phases of friction stir welding." *Model Simul Mater Sci Eng*, 17(7).

Guerra, M., Schmidt, C., Mcclure, J. C., Murr, L. E., and Nunes, A. C. (2003). "Flow patterns during friction stir welding." *Mater Charact*, 49(1), 95–101.

Gungor, B., Kaluc, E., Taban, E., and Sik, A. (2014). "Mechanical, fatigue and microstructural properties of friction stir welded 5083-H111 and 6082-T651 aluminum alloys." *Mater Des*, 56, 84–90.

Guo, J. F., Chen, H. C., Sun, C. N., Bi, G., Sun, Z., and Wei, J. (2014). "Friction stir welding of dissimilar materials between AA6061 and AA7075 Al alloys effects of process parameters." *Mater Des*, 56, 185–192.

Gupta, S. K., Pandey, K. N., and Kumar, R. (2018a). "Multi-objective optimization of friction stir welding process parameters for joining of dissimilar AA5083/AA6063 aluminum alloys using hybrid approach." *Proc Inst Mech Eng Part L J Mater Des Appl*, 232(4), 343–353.

Gupta, S. K., Pandey, K. N., and Kumar, R. (2018b). "Artificial intelligence-based modelling and multi-objective optimization of friction stir welding of dissimilar AA5083-O and AA6063-T6 aluminium alloys." *Proc Inst Mech Eng Part L J Mater Des Appl*, 232(4), 333–342.

Habibnia, M., Shakeri, M., Nourouzi, S., Karimi, N., and Nourouzi, S. (2012). "Effect of tool rotation speed and feed rate on friction stir welding of 1100 aluminum alloy to carbon steel." *Adv Mater Res Tech Publ*, 445(1), 741–746.

Hamilton, C., Dymek, S., and Blicharski, M. (2008a). "A model of material flow during friction stir welding." *Mater Charact*, 59(9), 1206–1214.

Hamilton, C., Dymek, S., and Sommers, A. (2008b). "A thermal model of friction stir welding in aluminum alloys." *Int J Mach Tools Manuf*, 48(10), 1120–1130.

Han, B., Huang, Y., Lv, S., Wan, L., Feng, J., and Fu, G. (2013). "AA7075 bit for repairing AA2219 keyhole by filling friction stir welding." *Mater Des*, 51, 25–33.

Han, M. S., Lee, S. J., Park, J. C., Ko, S. C., Woo, Y. Bin, and Kim, S. J. (2009). "Optimum condition by mechanical characteristic evaluation in friction stir welding for 5083-O Al alloy." *Trans Nonferrous Met Soc China (English Ed*, 19(SUPPL. 1), s17–s22.

Hao, H. L., Ni, D. R., Huang, H., Wang, D., Xiao, B. L., Nie, Z. R., and Ma, Z. Y. (2013a). "Effect of welding parameters on microstructure and mechanical properties of friction stir welded Al-Mg-Er alloy." *Mater Sci Eng A*, 559, 889–896.

Hao, H. L., Ni, D. R., Zhang, Z., Wang, D., Xiao, B. L., and Ma, Z. Y. (2013b). "Microstructure and mechanical properties of Al-Mg-Er sheets jointed by friction stir welding." *Mater Des*, 52, 706–712.

Hasan, M., Abdi, R., and Akbari, M. (2013). "Modelling and Pareto optimization of mechanical properties of friction stir welded AA7075 / AA5083 butt joints using neural network and particle swarm algorithm." *Mater Des J*, 44, 190–198.

Hasan, M. M., Ishak, M., and Rejab, M. R. M. (2018). "Effect of pin tool flute radius on the material flow and tensile properties of dissimilar friction stir welded aluminum

alloys." *Int J Adv Manuf Technol*, 98(9–12), 2747–2758.

Hassan, K. A. A., Norman, A. F., Price, D. A., and Prangnell, P. B. (2003a). "Stability of nugget zone grain structures in high strength Al-alloy friction stir welds during solution treatment." *Acta Mater*, 51(7), 1923–1936.

Hassan, K. A. A., Prangnell, P. B., Norman, A. F., Price, D. A., and Williams, S. W. (2003b). "Effect of welding parameters on nugget zone microstructure and properties in high strength aluminium alloy friction stir welds." *Sci Technol Weld Join*, 8(4), 257–268.

Hattingh, D. G., Blignault, C., Niekerk, T. I. van, James, M. N., Niekerk, T. I. Van, and James, M. N. (2008). "Characterization of the influences of FSW tool geometry on welding forces and weld tensile strength using an instrumented tool." *J Mater Process Technol*, 3(1–3), 46–57.

Hawksworth, A., Rainforth, W. M., and Jones, H. (1999). "Solidification microstructure selection in the Al-rich Al-La, Al-Ce and Al-Nd systems." *J Cryst Growth*, 197(1–2), 286–296.

Haykin, S. (2007). *Neural networks: a comprehensive foundation*.

He, Z. B., Peng, Y. Y., Yin, Z. M., and Lei, X. F. (2011). "Comparison of FSW and TIG welded joints in Al-Mg-Mn-Sc-Zr alloy plates." *Trans Nonferrous Met Soc China (English Ed*, 21(8), 1685–1691.

Heidarzadeh, A., Barenji, R. V., Esmaily, M., and Ilkhichi, A. R. (2015). "Tensile Properties of Friction Stir Welds of AA 7020 Aluminum Alloy." *Trans Indian Inst Met*, 68(5), 757–767.

Heidarzadeh, A., Khodaverdizadeh, H., Mahmoudi, A., and Nazari, E. (2012). "Tensile behavior of friction stir welded AA 6061-T4 aluminum alloy joints." *Mater Des*, 37(2012), 166–173.

Heinz, A., Haszler, A., Keidel, C., Moldenhauer, S., Benedictus, R., and Miller, W. S. (2000). "Recent development in aluminium alloys for aerospace applications." *Mater Sci Eng A*, 280(1), 102–107.

Heinz, B., and Skrotzki, B. (2002). "Characterization of a friction-stir-welded aluminum alloy 6013." *Metall Mater Trans B Process Metall Mater Process Sci*, 33(3), 489–498.

Herbert, M. A., Shettigar, A. K., Nigalye, A. V, and Rao, S. S. (2016). "Investigation on microstructure and mechanical properties of Friction Stir Welded AA6061-4 . 5Cu-10SiC composite." *Mater Sci Eng*, 114(1), 1–9.

Heurtier, P., Jones, M. J., Desrayaud, C., Driver, J. H., Montheillet, F., and Allehaux, D. (2006). "Mechanical and thermal modelling of Friction Stir Welding." *J Mater Process Technol*, 171, 348–357.

Hind, A. R., Bhargava, S. K., and Grocott, S. C. (1999). "The surface chemistry of Bayer process solids: A review." *Colloids Surfaces A Physicochem Eng Asp*, Elsevier.

Hirasawa, S., Badarinarayan, H., Okamoto, K., Tomimura, T., and Kawanami, T. (2010). "Analysis of effect of tool geometry on plastic flow during friction stir spot welding using particle method." *J Mater Process Technol*, 210(11), 1455–1463.

Hirata, T., Oguri, T., Hagino, H., Tanaka, T., Chung, S. W., Takigawa, Y., and Higashi, K. (2007). "Influence of friction stir welding parameters on grain size and formability in 5083 aluminum alloy." *Mater Sci Eng A*, 456(1–2), 344–349.

Hirsch, J. (2014). "Recent development in aluminium for automotive applications." *Trans Nonferrous Met Soc China (English Ed*, 24(7), 1995–2002.

Hirsch, J., and Lücke, K. (1988). "Overview no. 76. Mechanism of deformation and development of rolling textures in polycrystalline f.c.c. metals-I. Description of rolling texture development in homogeneous CuZn alloys." *Acta Metall*, 36(11), 2863–2882.

Hou, X., Yang, X., Cui, L., and Zhou, G. (2014). "Influences of joint geometry on defects and mechanical properties of friction stir welded AA6061-T4 T-joints." *Mater Des*, 53, 106–117.

Hovanski, Y., Upadhyay, P., Carsley, J., Luzanski, T., Carlson, B., Eisenmenger, M., Soulami, A., Marshall, D., Landino, B., and Hartfield-Wunsch, S. (2015). "High-speed friction-stir welding to enable aluminum tailor-welded blanks." *JOM*, 67(5), 1045–

1053.

Hoyos, E., López, D., and Alvarez, H. (2016). "A phenomenologically based material flow model for friction stir welding." *Mater Des*, 111, 321–330.

Hu, Z. L., Wang, X. S., Pang, Q., Huang, F., Qin, X. P., and Hua, L. (2015). "The effect of postprocessing on tensile property and microstructure evolution of friction stir welding aluminum alloy joint." *Mater Charact*, 99, 180–187.

Hu, Z. L., Wang, X. S., and Yuan, S. J. (2012a). "Quantitative investigation of the tensile plastic deformation characteristic and microstructure for friction stir welded 2024 aluminum alloy." *Mater Charact*, 73, 114–123.

Hu, Z. L., Yuan, S. J., Wang, X. S., Liu, G., and Liu, H. J. (2012b). "Microstructure and mechanical properties of Al-Cu-Mg alloy tube fabricated by friction stir welding and tube spinning." *Scr Mater*, 66(7), 427–430.

Huang, G., Wu, J., and Shen, Y. (2018a). "A strategy for improving the mechanical properties of FSWed joints of non-heat-treatable Al alloys through a combination of water cooling and particle addition." *J Manuf Process*, 34(March), 667–677.

Huang, Y., Meng, X., Wang, Y., Xie, Y., and Zhou, L. (2018b). "Joining of aluminum alloy and polymer via friction stir lap welding." *J Mater Process Technol*, 257(March), 148–154.

Huang, Y., Meng, X., Zhang, Y., Cao, J., and Feng, J. (2017). "Micro friction stir welding of ultra-thin Al-6061 sheets." *J Mater Process Technol*, 250, 313–319.

Huang, Y. X., Han, B., Tian, Y., Liu, H. J., Lv, S. X., Feng, J. C., Leng, J. S., and Li, Y. (2011). "New technique of filling friction stir welding." *Sci Technol Weld Join*, 16(6), 497–501.

Ikuta, A., Yin, Y. H., and North, T. H. (2012). "Influence of tool thread on mechanical properties of dissimilar Al alloy friction stir spot welds." *Sci Technol Weld Join*, 17(8), 622–629.

Ilangovan, M., Boopathy, S. R., and Balasubramanian, V. (2015a). "Microstructure and tensile properties of friction stir welded dissimilar AA6061-AA5086 aluminium alloy

joints." *Trans Nonferrous Met Soc China (English Ed*, 25(4), 1080–1090.

Ilangovan, M., Boopathy, S. R., and Balasubramanian, V. (2015b). "Effect of tool pin profile on microstructure and tensile properties of friction stir welded dissimilar AA 6061–AA 5086 aluminium alloy joints." *Def Technol*, 11(2), 174–184.

Ilkhichi, A. R., Soufi, R., Hussain, G., Barenji, R. V., and Heidarzadeh, A. (2015). "Establishing Mathematical Models to Predict Grain Size and Hardness of the Friction Stir-Welded AA 7020 Aluminum Alloy Joints." *Metall Mater Trans B Process Metall Mater Process Sci*, 46B(1), 357–365.

Ilyushenko, R., and Nesterenkov, V. (2006). "Novel technique for joining of thick section difficult-to-weld aluminium alloys." *Mater Sci Forum*, 519–521(PART 2), 1125–1130.

Jain, R., Kumari, K., Kesharwani, Ram Kumar Kumar, S., Pal, S. K., Singh, S. B., Panda, S. K., and Samantaray, A. K. (2015). *Friction Stir Welding: Scope and Recent Development*. Springer International Publishing Switzerland 2015.

Jamshidi Aval, H., Serajzadeh, S., Kokabi, A. H., and Loureiro, A. (2011). "Effect of tool geometry on mechanical and microstructural behaviours in dissimilar friction stir welding of AA 5086–AA 6061." *Sci Technol Weld Join*, 16(7), 597–604.

Jannet, S., Mathews, K., Raja, R., Mathews, P. K., and Raja, R. (2014). "Comparative investigation of friction stir welding and fusion welding of 6061 T6 – 5083 O aluminum alloy based on mechanical properties and microstructure." *Bull polish Acad Sci*, 62(4), 791–795.

Jaradeh, M., and Carlberg, T. (2007). "Light metals 2007 : proceedings of the technical sessions presented by the TMS Aluminum Committee at the TMS 2007 Annual Meeting & Exhibition : Orlando, Florida, USA, February 25 - March 1, 2007." *Light Met 2007 Proc Tech Sess Present by TMS Alum Comm TMS 2007 Annu Meet Exhib Orlando, Florida, USA, Febr 25 - March 1, 2007*, 679–684.

Jarrett, N. (1987). *Future Developments in the Bayer--Hall--Heroult Process*.

Jata, K. V. (2000). "Friction stir welding of high strength aluminum alloys." *Mater Sci*

Forum, 331(1), 1701–1712.

Jayaraman, M., and Balasubramanian, V. (2013). "Effect of process parameters on tensile strength of friction stir welded cast A356 aluminium alloy joints." *Trans Nonferrous Met Soc China (English Ed*, 23(3), 605–615.

Jayaraman, M., Sivasubramanian, R., and Balasubramanian, V. (2010). "Establishing relationship between the base metal properties and friction stir welding process parameters of cast aluminium alloys." *Mater Des*, 31(9), 4567–4576.

Jayaraman, M., Sivasubramanian, R., Balasubramanian, V., and Lakshminarayanan, A. K. (2009a). "Optimization of process parameters for friction stir welding of cast aluminium alloy A319 by Taguchi method." *J Sci Ind Res (India)*, 68(1), 36–43.

Jayaraman, M., Sivasubramanian, R., Balasubramanian, V., and Lakshminarayanan, A. K. (2009b). "Application of RSM and ANN to predict the tensile strength of Friction Stir Welded A319 cast aluminium alloy." *Int J Manuf Res*, 4(3), 306–323.

Jazaeri, H., and Humphreys, F. J. (2004). "The transition from discontinuous to continuous recrystallization in some aluminium alloys I - The deformed state." *Acta Mater*, 52(11), 3239–3250.

Ji, S. D., Meng, X. C., Li, Z. W., Ma, L., and Gao, S. S. (2016a). "Investigation of vertical compensation friction stir-welded 7N01-T4 aluminum alloy." *Int J Adv Manuf Technol*, 84(9–12), 2391–2399.

Ji, S. D., Meng, X. C., Ma, L., and Gao, S. S. (2016b). "Effect of groove distribution in shoulder on formation, macrostructures, and mechanical properties of pinless friction stir welding of 6061-O aluminum alloy." *Int J Adv Manuf Technol*, 87(9–12), 3051–3058.

Ji, S., Meng, X., Liu, Z., Huang, R., and Li, Z. (2017). "Dissimilar friction stir welding of 6061 aluminum alloy and AZ31 magnesium alloy assisted with ultrasonic." *Mater Lett*, 201, 173–176.

Johari, O., Corvin, I., and Staschke, J. (1973). *Failure Analysis of Aluminium Alloy Components*.

Jones, M. J., Heurtier, P., Desrayaud, C., Montheillet, F., Allehaux, D., and Driver, J. H. (2005). "Correlation between microstructure and microhardness in a friction stir welded 2024 aluminium alloy." *Scr Mater*, 52(8), 693–697.

Jordan, M. (1995). "Why the logistic function? A tutorial discussion on probabilities and neural networks." *Comput Cogn Sci Tech Rep 9503*, 1–13.

Jung, H., Bell, R., and Wang, X. (2009). *The fatigue characteristics of friction stir welded stiffened panel structure*. *12th Int Conf Fract 2009, ICF-12*.

Kadaganchi, R., Gankidi, M. R., and Gokhale, H. (2015). "Optimization of process parameters of aluminum alloy AA 2014-T6 friction stir welds by response surface methodology." *Def Technol*, 11(3), 209–219.

Kadlec, M., Růžek, R., and Nováková, L. (2015). "Mechanical behaviour of AA 7475 friction stir welds with the kissing bond defect." *Int J Fatigue*, 74(1), 7–19.

Kah, P., Rajan, R., Martikainen, J., and Suoranta, R. (2015). "Investigation of weld defects in friction-stir welding and fusion welding of aluminium alloys." *Int J Mech Mater Eng*, 10(1), 26.

Kalemba-Rec, I., Wróbel, M., and Kopyściański, M. (2016). "Investigations of friction stir welds between 5083 and 7075 aluminum alloys using EBSD and X-ray techniques." *Acta Phys Pol A*, 130(4), 996–999.

Kallee, S., and Nicholas, D. (2000). "Friction Stir Welding at TWI Friction Stir Welding - Process advantages Friction Stir Welding - Materials and thicknesses Friction Stir Welding - Superior weld quality." 1–7.

Kamp, N., Reynolds, A. P., and Robson, J. D. (2009). "Modelling of 7050 aluminium alloy friction stir welding." *Sci Technol Weld Join*, 14(7), 589–596.

Kamp, N., Sullivan, A., and Robson, J. D. (2007). "Modelling of friction stir welding of 7xxx aluminium alloys." *Mater Sci Eng A*, 466(1–2), 246–255.

Kang, S. H., Han, H. N., Oh, K. H., Cho, J. H., Lee, C. G., and Kim, S. J. (2009). "Investigation of the material flow and texture evolution in friction-stir welded aluminum alloy." *Met Mater Int*, 15(6), 1027–1031.

297

Karthikeyan, L., and Senthil Kumar, V. S. (2011). "Relationship between process parameters and mechanical properties of friction stir processed AA6063-T6 aluminum alloy." *Mater Des*, 32(5), 3085–3091.

Kasman, Ş., and Yenier, Z. (2014). "Analyzing dissimilar friction stir welding of AA5754/AA7075." *Int J Adv Manuf Technol*, 70(1–4), 145–156.

Katoh, M., and Kerr, H. W. (1987). "Investigation of heat-affected zone cracking of gta welds of al-mg-si alloys using the varestraint test." *Weld J (Miami, Fla)*, 66(12), 360–368.

Kaufman, J. G., and Rooy, E. L. (2014). *Aluminum Alloy Castings-Properties, Processes and Applications*. ASM Int.

Kawasaki, T., Makino, T., Todori, S., Takai, H., and Ezumi, M. (2000). "Application of friction stir welding to the manufacturing of the next generation." *Proc 2nd Int symp FSW, Gothenburg, Sweden*.

Khaled, T. (2005). *An Outsider Looks At Friction Stir Welding*.

Khan, N. Z., Khan, Z. A., and Siddiquee, A. N. (2015a). "Effect of Shoulder Diameter to Pin Diameter (D/d) Ratio on Tensile Strength of Friction Stir Welded 6063 Aluminium Alloy." *Mater Today Proc*, 2(4–5), 1450–1457.

Khan, N. Z., Siddiquee, A. N., Khan, Z. A., and Mukhopadhyay, A. K. (2017). "Mechanical and microstructural behavior of friction stir welded similar and dissimilar sheets of AA2219 and AA7475 aluminium alloys." *J Alloys Compd*, 695, 2902–2908.

Khan, N. Z., Siddiquee, A. N., Khan, Z. A., and Shihab, S. K. (2015b). "Investigations on tunneling and kissing bond defects in FSW joints for dissimilar aluminum alloys." *J Alloys Compd*, 648(1), 360–367.

Khodir, S. A., and Shibayanagi, T. (2008). "Friction stir welding of dissimilar AA2024 and AA7075 aluminum alloys." *Mater Sci Eng B Solid-State Mater Adv Technol*, 148(1–3), 82–87.

Khorrami, M. S., Kazeminezhad, M., and Kokabi, A. H. (2012). "Mechanical properties of severely plastic deformed aluminum sheets joined by friction stir welding." *Mater*

Sci Eng A, 543, 243–248.

Khourshid, A. M., El-Kassas, A. M., and Sabry, I. (2015). "Integration between Artificial Neural Network and Responses Surfaces Methodology for Modeling of Friction Stir welding." *Int J Adv Eng Res Sci*, 2(8), 67–73.

Kim, S., Lee, C. G., and Kim, S. J. (2008). "Fatigue crack propagation behavior of friction stir welded 5083-H32 and 6061-T651 aluminum alloys." *Mater Sci Eng A*, 478(1–2), 56–64.

Klobčar, D., Nagode, A., Smolej, A., and Tušek, J. (2013). "FSW of aluminium alloy AlSi12." *RMZ - Mater geoenvironment*, 3(60), 183–189.

Koilraj, M., Sundareswaran, V., Vijayan, S., and Koteswara Rao, S. R. (2012). "Friction stir welding of dissimilar aluminum alloys AA2219 to AA5083 - Optimization of process parameters using Taguchi technique." *Mater Des*, 42, 1–7.

Kori, S. A., Murty, B. S., and Chakraborty, M. (1999). "Influence of silicon and magnesium on grain refinement in aluminium alloys." *Mater Sci Technol*, 15(9), 986–992.

Kou, S. (1987). *Welding Metallurgy, 1987*. Wiley-Interscience, New York.

Krasnowski, K., Hamilton, C., and Dymek, S. (2015). "Influence of the tool shape and weld configuration on microstructure and mechanical properties of the Al 6082 alloy FSW joints." *Arch Civ Mech Eng*, 15(1), 133–141.

Kubit, A., Bucior, M., Wydrzyński, D., Trzepieciński, T., and Pytel, M. (2018a). "Failure mechanisms of refill friction stir spot welded 7075-T6 aluminium alloy single-lap joints." *Int J Adv ManufTechnol*, 94, 4479–4491.

Kubit, A., Kluz, R., Ochałek, K., Wydrzyński, D., and Trzepieciński, T. (2018b). "Friction stir welding of 2024-T3 aluminium alloy sheet with sheet pre-heating." *Mater Tehnol*, 52(3), 283–288.

Kumagai, M. (2003). "Recent technological developments in welding of aluminium and its alloys." *Weld Int*, 17(3), 173–181.

Kumar, HM Anil, V. R., Kumar, H. M. A., and Ramana, V. V. (2014). "An overview of friction stir welding (FSW): A new perspective." *Int J Eng Sci*, 4(6), 1–4.

Kumar, A. A., Gautam, S. S., and Kumar, A. A. (2014). "Heat Input & Joint Efficiency of Three Welding Processes Tig , Mig and Fsw Using Aa6061." *Int J Mech Eng Rob Res*, 1(1), 89–94.

Kumar, A., Khurana, M. ., and Singh, G. (2018). "Modeling and Optimization of Friction Stir Welding Process Parameters for Dissimilar Aluminium Alloys." *Mater Today Proc*, 5(11), 25440–25449.

Kumar, A., Sharma, V. K., and Singh, J. (2015a). "Optimization of friction stir welding parameters for joining aluminum alloy 6105 using taguchi technique." *Int J Res Eng Technol*, 4(7), 185–189.

Kumar, B. A., and Murugan, N. (2014). "Optimization of friction stir welding process parameters to maximize tensile strength of stir cast AA6061-T6/AlNp composite." *Mater Des*, 57, 383–393.

Kumar, K., and Kailas, S. V. (2008). "The role of friction stir welding tool on material flow and weld formation." *Mater Sci Eng A*, 485(1), 367–374.

Kumar, K., Kailas, S. V, and Srivatsan, T. S. (2008). "Influence of tool geometry in friction stir welding." *Mater Manuf Process*, 23(2), 188–194.

Kumar, P. V., Reddy, G. M., and Rao, K. S. (2015b). "Microstructure, mechanical and corrosion behavior of high strength AA7075 aluminium alloy friction stir welds – Effect of post weld heat treatment." *Def Technol*, 11(4), 362–369.

Kumar, R. A., and Thansekhar, M. R. (2014). "Effects of tool pin profile and tool shoulder diameter on the tensile behaviour of friction stir welded joints of aluminium alloys." *Adv Mater Res*, 984–985(2014), 586–591.

Kumar, R., Chattopadhyaya, S., Hloch, S., Krolczyk, G., and Legutko, S. (2016a). "Wear characteristics and defects analysis of friction stir welded joint of aluminium alloy 6061-T6." *Maint Reliab 2016*, 18(1), 128–135.

Kumar, S., Kumar, S., and Kumar, A. (2013). "Optimization of process parameters for

friction stir welding of joining A6061 and A6082 alloys by Taguchi method." *Proc Inst Mech Eng Part C J Mech Eng Sci*, 227(6), 1150–1163.

Kumar, S. S., Murugan, N., and Ramachandran, K. K. (2016b). "Influence of tool material on mechanical and microstructural properties of friction stir welded 316L austenitic stainless steel butt joints." *Int J Refract Met Hard Mater*, 58, 196–205.

Kumar, U., Yadav, I., Kumari, S., Kumari, K., Ranjan, N., Kesharwani, R. K., Jain, R., Kumar, S., Pal, S. K. S., Chakravarty, D., and Pal, S. K. S. (2015c). "Defect identification in friction stir welding using discrete wavelet analysis." *Adv Eng Softw*, 85, 43–50.

Kumari, K., Pal, S. K., and BratSingh, S. (2015). "Friction stir welding by using counter-rotating twin tool." *J Mater Process Technol*, 215(1), 132–141.

Kumbhar, N. T., Dey, G. K., and Bhanumurthy, K. (2011a). "Friction stir welding of aluminium alloys." *Int J Mech Eng Technol*, (321), 11–17.

Kumbhar, N. T., Sahoo, S. K., Samajdar, I., Dey, G. K., and Bhanumurthy, K. (2011b). "Microstructure and microtextural studies of friction stir welded aluminium alloy 5052." *Mater Des*, 32(3), 1657–1666.

Kwon, Y. J., Shim, S. B., and Park, D. H. (2009). "Friction stir welding of 5052 aluminum alloy plates." *Trans Nonferrous Met Soc China (English Ed*, 19(SUPPL. 1), s23–s27.

Lafly, A. L., Alléhaux, D., Marie, F., Donne, D. C., and Biallas, G. (2006). "Microstructure and mechanical properties of the aluminium alloy 6056 welded by friction stir welding techniques." *Weld World*, 50(11–12), 98–106.

Lagos, M., and Das, R. (2016). "Brittle and ductile character of amorphous solids." *Adv Appl Math Mech*, 8(3), 485–498.

Lakshminarayanan, A. K., and Balasubramanian, V. (2008). "Process parameters optimization for friction stir welding of RDE-40 aluminium alloy using Taguchi technique." *Trans Nonferrous Met Soc China*, 18(2008), 548–554.

LAKSHMINARAYANAN, A. K., and Balasubramanian, V. (2009). "Comparison of

RSM with ANN in predicting tensile strength of friction stir welded AA7039 aluminium alloy joints." *Trans Nonferrous Met Soc China (English Ed*, 19(2009), 9–18.

Lakshminarayanan, A. K., Balasubramanian, V., and Elangovan, K. (2009). "Effect of welding processes on tensile properties of AA6061 aluminium alloy joints." *Int J Adv Manuf Technol*, 40(1), 286–296.

Lakshminarayanan, A. K., Malarvizhi, S., and Balasubramanian, V. (2011). "Developing friction stir welding window for AA2219 aluminium alloy." *Trans Nonferrous Met Soc China (English Ed*, 21(11), 2339–2347.

Lauro, A., Thompson, B., and Thomas, W. (2011). *Friction Stir Welding of Titanium Alloys. Weld Int*.

Leal, R., Loureiro, A., and Rui M. Leal, A. L. (2004). "Defects formation in friction stir welding of aluminium alloys." *Mater Sci Forum*, 1(2004), 299–302.

Leal, R. M., Leitão, C., Loureiro, A., Rodrigues, D. M., and Vilac, P. (2008). "Material flow in heterogeneous friction stir welding of thin aluminium sheets : Effect of shoulder geometry." 498, 384–391.

Leitão, C., Louro, R., and Rodrigues, D. M. (2012). "Analysis of high temperature plastic behaviour and its relation with weldability in friction stir welding for aluminium alloys AA5083-H111 and AA6082-T6." *Mater Des*, 37, 402–409.

Li, D., Yang, X., Cui, L., He, F., and Shen, H. (2014a). "Effect of welding parameters on microstructure and mechanical properties of AA6061-T6 butt welded joints by stationary shoulder friction stir welding." *Mater Des*, 64, 251–260.

Li, D., Yang, X., Cui, L., He, F., and Zhang, X. (2015). "Investigation of stationary shoulder friction stir welding of aluminum alloy 7075-T651." *J Mater Process Technol*, 222, 391–398.

Li, Q., Jensen, J. O., and Bjerrum, N. J. (2009). "Chemistry, Electrochemistry, and Electrochemical Applications | Aluminum." *Encycl Electrochem Power Sources*, 695–708.

Li, W. Y., Fu, T., Hütsch, L., Hilgert, J., Wang, F. F., Santos, J. F. dos, and Huber, N. (2014b). "Effects of tool rotational and welding speed on microstructure and mechanical properties of bobbin-tool friction-stir welded Mg AZ31." *Mater Des*, 64, 714–720.

Liang, X. peng, Li, H. zhong, Li, Z., Hong, T., Ma, B., Liu, S. dan, and Liu, Y. (2012). "Study on the microstructure in a friction stir welded 2519-T87 Al alloy." *Mater Des*, 35, 603–608.

Lim, C. C., and Gweon, C. G. (1999). "In-process joint strength estimation in pulsed laser spot welding using artificial neural networks." *J Manuf Process*, 1(1), 31–42.

Liu, F. C., Hovanski, Y., Miles, M. P., Sorensen, C. D., and Nelson, T. W. (2018a). "A review of friction stir welding of steels: Tool, material flow, microstructure, and properties." *J Mater Sci Technol*, 34(1), 39–57.

Liu, H. J., Chen, Y. C., and Feng, J. C. (2006). "Effect of heat treatment on tensile properties of friction stir welded joints of 2219-T6 aluminium alloy." *Mater Sci Technol*, 22(2), 237–241.

Liu, H. J., Feng, J. C., Fujii, H., and Nogi, K. (2005). "Wear characteristics of a WC-Co tool in friction stir welding of AC4A+30 vol%SiCp composite." *Int J Mach Tools Manuf*, 45(14), 1635–1639.

Liu, H. J., Fujii, H., Maeda, M., and Nogi, K. (2003). "Mechanical properties of friction stir welded joints of 1050-H24 aluminium alloy." *Sci Technol Weld Join*, 8(6), 450–454.

Liu, H. J., Fujii, H., Maeda, M., and Nogi, K. (2017). "Tensile properties and fracture locations of friction-stir-welded joints of 2017-T351 aluminum alloy." *J Mater Process Technol*, 142(2003), 692–696.

Liu, H. J., Fujii, H., and Nogi, K. (2004). "Microstructure and mechanical properties of friction stir welded joints of AC4A cast aluminium alloy." *Mater Sci Technol*, 20(3), 399–402.

Liu, H., Zhang, H., Pan, Q., and Yu, L. (2012). "Effect of friction stir welding

parameters on microstructural characteristics and mechanical properties of 2219-T6 aluminum alloy joints." *Int J Mater Form*, 5(3), 235–241.

Liu, X., Lan, S., and Ni, J. (2014). "Analysis of process parameters effects on friction stir welding of dissimilar aluminum alloy to advanced high strength steel." *Mater Des*, 59, 50–62.

Liu, X., Lan, S., Qiao, X., and Ni, J. (2015). "Study of plunge stage for a hybrid friction stir welding process based on electro-plastic effect." *ASME 2015 Int Manuf Sci Eng Conf MSEC 2015*, 1, 1–8.

Liu, X., Zhao, S., Chen, K., and Ni, J. (2018b). "Material flow visualization of dissimilar friction STIR welding process using nano-computed tomography." *J Manuf Sci Eng Trans ASME*, 140(11), 1–8.

Lohwasser, D., and Chen, Z. (2010). *Friction Stir Welding: From Basics to Applications - Google Books*.

Lombard, H., Hattingh, D. G., Steuwer, A., and James, M. N. (2008). "Optimising FSW process parameters to minimise defects and maximise fatigue life in 5083-H321 aluminium alloy." *Eng Fract Mech*, 75(3–4), 341–354.

Long, T., Tang, W., and Reynolds, A. P. (2007). "Process response parameter relationships in aluminium alloy friction stir welds." *Sci Technol Weld Join*, 12(4), 311–317.

Lorrain, O., Favier, V., Zahrouni, H., and Lawrjaniec, D. (2010). "Understanding the material flow path of friction stir welding process using unthreaded tools." *J Mater Process Technol*, 210(4), 603–609.

Luo, C., Li, X., Song, D., Zhou, N., Li, Y., and Qi, W. (2016). "Microstructure evolution and mechanical properties of friction stir welded dissimilar joints of Mg-Zn-Gd and Mg-Al-Zn alloys." *Mater Sci Eng A*, 664, 103–113.

Ma, Z. Y. (2008). "Friction Stir Processing Technology : A Review." *Metall Mater Trans A*, 39(A), 642–658.

Ma, Z. Y., Feng, A. H., Chen, D. L., and Shen, J. (2018). "Recent Advances in Friction

Stir Welding/Processing of Aluminum Alloys: Microstructural Evolution and Mechanical Properties." *Crit Rev Solid State Mater Sci*, 43(4), 269–333.

Ma, Z. Y., Sharma, S. R., and Mishra, R. S. (2006). "Microstructural modification of As-cast Al-Si-Mg alloy by friction stir processing." *Metall Mater Trans A Phys Metall Mater Sci*, 37(11), 3323–3336.

Maggiolino, S., and Schmid, C. (2008). "Corrosion resistance in FSW and in MIG welding techniques of AA6XXX." *J Mater Process Technol*, 197(1–3), 237–240.

Magnusson, L., and Kallman, L. (2000). "Mechanical properties of friction stir welds in thin sheet of aluminium 2024, 6013 and 7475." *Second Int Symp FSW, Gothenburg, Sweden*.

Mahmoud, T. S., Gaafer, A. M., and Khalifa, T. A. (2008). "Effect of tool rotational and welding speeds on microstructural and mechanical characteristics of friction stir welded A319 cast Al alloy." *Mater Sci Technol*, 24(5), 553–559.

Malarvizhi, S., and Balasubramanian, V. (2011). "Effect of welding processes on AA2219 aluminium alloy joint properties." *Trans Nonferrous Met Soc China (English Ed*, 21(5), 962–973.

Malarvizhi, S., Balasubramanian, V., Malarvizhi, S., and Balasubramanian, V. (2011). "Effects of Welding Processes and Post-Weld Aging Treatment on Fatigue Behavior of AA2219 Aluminium Alloy Joints." *J Mater Eng Perform*, 20(April), 359–367.

Malik, V., Sanjeev, N. K., Hebbar, H. S., and Kailas, S. V. (2014). "Investigations on the Effect of Various Tool Pin Profiles in Friction Stir Stir Welding Using Finite Element Simulations." *Procedia Eng Glob Congr Manuf Manag GCMM 2014*, 97, 1060–1068.

Manisegaran, L. V., Ahmad, N. A., Nazri, N., Noor, A. S. M., Ramachandran, V., Ismail, M., Ahmad, A., Ku, K. Z., and Daruis, D. D. I. (2018). "Optimizing friction stir weld parameters of aluminum and copper using conventional milling machine." *AIP Conf Proc*, 7.

Marzbanrad, J., Akbari, M., Asadi, P., and Safaee, S. (2014). "Characterization of the

Influence of Tool Pin Profile on Microstructural and Mechanical Properties of Friction Stir Welding." *Metall Mater Trans B Process Metall Mater Process Sci*, 45(5), 1887–1894.

Mastanaiah, P., Sharma, A., and Reddy, G. M. (2018). "Role of hybrid tool pin profile on enhancing welding speed and mechanical properties of AA2219-T6 friction stir welds." *J Mater Process Technol*, 257, 257–269.

Mathers, G. (2002). *The welding of aluminium and its alloys. Woodhead Publ Ltd (CRC Press*.

McLean, E. O. (1965). *Aluminum*.

McNelley, T. R., Swaminathan, S., and Su, J. Q. (2008). "Recrystallization mechanisms during friction stir welding/processing of aluminum alloys." *Scr Mater*, 58(5), 349–354.

Mehdi, H., and Mishra, R. S. (2016). "Mechanical properties and microstructure studies in Friction Stir Welding (FSW) joints of dissimilar alloy – a review." *J Achiev Mater Manuf Eng Microstruct*, 77(1), 31–40.

Mehta, M., Arora, A., De, A., and DebRoy, T. (2011). "Tool Geometry for Friction Stir Welding—Optimum Shoulder Diameter." *Miner Met Mater Soc ASM Int*, 42(9), 2716–2722.

Mehta, M., De, A., and DebRoy, T. (2013). "Probing load bearing capacity of circular and non-circular tool pins in friction stir welding." *ASM Proc Int Conf Trends Weld Res*, (June 2012), 563–571.

Mehta, M., Reddy, G. M., Rao, A. V., and De, A. (2015). "Numerical modeling of friction stir welding using the tools with polygonal pins." *Def Technol*, 11(3), 229–236.

Meilinger, A., and Torok, I. (2013). "the Importance of Friction Stir Welding Tool." *Prod Process Syst*, 6(1), 25–34.

Mendez, P. F., and Eagar, T. W. (2001). "Welding processes for aeronautics." *Adv Mater Process*, 159(5), 39–43.

Meshram S., M. R. (2018). "Influence of tool tilt angle on material flow and defect generation in friction stir welding of AA2219." *Def Sci J*, 68(5), 512–518.

Midling, O., and Kvale, J. (1999). "Industrialisation of the FSW Technology in Panels Production for the Maritime Sector." *First Int Symp Frict Stir Welding, Thousand Oaks, California, USA.*

Midling, O. T., Oosterkamp, L. D., and Bersaas, J. (2009). *Friction Stir Welding Process and Applications.*

Mijajlović, M., and Milčić, D. (2012). *Analytical Model for Estimating the Amount of Heat Generated During Friction Stir Welding: Application on Plates Made of Aluminium Alloy 2024 T351. Weld Process.*

Miller, W. S., Zhuang, L., Bottema, J., Wittebrood, A. J., Smet, P. De, Haszler, A., and Vieregge, A. (2000). "Recent development in aluminium alloys for the automotive industry." *Mater Sci Eng A*, 280(1), 37–49.

Miodownik, M. A. (2002). "A review of microstructural computer models used to simulate grain growth and recrystallisation in aluminium alloys." *J Light Met*, 2(3), 125–135.

Mishra, R. S., and Jain, S. (2019). "Friction stir welding (FSW) process on aluminum alloy 6082-T6 using taguchi technique." *Int J Res Eng Innov*, 3(5), 301–305.

Mishra, R. S., and Ma, Z. Y. (2005). "Friction stir welding and processing." *Mater Sci Eng*, 50, 1–78.

Mishra, R. S., Mahoney, M. W., and Murray, W. (2007). "Friction Stir Welding and Processing." *ASM Int*, 1(5), 359.

Mohanty, H. K., Mahapatra, M. M., Kumar, P., Biswas, P., and Mandal, N. R. (2013). "Predicting the effects of tool geometries on friction stirred aluminium welds using artificial neural networks and fuzzy logic techniques." *Int J Manuf Res*, 8(3), 296–312.

Montgomery, D. C. (2017). *Design and analysis of experiments*. John wiley & sons.

Moosabeiki, V., Azimi, G., and Ghayoor, M. (2012). "Influences of Tool pin Profile

and Tool Shoulder Curvature on the Formation of Friction Stir Welding Zone in AA6061 Aluminium Alloy." *Adv Mater Res*, 445(1), 789–794.

Moreira, P. M. G. P., Santos, T., Tavares, S. M. O., Richter-Trummer, V., Vilaça, P., and Castro, P. M. S. T. de. (2009). "Mechanical and metallurgical characterization of friction stir welding joints of AA6061-T6 with AA6082-T6." *Mater Des*, 30(1), 180–187.

Mosleh, A. O., Mahmoud, F. H., Mahmoud, T. S., and Khalifa, T. A. (2016). "Microstructure and static immersion corrosion behavior of AA7020-O Al plates joined by friction stir welding." *Proc Inst Mech Eng Part L J Mater Des Appl*, 230(6), 1030–1040.

Movahedi, M., Kokabi, A. H., Reihani, S. M. S., and Najafi, H. (2012). "Effect of tool travel and rotation speeds on weld zone defects and joint strength of aluminium steel lap joints made by friction stir welding." *Sci Technol Weld Join*, 17(2), 162–167.

Mroczka, K., Dutkiewicz, J., Lityñska-dobrzyñska, L., and Pietras, A. (2008). "Microstructure and properties of FSW joints of 2017A / 6013 aluminium alloys sheets." *Arch Mater Sci Eng*, 33(2), 93–96.

Mukhopadhyay, A., Prasad, K., and Kumar, V. (2006). "Key microstructural features responsible for improved stress corrosion cracking resistance and weldability in 7xxx series Al alloys containing micro/trace alloying." *Trans Tech Publ*, 519–521(1), 315–320.

Muñoz, A. C., Rückert, G., Huneau, B., Sauvage, X., and Marya, S. (2008). "Comparison of TIG welded and friction stir welded Al-4.5Mg-0.26Sc alloy." *J Mater Process Technol*, 197(1–3), 337–343.

Murr, L. E., Flores, R. D., Flores, O. V., McClure, J. C., Liu, G., and Brown, D. (1998). "Friction-stir welding: Microstructural characterization." *Mater Res Innov*, 1(4), 211–223.

Murthy, V., Kalmeshwar, U., Rajaprakash, B. M., and Rajashekar, R. (2018). "Study on influence of concave geometry shoulder tool in Friction Stir Welding (FSW) by

using Image Processing and Acoustic Emission Techniques." *Mater Today Proc*, Elsevier Ltd, 27004–27017.

Murugan, N., and Ashok Kumar, B. (2013). "Prediction of tensile strength of friction stir welded stir cast AA6061-T6/AlNp composite." *Mater Des*, 51, 998–1007.

Muthu Krishnan, M., Maniraj, J., Deepak, R., and Anganan, K. (2018). "Prediction of optimum welding parameters for FSW of aluminium alloys AA6063 and A319 using RSM and ANN." *Mater Today Proc*, 5(1), 716–723.

Muthukrishnan, M., and Marimuthu, M. (2010). "Some studies on mechanical properties of friction stir butt welded Al-6082-T6 plates." *Proc Int Conf Front Automob Mech Eng - 2010, FAME-2010*, 269–273.

Nadikudi, B. K. B., Davidson, M. J., Akasapu, N. R., and Govindaraju, M. (2015). "Formability analysis of dissimilar tailor welded blanks welded with different tool pin profiles." *Trans Nonferrous Met Soc China*, 25(6), 1787–1793.

Nafsin, N., and Rashed, H. M. M. A. (2013). "Effects of Copper and Magnesium on Microstructure and Hardness of Al-Cu-Mg Alloys." *Int J Eng Adv Technol*, 2(5), 533–536.

Nakata, K., Kim, Y. G., Ushio, M., Hashimoto, T., and Jyogan, S. (2000). "Weldability of high strength aluminum alloys by friction stir welding." *ISIJ Int*, 40(SUPPL.).

Nami, H., Adgi, H., Sharifitabar, M., and Shamabadi, H. (2011). "Microstructure and mechanical properties of friction stir welded Al/Mg2Si metal matrix cast composite." *Mater Des*, 32(2), 976–983.

Nandan, R., Debroy, T., and Bhadeshia, H. K. D. H. (2008). "Recent Advances in Friction Stir Welding – Process , Weldment Structure and Properties." *Prog Mater Sci*, 53(1), 980–1023.

Nigalye, A. (2013). "Modelling and Validation of Behaviour of Mushy State Rolled Al-4.5 Cu-5TiB2 Composite Using Neural Network Techniques."

Nik, Z. C., Ishak, M., and Othman, N. H. (2017). "The Effect of Tool Pin Shape of Friction Stir Welding (FSW) on Polypropylene." *Mater Sci Eng*.

Okuyucu, H., Kurt, A., and Arcaklioglu, E. (2007). "Artificial neural network application to the friction stir welding of aluminum plates." *Mater Des*, 28(1), 78–84.

Olabode, M., Kah, P., and Martikainen, J. (2013). "Aluminium alloys welding processes: Challenges, joint types and process selection." *Proc Inst Mech Eng Part B J Eng Manuf*, 227(8), 1129–1137.

Olsen, D. (n.d.). "What Is Conductivity in Metals? | MetalTek." *Met Int*, <https://www.metaltek.com/blog/conductivity-in-metals/> (Feb. 19, 2021).

Oosterkamp, A., Oosterkamp, L. D., and Nordeide, A. (2004). "'Kissing bond' phenomena in solid-state welds of aluminum alloys." *Weld J (Miami, Fla)*, 83(8), 225-S.

Otsuka, D., and On, Y. S. (2008). "Self-reacting pin tool application for railway car body assembly." *Proc 7th Int Symp Frict Stir Weld*, 20–22.

Ouyang, J. H., and Kovacevic, R. (2002). "Material flow and microstructure in the friction stir butt welds of the same and dissimilar aluminum alloys." *J Mater Eng Perform*, 11(1), 51–63.

Ouyang, J., Jandric, D., Kovacevic, R., Song, M., and Valant, M. (2002). "Visualization of material flow during friction stir welding (FSW) of the same and dissimilar aluminum alloys." *6th Int Trends Weld Res*, 229–40.

Ouyang, J., Yarrapareddy, E., and Kovacevic, R. (2006). "Microstructural evolution in the friction stir welded 6061 aluminum alloy (T6-temper condition) to copper." *J Mater Process Technol*, 172(1), 110–122.

Øye, H. A., and Huglen, R. (1990). "Managing aluminum reduction technology: Extracting the most from Hall-Héroult." *JOM*, 42(11), 23–28.

Padmanaban, G., and Balasubramanian, V. (2009). "Selection of FSW tool pin profile, shoulder diameter and material for joining AZ31B magnesium alloy - An experimental approach." *Mater Des*, 30(7), 2647–2656.

Paglia, C. S., Jata, K. V., and Buchheit, R. G. (2007). "The influence of artificial aging on the microstructure, mechanical properties, corrosion, and environmental cracking

susceptibility of a 7075 friction-stir-weld." *Mater Corros*, 58(10), 737–750.

Palani, K., Elanchezhian, C., and Bhaskar, G. B. (2015). "Multi Response DEA-Based Taguchi Optimization of Process Parameters on AA8011 Friction Stir Welded Aluminium Alloys." *Appl Mech Mater*, 766–767, 921–927.

Palanivel, R., Koshy Mathews, P., Dinaharan, I., and Murugan, N. (2014). "Mechanical and metallurgical properties of dissimilar friction stir welded AA5083-H111 and AA6351-T6 aluminum alloys." *Trans Nonferrous Met Soc China (English Ed*, 24(1), 58–65.

Palanivel, R., Koshy Mathews, P., Murugan, N., and Dinaharan, I. (2012). "Effect of tool rotational speed and pin profile on microstructure and tensile strength of dissimilar friction stir welded AA5083-H111 and AA6351-T6 aluminum alloys." *Mater Des*, 40(1), 7–16.

Palanivel, R., Mathews, P. K., and Murugan, N. (2011). "Development of mathematical model to predict the mechanical properties of friction stir welded AA6351 aluminum alloy Engineering Science and Technology Review." *J Eng Sci Technol Rev*, 4(1), 25–31.

Pang, J. S., Ansari, M. N. M., Zaroog, O. S., Ali, M. H., and Sapuan, S. M. (2014). "Taguchi design optimization of machining parameters on the CNC end milling process of halloysite nanotube with aluminium reinforced epoxy matrix (HNT/Al/Ep) hybrid composite." *HBRC J*, 10(2), 138–144.

Peel, M., Steuwer, A., Preuss, M., and Withers, P. J. (2003). "Microstructure, mechanical properties and residual stresses as a function of welding speed in aluminium AA5083 friction stir welds." *Acta Mater*, 51(16), 4791–4801.

Perovic, M., Veljic, D., Rakin, M., Radovic, N., Sedmak, A., and Bajic, N. (2012). "Friction-stir welding of high-strength aluminium alloys and a numerical simulation of the plunge stage." *Mater Tehnol*, 46(3), 215–221.

Podržaj, P., Jerman, B., and Klobčar, D. (2015). "Welding defects at friction stir welding." *Metalurgija*, 54(2), 387–389.

Polmear, I. (2005). *Light alloys: from traditional alloys to nanocrystals*.

Poznak, A., Freiberg, D., and Sanders, P. (2018). *Automotive Wrought Aluminium Alloys. Fundam Alum Metall*, Elsevier Ltd.

Prabhu, S., Shettigar, A. K., Rao, K., Rao, S., and Herbert, M. (2016). "Influence of Welding Process Parameters on Microstructure and Mechanical Properties of Friction Stir Welded Aluminium Matrix Composite." *Mater Sci Forum*, 880, 50–53.

Prangnell, P. B., and Heason, C. P. (2005). "Grain structure formation during friction stir welding observed by the 'stop action technique.'" *Acta Mater*, 53(11), 3179–3192.

Prapas, M., Jennarong, N., and Woraphot, P. (2017). "Effect of post-weld heat treatment on microstructure and mechanical properties of friction stir welded SSM7075 aluminium alloy." *J Wuhan Univ Technol Mater Sci Ed*, 32(6), 1420–1425.

Qian, J., Li, J., Xiong, F., Jiangtao, F., and XinLin, Z. (2013). "An analytical model to optimize rotation speed and travel speed of friction stir welding for defect." *Scr Mater*, 68(3–4), 175–178.

Qin, G., Zhang, K., Zhang, W., and Wu, C. (2010). "Effect of friction stir welding heat input on weld appearance and mechanical properties of 6013-T4 Al alloy joint." *Hanjie Xuebao/Transactions China Weld Inst*, 31(11), 5–8.

R. Nandan, T. DebRoy, H. K. D. H. Bhadeshia, Nandan, R., Debroy, T., and Bhadeshia, H. K. D. H. (2008). "Recent advances in friction-stir welding – Process, weldment structure and properties." *Prog Mater Sci*, 53(6), 980–1023.

Radisavljevic, I. (2014). "Influence of pin geometry on mechanical and structural properties of butt friction stir welded 2024-T351 aluminum alloy." (January).

Rahmi, M., and Abbasi, M. (2017). "Friction stir vibration welding process: modified version of friction stir welding process." *Int J Adv Manuf Technol*, 90(1–4), 141–151.

Rai, R., De, A., Bhadeshia, H. K. D. H., and DebRoy, T. (2011). "Review: friction stir welding tools." *Sci Technol Weld Join*, 16(4), 325–342.

Rajakumar, S., and Balasubramanian, V. (2012a). "Correlation between weld nugget

grain size, weld nugget hardness and tensile strength of friction stir welded commercial grade aluminium alloy joints." *Mater Des*, 34, 242–251.

Rajakumar, S., and Balasubramanian, V. (2012b). "Predicting grain size and tensile strength of friction stir welded joints of AA7075-T 6 aluminium alloy." *Mater Manuf Process*, 27(1), 78–83.

Rajakumar, S., and Balasubramanian, V. (2012c). "Establishing relationships between mechanical properties of aluminium alloys and optimised friction stir welding process parameters." *Mater Des*, 40(1), 17–35.

Rajakumar, S., Muralidharan, C., and Balasubramanian, V. (2010a). "Optimization of the friction-stir-welding process and tool parameters to attain a maximum tensile strength of AA7075-T6 aluminium alloy." *Proc Inst Mech Eng Part B J Eng Manuf*, 224(8), 1175–1191.

Rajakumar, S., Muralidharan, C., and Balasubramanian, V. (2010b). "Establishing empirical relationships to predict grain size and tensile strength of friction stir welded AA 6061-T6 aluminium alloy joints." *Trans Nonferrous Met Soc China (English Ed*, 20(10), 1863–1872.

Rajakumar, S., Muralidharan, C., and Balasubramanian, V. (2011). "Influence of friction stir welding process and tool parameters on strength properties of AA7075-T6 aluminium alloy joints." *Mater Des*, 32(2), 535–549.

Rajamanickam, N., Balusamy, V., Madhusudhanna Reddy, G., and Natarajan, K. (2009). "Effect of process parameters on thermal history and mechanical properties of friction stir welds." *Mater Des*, 30(7), 2726–2731.

Rambabu, G., Naik, D. B., Rao, C. H. V., Rao, K. S., and Reddy, G. M. (2015). "Optimization of friction stir welding parameters for improved corrosion resistance of AA2219 aluminum alloy joints." *Def Technol*, 11(4), 330–337.

Rambabu, P., Eswara Prasad, N., Kutumbarao, V. V., and Wanhill, R. J. H. (2017). *Aluminium Alloys for Aerospace Applications*. Springer, Singapore.

Rao, A. C. U., Vasu, V., Govindaraju, M., and Srinadh, K. V. S. (2016). "Stress

corrosion cracking behaviour of 7xxx aluminum alloys: A literature review." *Trans Nonferrous Met Soc China (English Ed*, 26(6), 1447–1471.

Rao, D., Huber, K., Heerens, J., Santos, J. F. dos, and Huber, N. (2013). "Asymmetric mechanical properties and tensile behaviour prediction of aluminium alloy 5083 friction stir welding joints." *Mater Sci Eng A*, 565, 44–50.

Rao, T. S., Reddy, G. M., and Rao, S. R. K. (2015). "Microstructure and mechanical properties of friction stir welded AA7075-T651 aluminum alloy thick plates." *Trans Nonferrous Met Soc China (English Ed*, 25(6), 1770–1778.

Reddy, N. S., Prasada Rao, A. K., Chakraborty, M., and Murty, B. S. (2005). "Prediction of grain size of Al-7Si Alloy by neural networks." *Mater Sci Eng A*, 391(1–2), 131–140.

Reynolds, A. P. (2000). "Visualisation of material flow in autogenous friction stir welds." *Sci Technol Weld Join*, 5(2), 120–124.

Reynolds, A. P. (2008). "Flow visualization and simulation in FSW." *Scr Mater*, 58(5), 338–342.

Rezaei, H., Mirbeik, M. H., and Bisadi, H. (2011). "Effect of rotational speeds on microstructure and mechanical properties of friction stir-welded 7075-T6 aluminium alloy." *Proc Inst Mech Eng Part C J Mech Eng Sci*, 225(8), 1761–1773.

Rhodes, C. G., Mahoney, M. W., Bingel, W. H., Spurling, R. A., and Bampton, C. (1997). "Effects of friction stir welding on microstructure of 7075 aluminum." *Scr Mater*, 36(6), 69–75.

Rios, O., Geer, T., Weiss, D., Turchi, P. A. E., McCall, S. K., Sims, Z. C., Ott, R. T., and McGuire, M. A. (2016). "Cerium-Based, Intermetallic-Strengthened Aluminum Casting Alloy: High-Volume Co-product Development." *Jom*, 68(7), 1940–1947.

Rizi, M. S., and Kokabi, A. H. (2014). "Microstructure evolution and microhardness of friction stir welded cast aluminum bronze." *J Mater Process Technol*, 214(8), 1524–1529.

Roberge, P. R. (1999). *Handbook of Corrosion Engineering, McGraw-Hill, New York,*

USA.

Robinson, J. S., Tanner, D. A., and Truman, C. E. (2014). "The origin and management of residual stress in heat-treatable aluminium alloys." *Strain*, 50(3), 185–207.

Robson, J. D., and Campbell, L. (2010). "Model for grain evolution during friction stir welding of aluminium alloys." *Sci Technol Weld Join*, 15(2), 171–176.

Rodrigues, D. M., Loureiro, A., Leitao, C., Leal, R. M., Chaparro, B. M., and Vilaça, P. (2009). "Influence of friction stir welding parameters on the microstructural and mechanical properties of AA 6016-T4 thin welds." *Mater Des*, 30(6), 1913–1921.

Rodriguez, R. I., Jordon, J. B., Allison, P. G., Rushing, T., and Garcia, L. (2015). "Microstructure and mechanical properties of dissimilar friction stir welding of 6061-to-7050 aluminum alloys." *Mater Des*, 83, 60–65.

Rometsch, P. A., Zhang, Y., and Knight, S. (2014). "Heat treatment of 7xxx series aluminium alloys - Some recent developments." *Trans Nonferrous Met Soc China (English Ed*, 24(7), 2003–2017.

Rongshi, X., Wuxiong, Y., and Kai, C. (2007). "Porosity characterization in laser welds of Al-Li alloy 1420." *Appl laser*, 1(2007).

Roshan, S. B., Jooibari, M. B., Teimouri, R., Ahmadi, G. A., Naghibi, M. F., and Sohrabpoor, H. (2013). "Optimization of friction stir welding process of AA7075 aluminum alloy to achieve desirable mechanical properties using ANFIS models and simulated annealing algorithm." *Int J Adv Manuf Technol*, 69(5–8), 1803–1818.

Rumelhart, D. E., Hinton, G. E., and Williams, R. J. (1986). "Learning internal representations by error propagation. In: Rumelhart D E, McClelland J L et al. (eds.) Parallel Distributed Processing: Explorations in the Microstructure of Cognition." *MIT Press Cambridge, MA*, 1(V), 318–362.

Russo, D., Russo, E. Di, and Conserva, M. (1970). "Thermomechancal treatment process for heat treatable alumnium alloys."

Ryan, B. F., Ryan, T. A. J., and Joiner, B. L. (2020). "Minitab 10.X® Statistical software by Pennsylvania State University." Minitab Inc, USA.

Sabari, S. S., Malarvizhi, S., and Balasubramanian, V. (2016). "Influences of tool traverse speed on tensile properties of air cooled and water cooled friction stir welded AA2519-T87 aluminium alloy joints." *J Mater Process Technol*, 237, 286–300.

Sabatino, M. Di, and Arnberg, L. (2009). "Castability of aluminium alloys." *Trans Indian Inst Met*, 62(4–5), 321–325.

Sabatino, M. Di, Arnberg, L., Rørvik, S., and Prestmo, A. (2005). "The influence of oxide inclusions on the fluidity of Al-7 wt.%Si alloy." *Mater Sci Eng A*, 413–414, 272–276.

Sajadifar, S. V., Moeini, G., Scharifi, E., Lauhoff, C., Böhm, S., and Niendorf, T. (2019). "On the Effect of Quenching on Postweld Heat Treatment of Friction-Stir-Welded Aluminum 7075 Alloy." *J Mater Eng Perform*, 28(8), 5255–5265.

Salih, O. S., Ou, H., Sun, W., and McCartney, D. G. (2015). "A review of friction stir welding of aluminium matrix composites." *Mater Des*, 86, 61–71.

Sanders, R. E., Baumann, S. F., and Stumpf, H. C. (1989). *Wrought-Non-Heat-Treatable Aluminum Alloys-Contemporary Research and Applications*. *Cambridge, MA Acad Press Inc*.

Sashank, J. S., Sampath, P., Krishna, P. S., Sagar, R., Venukumar, S., and Muthukumaran, S. (2018). "Effects of friction stir welding on microstructure and mechanical properties of 6063 aluminium alloy." *Mater Today Proc*, 5(2), 8348–8353.

Sasidharan, B., Narayanan, K. P., and Prakash, R. S. (2017). "Tensile and Microstructural Characteris-tics of DCSP TIG welded and Friction Stir Welded AA2219 Aluminium Alloy." *Int J Des Manuf*, 5(3), 121–129.

Sato, Y. S., Kokawa, H., Enomoto, M., and Jogan, S. (1999). "Microstructural Evolution of 6063 Aluminum during Friction- Stir Welding." *Metall Mater Trans A*, 30A(September), 2429–2437.

Sato, Y. S., Park, S. H. C., and Kokawa, H. (2001). "Microstructural factors governing hardness in friction-stir welds of solid-solution-hardened Al alloys." *Metall Mater Trans A Phys Metall Mater Sci*, 32(12), 3033–3042.

Sato, Y. S., Takauchi, H., Park, S. H. C., and Kokawa, H. (2005). "Characteristics of the kissing-bond in friction stir welded Al alloy 1050." *Mater Sci Eng A*, 405(1–2), 333–338.

Sato, Y. S., Urata, M., and Kokawa, H. (2002). "Parameters controlling microstructure and hardness during friction-stir welding of precipitation-hardenable aluminum alloy 6063." *Metall Mater Trans A*, 33(3), 625–635.

Sato, Y. S., Urata, M., Kokawa, H., and Ikeda, K. (2003). "Hall-Petch relationship in friction stir welds of equal channel angular-pressed aluminium alloys." *Mater Sci Eng A*, 354(1–2), 298–305.

Schneider, J. A., Nunes, A. C., and Brendel, M. S. (1991). "The Influence of Friction Stir Weld Tool Form and Welding Parameters on Weld Structure and Properties : Nugget Bulge in Self- Reacting Friction Stir Welds The Influence of Friction Stir Weld Tool Form and Welding Parameters on Weld Structure and Propertie." *Int Symp Frict Stir Weld*.

Schwerdt, D., Pyttel, B., and Berger, C. (2010). "Fatigue strength and failure mechanism for the aluminium wrought alloy en AW 6056 in the VHCF-region and influence of notches and compressive residual stresses." *Procedia Eng*, 2(1), 1505–1514.

Scialpi, A., Filippis, L. A. C. De, and Cavaliere, P. (2007). "Influence of shoulder geometry on microstructure and mechanical properties of friction stir welded 6082 aluminium alloy." *Mater Des*, 28(4), 1124–1129.

Seidel, T. U., and Reynolds, A. P. (2001). "Visualization of the material flow in AA2195 friction-stir welds using a marker insert technique." *Metall Mater Trans A Phys Metall Mater Sci*, 32(11), 2879–2884.

Seidel, T. U., and Reynolds, A. P. (2003). "Two-dimensional friction stir welding process model based on fluid mechanics." *Sci Technol Weld Join*, 8(3), 175–183.

Seighalani, K. R., Givi, M. K. B., Nasiri, A. M., and Bahemmat, P. (2010). "Investigations on the effects of the tool material, geometry, and tilt angle on friction

stir welding of pure titanium." *J Mater Eng Perform*, 19(7), 955–962.

Selamat, N. F. M., Baghdadi, A. H., Sajuri, Z., and Kokabi, A. H. (2016). "Friction stir welding of similar and dissimilar aluminium alloys for automotive applications." *Int J Automot Mech Eng*, 13(2), 3401–3412.

Seniw, M. E., Conley, J. G., and Fine, M. E. (2000). "The effect of microscopic inclusion locations and silicon segregation on fatigue lifetimes of aluminum alloy A356 castings." *Mater Sci Eng A*, 285(1–2), 43–48.

Senthil, S. M., Parameshwaran, R., Ragu Nathan, S., Bhuvanesh Kumar, M., and Deepandurai, K. (2020). "A multi-objective optimization of the friction stir welding process using RSM-based-desirability function approach for joining aluminum alloy 6063-T6 pipes." *Struct Multidiscip Optim*, 17.

Shah, P. H., and Badheka, V. (2016). "An Experimental Investigation of Temperature Distribution and Joint Properties of Al 7075 T651 Friction Stir Welded Aluminium Alloys." *Procedia Technol*, 23, 543–550.

Shanavas, S., and Dhas, J. E. R. (2018a). "Quality Prediction of Friction Stir Weld Joints on Aa 5052 H32 Aluminium Alloy Using Fuzzy Logic Technique." *Mater Today Proc*, 5(5), 12124–12132.

Shanavas, S., and Dhas, J. E. R. (2018b). "Weld quality prediction of AA 5052-H32 aluminium alloy using neural network approach." *Mater Today Proc*, 5(2), 8256–8262.

Shanmuga Sundaram, N., and Murugan, N. (2010). "Tensile behavior of dissimilar friction stir welded joints of aluminium alloys." *Mater Des*, 31(9), 4184–4193.

Sharma, C., Dwivedi, D. K., and Kumar, P. (2012a). "Effect of welding parameters on microstructure and mechanical properties of friction stir welded joints of AA7039 aluminum alloy." *Mater Des*, 36, 379–390.

Sharma, C., Dwivedi, D. K., and Kumar, P. (2012b). "Influence of in-process cooling on tensile behaviour of friction stir welded joints of AA7039." *Mater Sci Eng A*, 556(1), 479–487.

Shehabeldeen, T. A., Elaziz, M. A., Elsheikh, A. H., and Zhou, J. (2019). "Modeling of

friction stir welding process using adaptive neuro-fuzzy inference system integrated with harris hawks optimizer." *J Mater Res Technol*, 8(6), 5882–5892.

Sheikhi, M., Ghaini, F. M., Torkamany, M. J., and Sabbaghzadeh, J. (2009). "Characterisation of solidification cracking in pulsed Nd:YAG laser welding of 2024 aluminium alloy." *Sci Technol Weld Join*, 14(2), 161–165.

Shen, J. J., Liu, H. J., and Cui, F. (2010). "Effect of welding speed on microstructure and mechanical properties of friction stir welded copper." *Mater Des*, 31(8), 3937–3942.

Shen, Z., Yang, X., Zhang, Z., Cui, L., and Yin, Y. (2013). "Mechanical properties and failure mechanisms of friction stir spot welds of AA 6061-T4 sheets." *Mater Des*, 49, 181–191.

Shercliff, H. R., Russell, M. J., Taylor, A., and Dickerson, T. L. (2005). "Microstructural modelling in friction stir welding of 2000 series aluminium alloys." *Mec Ind*, 6(1), 25–35.

Shettigar, A. K., and Manjaiah, M. (2017a). "Friction Stir Welding—An Overview." *Adv Manuf Technol*, 1(2017), 161–184.

Shettigar, A. K., and Manjaiah, M. (2017b). *Friction Stir Welding—An Overview*. Springer, Cham.

Shettigar, A. K., Prabhu, S., Malghan, R., Rao, S., and Herbert, M. (2016). "Application of Neural Network for the Prediction of Tensile Properties of Friction Stir Welded Composites." *Mater Sci Forum*, 880, 128–131.

Siddiqui, M. A., Jafri, S. a. ., Bharti, P. ., and Kumar, P. (2014). "Friction Stir Welding as a Joining Process through Modified Conventional Milling Machine : A Review." *Int J Innov Res Dev*, 3(7), 149–153.

Sidhu, M. S., and Chatha, S. S. (2012). "Friction Stir Welding – Process and its Variables : A Review." *Int J Emerg Technol Adv Eng*, 2(12), 275–279.

Silva, A. A. M. da, Arruti, E., Janeiro, G., Aldanondo, E., Alvarez, P., and Echeverria, A. (2011). "Material flow and mechanical behaviour of dissimilar AA2024-T3 and

AA7075-T6 aluminium alloys friction stir welds." *Mater Des*, 32(4), 2021–2027.

Silva, A. C. F., Braga, D. F. O., Figueiredo, M. A. V. de, and Moreira, P. M. G. P. (2015). "Ultimate tensile strength optimization of different FSW aluminium alloy joints." *Int J Adv Manuf Technol*, 79(5–8), 805–814.

Sims, Z. C., Weiss, D., McCall, S. K., McGuire, M. A., Ott, R. T., Geer, T., Rios, O., and Turchi, P. A. E. (2016). "Cerium based, intermetallic strengthened aluminum casting alloy: high volume co-product development." *Jom*, 68(7), 1940–1947.

Singh, B. R. (2012). *A Hand Book on Friction Stir Welding*. *ResearchGate*.

Singh, G., Singh, K., and Singh, J. (2011a). "Effect of process parameters on microstructure and mechanical properties in friction stir welding of aluminum alloy." *Trans Indian Inst Met*, 64(4–5), 325–330.

Singh, R. K. R., Sharma, C., Dwivedi, D. K., Mehta, N. K., and Kumar, P. (2011b). "The microstructure and mechanical properties of friction stir welded Al-Zn-Mg alloy in as welded and heat treated conditions." *Mater Des*, 32(2), 682–687.

Sinha, P., Muthukumaran, S., and Mukherjee, S. K. (2008). "Analysis of first mode of metal transfer in friction stir welded plates by image processing technique." *J Mater Process Technol*, 197(1–3), 17–21.

Sivaraj, P., Kanagarajan, D., and Balasubramanian, V. (2014). "Effect of post weld heat treatment on tensile properties and microstructure characteristics of friction stir welded armour grade AA7075-T651 aluminium alloy." *Def Technol*, 10(1), 1–8.

Smith, G., Steele, N., and Albrecht, R. (1997). *Artificial Neural Networks and Genetic Algorithms*.

Somasekharan, A. C., and Murr, L. E. (2004). "Microstructures in friction-stir welded dissimilar magnesium alloys and magnesium alloys to 6061-T6 aluminum alloy." *Mater Charact*, 52(1), 49–64.

Sorensen, C. D., and Stahl, A. L. (2007). "Experimental measurements of load distributions on friction stir weld pin tools." *Metall Mater Trans B Process Metall Mater Process Sci*, 38(3), 451–459.

Soundararajan, V., Zekovic, S., and Kovacevic, R. (2005). "Thermo-mechanical model with adaptive boundary conditions for friction stir welding of Al 6061." *Int J Mach Tools Manuf*, 45(14), 1577–1587.

Squillace, A., Fenzo, A. De, Giorleo, G., and Bellucci, F. (2004). "A comparison between FSW and TIG welding techniques: Modifications of microstructure and pitting corrosion resistance in AA 2024-T3 butt joints." *J Mater Process Technol*, 152(1), 97–105.

Starke, E. A., and Staley, J. T. (2010). "Application of modern aluminium alloys to aircraft." *Fundam Alum Metall Prod Process Appl*, Elsevier Ltd., 747–783.

Starke, E. A., and Staleyt, J. T. (1996). "Application of modern aluminum alloys to aircraft, Progress in Aerospace Sciences." *Prog Aerosp Sci*, 32(95), 131–172.

Strombeck, A. V., Santos, J. F. dos, Torster, F., Laureano, P., and Kocak, M. (2000). *Fracture Toughness Behaviour of FSW Joints on Aluminium Alloys*.

Strombeck, A. von, and Santos, J. dos. (1999). "F. T orster, P. L aureano, M. K ocak." *First Int Symp Frict Stir Welding, Thousand Oaks, CA, USA*.

Su, H., Wu, C. S., Bachmann, M., and Rethmeier, M. (2015). "Numerical modeling for the effect of pin profiles on thermal and material flow characteristics in friction stir welding." *Mater Des*, 77, 114–125.

Su, J., Nelson, T. W., Mishra, R., and Mahoney, M. (2003). "Microstructural investigation of friction stir welded 7050- T651 aluminium." *Acta Mater*, 51, 713–729.

Sued, M. ., Pons, D., and Lavroff, J. (2014). "Compression ratio effects in bobbin friction stir welding." *10th Int Symp Frict Stir Weld*, 16.

Sulka, G. D., and Stepniowski, W. J. (2009). "Structural features of self-organized nanopore arrays formed by anodization of aluminum in oxalic acid at relatively high temperatures." *Electrochim Acta*, 54(14), 3683–3691.

Sumathi, S., and Paneerselvam, S. (2010). *Computational intelligence paradigms: theory & applications using MATLAB*.

Suresha, C. N., Rajaprakash, B. M., and Upadhya, S. (2011). "A study of the effect of tool pin profiles on tensile strength of welded joints produced using friction stir welding process." *Mater Manuf Process*, 26(9), 1111–1116.

Sutton, M. A., Yang, B., Reynolds, A. P., and Taylor, R. (2002). "Microstructural studies of friction stir welds in 2024-T3 aluminum." *Mater Sci Eng A*, 323(1–2), 160–166.

Svensson, L.-E., Karlsson, L., Larsson, H., Karlsson, B., Fazzini, M., and Karlsson, J. (2000a). "Microstructure and Mechanical Properties of Friction Stir Welded 5083 and 7075 Aluminum Alloys." *Sci Technol ofWelding Join*, 5(5), 285–296.

Svensson, L. E., Karlsson, L., Larsson, H., Karlsson, B., Fazzini, M., and Karlsson, J. (2000b). "Microstructure and mechanical properties of friction stir welded aluminium alloys with special reference to AA 5083 and AA 6082." *Sci Technol Weld Join*, 5(5), 285–296.

Taheri, H., Kilpatrick, M., Norvalls, M., Harper, W. J., Koester, L. W., Bigelow, T., and Bond, L. J. (2019). "Investigation of Nondestructive Testing Methods for Friction Stir Welding." *Met - MDPI*, 9(624), 1–22.

Tait, W. S. (2005). "Handbook of Environmental Degradation of Materials." *Handb Environ Degrad Mater*, 565–581.

Takhakh, A. M., and Abdullah, A. M. (2012). "The Optimization Conditions of Friction Stir Welding (FSW) for Different Rotational and Weld speeds." *Nahrain Univ Coll Eng J*, 15(2), 187–196.

Tamadon, Pons, and Clucas. (2019). "AFM Characterization of Stir-Induced Micro-Flow Features within the AA6082-T6 BFSW Welds." *Technologies*, 7(4), 80.

Tang, W., Reynolds, A. P., Tang, W., and Reynolds, A. P. (2015). "Effect of tool pin features on process response variables during friction stir welding of dissimilar aluminum alloys Effect of tool pin features on process response variables during friction stir welding of dissimilar aluminum alloys." *Sci Technol Weld Join*, 20(5), 425–432.

Tansel, I. N., Demetgul, M., Okuyucu, H., Ahmet, Y., Tansel, I. N., Demetgul, M., Okuyucu, H., and Yapici, A. (2010). "Optimizations of friction stir welding of aluminum alloy by using genetically optimized neural network." *Int J Adv Manuf Technol*, 48(1–4), 95–101.

Tao, Y., Ni, D. R., Xiao, B. L., Ma, Z. Y., Wu, W., Zhang, R. X., and Zeng, Y. S. (2017). "Origin of unusual fracture in stirred zone for friction stir welded 2198-T8 Al-Li alloy joints." *Mater Sci Eng A*, 693(January), 1–13.

Taylor, J. A. (1996). "Metal-related castability effects in aluminium foundry alloys." *Cast Met*, 8(4), 225–252.

Thangaiah, S., Sevvel, P., Satheesh, C., and Mahadevan, S. (2018). "Experimental study on the role of tool geometry in determining the strength & soundness of wrought Az80a Mg alloy joints during FSW process." *FME Trans*, 46(4), 612–622.

Thomas, B. W. M., Johnson, K. I., and Wiesner, C. S. (2003). "Friction Stir Welding - Recent Developments in Tool and Process Technologies." *Adv Eng Mater*, 5(7), 485–490.

Thomas, W. M., and Dolby, R. E. (2002). "Friction Stir Welding Developments." *6TH Int Conf Trends Weld Res*, 10.

Thomas, W. M., and Nicholas, E. D. (1997). "Friction stir welding for the transportation industries." *J Mater Des*, 18(4/6), 269–273.

Thomas, W. M., Nicholas, E. D., and Kallee, S. W. (2001). "Friction Based Technologies for Joining and Processing - TWI." *TWI Ltd*, <https://www.twi-global.com/technical-knowledge/published-papers/friction-based-technologies-for-joining-and-processing-september-2001> (Feb. 26, 2020).

Threadgilll, P. L., Leonard, A. J., Shercliff, H. R., and Withers, P. J. (2009). "Friction stir welding of aluminium alloys." *Int Mater Rev*, 54(2), 49–93.

Thube, R. S. (2014). "Effect of Tool Pin Profile and Welding Parameters on Friction Stir Processing Zone, Tensile Properties and Micro-hardness of AA5083 Joints Produced by Friction Stir Welding." *Int J Eng Adv Technol*, 3(5), 2249–8958.

Timothy Masters. (1993). *Practical Neural Network Recipes in C++*.

Tiwari, S. K., Shukla, D. K., and Chandra, R. (2013). "Friction stir welding of aluminum alloys- A Review." *Int J Mech Aerospace, Ind Mechatronics Eng*, 7(12), 1315–1320.

Topic, I., Höppel, H. W., and Göken, M. (2009). "Friction stir welding of accumulative roll-bonded commercial-purity aluminium AA1050 and aluminium alloy AA6016." *Mater Sci Eng A*, 503(1–2), 163–166.

Toschi, S. (2018). "Optimization of A354 Al-Si-Cu-Mg alloy heat treatment: Effect on microstructure, hardness, and tensile properties of peak aged and overaged alloy." *Metals (Basel)*, 8(11), 16.

Tra, T. H., Okazaki, M., and Suzuki, K. (2012). "Fatigue crack propagation behavior in friction stir welding of AA6063-T5: Roles of residual stress and microstructure." *Int J Fatigue*, 43, 23–29.

Trimble, D., Mitrogiannopoulos, H., O'Donnell, G. E., and McFadden, S. (2015a). "Friction stir welding of AA2024-T3 plate - The influence of different pin types." *Mech Sci*, 6(1), 51–55.

Trimble, D., O'Donnell, G. E., and Monaghan, J. (2015b). "Characterisation of tool shape and rotational speed for increased speed during friction stir welding of AA2024-T3." *J Manuf Process*, 17, 141–150.

Trueba, L., Heredia, G., Rybicki, D., and Johannes, L. B. (2015). "Effect of tool shoulder features on defects and tensile properties of friction stir welded aluminum 6061-T6." *J Mater Process Technol*, 219, 271–277.

Uday, M. B., Fauzi, M. N. A., Zuhailawati, H., Ismail, A. B., Fauzi, M. N. A., Zuhailawati, H., Ismail, A. B., Uday, M. B., Fauzi, M. N. A., Zuhailawati, H., and Ismail, A. B. (2016). "Advances in friction welding process : a review Advances in friction welding process : a review." *Sci Technol Weld Join*, 15(7), 534–558.

Ugender, S., Kumar, A., and Reddy, A. S. (2014). "Microstructure and Mechanical Properties of AZ31B Magnesium alloy by Friction stir Welding." *Procedia Mater Sci*,

6(Icmpc), 1600–1609.

Ulysse, P. (2002). "Three-dimensional modeling of the friction stir-welding process." *Int J Mach Tools Manuf*, 42(July), 1549–1557.

Vaira, V. R., and Padmanaban, R. (2018). "Artificial neural network model for predicting the tensile strength of friction stir welded aluminium alloy AA1100." *Mater Today Proc*, 5(8), 16716–16723.

Vasudevan, A. K., and Doherty, R. D. (1989). *Aluminum Alloys-Contemporary Research and Applications*. *Acad Press Inc*.

Venkateswarlu, D., Mandal, N. R., Mahapatra, M. M., and Harsh, S. P. (2013). "Tool design effects for FSW of AA7039." *Weld J*, 92(2), 7.

Verma, S., and Misra, J. P. (2015). *A Critical Review of Friction Stir Welding Process*. DAAAM International Scientific Book 2015.

Vidakis, N., Vairis, A., Diouf, D., Petousis, M., Savvakis, K., and Tsainis, A. M. (2016). "Effect of the tool rotational speed on the mechanical properties of thin AA1050 friction stir welded sheets." *J Eng Sci Technol*, 9(3), 123–129.

Vijayavel, P., and Balasubramanian, V. (2018). "Effect of pin volume ratio on wear behaviour of friction stir processed LM25AA-5%SiCp metal matrix composites." *Alexandria Eng J*, 57(4), 2939–2950.

Vilaça, P., and Thomas, W. (2011). *Friction Stir Welding Technology*. Springer, Berlin, Heidelberg.

Wagner, D. C., Chai, X., Tang, X., and Kou, S. (2015). "Liquation Cracking in Arc and Friction-Stir Welding of Mg-Zn Alloys." *Metall Mater Trans A Phys Metall Mater Sci*, 46(1), 315–327.

Waheed, M. A., Jayesimi, L. O., Ismail, S. O., and Dairo, O. U. (2017). "Modeling of heat generations for different tool profiles in friction stir welding: study of tool geometry and contact conditions." *J Appl Comput Mech*, 3(1), 37–59.

Wan, L., and Huang, Y. (2018). "Friction stir welding of dissimilar aluminum alloys

and steels: a review." *Int J Adv Manuf Technol*, 99(5–8), 1781–1811.

Wan, L., Huang, Y., Lv, Z., Lv, S., and Feng, J. (2014). "Effect of self-support friction stir welding on microstructure and microhardness of 6082-T6 aluminum alloy joint." *Mater Des*, 55(1), 197–203.

Wang, J., Su, J., Mishra, R. S., Xu, R., and Baumann, J. A. (2014). "Tool wear mechanisms in friction stir welding of Ti-6Al-4V alloy." *Wear*, 321, 25–32.

Wang, S. C., Lefebvre, F., Yan, J. L., Sinclair, I., and Starink, M. J. (2006). "VPPA welds of Al-2024 alloys: Analysis and modelling of local microstructure and strength." *Mater Sci Eng A*, 431(1–2), 123–136.

Wang, X., Wang, K., Shen, Y., and Hu, K. (2008). "Comparison of fatigue property between friction stir and TIG welds." *J Univ Sci Technol Beijing Miner Metall Mater (Eng Ed)*, 15(3), 280–284.

Wanhill, R. J. H. (2013). *Aerospace Applications of Aluminum-Lithium Alloys. Aluminum-Lithium Alloy Process Prop Appl*, Elsevier Inc.

Warrington, D., and Mccartney, D. G. (1989). "Development of a New Hot-cracking Test for Aluminium Alloys." *Cast Met*, 2(3), 134–143.

Waterloo, G., and Jones, H. (1996). "Microstructure and thermal stability of melt-spun Al-Nd and Al-Ce alloy ribbons." *J Mater Sci*, 31(9), 2301–2310.

Weglowski, M. S. (2013). "An experimental study on the friction stir processing process of aluminium alloy." *Key Eng Mater*, 554–557, 1787–1792.

Whittington, B. I. (1996). "The chemistry of CaO and Ca(OH)2 relating to the Bayer process." *Hydrometallurgy*, 43(1–3), 13–35.

Woo, W., Choo, H., Brown, D. W., Feng, Z., and Liaw, P. K. (2006). "Angular distortion and through-thickness residual stress distribution in the friction-stir processed 6061-T6 aluminum alloy." *Mater Sci Eng A*, 437(1), 64–69.

Woodward, N. J., Richardson, I. M., and Thomas, A. (2000). "Variable polarity plasma arc welding of 6.35 mm aluminium alloys: Parameter development and preliminary

analysis." *Sci Technol Weld Join*, 5(1), 21–25.

Xiao, R., and Zhang, X. (2014). "Problems and issues in laser beam welding of aluminum-lithium alloys." *J Manuf Process*, Elsevier BV.

Xie, G. M., Cui, H. B., Luo, Z. A., Misra, R. D. K., and Wang, G. D. (2017). "Microstructrual evolution and mechanical properties of the stir zone during friction stir processing a lean duplex stainless steel." *Mater Sci Eng A*, 704, 311–321.

Xie, G. M., Ma, Z. Y., and Geng, L. (2007). "Development of a fine-grained microstructure and the properties of a nugget zone in friction stir welded pure copper." *Scr Mater*, 57(2), 73–76.

Xie, G. M., Ma, Z. Y., and Geng, L. (2008). "Effects of friction stir welding parameters on microstructures and mechanical properties of brass joints." *Mater Trans*, 49(7), 1698–1701.

Xu, S., Deng, X., Reynolds, A. P., and Seidel, T. U. (2001). "Finite element simulation of material flow in friction stir welding." *Sci Technol Weld Join*, 6(3), 191–193.

Xu, W., Liu, J., Luan, G., and Dong, C. (2009). "Microstructure and mechanical properties of friction stir welded joints in 2219-T6 aluminum alloy." *Mater Des*, 30(9), 3460–3467.

Xu, W., Liu, J., Zhu, H., and Fu, L. (2013). "Influence of welding parameters and tool pin profile on microstructure and mechanical properties along the thickness in a friction stir welded aluminum alloy." *Mater Des*, 47, 599–606.

Yadav, D., and Bauri, R. (2012). "Effect of friction stir processing on microstructure and mechanical properties of aluminium." *Mater Sci Eng A*, 539, 85–92.

Yaduwanshi, D. K., Bag, S., and Pal, S. (2014). "Effect of Preheating in Hybrid Friction Stir Welding of Aluminum Alloy." *J Mater Eng Perform*, 23(10), 3794–3803.

Yamamoto, H., Hairada, S., Ueyama, T., and Ogawa, S. (1992). "Development of low-frequency pulsed MIG wellding for ailuminium alloys." *Weld Int*, 6(7), 580–583.

Yan, J., Sutton, M. A., and Reynolds, A. P. (2005). "Process-structure-property

relationships for nugget and heat affected zone regions of AA2524-T351 friction stir welds." *Sci Technol Weld Join*, 10(6), 725–736.

Yang, J., Ni, D. R., Wang, D., Xiao, B. L., and Ma, Z. Y. (2014). "Friction stir welding of as-extruded Mg-Al-Zn alloy with higher Al content. Part I: Formation of banded and line structures." *Mater Charact*, 96, 142–150.

Yang, Q., Xiao, B. L., and Ma, Z. Y. (2012). "Influence of process parameters on microstructure and mechanical properties of friction-stir-processed mg-gd-y-zr casting." *Metall Mater Trans A Phys Metall Mater Sci*, 43(6), 2094–2109.

Yeni, C., Sayer, S., Ertu, O., and Pakdil, M. (2008). "Effect of post-weld aging on the mechanical and microstructural properties of friction stir welded aluminum alloy 7075." *Arch Mater Sci Eng*, 34(2), 105–109.

Younes, Y. (2010). "Corrosion Control of Friction Stir Welded AA2024-T351 Aluminium Alloys."

Yousif, Y. K., Daws, K. M., and Kazem, B. I. (2008). "Prediction of Friction Stir Welding Characteristic Using Neural Network." *Jordan J Mech Ind Eng*, 2(3), 151–155.

Yu, H., Zheng, B., and Lai, X. (2018). "A modeling study of welding stress induced by friction stir welding." *J Mater Process Technol*, 254(June 2017), 213–220.

Yuqing, M., Liming, K., Fencheng, L., Yuhua, C., and Li, X. (2017). "Effect of tool pin-tip profiles on material flow and mechanical properties of friction stir welding thick AA7075-T6 alloy joints." *Int J Adv Manuf Technol*, 88(1–4), 949–960.

Zaraska, L., Sulka, G. D., Szeremeta, J., and Jaskuła, M. (2010). "Porous anodic alumina formed by anodization of aluminum alloy (AA1050) and high purity aluminum." *Electrochim Acta*, 55(14), 4377–4386.

Zeng, W. M., Wu, H. L., and Zhang, J. (2006). "Effect of tool wear on microstructure, mechanical properties and acoustic emission of friction stir welded 6061 Al alloy." *Acta Metall Sin (English Lett*, 19(1), 9–19.

Zeng, X. H., Xue, P., Wu, L. H., Ni, D. R., Xiao, B. L., Wang, K. S., and Ma, Z. Y.

(2019). "Microstructural evolution of aluminum alloy during friction stir welding under different tool rotation rates and cooling conditions." *J Mater Sci Technol*, 35(6), 972–981.

Zettler, R., Lomolino, S., Santos, J. F. Dos, Donath, T., Beckmann, F., Lippman, T., and Lohwasser, D. (2005). "Effect of tool geometry and process parameters on material flow in FSW of AN AA 2024-T351 alloy." *Weld World*, Institut International de la Soudure, 41–46.

Zhang, D. L., and Zheng, L. (1996). "The quench sensitivity of cast Al-7 Wt Pet Si-0.4 Wt pct Mg alloy." *Metall Mater Trans A Phys Metall Mater Sci*, 27(12), 3983–3991.

Zhang, F., Su, X., Chen, Z., and Nie, Z. (2015). "Effect of welding parameters on microstructure and mechanical properties of friction stir welded joints of a super high strength Al-Zn-Mg-Cu aluminum alloy." *Mater Des*, 67, 483–491.

Zhang, G. F., Jiao, W. M., and Zhang, J. X. (2014). "Filling friction stir weld keyhole using pin free tool and T shaped filler bit." *Sci Technol Weld Join*, 19(2), 98–104.

Zhang, H. J., Liu, H. J., and Yu, L. (2011). "Microstructural evolution and its effect on mechanical performance of joint in underwater friction stir welded 2219-T6 aluminium alloy." *Sci Technol Weld Join*, 16(5), 459–464.

Zhang, H., Lin, S. B., Wu, L., Feng, J. C., and Ma, S. L. (2006). "Defects formation procedure and mathematic model for defect free friction stir welding of magnesium alloy." *Mater Des*, 27(9), 805–809.

Zhang, H. W., Zhang, Z., and Chen, J. T. (2007). "3D modeling of material flow in friction stir welding under different process parameters." *J Mater Process Technol*, 183(1), 62–70.

Zhang, J., Feng, X. S., Gao, J. S., Huang, H., Ma, Z. Q., and Guo, L. J. (2018). "Effects of welding parameters and post-heat treatment on mechanical properties of friction stir welded AA2195-T8 Al-Li alloy." *J Mater Sci Technol*, 34(1), 219–227.

Zhang, Y. N., Cao, X., Larose, S., and Wanjara, P. (2012). "Review of tools for friction stir welding and processing." *Can Metall Q*, 51(3), 250–261.

Zhang, Z., Wang, Y., and Bian, X. (2004). "Microstructure selection map for rapidly solidified Al-rich Al-Ce alloys." *J Cryst Growth*, 260(3–4), 557–565.

Zhang, Z., and Zhang, H. W. (2008). "A fully coupled thermo-mechanical model of friction stir welding." *Int J Adv Manuf Technol*, 37, 279–293.

Zhao, J., Jiang, F., Jian, H., Wen, K., Jiang, L., and Chen, X. (2010). "Comparative investigation of tungsten inert gas and friction stir welding characteristics of Al-Mg-Sc alloy plates." *Mater Des*, 31(1), 306–311.

Zhao, K., Liu, Z., Xiao, B., and Ma, Z. (2017a). "Friction stir welding of carbon nanotubes reinforced Al-Cu-Mg alloy composite plates." *J Mater Sci Technol*, 33(9), 1004–1008.

Zhao, S., Bi, Q., Wang, Y., and Shi, J. (2017b). "Empirical modeling for the effects of welding factors on tensile properties of bobbin tool friction stir-welded 2219-T87 aluminum alloy." *Int J Adv Manuf Technol*, 90(1–4), 1105–1118.

Zhao, Y. H., Lin, S. B., Qu, F. X., and Wu, L. (2006). "Influence of pin geometry on material flow in friction stir welding process." *Mater Sci Technol*, 22(1), 45–50.

Zhou, C., Yang, X., and Luan, G. (2006). "Effect of kissing bond on fatigue behavior of friction stir welds on Al 5083 alloy." *J Mater Sci*, 41(10), 2771–2777.

Zhou, L., Liu, D., Nakata, K., Tsumura, T., Fujii, H., Ikeuchi, K., Michishita, Y., Fujiya, Y., and Morimoto, M. (2012). "New technique of self-refilling friction stir welding to repair keyhole." *Sci Technol Weld Join*, 17(8), 649–655.

Zhou, L., Wang, T., Zhou, W. L., Li, Z. Y., Huang, Y. X., and Feng, J. C. (2016). "Microstructural Characteristics and Mechanical Properties of 7050-T7451 Aluminum Alloy Friction Stir-Welded Joints." *J Mater Eng Perform*, 25(6), 2542–2550.

Zhu, Y., Chen, G., Chen, Q., Zhang, G., and Shi, Q. (2016). "Simulation of material plastic flow driven by non-uniform friction force during friction stir welding and related defect prediction." *Mater Des*, 108, 400–410.

Zurada, J. M. (1992). "Introduction to artificial neural systems." *Neurocomputing*, 8(1), 764.

LIST OF PUBLICATIONS BASED ON Ph.D. WORK

International Journal Publications:

1. D'Souza, A. D., Rao, S. S., and Herbert, M. A. (2019). "Assessment of influence of process parameters on properties of friction stir welded Al-Ce-Si-Mg aluminium alloy." *Mater. Res. Express - IOP Sci.*, 10. – (*Published on May 1, 2019*)

2. D'Souza, A. D., Rao, S. S., and Herbert, M. A. (2019). "Evaluation of Microstructure, hardness and mechanical properties of friction stir welded Al-Ce-Si-Mg Aluminium alloy." *Met. Mater. Int. Springer.*, 12 – (*Published on July 30, 2019*)

International Conference Proceedings:

1. D'Souza, A. D., Rao, S. S., and Herbert, M. A. (2021). "Taguchi method of optimization of process variables for ultimate tensile strength of friction stir welded joint of Al-Ce-Si-Mg aluminium alloy plates." *Proceedings of 2nd International Conference on Smart and Sustainable Developments in Materials, Manufacturing and Energy Engineering, December 22 & 23, 2020 - NMAM Institute of Technology, Nitte, Karnataka, India. Published in Mater. Today Proc., 46(7), 2691–2698.*

Communicated to International Journal Publications:

1. D'Souza, A. D., Rao, S. S., and Herbert, M. A. (2020). "Process parameter optimization for ultimate tensile strength of friction stir weld joint of Al-10Mg-8Ce-3.5Si aluminium alloy plates using Taguchi technique", *Mater. Today Proceedings,* an International Conference Proceedings Journal – Springer - (*Communicated & Review completed*)

2. D'Souza, A. D., Rao, S. S., and Herbert, M. A. (2020). "A Study of Microstructure and Mechanical properties of Friction Stir Welded joint of Al-Ce-Si-Mg Aluminium Alloy Plates and Optimization cum Prediction techniques using Taguchi and ANN", Sādhanā,, Springer Nature. - (*Communicated*)

APPENDIX – I

Prediction Programs for ANN

Sample Program for Training Data

```
%  %46Training data no.
clear all;
% g=1;
% h=8;
for(k=1:30)
  A = xlsread('addatttbfg6.xlsx','M5:P50');
  P = A';
  B = xlsread('addatttbfg6.xlsx','Q5:V50');
  T = B';
  n=length(P);
  m=length(T);
  % [pn,ps1] = mapstd(P);
  % [ptrans,ps2] = processpca(pn,0.001);
  net=newff(P,T,k,{'tansig'});
  net.performFcn='mse';
  net.initFcn='initlay';
  net.trainFcn='trainbfg';
  net.trainParam.epochs= 1000;
  %net.trainParam.lr = 0.01;
  net.trainParam.goal=1E-3;
  net.divideFcn = '';
  [net1,tr] = train(net,P,T);
  Y1 = sim(net1,P);
  R=Y1';
  C=T';
  %for i=1:m
```

```matlab
%e=((R-T).^2)/2;
%e=abs(R-T)/R;
xlswrite('addatttbfg6.xlsx',R,'X5:AC50');
% end
%
% Testing 8 datas
O = xlsread('addatttbfg6.xlsx','M51:P58');
S = O';
Y2 = sim(net1,S);
Z =Y2';
xlswrite('addatttbfg6.xlsx',Z,'X51:AC58');  %test network output%
%training accuracy(For calculating minium mse and error for training data)
for(i=1:m)
    e=abs(C-R);
    mse=(e.^2)/2;
    xlswrite('addatttbfg6.xlsx',mse,'BE5:BJ50');
end

for(j=1:m)
    er=abs(R-C);
    xlswrite('addatttbfg6.xlsx',er,'BL5:BQ50');%%DIFFFERENCE
end
% % Test accuracy(For calculating minium mse and error for test data)
V = xlsread('addatttbfg6.xlsx','X51:AC58');
W = xlsread('addatttbfg6.xlsx','Q51:V58');
te=abs(V-W);
    tmse=(te.^2)/2;
    xlswrite('addatttbfg6.xlsx',tmse,'BE51:BJ58');
ter=abs(V-W);
xlswrite('addatttbfg6.xlsx',ter,'BL51:BQ58');
% %
```

```
% F = xlsread('addatttbfg6.xlsx','Q5:V50');%%READ ACTUAL TEST
OUTPUT%
% % %%for validation
% L = xlsread('addatttbfg6.xlsx','M51:P58');
% M = xlsread('addatttbfg6.xlsx','Q51:V58');
% N=L';
% QQ = sim(net1,N);
% O=QQ';
% xlswrite('addatttbfg6.xlsx',O,'Y59:Y63');
% % D =abs(M-O);
% % xlswrite('addatttbfg6.xls',D,'O238:O242');
% % For calculating minium mse and error for training data
% g=g+10;
% a = num2str(g);
% b = 'C' ;
% c = [b a] ;
% h=h+10;
% d = num2str(h);
% e = 'H' ;
% f = [e d] ;
% xlswrite('Restrainttbfg6.xlsx',U, 'c:f' );
U = xlsread('addatttbfg6.xlsx','X5:AC58');
if k == 1
    xlswrite('Restrainttbfg6.xlsx',U, 'O5:T58' );
elseif k == 2
    xlswrite('Restrainttbfg6.xlsx',U, 'O65:T118' );
elseif k == 3
    xlswrite('Restrainttbfg6.xlsx',U, 'O125:T178' );
elseif k == 4
    xlswrite('Restrainttbfg6.xlsx',U, 'O185:T238' );
elseif k == 5
    xlswrite('Restrainttbfg6.xlsx',U, 'O245:T298' );
```

```
elseif k == 6
    xlswrite('Restrainttbfg6.xlsx',U, 'O305:T358' );
elseif k == 7
    xlswrite('Restrainttbfg6.xlsx',U, 'O365:T418' );
elseif k == 8
    xlswrite('Restrainttbfg6.xlsx',U, 'O425:T478' );
elseif k == 9
    xlswrite('Restrainttbfg6.xlsx',U, 'O485:T538' );
elseif k == 10
    xlswrite('Restrainttbfg6.xlsx',U, 'O545:T598' );
elseif k == 11
    xlswrite('Restrainttbfg6.xlsx',U, 'O605:T658' );
elseif k == 12
    xlswrite('Restrainttbfg6.xlsx',U, 'O665:T718' );
elseif k == 13
    xlswrite('Restrainttbfg6.xlsx',U, 'O725:T778' );
elseif k == 14
    xlswrite('Restrainttbfg6.xlsx',U, 'O785:T838' );
elseif k == 15
    xlswrite('Restrainttbfg6.xlsx',U, 'O845:T898' );
elseif k == 16
    xlswrite('Restrainttbfg6.xlsx',U, 'O905:T958' );
elseif k == 17
    xlswrite('Restrainttbfg6.xlsx',U, 'O965:T1018' );
elseif k == 18
    xlswrite('Restrainttbfg6.xlsx',U, 'O1025:T1078' );
elseif k == 19
    xlswrite('Restrainttbfg6.xlsx',U, 'O1085:T1138' );
elseif k == 20
    xlswrite('Restrainttbfg6.xlsx',U, 'O1145:T1198' );
elseif k == 21
    xlswrite('Restrainttbfg6.xlsx',U, 'O1205:T1258' );
```

```
    elseif k == 22
        xlswrite('Restrainttbfg6.xlsx',U, 'O1265:T1318' );
    elseif k == 23
        xlswrite('Restrainttbfg6.xlsx',U, 'O1325:T1378' );
    elseif k == 24
        xlswrite('Restrainttbfg6.xlsx',U, 'O1385:T1438' );
    elseif k == 25
        xlswrite('Restrainttbfg6.xlsx',U, 'O1445:T1498' );
    elseif k == 26
        xlswrite('Restrainttbfg6.xlsx',U, 'O1505:T1558' );
    elseif k == 27
        xlswrite('Restrainttbfg6.xlsx',U, 'O1565:T1618' );
    elseif k == 28
        xlswrite('Restrainttbfg6.xlsx',U, 'O1625:T1678' );
    elseif k == 29
        xlswrite('Restrainttbfg6.xlsx',U, 'O1685:T1738' );
    elseif k == 30
        xlswrite('Restrainttbfg6.xlsx',U, 'O1745:T1798' );
    else
    end
end
```

Sample Program for Test & Validation Data

```
%  %56Test & Validation data no.
clear all;
% g=1;
% h=8;
for(k=1:3)
  A = xlsread('addatttbfg6HL3.xlsx','M5:P50');
  P = A';
```

```
B = xlsread('addatttbfg6HL3.xlsx','Q5:V50');
T = B';
n=length(P);
m=length(T);
% [pn,ps1] = mapstd(P);
% [ptrans,ps2] = processpca(pn,0.001);
net=newff(P,T,k,{'tansig'});
net.performFcn='mse';
net.initFcn='initlay';
net.trainFcn='trainbfg';
net.trainParam.epochs= 100000;
%net.trainParam.lr = 0.01;
net.trainParam.goal=1E-5;
net.divideFcn = '';
[net1,tr] = train(net,P,T);
Y1 = sim(net1,P);
R=Y1';
C=T';
%for i=1:m
%e=((R-T).^2)/2;
%e=abs(R-T)/R;
xlswrite('addatttbfg6HL3.xlsx',R,'X5:AC50');
% end
%
% Testing 8 datas
O = xlsread('addatttbfg6HL3.xlsx','M51:P58');
S = O';
Y2 = sim(net1,S);
Z =Y2';
xlswrite('addatttbfg6HL3.xlsx',Z,'X51:AC58');  %test network output%
%training accuracy(For calculating minium mse and error for training data)
for(i=1:m)
```

```
    e=abs(C-R);
    mse=(e.^2)/2;
    xlswrite('addatttbfg6HL3.xlsx',mse,'BE5:BJ50');
end

for(j=1:m)
    er=abs(R-C);
    xlswrite('addatttbfg6HL3.xlsx',er,'BL5:BQ50');%%DIFFFERENCE
end
% % Test accuracy(For calculating minium mse and error for test data)
V = xlsread('addatttbfg6HL3.xlsx','X51:AC58');
W = xlsread('addatttbfg6HL3.xlsx','Q51:V58');
te=abs(V-W);
    tmse=(te.^2)/2;
    xlswrite('addatttbfg6HL3.xlsx',tmse,'BE51:BJ58');
ter=abs(V-W);
xlswrite('addatttbfg6HL3.xlsx',ter,'BL51:BQ58');
% %
% F = xlsread('addatttbfg6HL3.xlsx','Q5:V50');%%READ ACTUAL TEST
OUTPUT%
% % %%for validation
% L = xlsread('addatttbfg6HL3.xlsx','M51:P58');
% M = xlsread('addatttbfg6HL3.xlsx','Q51:V58');
% N=L';
% QQ = sim(net1,N);
% O=QQ';
% xlswrite('addatttbfg6HL3.xlsx',O,'Y59:Y63');
% % D =abs(M-O);
% % xlswrite('addatttbfg6HL3.xls',D,'O238:O242');
% % For calculating minium mse and error for training data
% g=g+10;
% a = num2str(g);
```

```matlab
% b = 'C' ;
% c = [b a] ;
% h=h+10;
% d = num2str(h);
% e = 'H' ;
% f = [e d] ;
% xlswrite('Restrainttbfg6HL3.xlsx',U, 'c:f' );
U = xlsread('addatttbfg6HL3.xlsx','X5:AC58');
if k == 1
    xlswrite('Restrainttbfg6HL3.xlsx',U, 'O5:T58' );
elseif k == 2
    xlswrite('Restrainttbfg6HL3.xlsx',U, 'O65:T118' );
elseif k == 3
    xlswrite('Restrainttbfg6HL3.xlsx',U, 'O125:T178' );
    else
    end
end
```

APPENDIX – II

Dynamic to Static volume ratio calculations

1) Triangular Profile Pin Tool (TPP)

r = 3.5 mm

6 mm
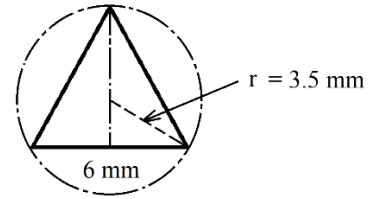
Static volume of the Triangular Profile Pin (SV) $= \frac{1}{2} \times b \times h \times l$

$$SV = \frac{1}{2} \times 6 \times 5.2 \times 5.8$$

$$= 90.5 \text{ mm}^3$$

Where,

b =. Side length of Triangular profile of pin   = 6 mm

h = Perpendicular height of Triangular profile   = 5.2 mm

l = Length of Triangular profiled tool pin   = 5.8 mm

Dynamic volume of the Triangular profile of pin during rotation resembles to cylindrical profile. Hence, Volume swept during rotation in a circular fashion is Dynamic volume.

Dynamic volume of the Triangular Profile Pin (DV) $= \pi r^2 \times l$

$$DV = \pi \times 3.5^2 \times 5.8$$

$$= 223.2 \text{ mm}^3$$

Where,

r =. Radius of sweep of Triangular profile of pin   = 3.5 mm

Ratio of Dynamic to Static volume of TPP $= \dfrac{DV}{SV} = \dfrac{223.2}{90.5} = \underline{\mathbf{2.47}}$

341

2) Square Profile Pin Tool (SPP)

r = 4.24 mm

6 mm

Static volume of the Square Profile Pin (SV) $\quad = b\ x\ h\ x\ l$

$$SV = 6\ x\ 6\ x\ 5.8$$

$$= 208.8\ mm^3$$

Where,

b =. Side length of Square profile of pin $\qquad = 6\ mm$

l = Length of Square profiled tool pin $\qquad = 5.8\ mm$

Dynamic volume of the Square profile of pin during rotation resembles to cylindrical profile. Hence, Volume swept during rotation in a circular fashion is Dynamic volume.
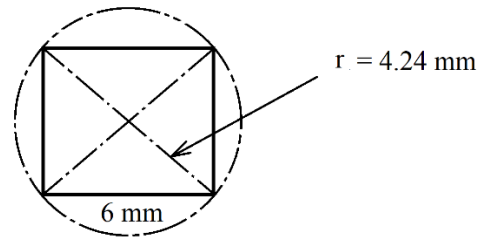
Dynamic volume of the Square Profile Pin (DV) $= \pi r^2\ x\ l$

$$DV = \pi\ x\ 4.24^2\ x\ 5.8$$

$$= 327.6\ mm^3$$

Where,

r =. Radius of sweep of Square profile of pin $\qquad = 4.24\ mm$

Ratio of Dynamic to Static volume of SPP $= \dfrac{DV}{SV} = \dfrac{327.6}{208.8} = \underline{\mathbf{1.57}}$

3) Circular Profile Pin Tool (CPP)

r = 3 mm

6 mm

Static volume of the Circular Profile Pin (SV) $= \pi r^2 \times l$

$$SV = \pi \times 3^2 \times 5.8$$

$$= 164 \text{ mm}^3$$

Where,

r =. Radius of Circular profile of pin   = 3 mm

l = Length of Circular profiled tool pin   = 5.8 mm

Dynamic volume of the Circular profile of pin during rotation resembles to cylindrical profile. Hence, Volume swept during rotation in a circular fashion is Dynamic volume.

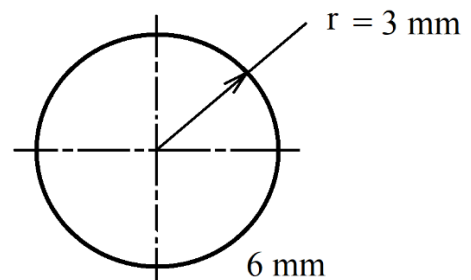Dynamic volume of the Circular Profile Pin (DV) $= \pi r^2 \times l$

$$DV = \pi \times 3^2 \times 5.8$$

$$= 164 \text{ mm}^3$$

Where,

r =. Radius of sweep of Circular profile of pin   = 3 mm

Ratio of Dynamic to Static volume of CPP $= \dfrac{DV}{SV} = \dfrac{164}{164} = \underline{\mathbf{1}}$

APPENDIX – III

FSW Machine Specifications

Machine Type	CNC Vertical Machining Center
Model	BMV45T 20
Make	BFW Bangalore INDIA

Table

Clamping area	450 mm x 900 mm
Max. load	50 kg

Traverse

X-Axis	600 mm
Y-Axis	450 mm
Z-Axis	500 mm

Axis Drive

Feed rates	1 – 10000 mm / min
Rapid traverse X/ Y / Z	24 / 24 /15 m/min

Spindle

Power	3.5 / 7.5 kW
Speed	6000 rpm
	(8000 / 10000)
Tool format	BT40

Automatic tool changer

No. of tools	20 No.
CNC System	Fanuc

APPENDIX – IV

CNC Machine Programming

G codes

G00 - Positioning at rapid speed

G01 - Linear interpolation (machining a straight line)

G02 - Circular interpolation clockwise (machining arcs)

G03 - Circular interpolation, counter-clockwise

G04 - Dwell

G09 - Exact stop

G10 - Setting offsets in the program

G12 - Circular pocket milling, clockwise

G13 - Circular pocket milling, counter-clockwise

G17 - X-Y plane for arc machining

G18 - Z-X plane for arc machining

G19 - Z-Y plane for arc machining

G20 - Inch units

G21 - Metric units

G27 - Reference return check

G28 - Automatic return through reference point

G29 - Move to location through reference point

G31 - Skip function

G32 - Thread cutting

G33 - Thread cutting

G40 - Cancel diameter offset

G41 - Cutter compensation left

G42 - Cutter compensation right

G43 - Tool length compensation

G44 - Tool length compensation cancel

G50 - Set coordinate system and maximum RPM

G52 - Local coordinate system setting

G53 - Machine coordinate system setting

G54~G59 - Workpiece coordinate system settings

G61 - Exact stop check

G65 - Custom macro call

G70 - Finish cycle

G71 - Rough turning cycle

G72 - Rough facing cycle

G73 - Irregular rough turning cycle

G73 - Chip break drilling cycle

G74 - Left hand tapping

G74 - Face grooving or chip break drilling

G75 - OD groove pecking

G76 - Fine boring cycle

G76 - Threading cycle

G80 - Cancel cycles

G81 - Drill cycle

G82 - Drill cycle with dwell

G83 - Peck drilling cycle

G84 - Tapping cycle

G85 - Bore in, bore out

G86 - Bore in, rapid out

G87 - Back boring cycle

G90 - Absolute programming

G91 - Incremental programming

G92 - Reposition origin point

G92 - Thread cutting cycle

G94 - Per minute feed

G95 - Per revolution feed

G96 - Constant surface speed control

G97 - Constant surface speed cancel

G98 - Per minute feed

G99 - Per revolution feed

M codes

M00 - Program stop

M01 - Optional program stop

M02 - Program end

M03 - Spindle on clockwise

M04 - Spindle on counter-clockwise

M05 - Spindle off

M06 – Tool change

M08 - Coolant on

M09 - Coolant off

M10 - Chuck or rotary table clamp

M11 - Chuck or rotary table clamp off

M19 - Orient spindle

M30 - Program end, return to start

M97 - Local sub-routine call

M98 - Sub-program call

M99 - End of sub program

APPENDIX – V

Chemical Analysis (Optical Emission Spectrometry) Report

MATERIAL TESTING LABORATORY
केमिकल लेबोरेटरी
NABL ACCREDITED
CHEMICAL ANALYSIS REPORT
केमिकल एनालिसिस रिपोर्ट

NABL Cert. No. T-022

Page \ of \

Report & Date	:	7493-94		20-07-2018

Customer : M/s AUSTIN DINESH D'SOUZA,NMAMIT,KARKALA. BANGALORE.

Ref No. & Date	:	NIL	20-07-2018
Sample Received On	:	20-07-2018	
Date of test	:	20-07-2018	

Description of sample : ALUMINIUM LLOY
Procedure Adopted : Optical Emission Spectrometry as per
ASTM E1251-11

RESULT:

SI NO.	Sample ID	Content %							
		Al	Mg	Si	Fe	Mn	Ce	Zn	Ti
1	1	79.28	9.942	3.239	0.188	0.122	7.109	0.085	0.042
2	2	82.48	5.016	3.821	0.309	0.191	8.003	0.142	0.039

Reporting of any discrepancies & collection of tested sample shall be made within 15 days from the date of report

Traceability : Certified reference masters used are traceable to International Standards.
Sampling : Sampling is not carried out by CMTI

This report refers only to the samples supplied and may not be reproduced except in full without the written permission from the Director, Central Manufacturing Technology Institute

सेन्ट्रल मैन्युफैक्चरिंग टेक्नोलॉजि इंस्टिट्यूट
CENTRAL MANUFACTURING TECHNOLOGY INSTITUTE
(Govt. of India Society) Tumkur Road, Bangalore - 560 022, India
Ph : 080-22188289, 22188287, Fax : 23370428,
E-mail : avadhani.cmti@nic.in, Web : www.cmti-india.net

Authorised Signatory

Bio - Data

The author, Austine Dinesh D'Souza was born on 5th July 1966 in Shirva of Udupi District in Karnataka State, India. He obtained his primary education from Christ King Higher Primary School, Karkala, Karnataka. He completed his secondary education from S.B. High School, Karkala. and higher secondary education from S. B. College, Karkala, Karnataka. He completed his Bachelor 's Degree in Mechanical Engineering in 1989 from M.S. Ramaiah Institute of Technology, Bengaluru, securing 4th Rank to Bangalore University and Master 's Degree in Machine Design in 2015 from N.M.A.M. Institute of Technology, Karkala, Karnataka. He has obtained his Ph.D. Doctorate Degree from N.I.T.K., Surathkal in the year 2021. He worked as a Design Engineer in Bangalore for Research Institutes and Industries like CMTI (Central Manufacturing Technology Institute), WIPRO Fluid Power and BFW for 7 years. Then he moved to U.A.E. (United Arab Emirates) to work as Machine Design Engineer in Industries like Danway Dubai, E.W. Cox Pty. Ltd., Australia, Emirates Truck Factory Pty. Ltd., Holland, Fortuna Engineering LLC. for 16 years. Then he joined as an Assistant Professor, Grade-II in the Department of Mechanical Engineering of N.M.AM. Institute of Technology, Nitte, Karkala, Karnataka, in the year 2012. Currently, he is working in the same college as an Assistant Professor, Grade-III, in the Department of Mechanical Engineering.

The author has published a part of his research work based on FSW related to this Ph.D., in the form of papers in two International Journals, one paper in International Conference and another two communicated to International Journals and awaiting review comments. The author has also published papers related to other fields like Condition monitoring studies in mechanical industries. These include two papers published in National journals and two in International Conference proceedings.

The author is an active member of various Professional Societies or Bodies, like CMSI (Condition monitoring society of India), IWS (Indian welding society), FPSI (Fluid power society of India) etc. The author has also organised or attended twelve FDPs, ten Technical workshops, twelve technical Seminars, eight Industry visits, and two Guest lectures. He has worked as a Resource person, Co-ordinator, or Organising Committee

Member for various FDPs, workshops, seminars, and industry visits both within the employed organisation and other outside Institutes.

In addition to this, the author is well versed with many modern computer software & programming languages used in the Design and analysis of Machine components, materials, and structures.

The authors address for communication is as below.

Austine Dinesh D'Souza

56/3, Near Ramasamudra,

Karkala Post, Karkala Taluq,

Udupi District, Karnataka State

INDIA – **574104**

Mobile: +91-**8762698926**
             +91-**9620975100**

Email: austindinesh@hotmail.com
             austindineshdsouza@gmail.com

```
* * * * * * * * *
 * * * * * * * *
  * * * * * * *
   * * * * * *
    * * * * *
     * * * *
      * *
       *
```